TECHNICAL REPORT STANDARD TITLE PAGE

1. Report No.	2. Government Accession No.	3. Recipient's Catalog No.
FHWA/TX-88+463-1F		

4. Title and Subtitle
DISTRIBUTION OF POST-TENSIONING FORCES PRIOR TO GROUTING TENDONS

5. Report Date
January 1988

6. Performing Organization Code

7. Author(s)
N. H. Burns and Charles E. Quade

8. Performing Organization Report No.
Research Report 463-1F

9. Performing Organization Name and Address
Center for Transportation Research
The University of Texas at Austin
Austin, Texas 78712-1075

10. Work Unit No.

11. Contract or Grant No.
Research Study 3-5-86-463

12. Sponsoring Agency Name and Address
Texas State Department of Highways and Public Transportation; Transportation Planning Division
P. O. Box 5051
Austin, Texas 78763-5051

13. Type of Report and Period Covered
Final

14. Sponsoring Agency Code

15. Supplementary Notes
Study conducted in cooperation with the U. S. Department of Transportation, Federal Highway Administration. Research Study Title: "Distribution of Post-Tensioning Forces Prior to Grouting Tendons"

16. Abstract

The objective of this study was to evaluate the simplification of design procedures for continuous post-tensioned members using an average-tendon stress as opposed to the current-design procedure of using a variable-tendon stress at different design control points along the length of a tendon profile.

This report evaluates the tendon stress distribution due to frictional effects during jacking and seating of several tendon profiles. Measured strand stress values along the tendon profile are compared to predicted theoretical stress values. After seating, the redistribution of strand stresses was observed to determine the magnitude of tendon stress equalization and the necessary time period for redistribution to occur. The results of laboratory and field experimental studies are summarized in this report.

17. Key Words	18. Distribution Statement
post-tensioning forces, distribution, grouting, tendons, average-tendon stress, variable-tendon stress, design procedures, distribution, continuous	No restrictions. This document is available to the public through the National Technical Information Service, Springfield, Virginia 22161.

19. Security Classif. (of this report)	20. Security Classif. (of this page)	21. No. of Pages	22. Price
Unclassified	Unclassified	174	

Form DOT F 1700.7 (8-69)

DISTRIBUTION OF POST-TENSIONING FORCES PRIOR TO GROUTING TENDONS

by

N. H. Burns and Charles E. Quade

Research Report No. 463-1F

Research Project 3-5-86-463

"Distribution of Post-Tensioning Forces
Prior to Grouting Tendons"

Conducted for

Texas

State Department of Highways and Public Transportation

In Cooperation with the
U. S. Department of Transportation
Federal Highway Administration

by

CENTER FOR TRANSPORTATION RESEARCH
BUREAU OF ENGINEERING RESEARCH
THE UNIVERSITY OF TEXAS AT AUSTIN

January 1988

The contents of this report reflect the views of the authors, who are responsible for the facts and the accuracy of the data presented herein. The contents do not necessarily reflect the official views or policies of the Federal Highway Administration. This report does not constitute a standard, specification, or regulation.

There was no invention or discovery conceived or first actually reduced to practice in the course of or under this contract, including any art, method, process, machine, manufacture, design or composition of matter, or any new and useful improvement thereof, or any variety of plant which is or may be patentable under the patent laws of the United States of America or any foreign country.

PREFACE

Field observations for post-tensioned structures have suggested that post-tensioned tendon forces along a tendon profile tend to redistribute and equalize the tendon-stress variation induced by friction and anchorage-seating losses. This phenomenon is widely acknowledged in the post-tensioned industry but no research data has been available to predict the magnitude to tendon-stress redistribution or the time period over which the redistribution occurs.

The research described here is that of Research Project 463-1F of which the overall objective was to determine the distribution of post-tensioned tendon forces prior to grouting of the tendon. Tendon-stress distribution was monitored for three phases:

1. jacking phase– tendon-stress variation induced by the friction and wobble effects during stressing;

2. anchorage seating phase– change in the tendon-stress variation resulting from the anchorage-seating transformation loss; and

3. prior-to-grouting phase– redistribution of the tendon-stress variation following seating and prior to grouting of the tendon.

Factors considered in this study to influence the magnitude of distribution were:

1. type of prestressing strand;

2. tendon size (number of strands per tendon);

3. tendon curvature; and

4. stressing technique.

IMPLEMENTATION

The determination of the distribution of post-tensioned forces prior to grouting tendons is an important part of the design of continuous post-tensioned concrete members. Prior to grouting the tendons, the adjustments of the tendon-stress variation to an average tendon stress along the length will greatly simplify design of continuous beams. This report compares current design procedures for determining the tendon-stress variation due to friction and anchorage seating losses along a tendon profile with the measured tendon-stress variation.

SUMMARY

The objective of this study was to evaluate the simplification of design procedures for continuous post-tensioned members using an average-tendon stress as opposed to the current-design procedure of using a variable-tendon stress at different design control points along the length of a tendon profile.

This report evaluates the tendon stress distribution due to frictional effects during jacking and seating of several tendon profiles. Measured strand stress values along the tendon profile are compared to predicted theoretical stress values. After seating, the redistribution of strand stresses was observed to determine the magnitude of tendon stress equalization and the necessary time period for redistribution to occur. The results of laboratory and field experimental studies are summarized in this report.

TABLE OF CONTENTS

LIST OF TABLES

LIST OF FIGURES

CHAPTER ONE INTRODUCTION

1.1 General

An accurate estimation of the prestress force in continuous post-tensioned structures is an important design consideration. Both serviceability and, in some cases, ultimate moment capacity rely on the final effective prestress force. Continuous post-tensioned structures usually have several design control points. The final effective prestress force at design control points is dependent on the initial jacking force, losses due to friction coefficient and curvature of the tendon profile, and anchorage seating losses. After seating, time dependent losses result from creep and shrinkage of concrete and prestressing steel relaxation. These losses are interdependent for a prestressed concrete structure.

Frictional resistance along a tendon profile during post-tensioning often induces a major loss in prestress force over a long tendon length with significant curvature along the path from jacking end to holding end. Other losses generally total approximately 15% of the initial prestress and are more nearly uniform along the entire length. Frictional losses occasionally may reduce the initial prestress by 30% or more. Also, friction losses are characterized by the variation in the prestress force along the length of a tendon profile. This variation often complicates the design and analysis.

1.2 Friction Losses

1.2.1 Theory. Three different forces act on a structure due to a post-tensioned tendon: axial compression, radial pressure, and frictional resistance. The axial force acts through end anchorages actively compressing the concrete. The radial pressure force is distributed along the tendon length and is directed through the radius of curvature. Frictional resistance is a tangential force which acts in a direction opposite to the movement of prestressing strand during stressing. Both axial compression and the radial pressure combine to resist dead and externally applied loads. Friction diminishes the influence of both these beneficial effects of post-tensioning.

Friction is the resistance that develops when two surfaces slide or tend to slide against each other. The resisting friction force is directly proportional to the normal force (radial pressure) pressing the two surfaces together. For post-tensioning systems, friction develops between the prestressing strand and the surrounding sheathing. Friction losses result from two primary effects: length and curvature. The length effect is considered to account for the unintentional misalignment, referred to as wobble, of a tendon profile which is intended to be straight. The amount of wobble depends on the stiffness of sheathing and cable, spacing and rigidity of supports, amount of vibration during concrete placement, and the workmanship of conduit (sheathing) placement.

The curvature effect accounts for the intentional bending of the tendon, often called the tendon profile, in the vertical plane.

The loss of prestress due to length and curvature is dependent on the coefficient of friction between strands and surrounding sheathing plus the normal pressure force exerted by the tendon on the post-tensioned member. The effect of friction loss can be computed by the following equation:

$$F_x = F_J e^{-KL_x - \mu\alpha} \tag{1.1}$$

where

F_x = prestress tendon force at any point x from the jacking end

F_J = prestress tendon force at jacking end

e = base of Napierian logarithms

K = wobble coefficient

L_x = length of tendon element from jacking end to a distance x

μ = friction coefficient

α = radius of curvature

This equation is well known and recommended by ACI 318-83 (1), Post-Tensioning Manual (2), and A.A.S.H.T.O. (3). The equation is derived from basic theory of friction loss of a cable around a curve. Figure 1.1 shows the derivation of the equation as outlined by Lin and Burns (4).

The friction and wobble coefficients depend on the material properties of sheathing, prestressing steel, and the usage and nature of lubricants. These coefficients have been determined experimentally for a variety of post-tensioned systems. Usually the wobble coefficient is first determined for a straight tendon layout. Next the friction coefficient is determined for an intentionally draped tendon profile of know curvature. The friction coefficient is thus obtained from the following equation:

$$\mu = \left[ln\left(\frac{F_J}{F_H}\right) - KL \right] / \alpha \tag{1.2}$$

where

F_J = measured prestress tendon force at jacking end

F_H = measured prestress tendon force at holding end

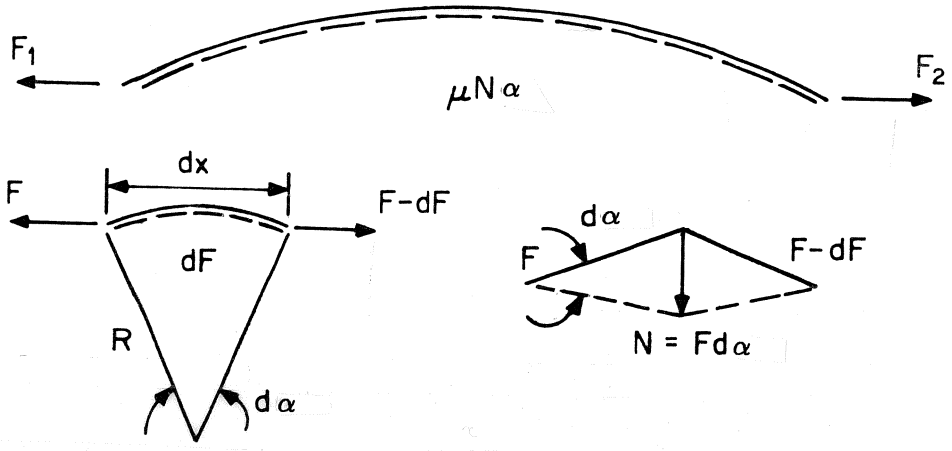

N = Normal Pressure
F = Stress Along Profile
R = Radius of Curvature
μ = Friction Coefficient
$d\alpha$ = Infinitesimal Angle Change
dx = Infinitesimal Length
dF = Frictional Loss

Considering that an infinitesimal length dx of a prestressing tendon whose centroid follows the arc of a circle of radius R, then the change in angle of the tendon as it goes around the length dx is:

$$d\alpha = \frac{dx}{R}$$

For this infinitesimal length dx, the stress in the tendon may be considered constant and equal to F; then the normal component of pressure produced by the stress F bending around an angle $d\alpha$ is given by:

$$N = F\,d\alpha = \frac{F\,dx}{R}$$

The amount of friction loss dF around the length dx is given by the pressure times a coefficient of friction, μ, thus:

$$dF = -\mu N = \frac{-\mu F\,dx}{N} = -\mu F\,d\alpha$$

Transposing and integrating on both sides yields:

$$\frac{dF}{F} = -\mu\alpha \quad \rightarrow \quad log_e F = -\mu\alpha$$

Using the limits F_1 and F_2 gives:

$$F_2 = F_1 e - \mu\alpha$$

By applying the same procedure to the wobble effect and combining with the friction effect gives the conventional friction-loss formula:

$$F_2 = F_1\, e^{-KL - \mu\alpha}$$

Fig. 1.1 Derivation of friction-loss formula

K = known or assumed wobble coefficient

L = known tendon profile length

α = known radius of curvature for tendon profile

Note that the wobble and friction coefficients are based on experimental research and are assumed to be uniform coefficients between the jacking and holding ends.

1.2.2 Friction and Wobble Coefficients. Extensive research has been conducted to determine coefficients for friction and wobble for a large variety of sheathing and prestressing steel types. T.Y. Lin summarizes many laboratorial and field experimental studies covering a wide range of different materials and stressing systems (5). It is evident that the friction coefficient is highly variable as tests show coefficient values for similar materials can range between wide limits. Lin states,

> ...any assumed coefficient of friction is simply quesswork based on past performance which may not be completely repeated in the structure. More tests are undoubtedly desired to furnish better guidance, but the estimation of actual field conditions may always remain a matter of judgment.

Approximate values for friction and wobble coefficients are given in the commentary of ACI 318-83, Post-Tensioning Manual, and A.A.S.H.T.O. These values are intended only as a guide for normal conditions. Friction coefficients for a particular prestressing steel and conduit can be obtained from the tendon manufacturer.

1.2.3 Epoxy Coated Strand Test Report. In a test report by Florida Wire and Cable Company (6), friction and wobble coefficients were determined for .600-in. diameter grit-impregnated epoxy coated strand. They concluded that friction values and tendon losses for the epoxy coated strand were slightly higher when compared to uncoated strand. Friction tests were conducted for both plastic and galvanized rigid metal conduit. The test specimen was 60-ft long and included a total tendon angle change of 1.689 radians. For the plastic conduit, measured wobble and friction coefficients were .0034/ft and .172, respectively. Based on an assumed wobble coefficient of .001/ft, the measured friction coefficient for the galvanized metal conduit was .318. The above values are averaged for a series of repetitive tests.

1.3 Anchor Set Losses

For most post-tensioning systems an anchor set transformation loss occurs when the prestress force is transferred from the stressing jack to the permanent anchorage fixture. The

reduction in tendon stress which occurs during release of the jacking force depends on the amount of lost tendon elongation which was obtained during the stressing operation. This elongation transformation (anchor set) loss is dependent on the stressing system and operational technique implemented. Often the anchor set loss is compensated for by an initial over stressing of the tendon. The maximum over stressing allowed by the ACI Code during jacking is 0.85 f_{pu}.

The most common method of determining the resulting tendon stress variation caused by anchor set is based on the assumption that the anchor set curve is a mirror image of the friction loss curve. That is, frictional resistance between the strands and conduit opposes the strand movement along the tendon profile induced by the elongation transformation release. Thus the anchor set loss is dependent on the friction coefficient and tendon curvature in addition to the amount of seating transformation movement.

In Appendix Three of the Post-Tensioning Manual (2) a derivation of approximate formulas for calculating anchor set losses including the effect of friction are presented. These formulas are shown below:

$$\Delta f_s = \sqrt{\frac{E_s(\Delta L)d}{3L}} \tag{1.3}$$

where

$\Delta f_s =$ change in stress due to anchor set (ksi)

$E_s =$ modulus of elasticity (ksi)

$\Delta L =$ anchor set (in.)

$d =$ friction loss in length L (ksi)

$L =$ length to point where loss is known (ft)

The distance from the seating end where the anchor set curve intercepts the friction loss curve is given by:

$$x = \sqrt{\frac{E_s(\Delta L)L}{12\alpha}} \tag{1.4}$$

where $x =$ length influenced by anchor set (ft)

In order to simplify the computation effort of the anchorage deformation loss, the slope of the friction and anchor set curves are assumed to be linear (straight lines) between control points. Control points are the points which define the geometry of a tendon layout. Note that for a large seating loss, low friction, short span lengths, or shallow curvatures, the anchorage seating loss may be transferred to the holding end anchorage. Figure 1.2 shows the schematic for the derivation of the anchorage loss formulas.

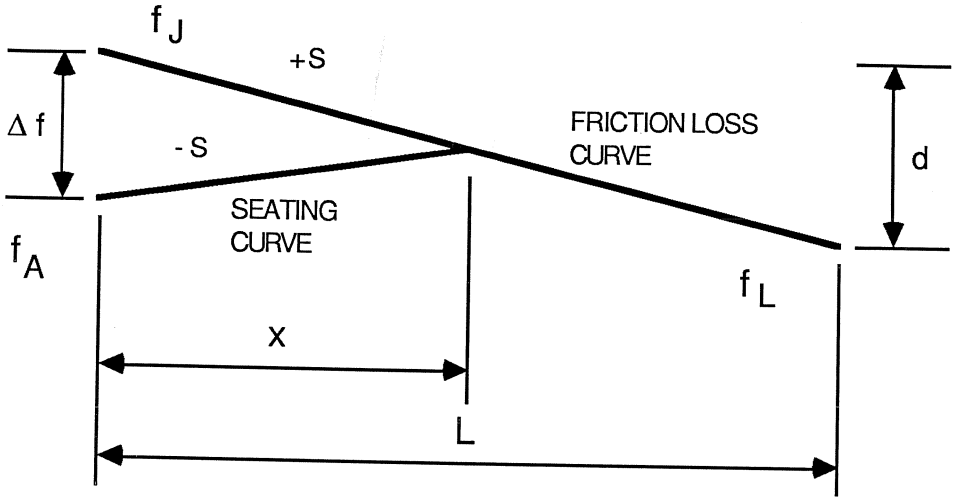

Δf = Change in stress due to anchor set

f_A = Known or assumed anchorage stress

f_J = Known or assumed jacking stress

f_L = Known or assumed stress at distance, L

d = Friction loss in length, L

x = Length influenced by anchor set

L = Length to point where loss is known

ΔL = Anchor set

E_S = Modulus of Elasticity

S = Slope of friction/seating curve

Fig. 1.2 Anchorage seating schematic

1.4 Computer Program *FLOSS*

The theoretical friction loss and assumed anchor set formulas described previously have been incorporated into a computer program called *FLOSS*. The program was written in Fortran 77 and is compatible with any fortran compiler. Computer program *FLOSS* is shown in Appendix A and is well documented with comment cards that describe important variables and calculation steps.

1.5 Time Dependent Losses

Prestress losses due to creep and shrinkage of concrete and steel relaxation are both time dependent and interdependent. Usually the total contribution of these losses are considered for the life of a structure. Extensive research has been conducted to determine these losses and is not discussed here. Time dependent losses for post-tensioned structures begin immediately following the stressing and seating operation. But prior to grouting the tendons, these losses are considered to be negligible as grouting usually occurs within 48 hours of stressing.

1.6 Objectives and Scope of Research

Tendon stress variation induced by friction and anchor seating tend to distribute and equalize themselves along the length of a tendon up until a tendon is grouted. Industry sources acknowledge this phenomenon but there has been no data about its magnitude or the time duration over which it takes place.

The objective of this study was to determine whether simplification of design calculations might be justified if flattening of the peaks and valleys along the stress profile can be shown to occur. Grouting of a tendon is assumed to lock the tendon stress variation in place and prevent further redistribution tendencies.

The determination of the distribution of post-tensioning forces prior to grouting considered three phases:

1. initial stressing and frictional effects;
2. anchor seating and transformation losses; and
3. time period following seating and prior to grouting to observe redistribution effects.

Initial stressing and anchor-seating stress distributions from tests conducted in this study are compared to those calculated using standard design methods. The magnitude of redistribution of the tendon stress after seating was determined for time periods of up to two weeks.

Other factors considered in this study to influence the magnitude of redistribution were:

1. type of prestressing strand;
2. tendon size (number of strands per tendon);
3. tendon curvature; and
4. stressing technique.

The scope of this experimental study was limited to the testing in the Ferguson Structural Engineering Laboratory of an 80-ft-long rigid body specimen containing three different layouts, tests in the field of two tendons of 275-ft length in an actual three span bridge during its construction, and a laboratory test of a single simply-supported T-beam specimen of 30-ft length. Chapter 2 describes the details of the laboratory tests while Chapter 3 describes the field test. Chapter 4 contains the analysis and discussion of test data. The conclusions are presented in Chapter 5.

CHAPTER TWO EXPERIMENTAL PROGRAM

2.1 Introduction

This study dealt primarily with multi-strand post-tensioning systems and the measurement of the force distribution associated with post-tensioning of concrete members. A galvanized semi-rigid steel conduit housing seven half in. diameter 7 wire low-relaxation strands, was chosen for the majority of the tests in the study.

Two different types of test specimens were constructed for laboratory observation of the tendon stress distribution along the path of the tendon profile during the jacking phase, anchor-set phase, and the time period prior to grouting. The first type was a restrained rigid body concrete specimen of considerable size and bulk which experienced no significant deformations while the second type was a 30 ft span T-section concrete beam.

2.2 Rigid Body Specimen

2.2.1 General. The rigid body specimen was rectangular in cross section with a width of 12 in. and a height of 48 in. The length was 80 ft. These dimensions provided a sufficient height to accommodate large tendon curvatures and an adequate width to place three different tendon layouts in the specimen. The tendon curvatures over the length were chosen to insure 1) that the tendon stress varied significantly from the jacking end to the dead end, and 2) that the anchorage seating losses were not transmitted along the entire specimen length to the dead end. Also, the dimensions allowed for rather easily constructed formwork.

The rigid body specimen was aligned in a north-south direction with the jacking end being south and the dead end north. For reference, the jacking end was given a station location of 0 ft and the dead end a station location of 80 ft. All points of location are referenced from the jacking end. For example, the four quarter points are 20, 40, 60, and 80 ft with the first quarter point being a distance of 20 ft from the jacking end.

The rigid body specimen housed the tendon layouts and provided ample mass to eliminate the possible transverse bending due to eccentricity of tendons placed in the section as described below.

2.2.2 Various Tendon Layouts. The chief criteria for the selection of the tendon profiles was to insure that significant frictional losses occurred during the stressing phase. Without significant losses, tendon stress variation and redistribution would be difficult to detect.

The three selected tendon layouts consisted of parabolically draped profiles with varying curvatures. These are shown in Figs. 2.1a, 2.2a, and 2.3a and are referred to as Profiles No.1, No.2, and No.3, respectively.

Profile No.1 is symmetrical about the midpoint and has an incremental angle change of .1667 radians within each of the four segments. The sharpest decrease in tendon stress occurs along segments (2) and (3); from 32 to 48 ft from the jacking end. Profile No.2 has a larger incremental angle change of .2222 radians in three of the segments with the sharpest decrease in tendon force in segment (3) located from 54 to 60 ft from jacking end. Profile No.3 had with the largest incremental angle change per segment of .3333 radians, with the sharpest decrease in tendon stress along segments (2) and (3) located from 26 to 34 ft from the jacking end as shown in Fig. 2.3a.

To provide space for mounting strain gages to measure the actual strand strains, polyethylene styrofoam blockouts were placed at various points along the tendon layouts (Fig. 2.3c). The primary blockout locations were points of inflection (P.I.) and the uppermost and lowermost portions of the parabolic drapes. Secondary blockouts were placed to obtain strand strain measurements at distances between the primary blockouts. The blockout length was 8 in.

Blockouts for Profile No.1 were located at 12, 24, 32, 40, 48, 56, and 68 ft from the stressing end; for Profile No.2: 15, 30, 40, 54, 60, and 70 ft from the stressing end; and for Profile No.3: 10, 26, 30, 34, 40, 50, and 74 ft from the stressing end. Figure 2.3c shows the blockout locations for Profile No.3 and a general description for the placement of strain gage instrumentation on the strands. This procedure was typical for the other two profiles.

Although the tendon profiles may not represent layouts commonly used in design practice, the principles derived in Chapter One for frictional losses are still valid.

Implementing the friction loss formula given in Eq. 2.1 in terms of unit stress, with the following assumptions typical of the materials and stressing system used give the tendon stress variations for each profile (Figs. 2.1b, 2.2b, and 2.3b).

$$f_2 = f_1 e^{Kl_x - \mu\alpha} \tag{2.1}$$

where

$f_1 = .8 f_{pu}$ (216 ksi) (Jacking stress)

$K = .0002$ (Wobble coefficient)

$\mu = .250$ (Friction coefficient)

$\Delta L =$ 0.5 in. (Anchor set)

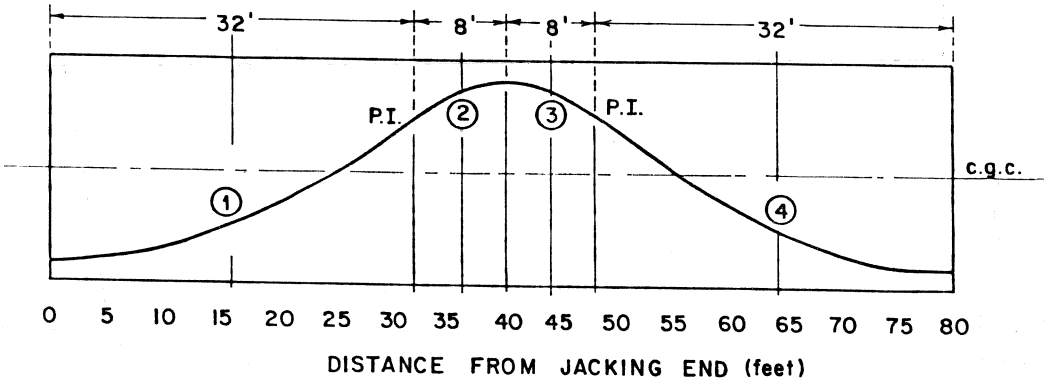

SEGMENT	ELEVATION DIFFERENCE	INCREMENTAL ANGLE CHANGE
①	32.0"	.1667
②	8.0"	.1667
③	8.0"	.1667
④	32.0"	.1667

Fig. 2.1a Tendon Profile No. 1

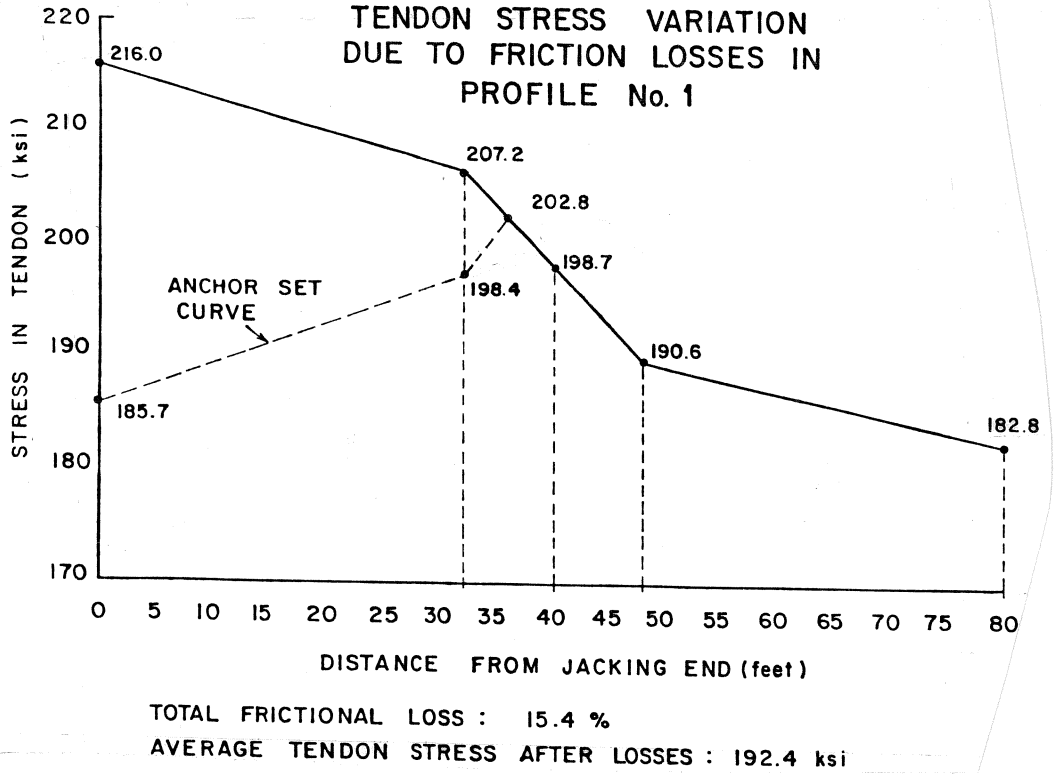

Fig. 2.1b Tendon-stress variation due to friction losses in Profile No. 1

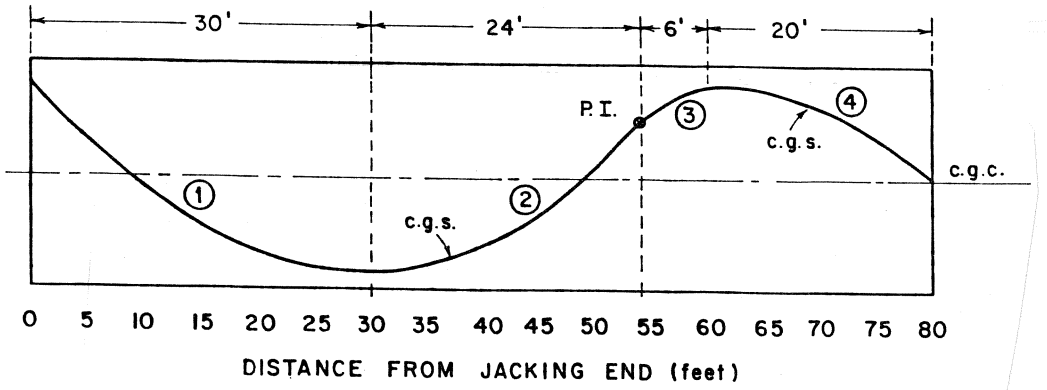

SEGMENT	ELEVATION DIFFERENCE	INCREMENTAL ANGLE CHANGE
①	40.0"	.2222
②	32.0"	.2222
③	8.0"	.2222
④	20.0"	.1667

Fig. 2.2a Tendon Profile No. 2

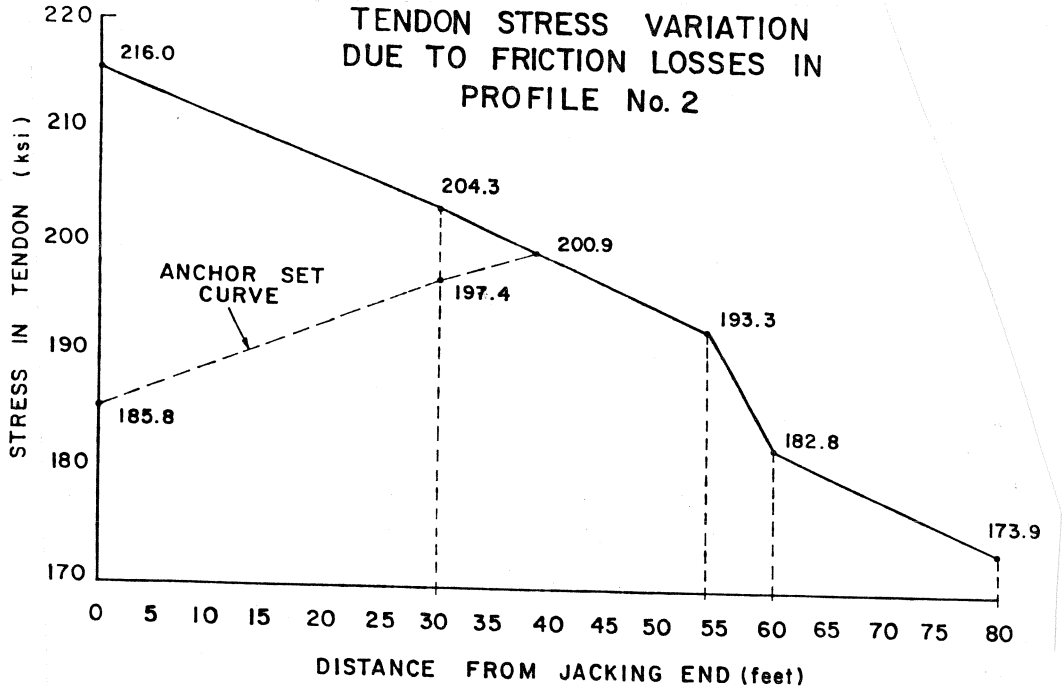

TOTAL FRICTIONAL LOSS : 19.5 %

AVERAGE TENDON STRESS AFTER LOSSES : 189.2 ksi

Fig. 2.2b Tendon-stress variation due to friction losses in Profile No. 2

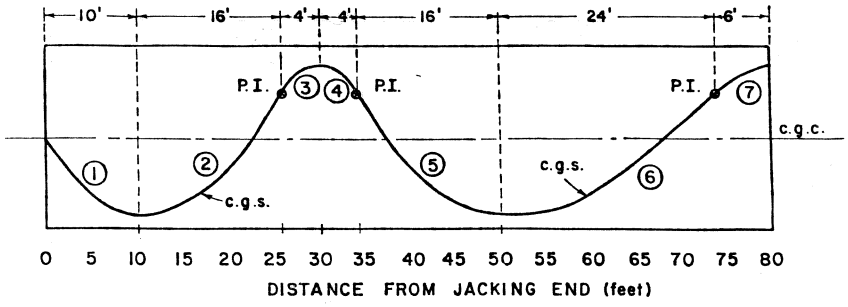

SEGMENT	ELEVATION DIFFERENCE	INCREMENTAL ANGLE CHANGE
①	20.0"	.3333
②	32.0"	.3333
③	8.0"	.3333
④	8.0"	.3333
⑤	32.0	.3333
⑥	32.0	.2222
⑦	8.0	.2222

Fig. 2.3a Tendon Profile No.3

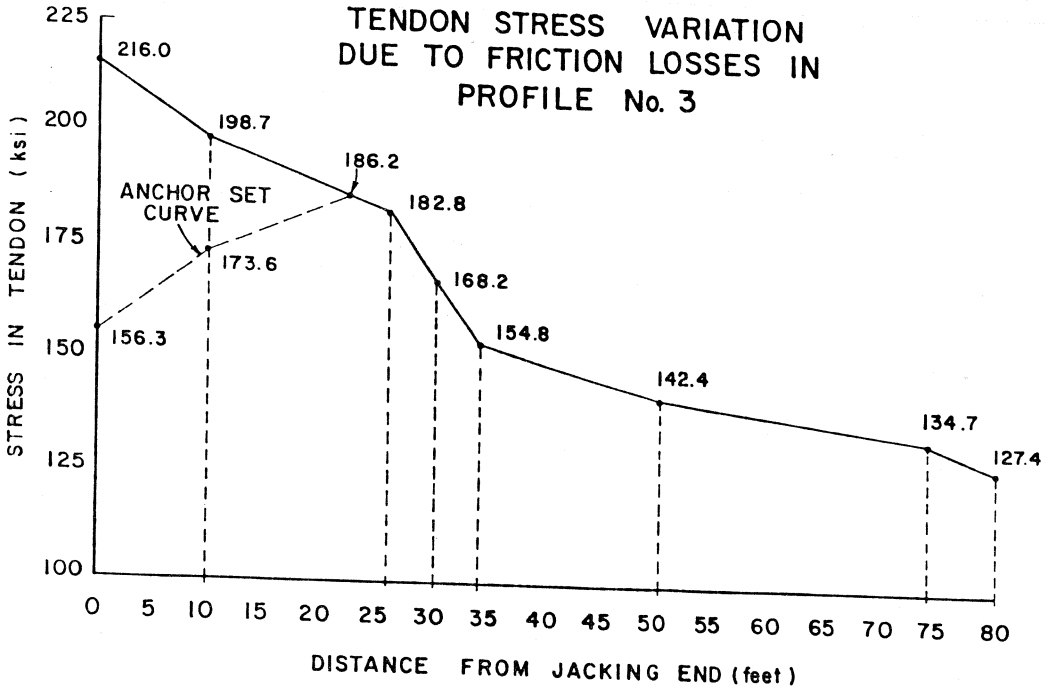

Fig. 2.3b Tendon-stress variation due to friction losses in Profile No. 3

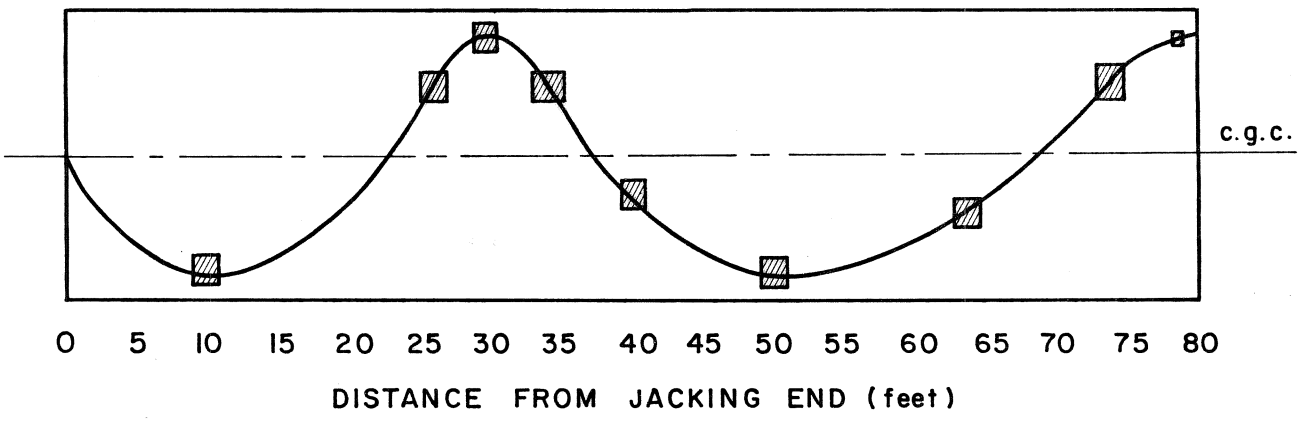

Fig. 2.3c Placement of strain gages: Profile No. 3

2.2.3 Material Used. The seven-strand anchor system, Prescon 'KD', consisted of a 7K5 double bearing anchor plate, 7K5 permanent anchorage block, and 3-piece wedge sets for half-in. strand (Fig. 2.4). The rated ultimate force capacity of the 7K5 system is 202, 231, and 289 kips for 70%, 80%, and 100% of the minimum guaranteed breaking strength of the prestressing strand. Spiral reinforcement for the anchorage zone stresses was designed in accordance with procedures developed by Stone and Breen(7).

The conduit was semi-rigid galvanized Gage 26 steel with a nominal diameter of 2.125 in. and a corrugated profile. When two sections of conduit had to be spliced together, a conduit coupler sleeve was used and then sealed with tape to prevent leakage of grout into conduit during grouting. For this type of conduit, the range of values for friction coefficient; μ, are 0.18-0.26 and wobble coefficient; K, 0.0005-.001 (2). In accordance with ACI 318-83(1), the inside cross sectional area of a grouted duct had more than twice the tendon area for the seven 1/2 in. diameter strands.

The prestressing steel was uncoated 0.5-in.-diameter, 7-wire stress relieved, low relaxation strand Grade 270 furnished by Shinko Wire America, Inc. The heat/ coil No. 62041 strand was manufactured in accordance with ASTM Specification A416 and the chemical composition conformed to AISI C1080. The manufacturer provided a test report with the strand shipment. An additional test conducted at the laboratory confirmed the values given in the test report (Table 2.1). The maximum relaxation loss was stated as 2.5% at 70% and 3.5% at 80% of the initial load after a time of 1000 hours.

The concrete for the rigid body specimen was a typical 6- sack mix ordered from a local ready-mix concrete company. The nominal concrete strength required was 5000 psi. Concrete was placed in cylinder molds and tested for 28-day strength. No instrumentation was provided for observing concrete strains during testing.

2.2.4 Construction. To save on formwork material costs and construction time, the rigid body specimen was cast in two segments, each forty ft in length. The segments were centered directly over a row of tie-down anchors. The tie-down anchors in the reaction floor at the Ferguson Structural Engineering Laboratory are spaced four ft in each direction. To insure no upward deflections and stability against possible overturning, Grade 100 steel tie down rods, one-in. diameter, encased in PVC pipe were placed along the length of the test specimen (Fig. 2.5). The rods were provided in pairs and spaced 4 in. off centerline at 2, 10, 25, 38, 42, 54, 69, and 78 ft from the south end of the specimen.

Due to the geometry of the tendon profiles, some of the end anchor bearing plates were placed at an inclination as shown in Fig. 2.6. This prevented large localized friction losses at either the jacking or holding end. Profiles No.1 and No.2 were placed with a 2.5 in. eccentricity

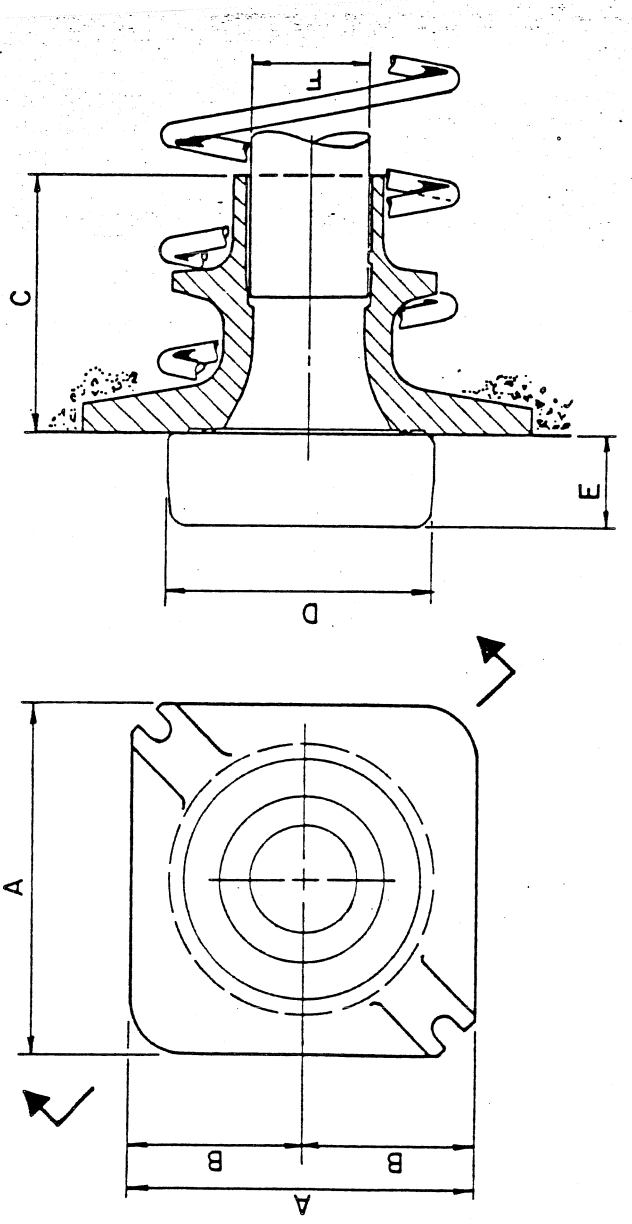

Type	Str Dia	No. Str.	A	B	C	D	E	F		RAM
7 K 5	0.5	7	6.9	3.45	5.12	4.72	1.97	2.125		200 T

Fig. 2.4 Anchorage hardware

Grade 270 Uncoated Seven-Wire Stress-Relieved
Low Relaxation Strand Properties

Nominal Diameter (inches)	.502	
Steel Area (sq. in.)	.153	(.153 min)
Breaking Strength (lb)	43,000	(41,300 min)
Load at 1% Extension (lb)	40,000	(35,100 min)
Elongation in 24 inches (%)	8.9	(3.5 min)
Modulus of Elasticity (psi)	28.0×10^6	

( ) Denotes ASTM Limits

Table 2.1 Properties of Uncoated Seven-Wire Strand

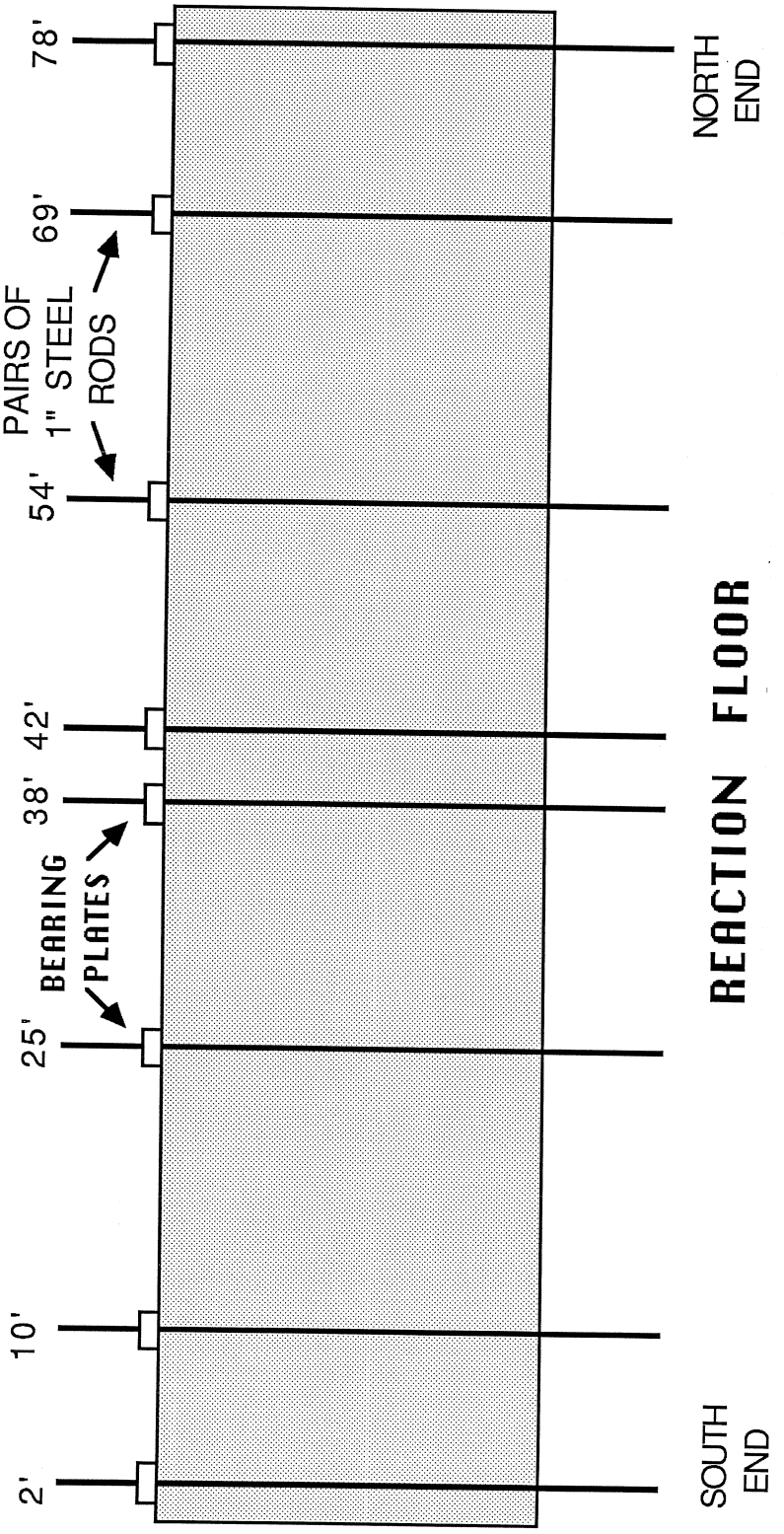

Fig. 2.5 Location of tie-down anchors

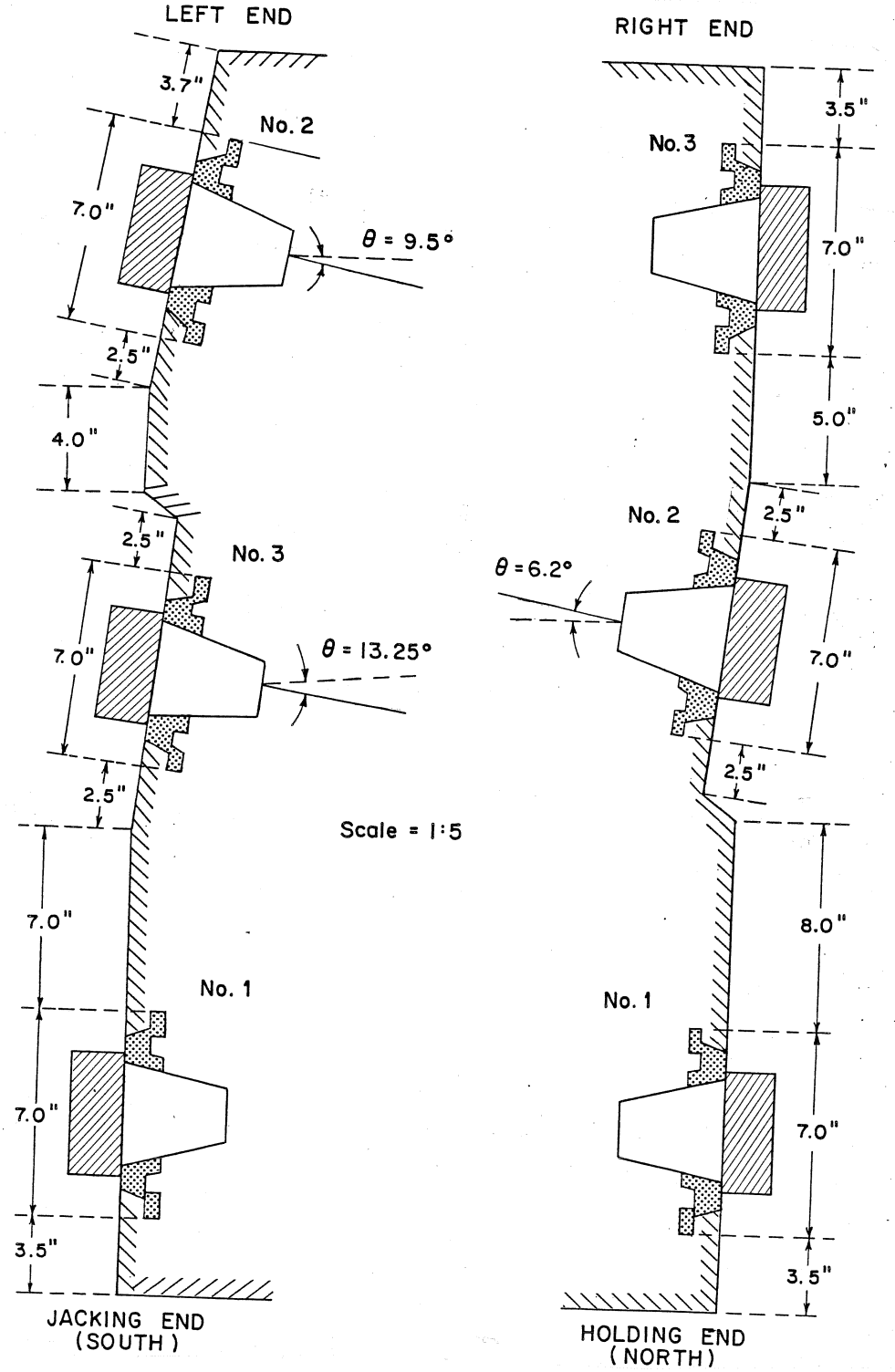

Fig. 2.6 Inclination of anchor-bearing plates

from the vertical centroidal axis of the cross section (Fig. 2.7). The offset was determined by the outside diameter of three conduits placed in three vertical planes next to one another. The centroid of the anchor bearing plates and conduit, for each profile, was aligned in the same vertical plane. Thus, the wobble effect was assumed to be consistent among the three profiles. Three practical considerations controlled the design of the reinforcement steel cage. First, the inside width between pairs of tie down rods had to allow for the placement of the three conduits. Second, the steel cage had to provide firm support to each conduit at regular intervals along its length. Finally, although the specimen was continuously supported by the reaction floor and experienced no externally applied moments or shear, the minimum shear reinforcement and spacing limits requirements of the ACI-318 Code were followed.

Figures 2.8 and 2.9 show the reinforcement cage dimensions in the longitudinal direction and cross sectional plane, respectively. The conduit was firmly secured at two foot intervals. Cross ties securely tied to the vertical legs of the stirrups provided support for the conduit in the vertical and horizontal directions.

The construction sequence was as follows. One sidewall of the formwork was erected, aligned, and leveled. The reinforcement cage was installed and fastened with spacers to the sidewall. The conduit for each of the three profiles was placed and secured (Figs. 2.1a, 2.2a, and 2.3a) as shown in the photos of Figs. 2.10a and b. Styrofoam blockouts were contoured and taped to fit tightly around the conduit. The remaining sidewall was placed to complete the formwork closure (Fig. 2.11). The concrete was poured in three lifts. Each lift was consolidated with mechanical vibrators.

The formwork was stripped within two days after casting. The styrofoam was then removed from around the conduit at each blockout position. Strands were cut to the desired length and individually hand fed through the profiles. During strand placement, it was observed that the strands aligned themselves in a consistent position relative to one another in the strand bundle and that no strand crossing over or entwinement occurred. A hacksaw was used to cut open the conduit for placement of strain gages on the strand (Fig. 2.12).

2.2.5 Variation of Strand Number. In multi-strand systems with draped layouts, the strands when post-tensioned are forced against the conduit into a tightly compacted bundle. The arrangement of the bundle is such that each individual strand could not be instrumented with a strain gage. Only those strands on the exterior provided a surface which was accessible for strain gage placement.

For each layout, two strands were chosen for instrumentation. They were color coded near the blockout with blue and green spray paint. At each blockout a strain gage was placed on both the blue and green marked strands.

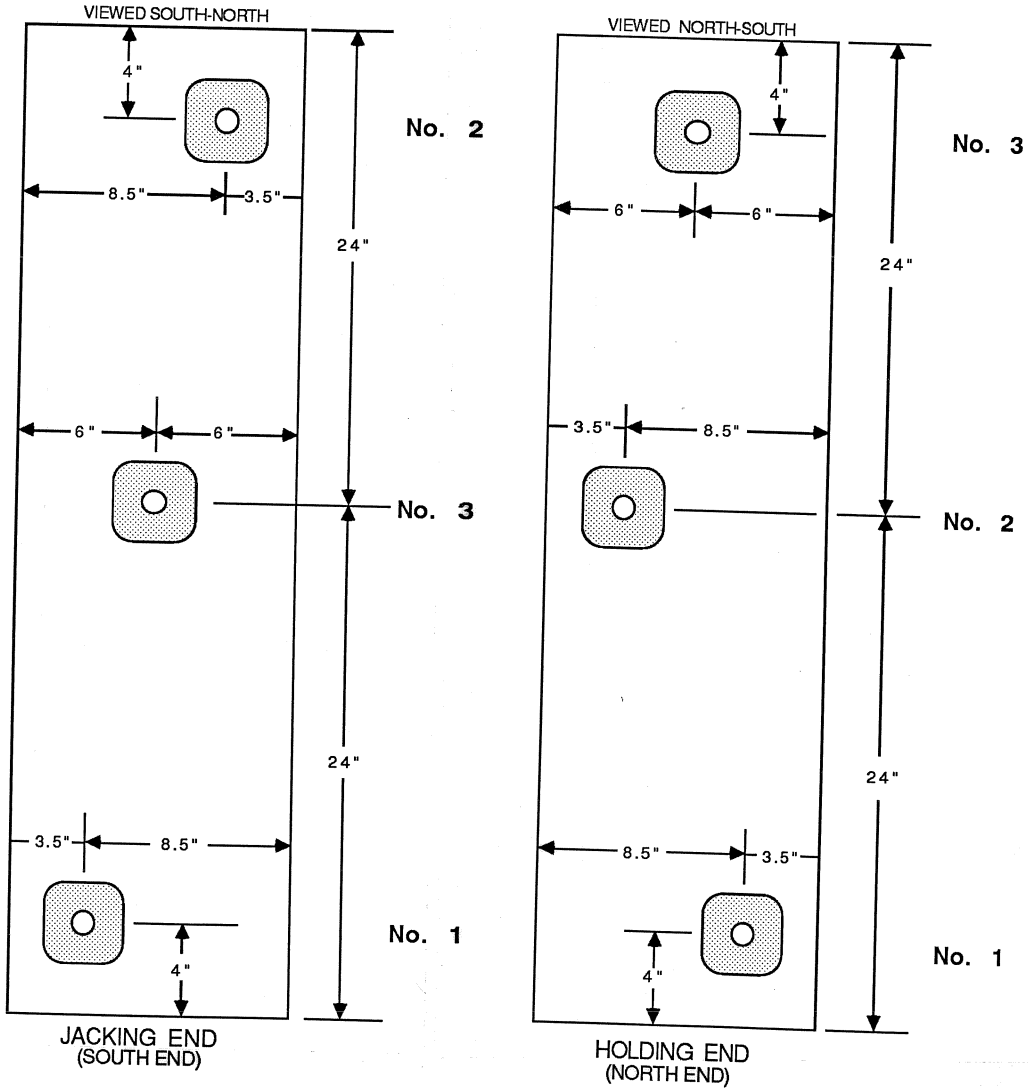

Fig. 2.7 Eccentricity of anchor-bearing plates

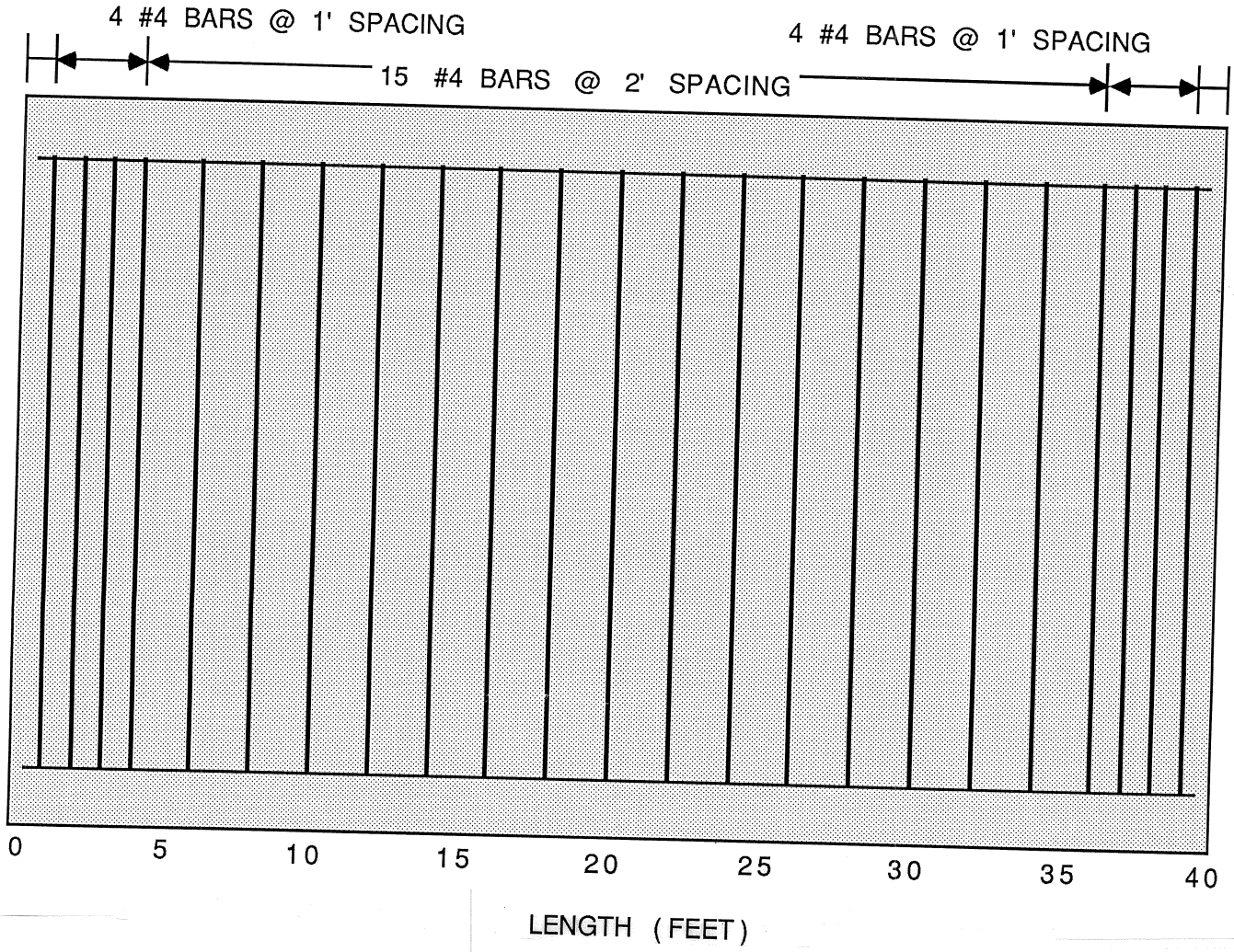

Fig. 2.8 Reinforcement cage longitudinal direction

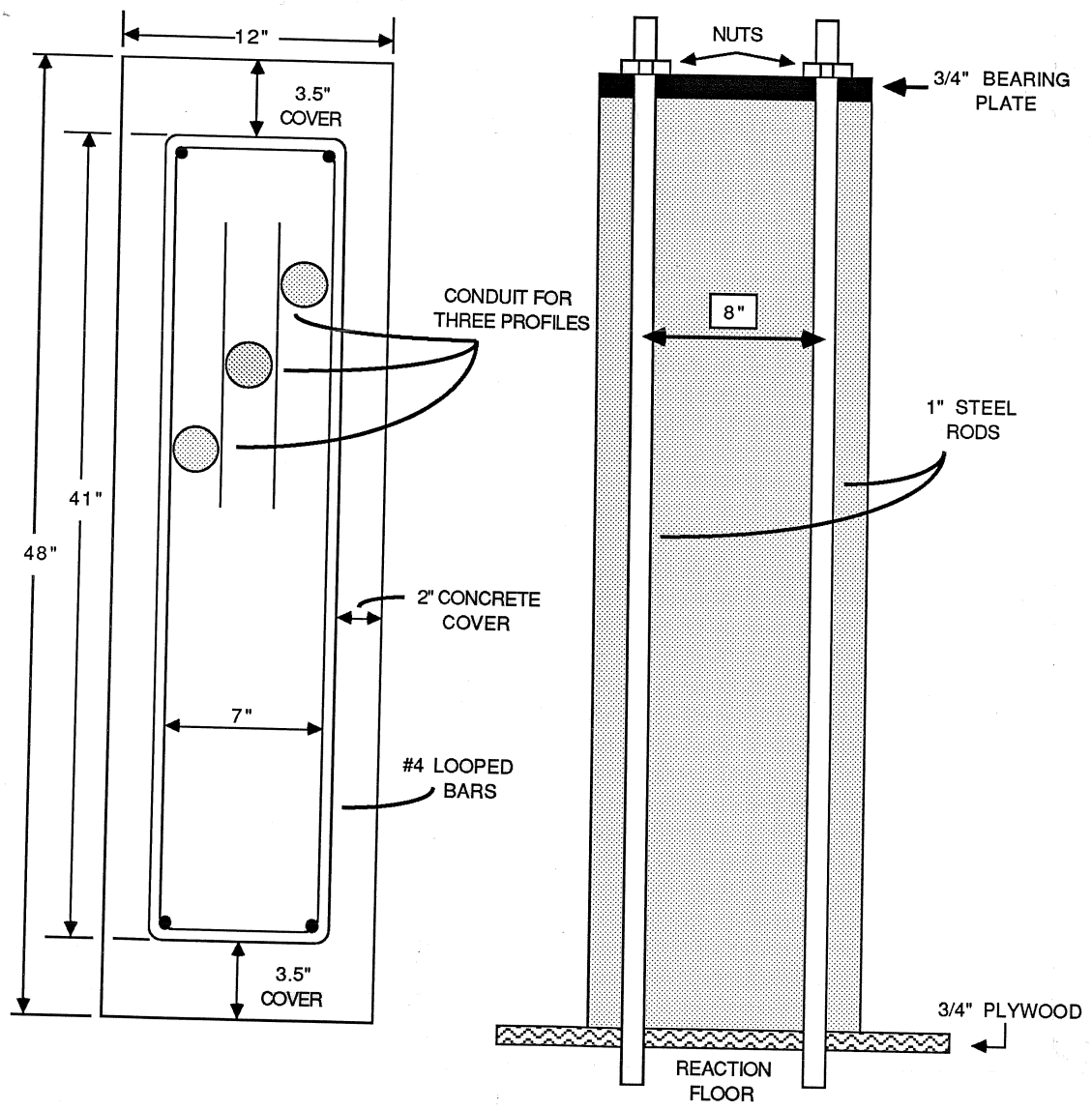

Fig. 2.9 Cross section of reinforcement cage

Fig. 2.10a Conduit placement 0 to 40 ft

Fig. 2.10b Conduit placement 40 to 80 ft

Fig. 2.11 Formwork prior to closure

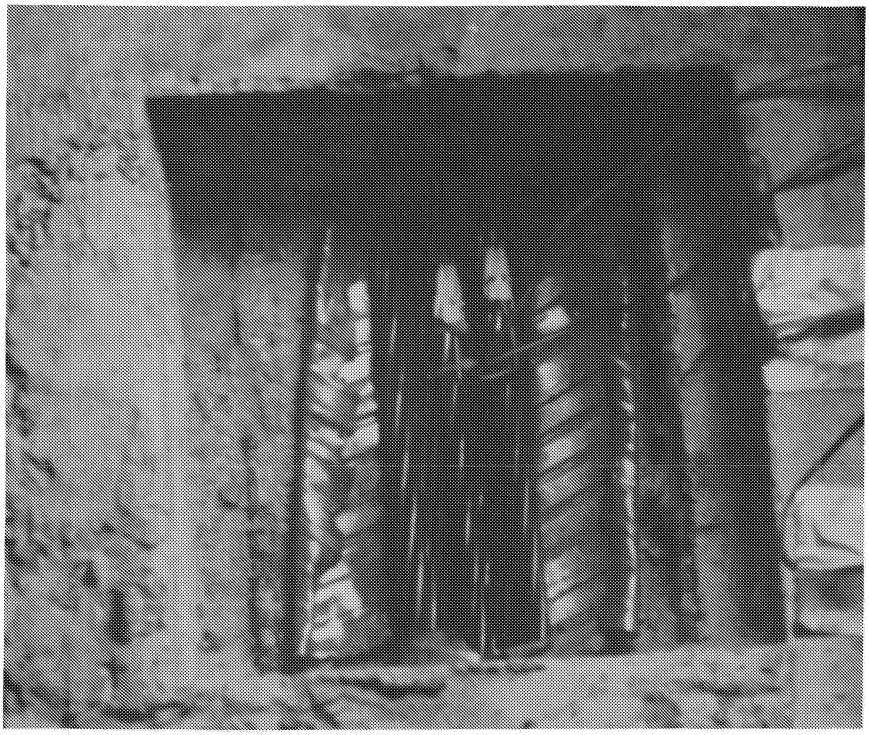

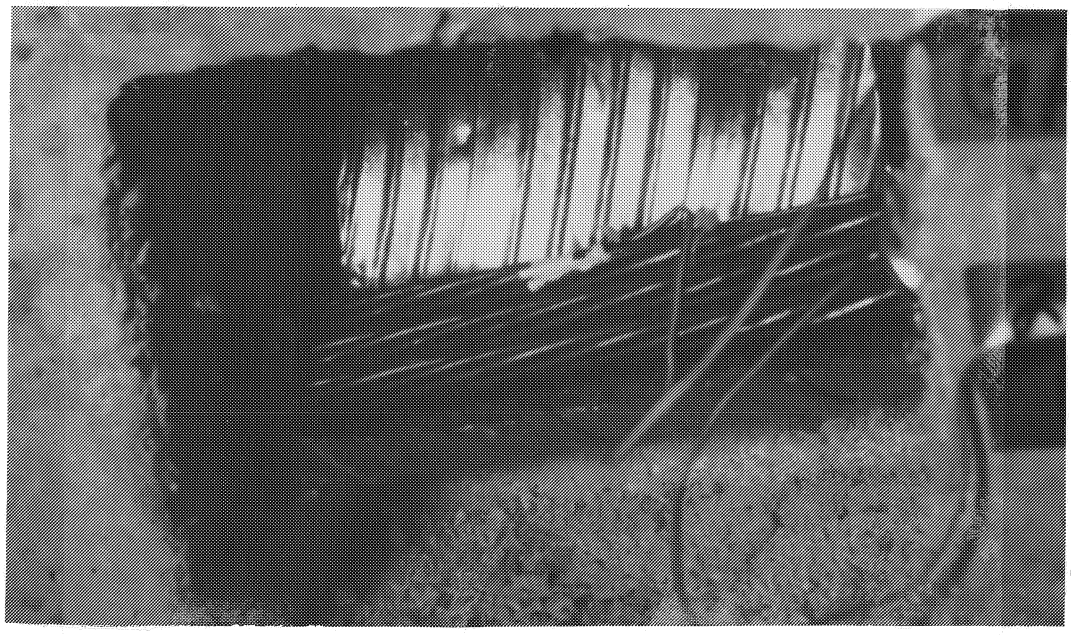

Fig. 2.12 Example of blockout and cut conduit

The first series of tests consisted of 7 strands per layout. The distribution of stresses for the two strand instrumented were affected by 1) frictional contact with the conduit, and 2) forces due to the interaction of the surrounding strands, i.e., friction coefficient and normal force. To determine the significance of the latter effect, the second and third test series consisted of 4 strands and 2 strands per layout, respectively. For the second test series, three non- instrumented strands were removed. For the third test series, the remaining two non instrumented strands were removed. In the third test series, the two instrumented strands were almost exclusively in contact with conduit. No significant force interaction occurred between the two strands. The same stressing system was used for all three series.

2.2.6 Epoxy Coated Strand. Half-in. diameter epoxy coated strand known as Flo-Bond was used for a comparative study with the uncoated bare strand (Sec. 2.2.3). The epoxy coating is intended to eliminate corrosion which can be detrimental to the prestressing steel. The epoxy coated strand's major properties, various test results, and recent applications are summarized in a paper by Dorsten, Hunt, and Preston(8).

The prestressing steel was low relaxation strand manufactured in accordance with ASTM A-416 and the epoxy coating covered the outside wires with a thickness of 30 $\pm$ 5 mils. To enhance the bonding strength, grit was thoroughly embedded in the coating. The detrimental effect of the epoxy coated strand with grit was an increased friction and wobble coefficient.

The epoxy coating slightly increases the axial stiffness of the strand. Strand properties and given in Table 2.2. Refer to Table 2.1 for comparison to the uncoated strand.

The manufacturer requires that for strand sizes half-in. and over, slightly modified wedges are necessary; however modified wedges were not used in this laboratory test. The anchorage system and stressing equipment was unchanged from that used with the bare strand.

Only one test series was performed on the epoxy coated strand. Seven strands were placed in each layout. It was extremely difficult to hand feed the last two strands due to the increased nominal diameter and the grit embedded coating. A wire brush grinder was needed to remove the epoxy coating at the various blockout locations. This allowed for direct strain gage placement on an individual strand wire instead of the epoxy. The epoxy coating was not removed at either the stressing or holding ends.

2.3 T-Section Girder

2.3.1 General. Externally applied loads in prestressed concrete beams produce a change in the prestressing steel stress. The change in stress due to applied loads is different for bonded and unbonded beams. Prior to grouting, a bonded beam (when grouted) behaves as an unbonded beam and slip between the tendon and conduit may occur.

Grade 270 Epoxy Coated Seven-Wire
Strand Properties

Nominal Diameter (inches)	.563
Steel Area (sq. in.)	.153
Breaking Strength (lb)	43,250
Load at 1% Extension (lb)	40,000
Ultimate Elongation (%)	6.25
Modulus of Elasticity (psi)	28.8×10^6

Table 2.2 Properties of Epoxy Coated Seven-Wire Strand

A simply supported concrete T-beam was studied in this test program to determine whether tendon stress redistribution effects occurred due to external loading. It is unlikely that prior to grouting, a structure would experience loads approaching full service loads allowed by the design codes. Therefore, various loading stages were monitored by increments up to first cracking. Before applying the external load, the tendon stress redistribution was monitored periodically due to the beam's own weight.

For economical use of time and resources, previously constructed formwork and an erected test frame of another research project being conducted at Ferguson Laboratory dictated the geometric properties of the T-beam described in the following sections.

2.3.2 Bonded and Unbonded Tendon Stresses. When concrete is bonded to the prestressing strand, the result is that the beam can be treated as elastic until cracking occurs. Using elastic theory, the change in steel stress is the concrete stress at the level of steel times the ratio E_S/E_c:

$$\Delta f_s = \frac{E_s}{E_c}\Delta f_c \tag{2.2}$$

The concrete stress due to an external moment, M_E, is:

$$\Delta f_c = \Delta M_E y/I \tag{2.3}$$

where

$I =$ transformed section modulus

$y =$ distance to level of steel from c.g.c.

For unbonded tendons, an external load will cause the tendon to slide with respect to the concrete. Hence, the tendon stress will be distributed throughout the beam's length. Therefore, an elastic analysis is no longer valid. The average tendon stress change can be obtained by integrating the concrete stress along the beam length as follows:

$$\Delta f_s = E_s/E_c L \int \Delta M_E y/I \, dx \tag{2.4}$$

where

$M_E =$ function of x

$y =$ function of x

$I =$ constant for a uniform cross section

$x =$ distance along the beam

A series of cyclic static loads were applied to the T-beam. This loading series should cause the variation in tendon stress due to friction and anchor-set losses to possibly equalize since the strands are unbonded.

2.3.3 Beam Design. The beam was simply supported over a 30 ft length. The symmetrical tendon profile (Referenced as No.4) was parabolic with a midspan drape of 12 in. The incremental angle change was .1333 radians over the length of the tendon. The end anchor bearing plates were located at the neutral axis with a 10 degree inclination (Fig. 2.13). Figure 2.14 shows dimensions and properties for the cross section available for this test. Anchor zone stresses required a web width of 12 in. at the ends rather than the reduced 6-in. web along the span. The web reduction occurred four ft from the ends. Spiral reinforcement was installed around the conduit.

A friction coefficient; μ, of .25, wobble coefficient; K, of .0002, and an anchor set of 0.50 in. were assumed for design. The anchorage seating loss was calculated to be transmitted to the dead end anchor. Tendon stress variation during jacking and anchor set with above parameters is shown in Fig. 2.15. The beam was tested with 7 strands using the same materials as described in previous sections for uncoated strands.

The beam was designed according to standard prestressed concrete principles with the limited allowable service load corresponding to $6\sqrt{f'_c}$ tension stress at the extreme fiber. The following criteria were in accordance with ACI-318 limits: extreme concrete fiber stresses, ductility parameter ω, shear reinforcement, minimum bonded reinforcement, and flexural strength.

2.3.4 Materials. The anchorage hardware, conduit, and strands were as described in Sec. 2.2.3. The concrete again had a nominal strength of 5000 psi. The largest aggregate size was limited to 3/8 in. to insure a uniform concrete mixture in the bottom flange. Epoxy coated strand was not used in this test set up.

2.3.5 Greased Strand. As a separate test series, two monostrand greased tendons were monitored for stress redistribution between the jacking and holding ends. The tendon profile (Referenced as No.5) had a parabolic drape similar to Profile No.4 (Fig. 2.13) except that the midspan drape was 6 in. The incremental angle change was .0667 radians over the 30 ft length. The unbonded greased strands were placed in the same T-beam test specimen with the 7-strand tendon in metal duct (grouted type tendon).

For the unbonded tendons, used in this beam, low relaxation Grade 270 prestressing strand was encased in lithium base grease with an extruded high density polyethylene jacket.

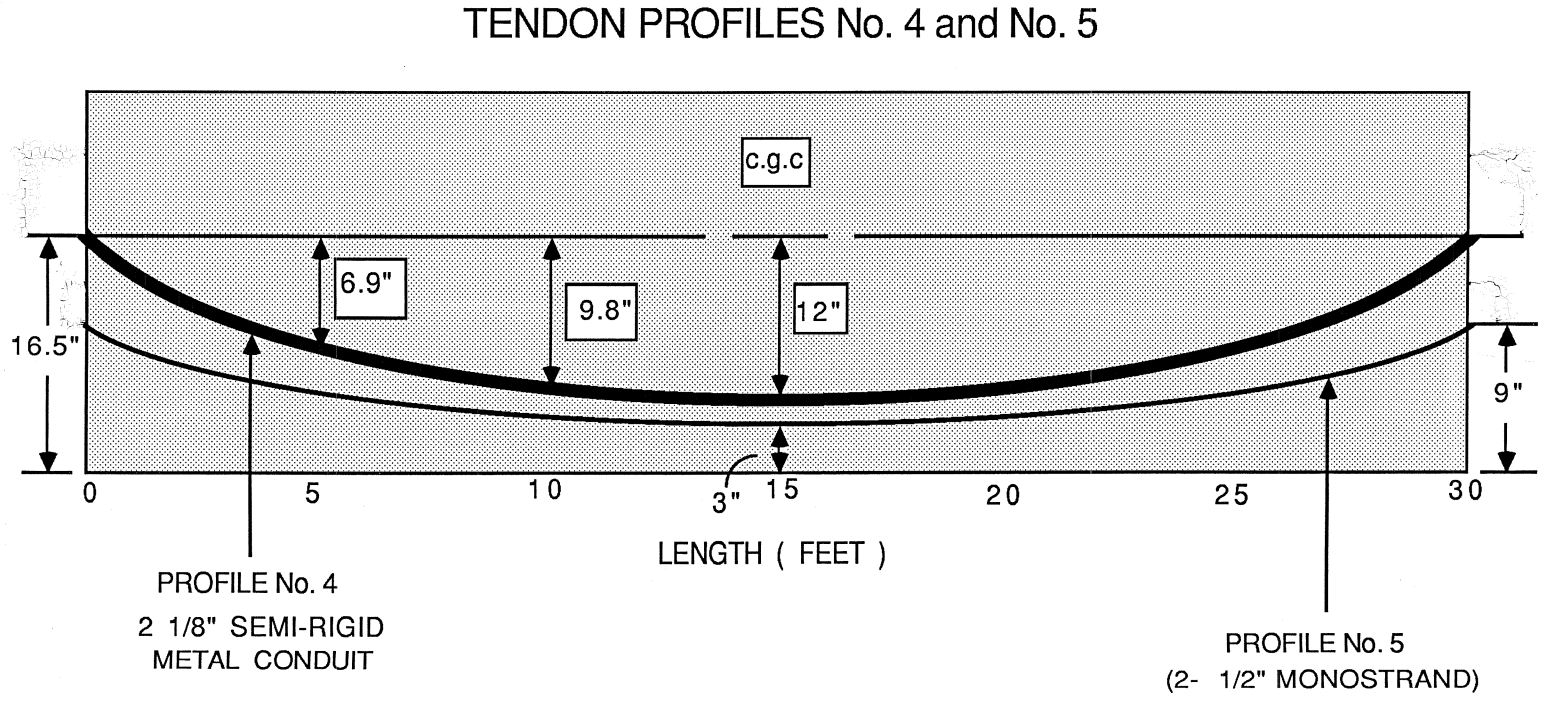

Fig. 2.13 Tendon Profile No. 4 and No. 5

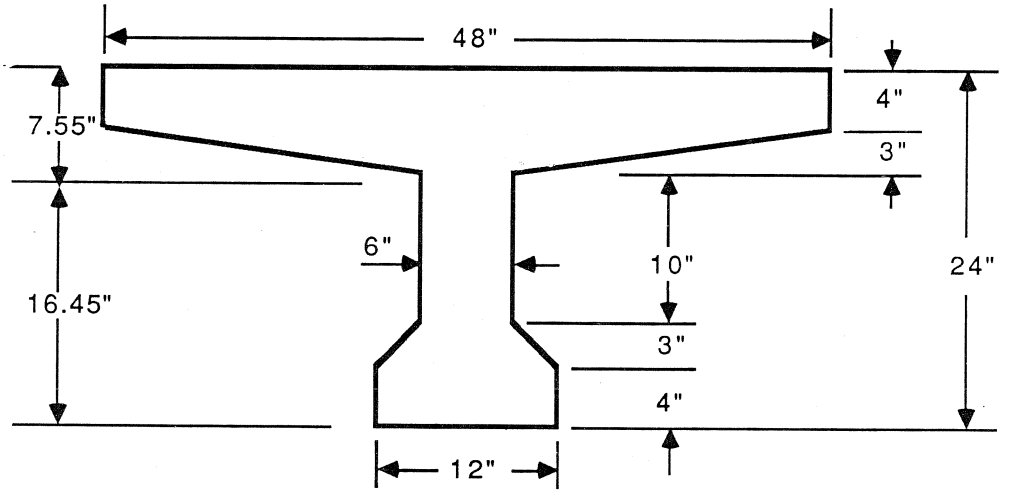

AREA: A	=	408 sq. in.
MOMENT OF INERTIA; I	=	21,831 in.
NEUTRAL AXIS; N.A. $\bar{y}_b$	=	16.45 inches
C_b	=	16.45 inches
C_t	=	7.55 inches
DEAD WEIGHT; w_b	=	.425 k/ ft

Fig. 2.14 T-beam cross section and properties

The grease prevents strand bonding with the concrete and provides a reduced friction coefficient as well as corrosion protection.

The range of values for the friction coefficient (2) μ, and wobble coefficient, K, are 0.05-0.15 and .0005-.0015, respectively. Assuming μ is 0.07, and K is .001, and the anchor set is .25 in., Fig. 2.16 shows the stress distribution.

2.3.6 Construction. The formwork was designed so that a series of beams could be cast in a previous study at Ferguson Structural Lab.. The sidewalls were attached by bolts through the formwork base. Threaded rods connected the two sidewalls, both top and bottom, to resist spreading of side forms due to the hydrostatic concrete forces. The anchor bearing plates were secured to the end panels which in turn were bolted to the sidewalls.

The steel cages were fabricated on racks. Cross ties were positioned according to the drape desired for the tendon profiles. The conduit and greased strands were then placed into the cage and secured. An overhead crane lowered the fabricated cage into the formwork. Figures 2.17 and 2.18 show the layout of the steel reinforcement cage.

Two contoured styrofoam blockouts were secured and taped to the conduit at a distance of 9.5 ft from each end. Continuing the reference scheme implemented previously, the blockout locations were 9.5 and 20.5 ft from the jacking end. The blockout length was 4 in. Blockouts were not placed around the greased strands since no gages were instrumented on these tendons.

The concrete was placed in two lifts, each consolidated with mechanical vibrators. Concrete was again placed in cylinder molds for casting representative cylinders for testing. After casting , the beam surface was finished with trowels. The beam was moist cured for one day with wet burlap and plastic sheets to prevent shrinkage cracks. The formwork was stripped after one day (Fig. 2.19).

The styrofoam was removed from around the conduit to allow access to strands. The conduit was cut open with a hacksaw. The seven 1/2 in. diameter strands were cut to length and hand fed into the conduit. Four of the seven strands were instrumented with strain gages at each blockout. The strands were color coded blue, green, red, and yellow for reference.

2.3.7 Loading Scheme. A two-point loading scheme (Fig. 2.20) was applied to the beam. The end supports were 12-in. wide and were bolted to the tie-down anchors in the reaction floor of the laboratory. The beam's end rested on one-in. thick by 9-in.-wide neoprene pads. Thus, an overhang of 3 in. was provided on each end. The ends were free to rotate during loading. Prior to post-tensioning, intermediate supports were placed 10 ft from the ends to support the loading apparatus on top of the beam without deflection. They were removed following stressing after upward camber developed and prior to applied loading of the beam.

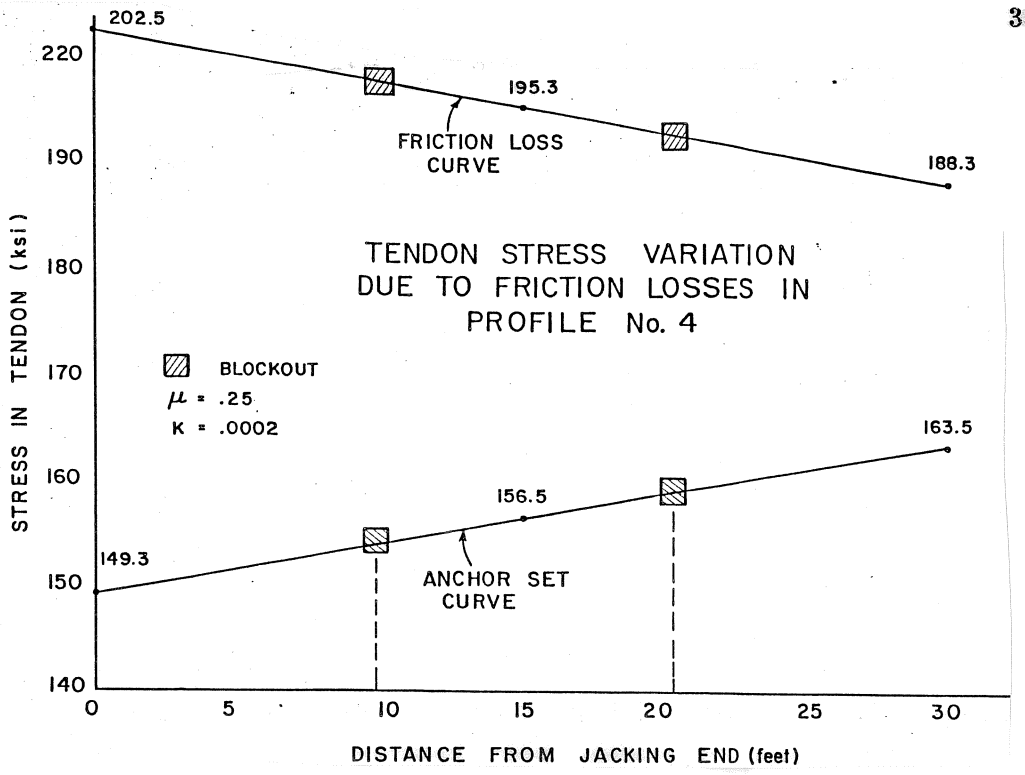

Fig. 2.15 Tendon-stress variation due to friction losses in Profile No. 4

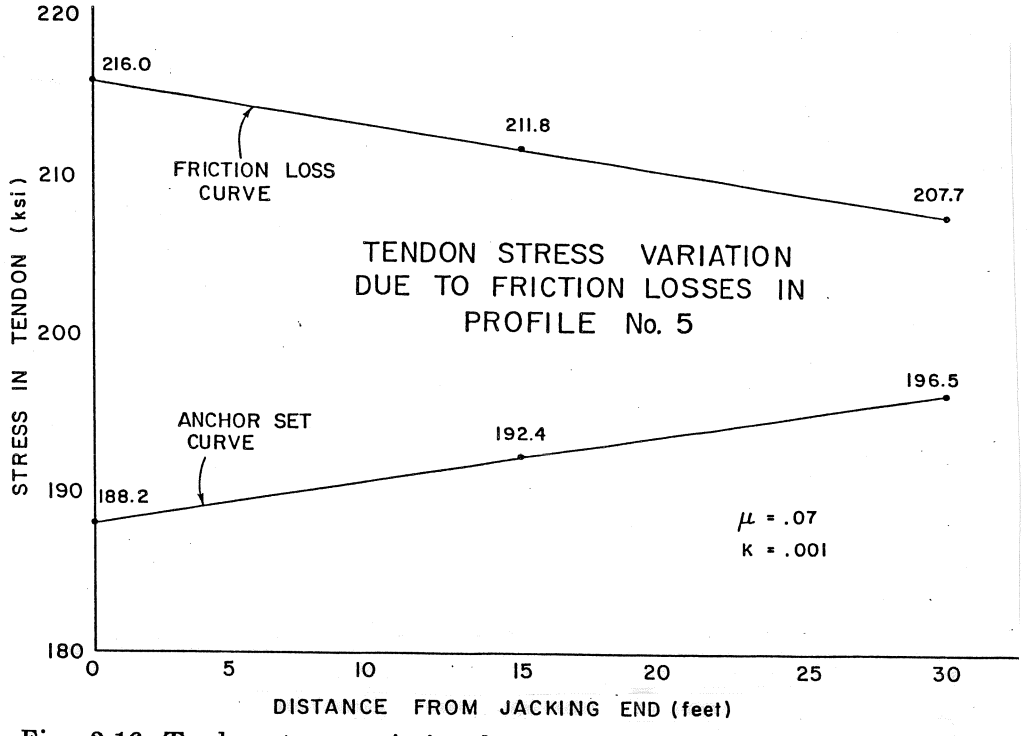

Fig. 2.16 Tendon-stress variation due to friction losses in Profile No. 5

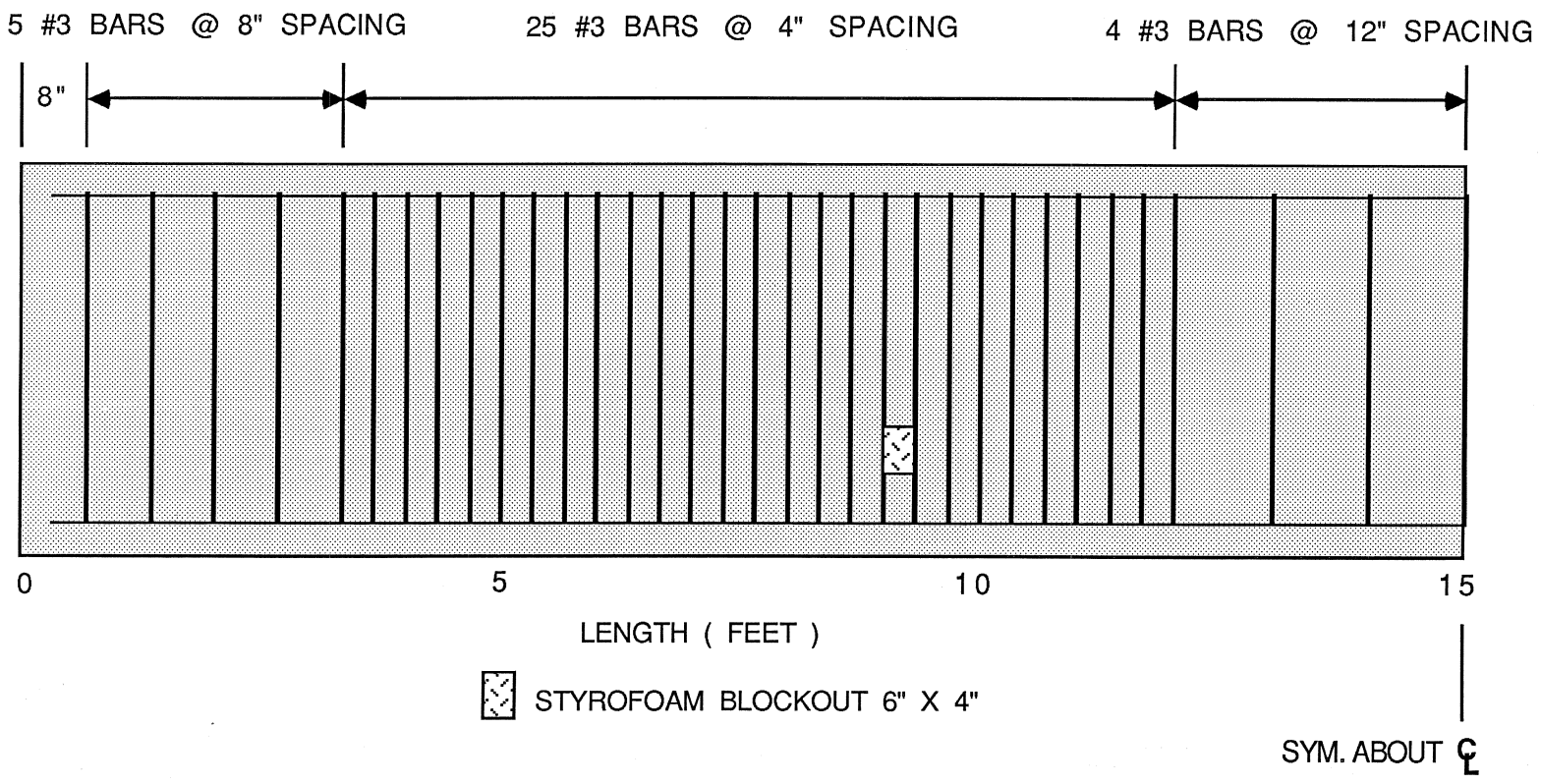

Fig. 2.17 Shear reinforcement: Profile No. 4

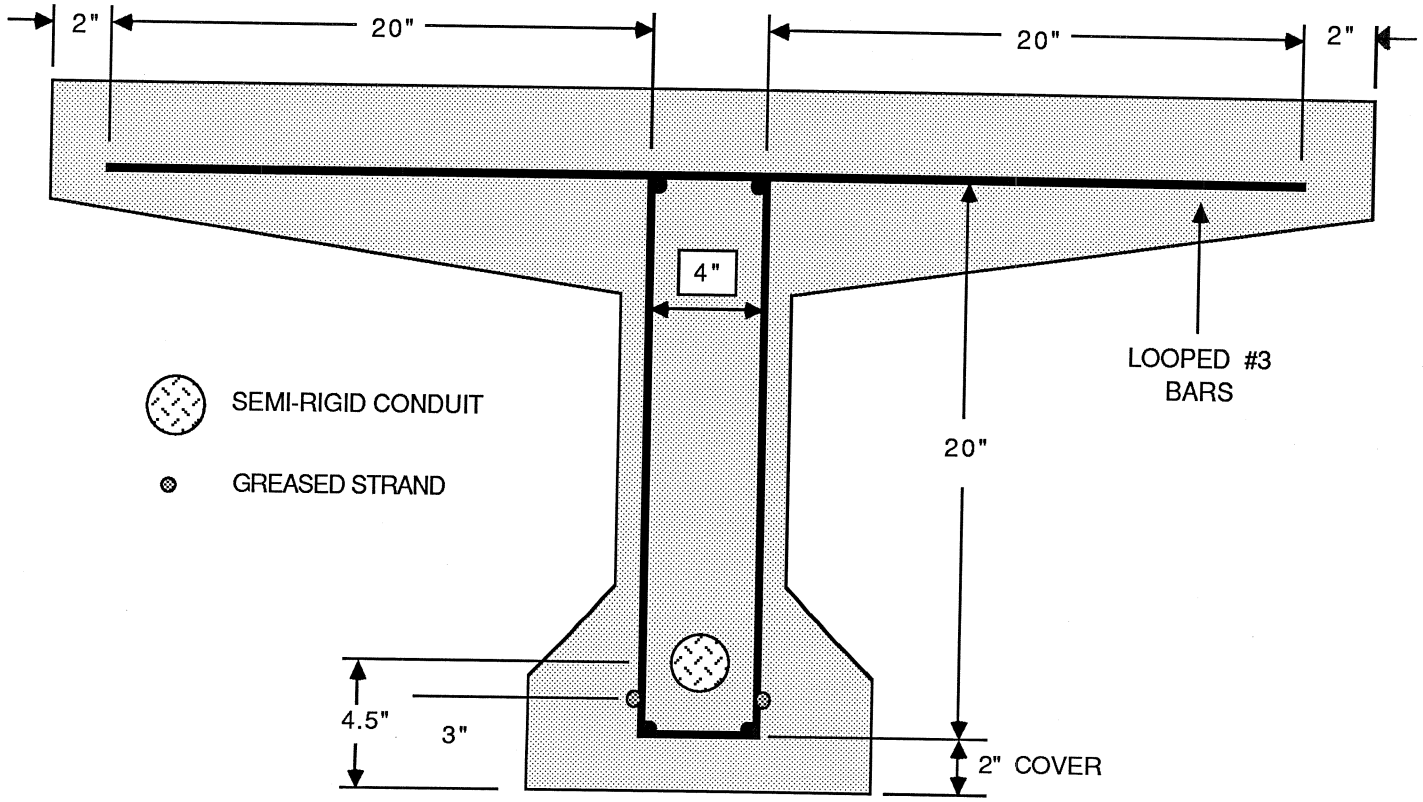

Fig. 2.18 Shear reinforcement cross section: Profile No. 4

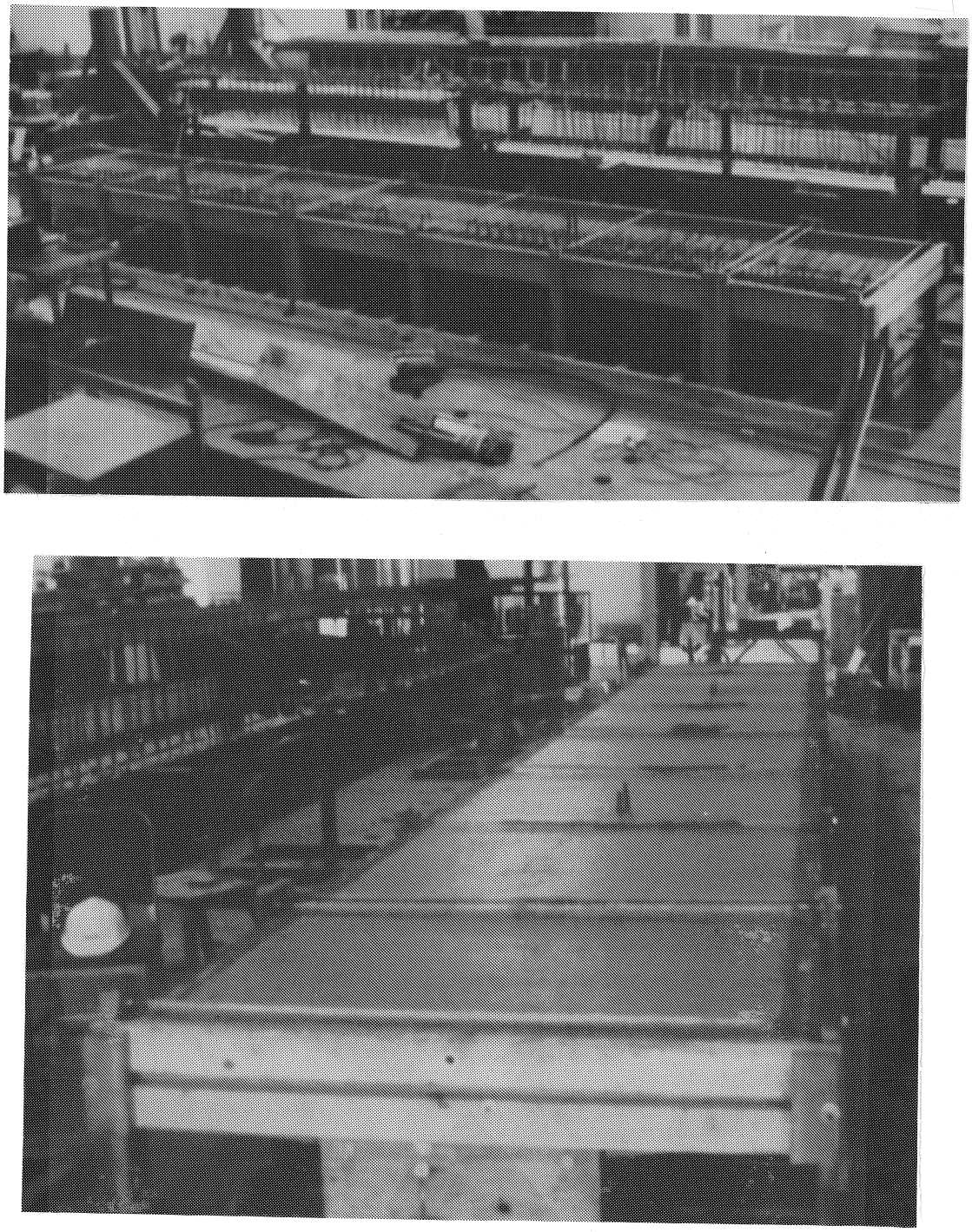

Fig. 2.19 Formwork prior to and after casting

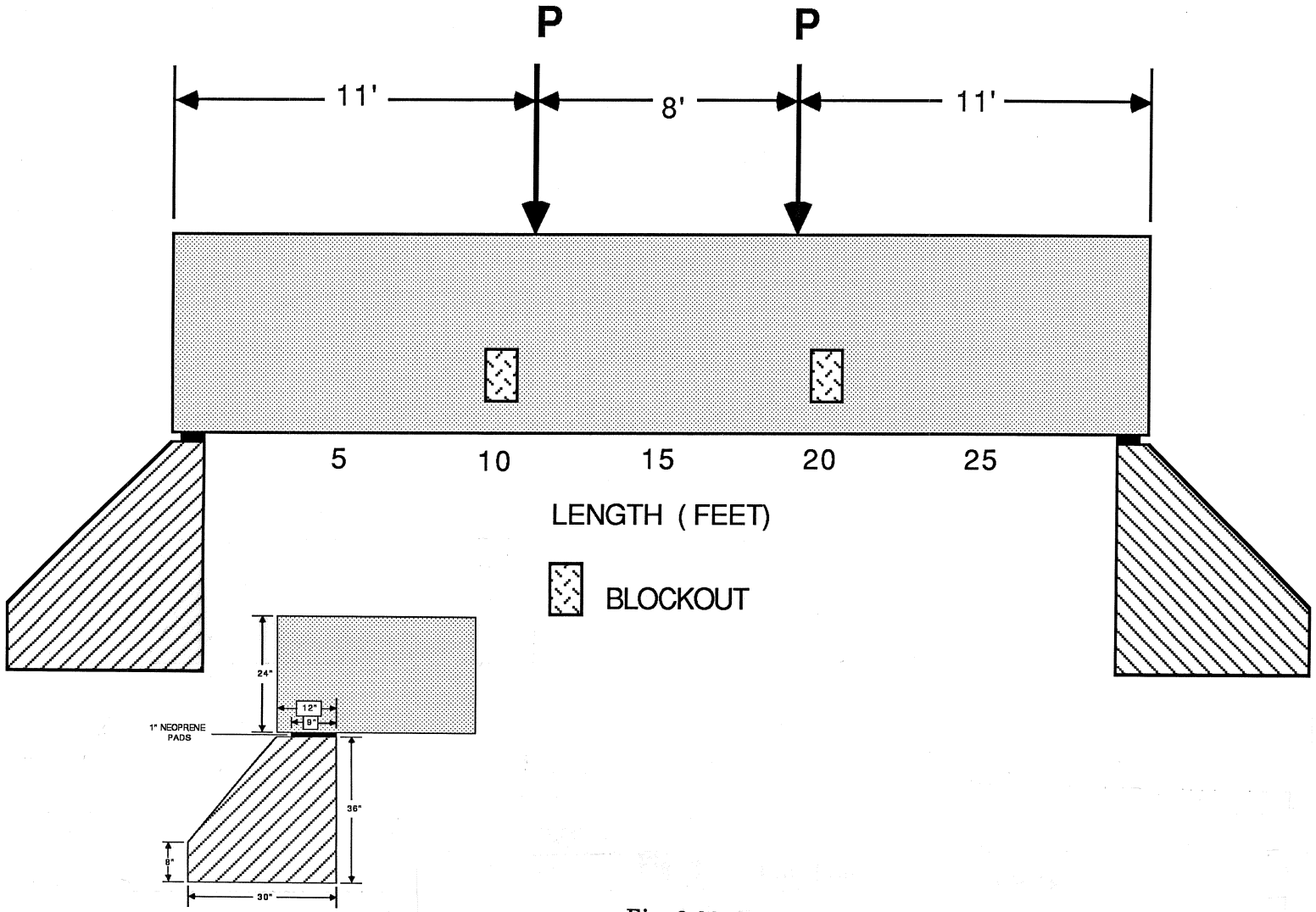

Fig. 2.20 Two point loading scheme

The load was applied to a transfer steel girder using a single hydraulic ram attached to a 100 kip load cell. Two steel columns with a steel cross beam supported the hydraulic ram. The transfer girder rested on two ball-in-cup assemblies which allowed rotation during loading as the beam deflected (Fig. 2.21).

2.4 Instrumentation

2.4.1 Load Cells. The holding force at the dead end was measured for tests of seven strand tendons using a 200 kip Universal Flat Load Cell. The load cell was manufactured by StrainSert model number FL200U-3SPKT, S/N Q6522-3. The resistance was 350 ohms and the voltage was 3 MV/V. The outside diameter was 12-1/4 in. with a 4-in. depth. The center hole diameter was 2-3/8 in.

The holding force system (Fig. 2.22) consisted of a front plate, load cell, circular back plate, anchor bearing plate, and anchor block all concentrically aligned. The prestressing strand passed through the center hole of the load cell.

For the greased strand, four load cells were necessary to measure the force at both the stressing and holding ends. The load cells had been manufactured in the laboratory and had a rated capacity of 100 kips. The holding system (Fig. 2.23) consisted of a front plate, load cell, back plate, and a monostrand anchor.

All the load cells were calibrated in a universal testing machine before and after testing. The load cells exhibited a linear behavior.

2.4.2 Stain Gages. Strain gages were placed on an individual wire of a tendon strand from the seven wire strand to measure strain. The gage was manufactured by Micro Measurements model number EA-06-062AP-120. The resistance was 120 ohms with a gage factor of 2.005. The gage length was .062 mils. Two different lead options, L and LE, were used. Option L was preattached with soft formable copper leads. Option LE had polyamide encapsulation of the leads.

The following procedure describes how the gage was attached to the wire. First, the wire surface was sanded with a fine grit sandpaper. Next, the surface was cleansed with acetone, metal conditioner, and metal neutralizer. The gage was then bonded to the wire with M-bond 200 adhesive in a direction parallel to the wire. An insulator was placed around the leads to prevent contact with the strand. The gages were protected by an epoxy sealant after the lead wires had been soldered in place. Finally, the gage was tested to insure proper electronic function.

2.4.3 Stressing Ram Pressure Readings. The stressing force was monitored by a pressure gage attached to the hydraulic ram. The stressing jack was a Prescon K200 No.24 type with

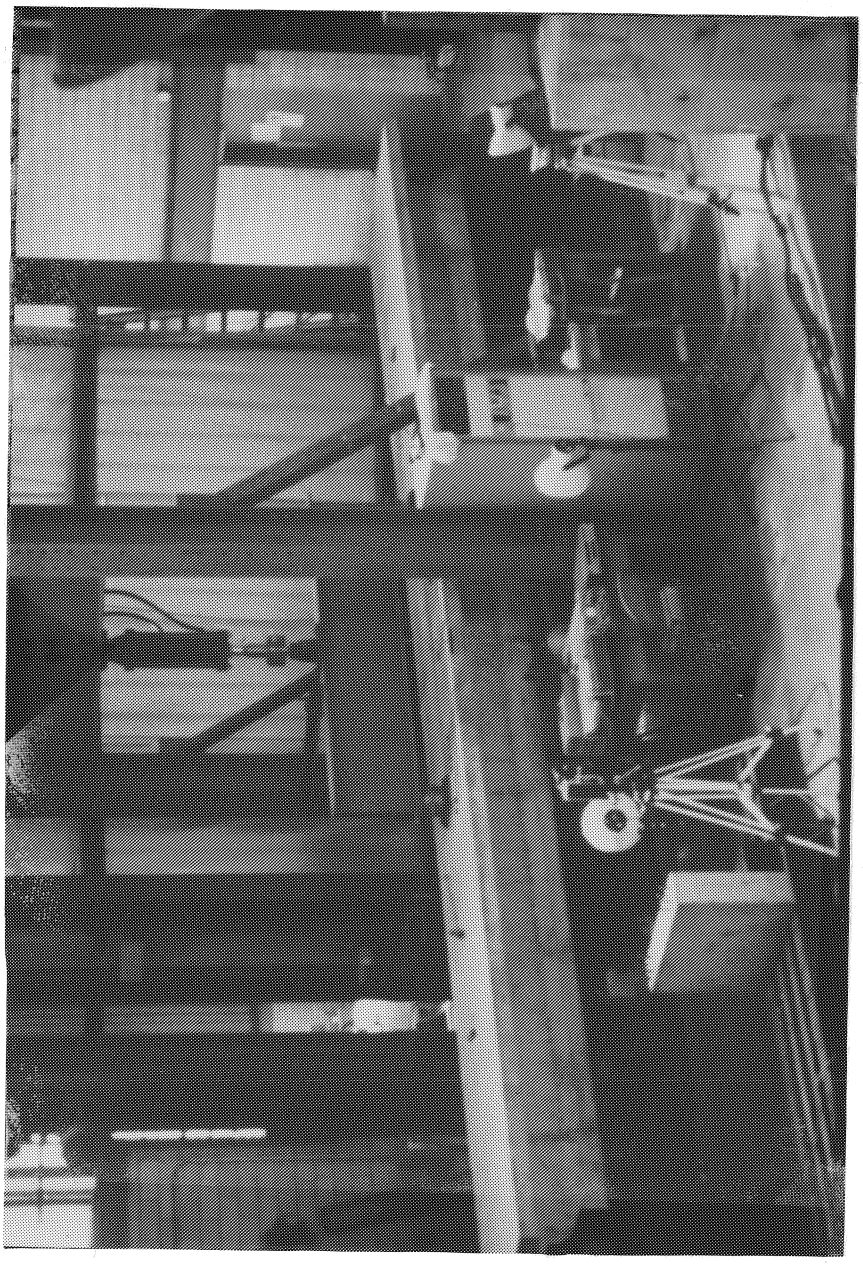

Fig. 2.21 Load-test set up

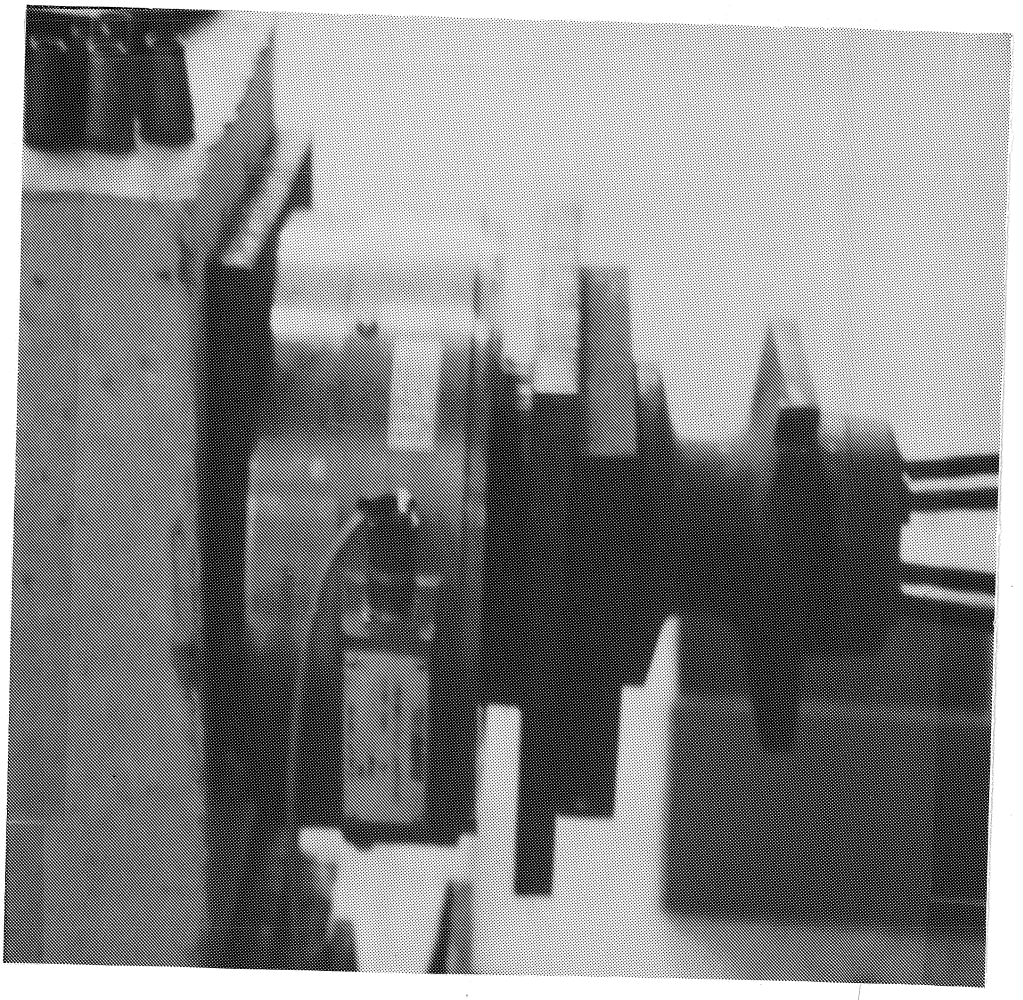

Fig. 2.22 Two-hundred-kip load-cell holding system

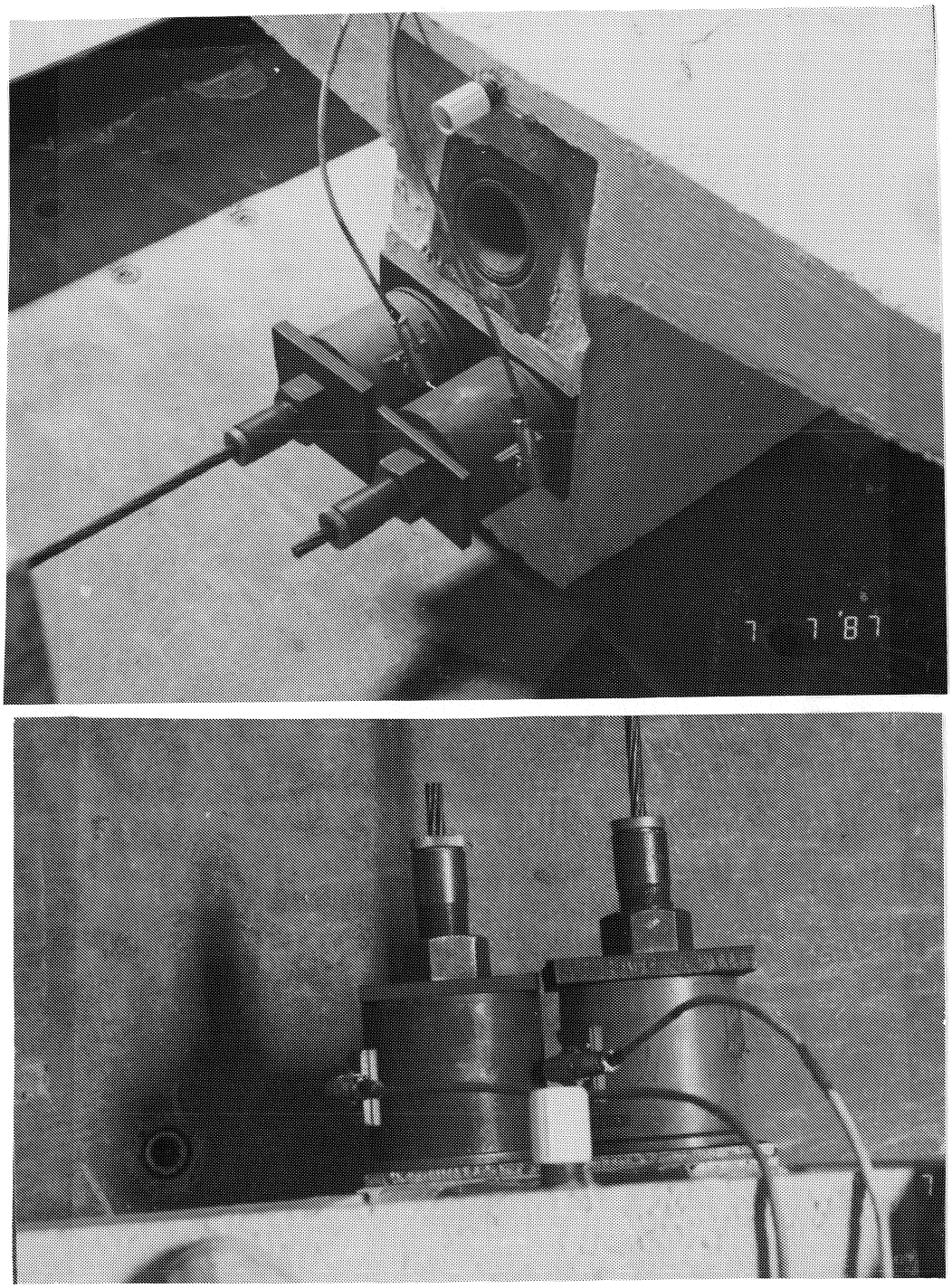

Fig. 2.23 Greased-strand holding system

an 8-in. stroke. The pressure gage was No. 215.102 with 100 psi divisions. Both the pressure gage and ram were calibrated as a unit prior to testing. Additional stressing equipment used in conjunction with the 'K' series jack was: rubber springs to decrease anchorage seating losses, pressure plate, pulling block, temporary stressing, and an electrical hydraulic pump. Figure 2.24 shows the stressing operation. The elongation of the tendons was measured as a check against the pressure gage indications.

The greased strand was stressed with a center hole two-in. stroke hydraulic ram. The load was monitored with a 5000 psi pressure transducer. The ram and pressure transducer as a unit were calibrated in a 60-kip universal testing machine.

2.4.4 Deflection Measurements. For the T-beam, vertical deflection readings were taken at the midspan and 10 ft from each end. Also, the lateral movement of the beam was measured at each end. Dial gages measured deflections at exactly the position of the blockouts. Therefore, the five dial gages were placed at 0, 10, 15, 20, and 30 ft. The deflection was measured by mechanical 0.001-in. dial gages.

2.4.5 Instrumentation Correlations.

2.4.5.1 Modulus of Elasticity. The modulus of elasticity is the ratio of the unit stress to corresponding unit deformation. Within the elastic limit, this ratio is constant. For prestressing strand, the modulus of elasticity is determined by loading a standard specimen length in tension. For each load increment, the change in elongation is measured up to the yield point. The modulus of elasticity is then obtained by:

$$E = \frac{PL}{A\Delta L} \tag{2.5}$$

where

$P =$ applied load

$A =$ cross sectional area of strand

$L =$ specimen length

$\Delta L =$ change in specimen length

A seven-wire strand consists of a straight center wire enclosed tightly by six helically wrapped outer wires. An individual helix wire is not elongated parallel to the direction of the overall strand. Therefore, the unit deformation detected by a strain gage placed on an outer wire

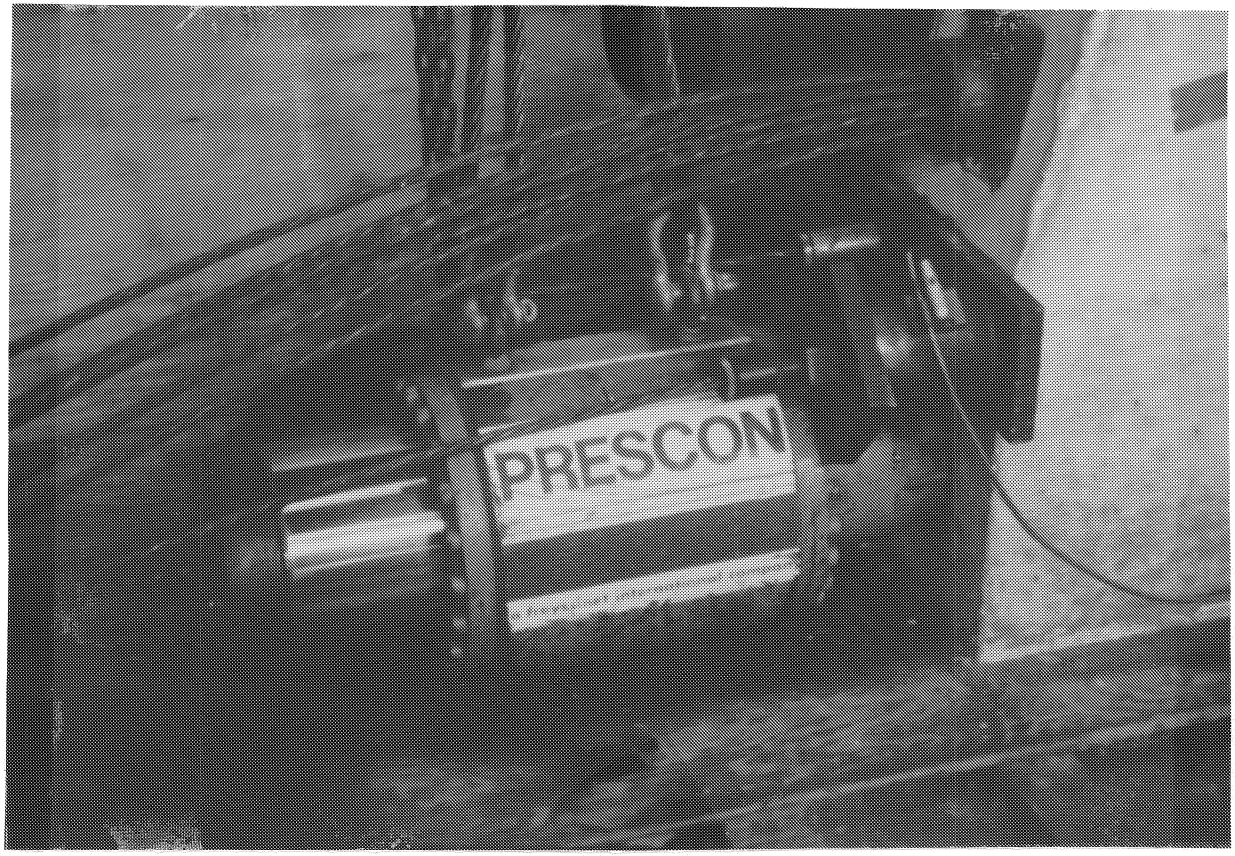

Fig. 2.24 Stressing operation

corresponding to the overall unit stress does not reproduce exactly the modulus of elasticity for the strand. The modulus of elasticity for a strain gage, E_{sg}, was determined in a separate test. A strand was instrumented with three strain gages. The gages were attached on every other outer wire in the same cross sectional plane. The strand was loaded in 2 kip increments up to the yield point. Corresponding strain increments were recorded. The strain gage modulus is given by:

$$E_{sg} = \frac{P}{L\epsilon} \tag{2.6}$$

where

$P =$ applied load

$A =$ cross sectional area of strand

$\epsilon =$ strain gage measurement

Figures 2.25a and 2.25b show a plot of the test results for the bare and epoxy coated strand. The average values of E_{sg} were 30,500 ksi and 31,750 ksi from the strain readings, respectively. These values were utilized to correlate the measured strains to the tendon stress.

2.4.5.2 Relaxation. Another test was conducted to determine the relaxation loss after anchor set. The test also confirmed the strain gage ability to measure tendon stress redistribution.

A strand, instrumented as in the elongation test, was stressed in a rigid steel prestressing bed. The strain gages were located at the midpoint. The "free air" strand, 20 ft in length, was stressed in the same manner as the greased strand (Sec. 2.5.2). Load cell and strain gage readings were recorded periodically for one week. Table 2.3 shows the measured stresses at jacking end load cell, holding end load cell, and strain gages at various stages. At maximum jacking force, strand stress was uniform along the length. Note that the average of strain gage measurements was close to load cell measurements although an 11 ksi differential occurred between the maximum and minimum. Since strain gages measure a local strain in an individual wire, each wire in a cross-sectional plane might register a slightly different stress although the summation of the local stresses for all the wires in a cross-sectional plane average out to be the applied force divided by the area. Following seating, strand stress at jacking end was 14.3 ksi larger than the holding end. Strain gage stresses ranged between jacking and holding end stresses with the average more closely approximating the holding end stress. Note that each strain gage on the respective strand wires detected exactly the same strain change during seating. This was also the case in the monitored time period following seating (Fig. 2.26a). The average stress loss after 142 hours was

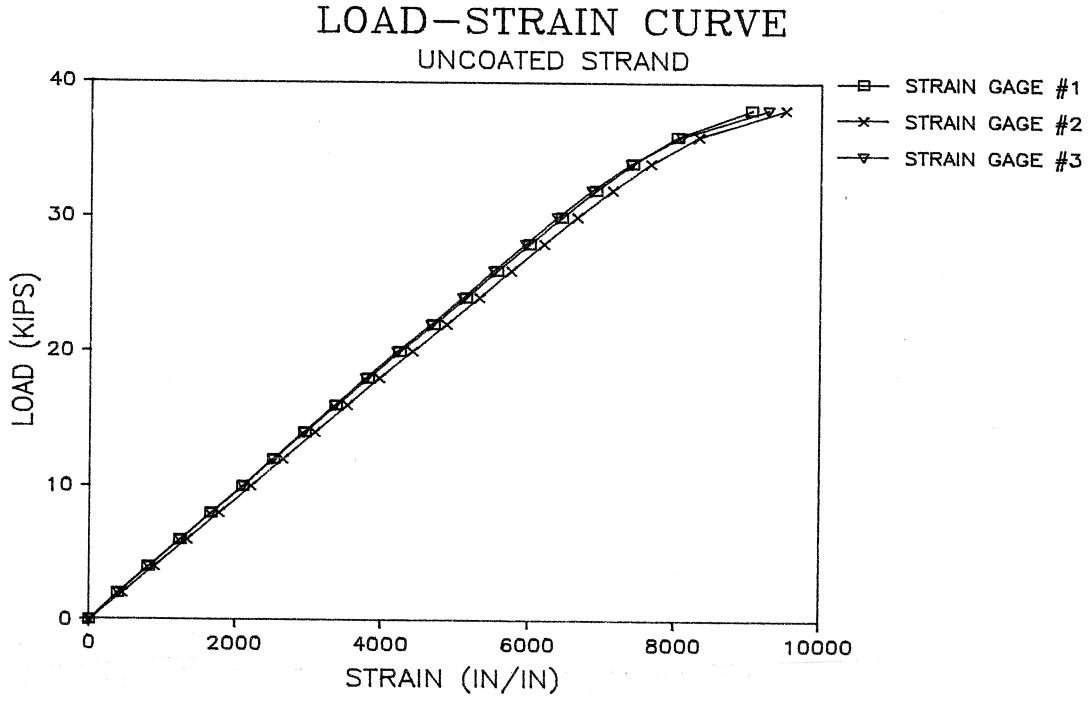

Fig. 2.25a Uncoated Strand: strain-gage modulus of elasticity

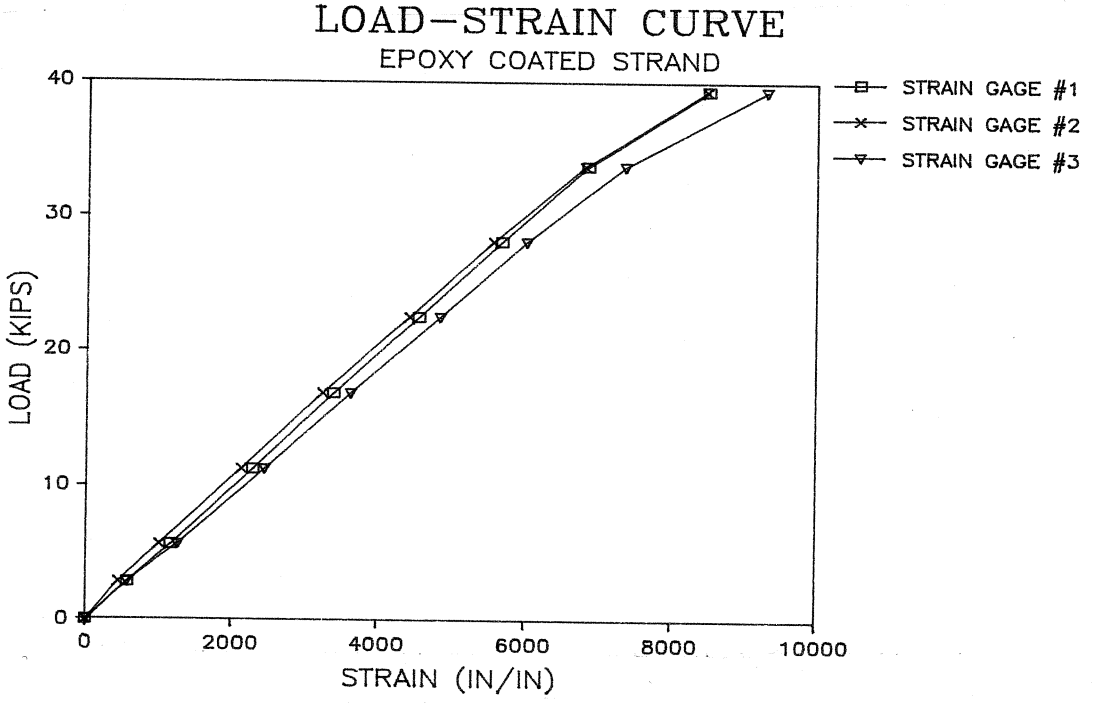

Fig. 2.25b Epoxy-coated strand: strain-gage modulus of elasticity

	Jacking End Load Cell (ksi)	Strain Gage #1 (ksi)	Strain Gage #2 (ksi)	Strain Gage #3 (ksi)	Strain Gage Ave. (ksi)	Holding End Load Cell (ksi)
Maximum Jacking Force	216.0	222.0	211.0	217.6	216.8	216.0
Anchor Set	201.9	195.3	184.4	191.2	190.3	187.6
2 Hours	199.5	193.5	182.6	189.1	188.4	185.3
25 Hours	196.0	192.5	181.7	188.1	187.4	183.2
73 Hours	196.0	190.9	179.8	186.3	185.7	183.2
156 Hours	196.0	188.7	177.6	184.3	183.5	183.2

Table 2.3 Strand Stress For Relaxation Test

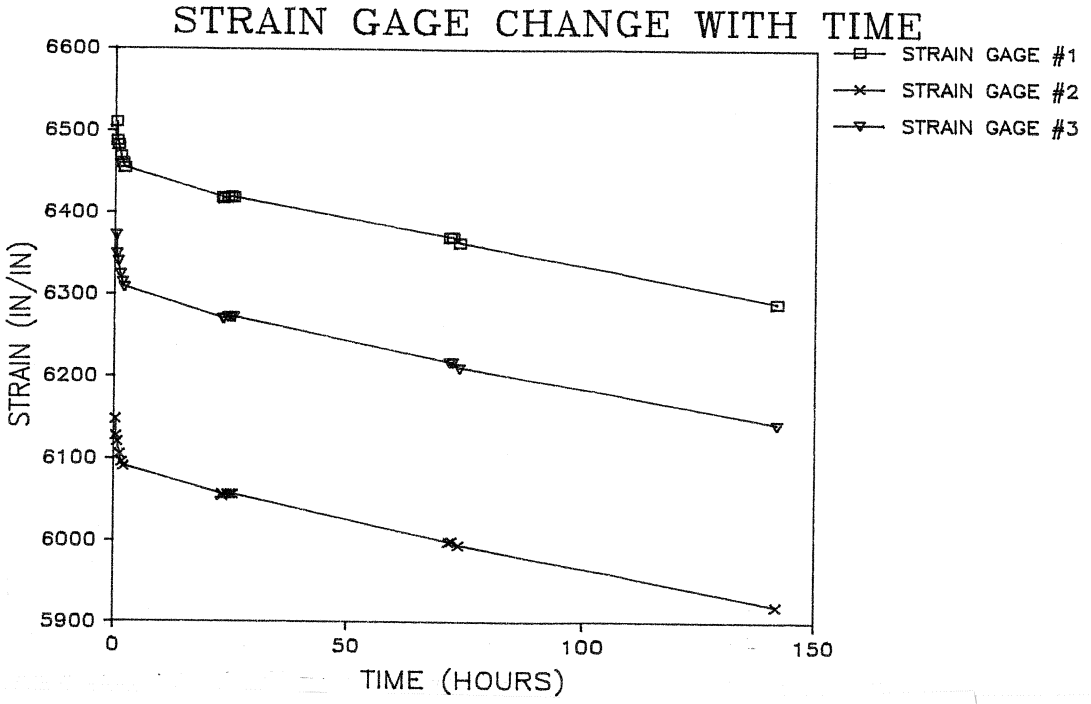

Fig. 2.26a Relaxation losses: strand-strain loss with time

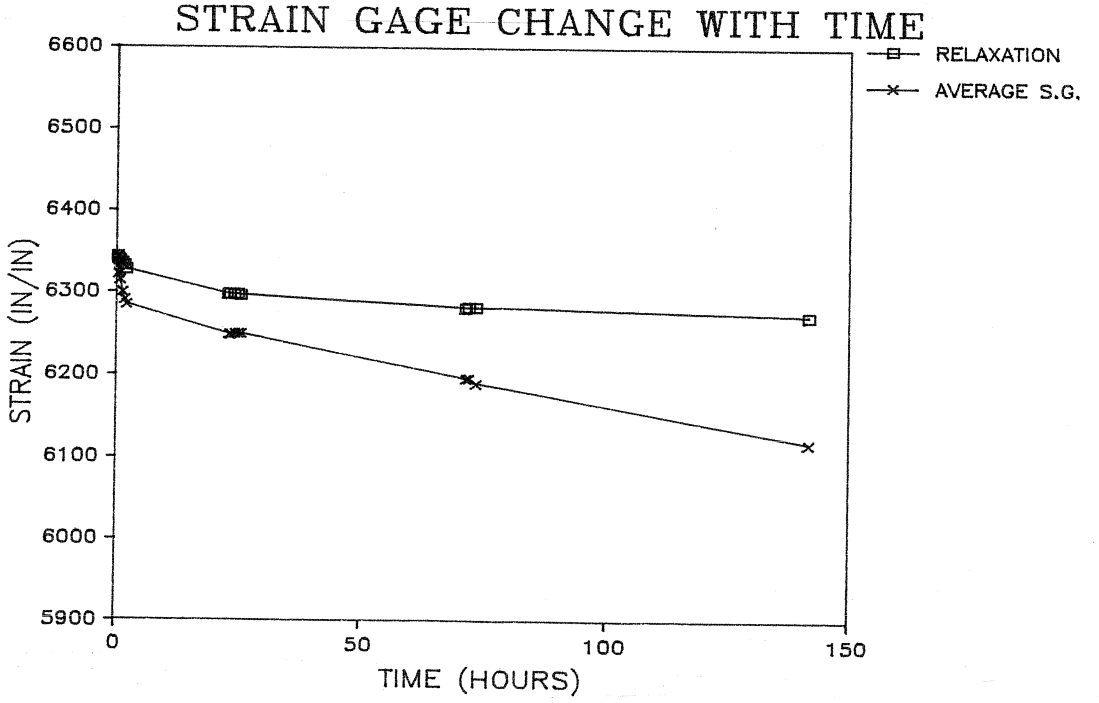

Fig. 2.26b Comparison of relaxation losses following seating

6.8 ksi corresponding to a stress reduction of 3.6%. Strain gages measured a larger stress loss than either load cell which were 5.9 and 4.4 ksi for jacking and holding ends, respectively.

Tests of prestressing steel with constant elongation maintained over a period of time have shown that the strand stress will decrease according to the following Eq (9):

$$f_{sr} = f_{si} \log t/10(f_{si}/f_{py} - 0.55) \tag{2.7}$$

where

f_{sr} = relaxation loss at time t

f_{si} = initial stress

$f_{py} = .9 f_{pu}$

Figure 2.26b shows the comparison between the above equation and strain gage measurements assuming f_{si} equaled the averaged measured strand stress following seating. The estimated equation relaxation loss was 2.1 ksi. Hence, strain gages measured over three times the estimated loss although a constant elongation was maintained.

2.4.6 Data Acquisition. Two different methods were implemented for data acquisition. In the first, the load cell and strain gage values were obtained with a strain indicator. The readings were recorded manually.

In the second, the load cell and strain gage values were read electronically using an Hewlett-Packard scanner. Each scan was recorded with data acquisition software by an IBM AT personal computer. The software, called HPDAS, was developed by the laboratory.

The rigid body test series used both types of data acquisition. For the T-beam, the strain indicator method was used.

2.5 Test Procedure

2.5.1 Rigid Body Specimen. Prior to stressing, the strands were feed into the permanent anchor block. The 3-piece wedge grips then were hand driven to insure they gripped the strand. The holding load cell was supported and aligned concentrically around the strands. All instrumentation was then tested for proper electrical function and zero readings were recorded.

For each layout, the strands were stressed at 500 psi increments by the stressing ram pressure gage readings. At each increment, the load cell, strain gage, and elongation readings were recorded. After the maximum prestressing force was released, readings were recorded to

CHAPTER THREE FIELD OBSERVATIONS

3.1 Introduction

For comparison with the laboratory test data, test data were acquired during field-stressing of a post-tensioned bridge on U.S. Highway 82 in Wichita Falls, Texas. The continuous 3-span bridge, known as the Taft St. Overpass Westbound, is a 274.5-ft post-tensioned concrete slab unit. The center span has a 94.5-ft length with end spans of 90 ft. The slab width is 58 ft with a 30-in. depth for the concrete.

Post-tensioning was applied in both the transverse and longitudinal directions. Transverse post-tensioning was positioned over the interior bents and at the end of the slab unit. The transverse tendon profile drape was very shallow and these strands were inaccessible for strain gage instrumentation. Post-tensioning in the longitudinal direction was applied from both ends to overcome the friction losses in the draped tendons within the three spans. Simultaneous stressing was not employed. High points over the interior bents were accessible for strain gage instrumentation as described below for this field test.

The bridge was designed by the Texas State Department of Highways and Public Transportation, Bridge Division, Austin, Texas, according to the 1983 AASHTO Standard Specifications; HS20 loading.

3.2 Bridge Design

3.2.1 Design Layout. To acheive the necessary longitudinal prestressing force, 36 tendons spaced 19 in. on center were used (Fig. 3.1). The numbers represent the stressing sequence, i.e., Tendon No.1 was the first tendon stressed, and the others followed the numbered sequence given. Each tendon consisted of 19 one-half-in. diameter low relaxation strands prestressed to an initial stress of approximately $.75f_{pu}$ (200.5 ksi). Tendons No.3 and No.4 were monitored for friction losses and tendon stress distribution. These two tendons are referred to as WF3 and WF4 for the alphanumeric scheme (Sec. 4.2).

The tendon profile (Fig. 3.2a) was parabolically draped with incremental angle changes ranging from .0417 to .0635 radians. At the ends, the profile was placed at the center of gravity of concrete (c.g.c.). For design, the friction coefficient; μ, wobble coefficient; K, and anchor set were assumed to be .25, .0002, and 0.5 in., respectively. Figure 3.2b shows the theoretical tendon stress variation due to the friction and anchor set losses for both the first and second end jacking.

Over the interior bent, the center of gravity of the conduit was 6 in. below top of slab. Steel reinforcement was located both top and bottom (Fig. 3.3) with the top bars being epoxy

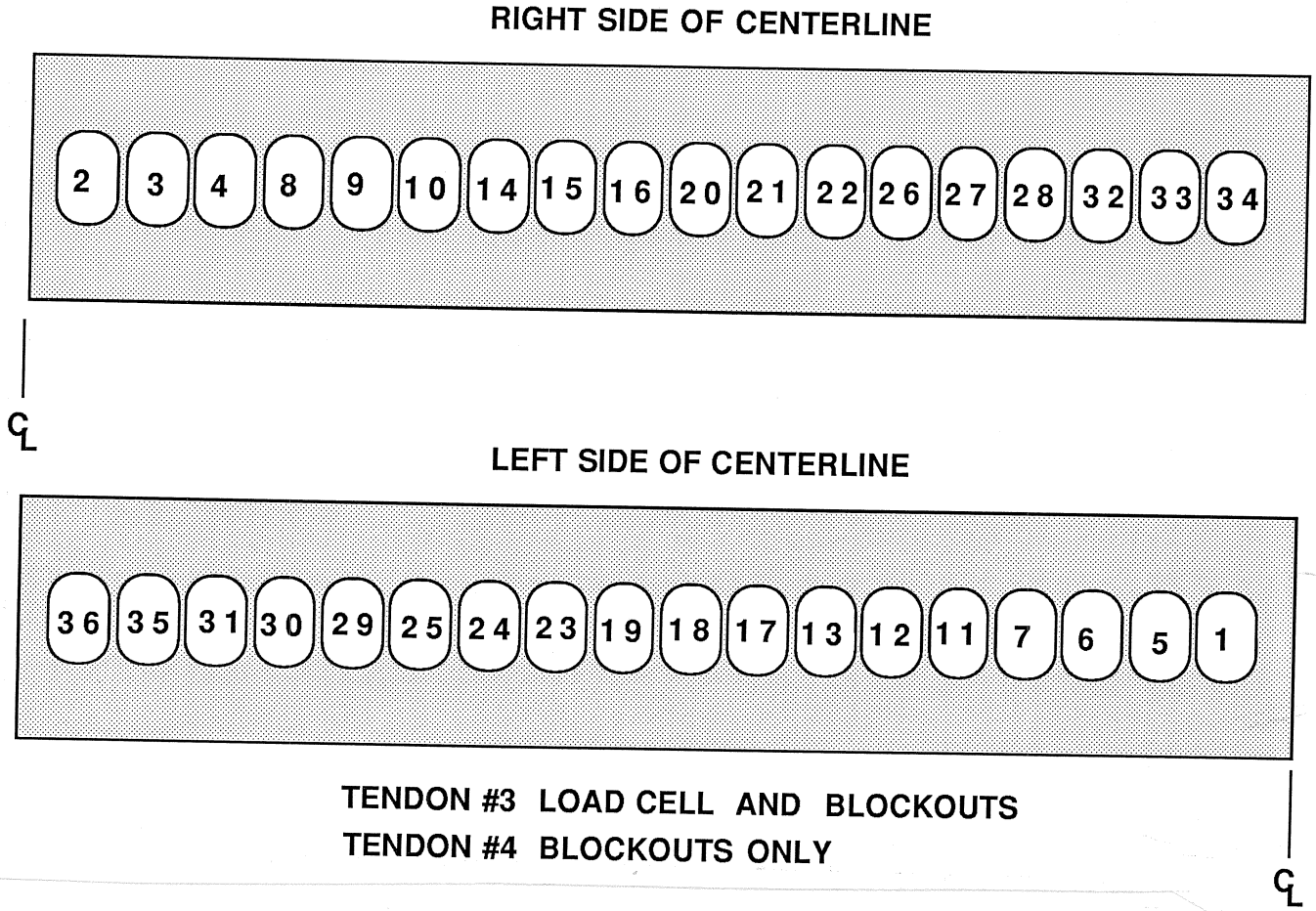

Fig. 3.1 Tendon-stressing sequence

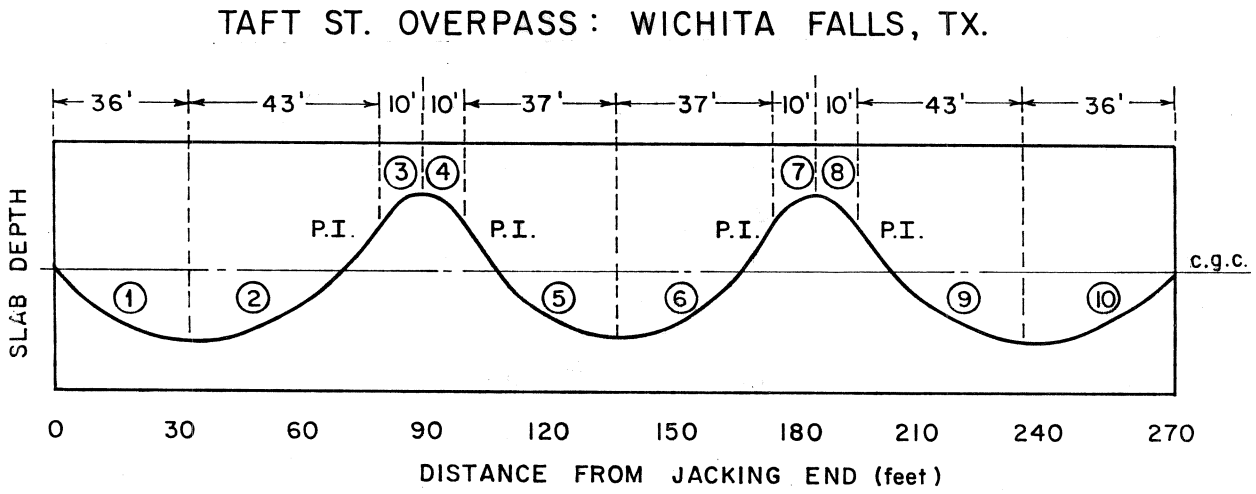

SEGMENT	ELEVATION DIFFERENCE	INCREMENTAL ANGLE CHANGE
①	9.0"	.0417
②	14.6"	.0566
③	3.4"	.0566
④	3.8"	.0635
⑤	14.2"	.0635
⑥	14.2"	.0635
⑦	3.8"	.0635
⑧	3.4"	.0566
⑨	14.6"	.0566
⑩	9.0"	.0417

Fig. 3.2a Wichita Falls tendon profile

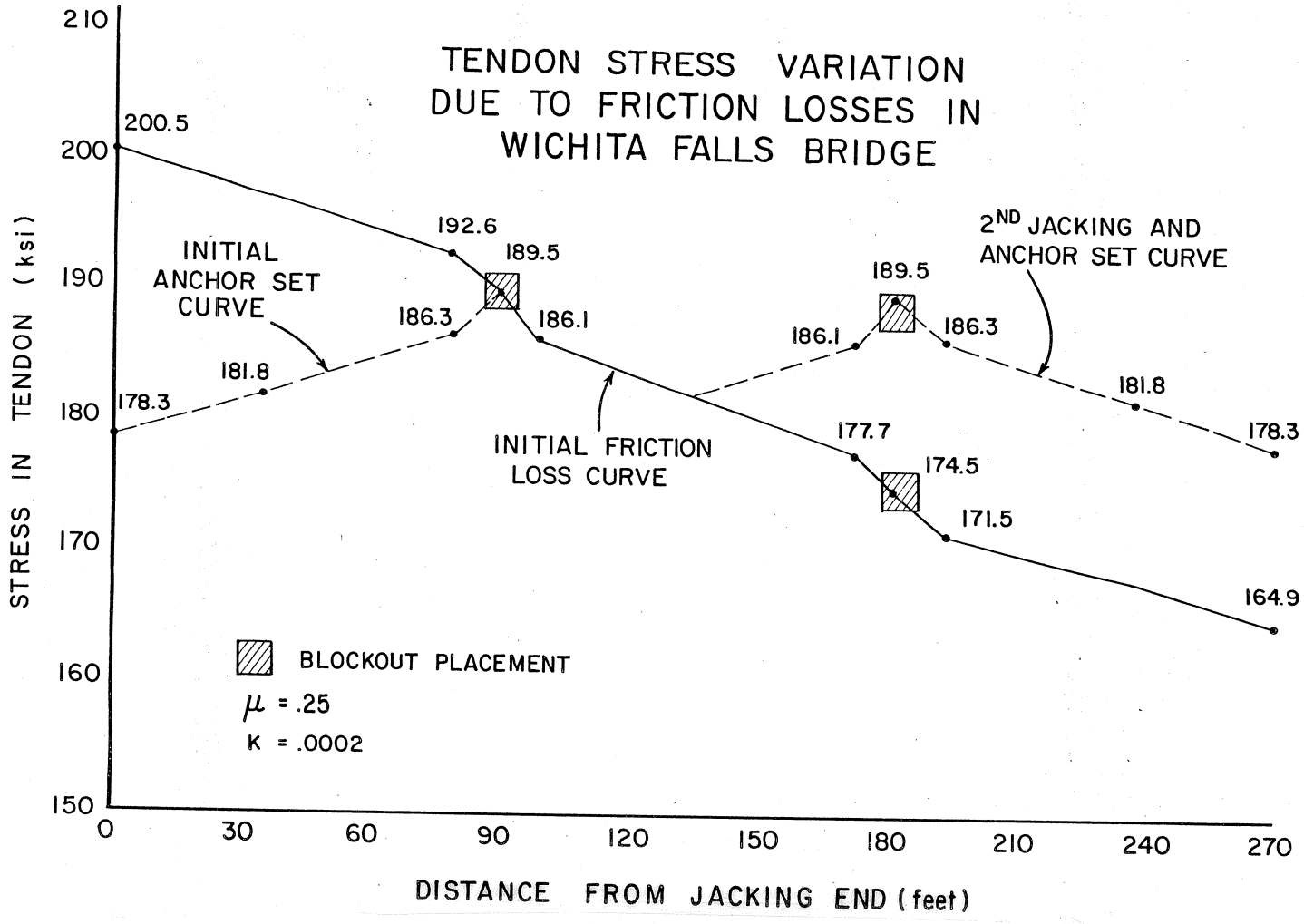

Fig. 3.2b Theoretical tendon stress variation

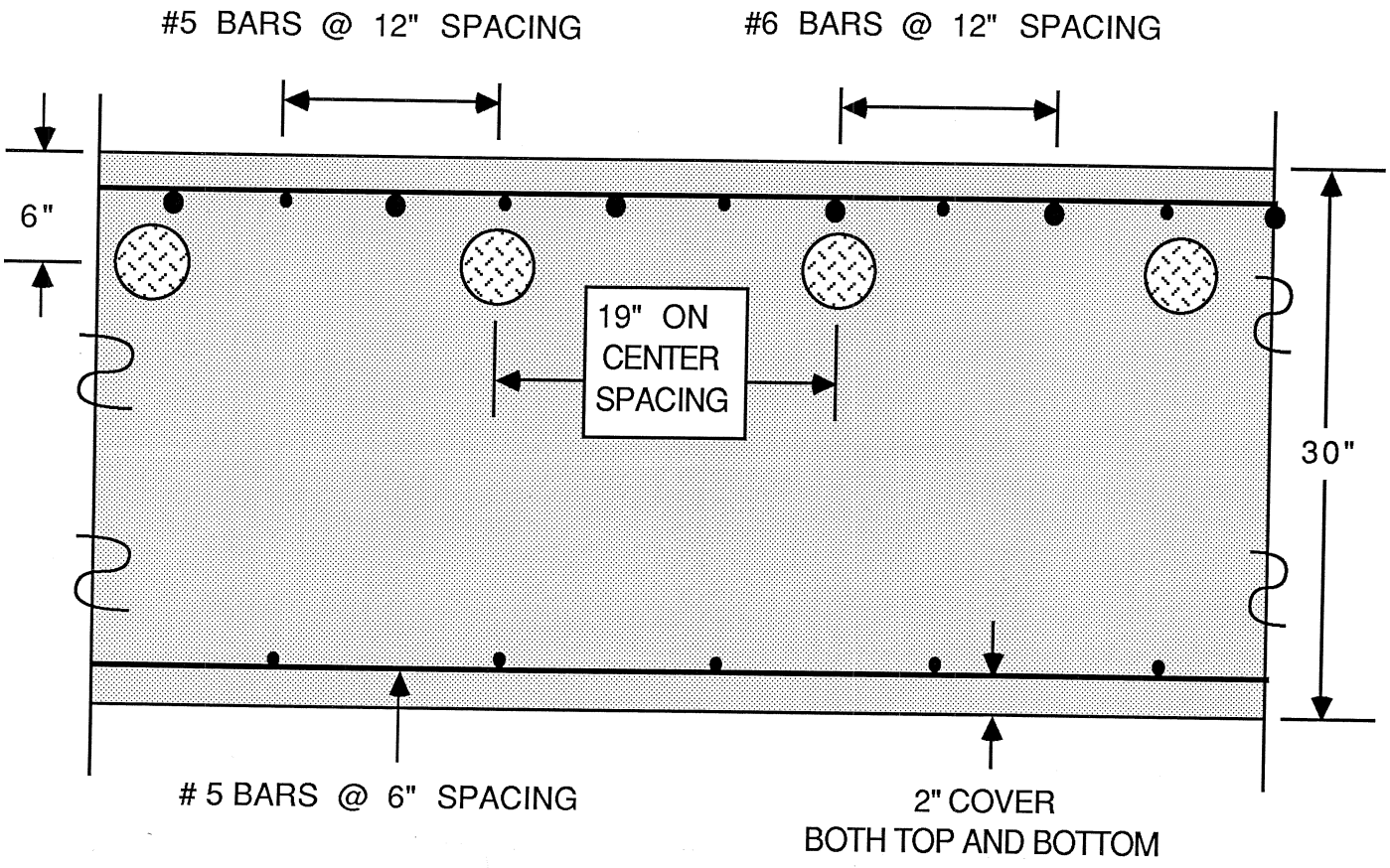

Fig. 3.3 Reinforcement along centerline- interior bent

coated. Grout vents were placed on the tendons along the center line of each bent. The grout vent distances from the initial jacking end were 89 and 183 ft.

3.2.2 Materials. Prescon supplied the post-tensioning anchorage system, conduit, and stressing equipment for the bridge project. A Prescon crew performed the field stressing operation. The materials were very similar to those used in the laboratory testing except that 19 strands were used in the field tendons compared to only seven strands in the laboratory tendons.

The multi-strand tendons consisted of 1/2-in.-diameter Grade 270 seven-wire low relaxation strand conforming to ASTM A-416. The material was tested in accordance with Texas S.D.H.P.T. 1982 Standard Specifications. Prior to placement, rust and other debris were removed with a wire brush. The strands were individually pushed through the profile with a mechanical feeder. Strand placement occurred one to three days prior to stressing.

The anchorage system, Prescon 'KP', consisted of a 19K5 cast bearing plate, 19K5 permanent anchor block, transition cone, and 3-piece wedge sets. The transition cone was Gage 16 sheet metal extending inward 9.5 in. from the concrete face. Spirals provided passive reinforcement to accommodate anchorage zone stresses for each anchorage assembly.

The conduit was the same as described in Sec. 2.2.3 except the nominal diameter was 3-1/4 in. At the high and low points of the profile drape, the center of gravity of the 19 strands was assumed to be 3/4 in. from the centroid of the conduit for design of the bridge.

3.3 Test Set-Up

3.3.1 Preparation. To gain access to the strands, the concrete had to be removed from around the conduit. Styrofoam blockouts were not used at the time concrete was cast for the 30-in.-thick bridge. The grout vents marked the high points over the support points for interior bents and located the individual tendon centerlines. A jackhammer removed the concrete to form a 6-in $\times$ 18-in. blockout for Tendons No.3 and No.4. Concrete was removed to a depth of 6 in. which coincided with the centroid of the conduit (Fig. 3.4). A total of four blockouts were formed, two each on WF3 and WF4. Care was taken not to damage the epoxy coated rebar above the tendon while jackhammering.

After strand placement, the conduit was cut along the top with a hacksaw. Next, the conduit was peeled back for an unobstructed view of the strands. Strain gages were then placed on four of the 19 strands which were color coded blue, green, red, and yellow. Two strain gages were placed on each instrumented strand at a spacing of 6 in. (Fig. 3.5). Thus a total of eight gages were placed per blockout. The main purpose of two strain gages was to check the correlation of strand strains measured over the short distance. A secondary effect was to allow observation of tendon strain redistribution along the short distance as well as total redistribution

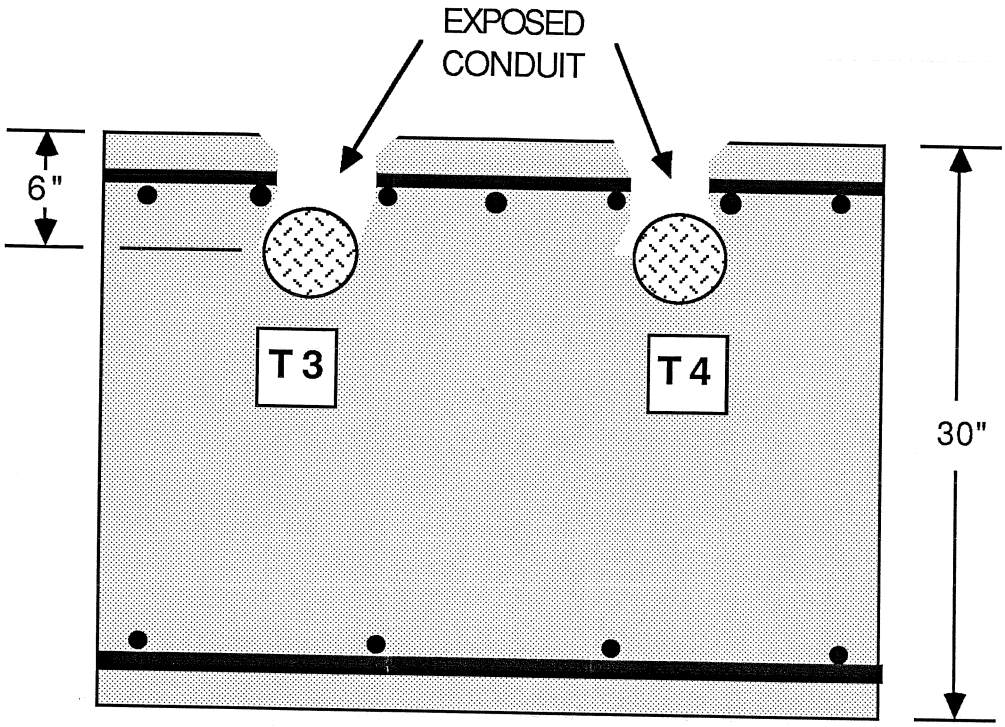

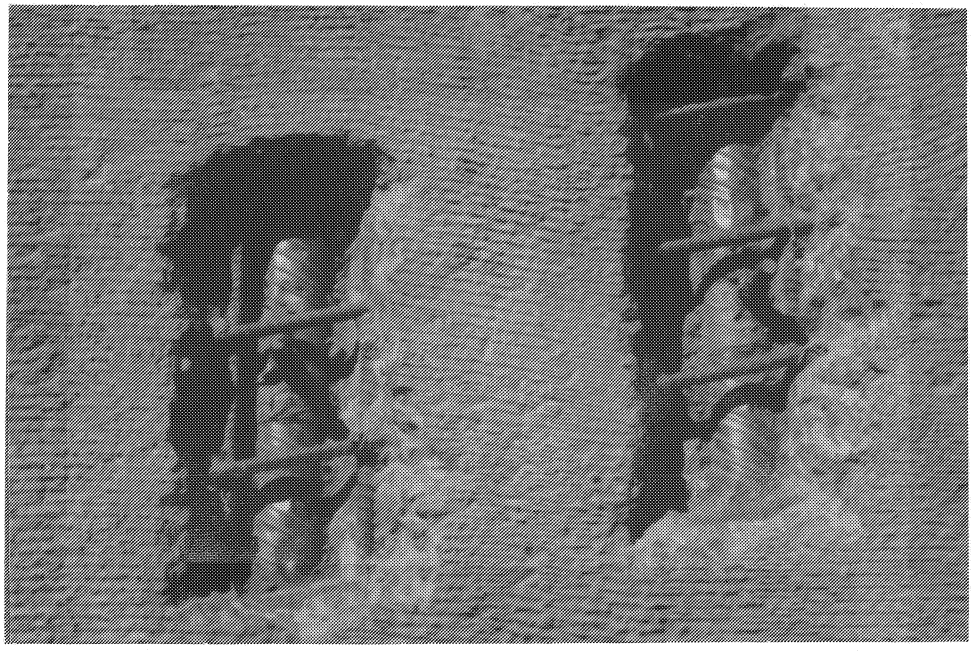

Fig. 3.4 Blockouts to conduit

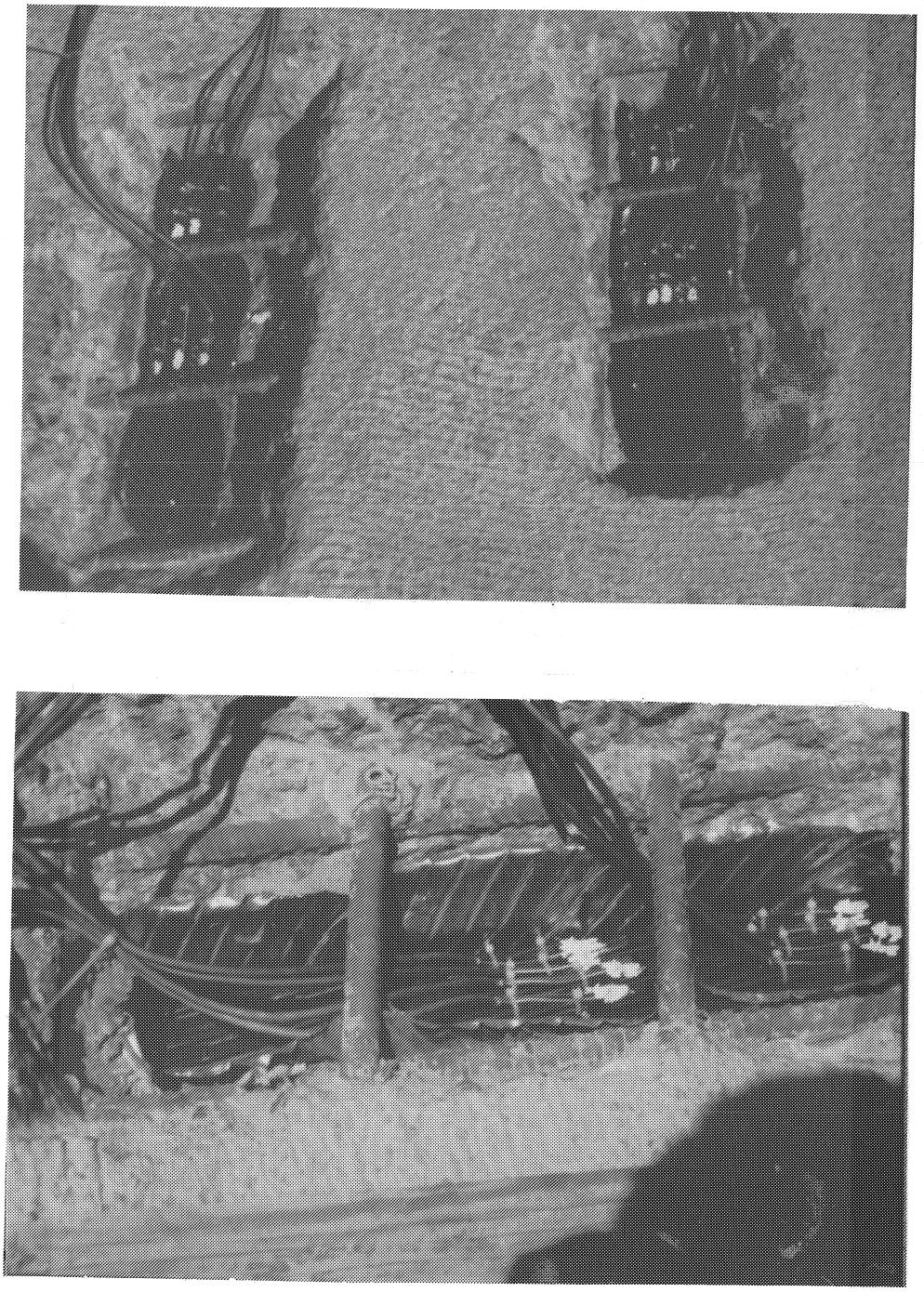

Fig. 3.5 Strain-gage placement

after stressing. The gages were not placed on the same wire but rather two different wires of the same strand.

Plywood and sheet plastic covered the blockouts to prevent debris or water from entering the conduit when strain readings were not being monitored. The project contractor assisted with forming the blockouts and repaired the conduit and blockouts after testing was completed.

3.3.2 Instrumentation. A load cell determined the holding force on WF3 (Fig. 3.6). The 1.5 million pound load cell was a Visham model, Serial No. 27740 with a gage factor of 0.540. Prescon supplied the load cell and provided a Certificate of Calibration. With the load cell on WF3, double end stressing could not be observed. Double end stressing was monitored on WF4 using the pressure gage readings from the hydraulic jack.

The hydraulic stressing ram was a member of Prescon 'K' series jacks. The ram was a K350 (350 ton capacity), No. 4035.003 with a 10-in. stroke. The pressure gage was No. 4215.003 with 100-psi increments. Prescon performed the calibrations for ram and pressure gage and provided a copy of the calibration data sheets.

Strain gage placement procedure and model type remained the same as described in Sec. 2.4.2. Strain indicators were used for the data acquisition on these field measurements.

3.3.3 Test Procedure. The test procedure had to be arranged to minimize the delay in the stressing operation by the bridge contractor. Also, the tendon stressing sequence could not be altered. Expected tendon elongations were such that multiple stroke jacking was required. The required number of strokes was three to achieve the total elongation.

On the first day of stressing (Fig. 3.7), Tendons 1 through 3 were stressed. Prior to stressing WF3, the load cell and strain gages were checked to insure proper electronic function. Instrumentation readings were recorded during stressing at 1000 psi increments. Tendon elongations were measured as a check on the pressure gage readings. A Texas Highway Department representative supervised elongation measurements. During stressing, the ram stroke was reset at pressure readings of 3000 and 6000 psi. For confirmation, instrumentation readings were recorded again at those pressure gage readings before the stressing operation was continued. The maximum pressure reading was 7800 psi. Upon transferring the jacking force from the ram to the permanent anchor block, anchor set was determined with a measuring tape and strain gage readings were recorded. Tendon stress redistribution was monitored for the 12 hours prior to stressing WF4.

Tendon WF4 was stressed and monitored using the same procedure as described for WF3 except that no load cell was installed to determine the holding force. Tendons 4 through 25 were stressed on the second day. No appreciable time elapsed between the stressing of Tendons

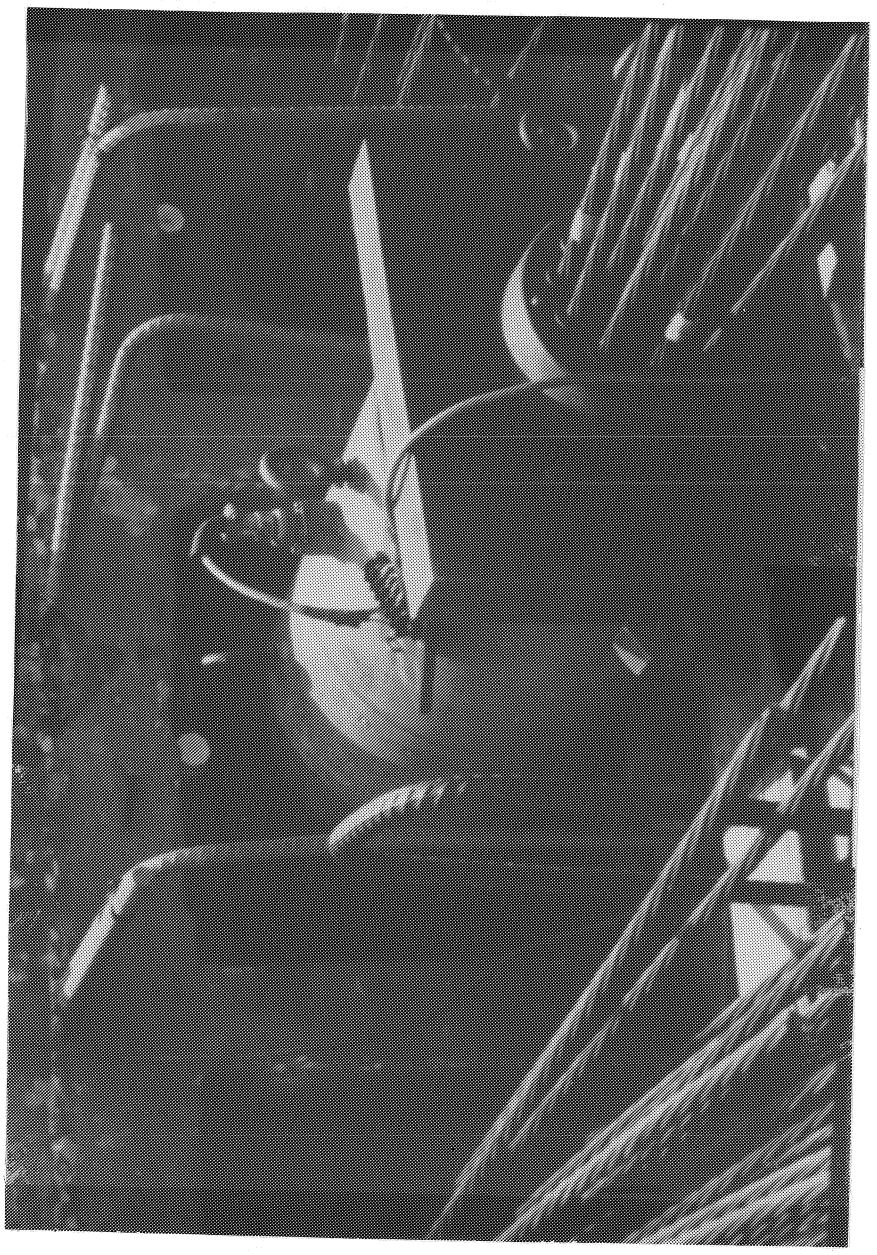

Fig. 3.6 Load cell on WF3

Fig. 3.7 Stressing operation

4 and 5. WF3 and WF4 were monitored at periodic intervals while the stressing operation continued. On the third day, the first end stressing of the 36 tendons was completed. Tendons 1, 2, and 4 were also stressed on this day from the second end. Instrumentation readings were recorded only at the final pressure gage readings of 7800 psi without the readings at 1000 psi increments as was done during the initial stressing. WF3 and WF4 were monitored for an additional 16 hours with no other tendons having been stressed from the second end. The total elapsed time between initial stressing of WF3 and the final readings was 64 hours.

CHAPTER FOUR PRESENTATION AND ANALYSIS OF TEST RESULTS

4.1 Introduction

In this chapter, the test results from the rigid body specimen, Wichita Falls bridge, and T-Beam specimen are presented and analyzed. The general behavior of tendon stress and strain for the tests are discussed for the jacking stage, anchor set stage, and the time period following anchor set. For friction and seating losses, the measured tendon stress variation along the layout's length is compared with that of theory. Change in the tendon strain and redistribution after seating is compared between the respective blockouts of each layout.

4.2 Test Results Presentation

For presentation of the test results, the following alphanumeric sequence was used to designate specimen profile and test description:

$$LTN : C - X$$

where

$L =$ represents the layout number for each tendon profile as discussed in Chapter's 2 and 3

$T =$ test series for a particular layout. Only the rigid specimen layouts and Tendon Profile No.5 were tested in a series. Hence, only these layouts contain the T term

$N =$ number of strands stressed for a particular test. An E after the number represents epoxy coated strands while a G a greased strand

$C =$ color code of strand instrumented with strain gages; Blue (BL), Green (GR), Red (RD), Yellow (YW)

$X =$ blockout distance from the stressing end

As an example, L3 T4 (7):GR-24 indicated Tendon Profile No.3, the fourth test in the series with seven strands stressed, the instrumented 'green' strand at the blockout located 24 ft from the stressing end.

A summary of the tests is presented in Table 4.1. The maximum initial tensile stress due to the jacking force was limited to $.85f_{pu}$ in accordance with ACI-318 Sec. 18.5. In testing, the jacking stress ranged from $.74f_{pu} - .87f_{pu}$ with a very slight overstress above $.85f_{pu}$ in four of the tests. Elongation measurements were used as a check during stressing. Due to test

Test	Jacking Stress (ksi)	% f_{pu} Ultimate Tensile Strength	Load Cell	Friction Coefficient	Total Elapsed Time (Hours)
L1 T1 (7)	202.5	.75	YES	.392	20.24
L1 T2 (7)	202.5	.75	YES	.398	19.21
L1 T3 (7)	202.5	.75	YES	.371	186.58
L1 T4 (7)	216.0	.80	NO	(.387)	124.22
L1 T5 (4)	232.0	.86	NO	(.387)	139.40
L1 T6 (2)	220.0	.81	NO	(.387)	71.20
L1 T7 (7E)	202.5	.75	YES	.530	50.21
L2 T1 (7)	196.0	.73	YES	.250	17.60
L2 T2 (7)	202.5	.75	YES	.290	2.94
L2 T3 (7)	202.5	.75	NO	(.275)	571.87
L2 T4 (7)	212.5	.79	YES	.285	124.33
L2 T5 (4)	232.0	.86	NO	(.275)	215.58
L2 T6 (2)	228.0	.84	YES	.390	71.20
L2 T7 (7E)*	157.5	.58	YES	.610	- - -
L3 T1 (7)	222.0	.82	YES	.289	44.58
L3 T2 (7)	202.5	.75	YES	.278	337.67
L3 T3 (7)	222.0	.82	NO	(.270)	118.59
L3 T4 (4)	232.0	.86	NO	(.270)	216.16
L3 T5 (2)	236.0	.87	YES	.244	42.67
L3 T6 (tE)*	135.0	.50	YES	.565	- - -
WF3 (19)	200.5	.74	YES	.301	62.00
WF4 (19)	200.5	.74	NO	(.301)	49.00
L4 TB (7)	202.5	.75	YES	.305	167.33
L5 T1 (1G)	216.0	.8	YES	.100	139.00
L5 T2 (1G)	216.0	.8	YES	.040	138.67

( ) Averaged Friction Coefficient
* Epoxy Coating Slipped Through Wedges at Holding End at this Jacking Stress

Table 4.1 Test Summary

time durations and only one available load cell with adequate capacity to measure the holding force, some tests were stressed without a load cell. In these tests, strain gages provided tendon measurements with the holding force estimated using an averaged friction coefficient from other tests in the same series. Also, as a separate test was not performed to determine the wobble coefficient, a representative median value of K=.0002 for galvanized rigid metal conduit was assumed for each layout. Due to the large profile curvatures, an assumed wobble was considered justified, i.e. friction coefficient contributed a substantially greater percentage of overall frictional losses. Hence, with a known initial jacking stress and wobble coefficient, the friction coefficient; μ, was computed by trial and error using program *FLOSS* to match the load cell holding end stress. In practically every test, the measured friction coefficient was greater than the 0.25 value recommended for galvanized rigid metal conduit. Measured values of μ ranged from .244 to .398 as shown in Table 4.1.

For the hydraulic stressing ram and electric pump used for jacking, release of final jacking pressure was rapid and instantaneous. With three seconds as an outside limit, the jacking force was transferred completely from pulling block to permanent anchorage block. The anchorage transformation or elongation loss consistently measured 0.5 inches. Hence, the theoretical anchor set curve was determined by *FLOSS* using an half-in.-seating loss. As shown in Table 4.1, the total elapsed time after seating varied from test to test, but each layout was monitored at least once for approximately 120 hours (5 days) or longer.

4.3 Rigid Body Specimen

4.3.1 General. A series of three figures describe test results for each rigid body specimen layout. The first figure in the series shows jacking, seating, and final strand stress variation along the layout length. Stressing and holding end forces represent a collective value of all stressed tendons. Strand stresses were based upon strain gage measurements which were unique to an individual wire in a particular strand. Referring to Fig. 4.1a, a solid line connects strand stresses as detected by strain gages between each respective blockout. A dashed line represents the distribution along the length of the specimen for tendon stresses obtained with *FLOSS* based upon jacking and holding end forces, friction and wobble coefficients, and an assumed half-in. transformation seating loss. The tendon stresses (converted from measured strain) are shown at maximum jacking stress, immediately after seating the wedges to permanent anchor head, and final stress readings just prior to detensioning.

After anchorage seating, change in tendon strain with time for each blockout is shown in the second of the series of three figures (Fig. 4.1b). Any tendencies for redistribution of strains to flatten out tendon force peaks and valleys caused by jacking and anchorage seating can be observed in this figure (Fig. 4.1b). The last figure in the series (Fig. 4.1c) is a bar chart showing

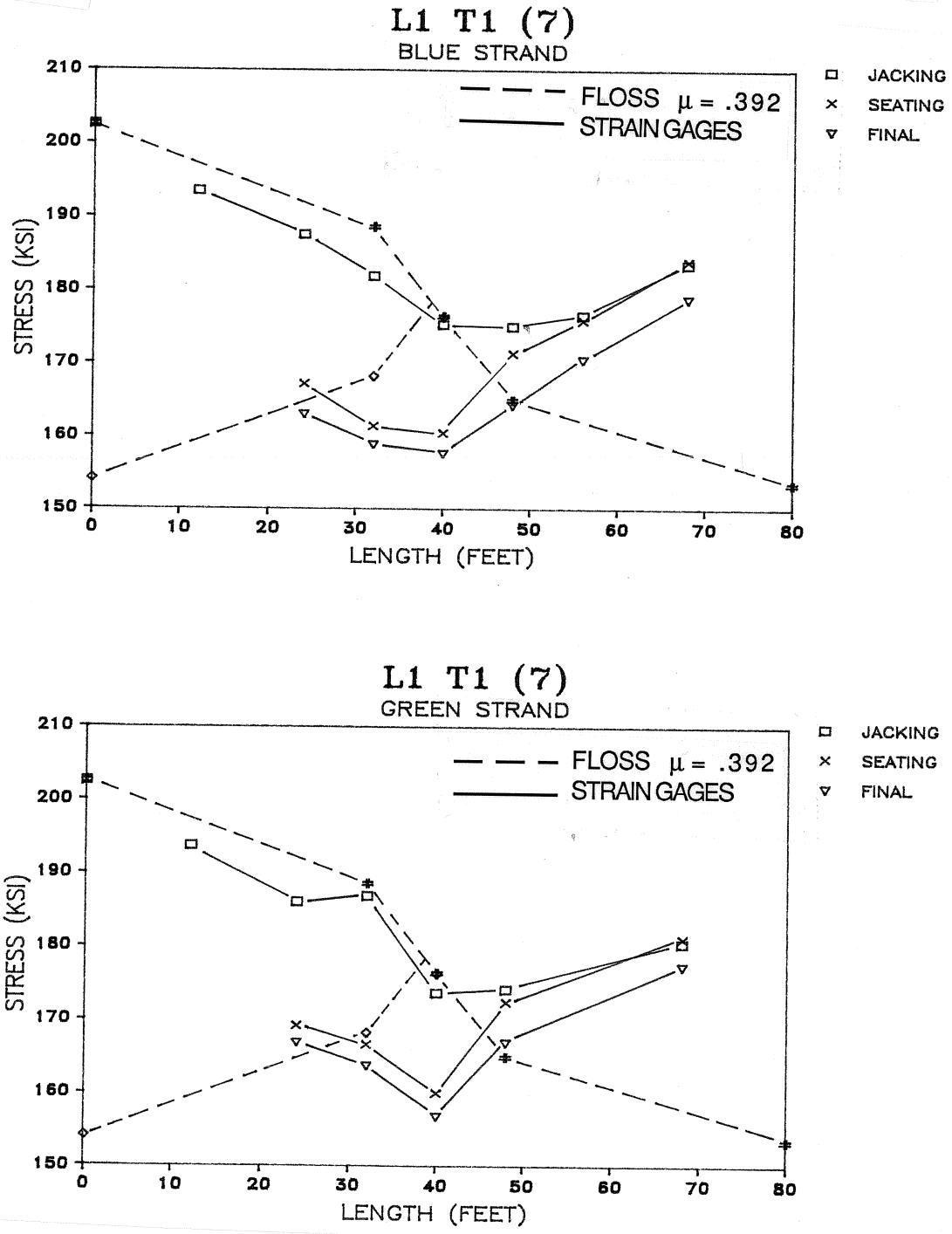

Fig. 4.1a L1 T1 (7): Jacking, seating, and final strand-stress variation

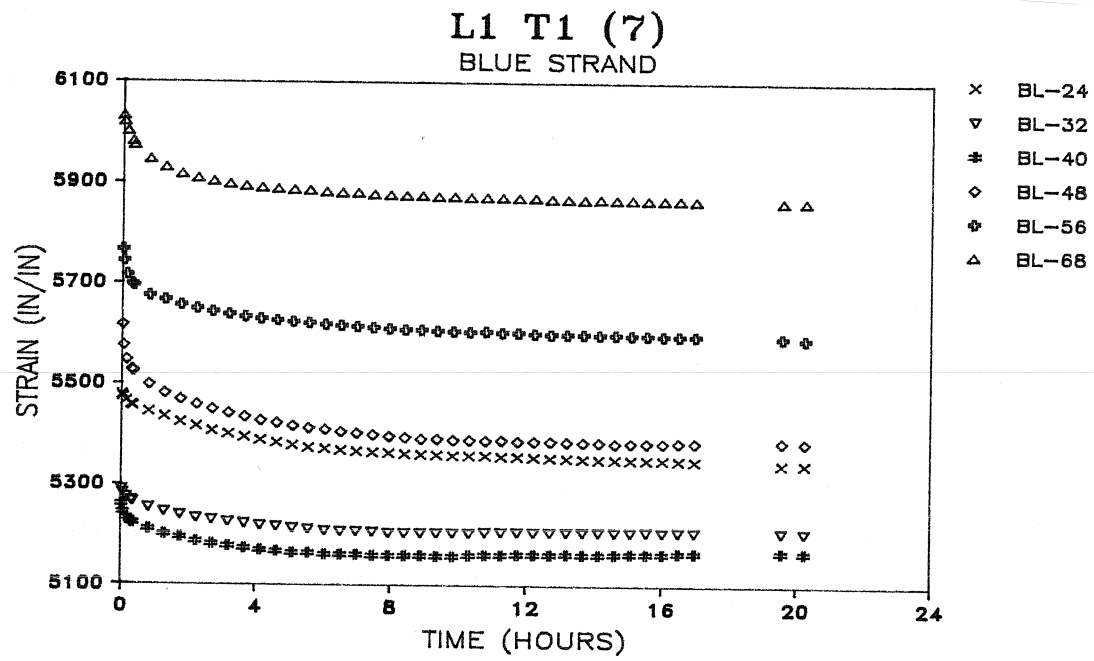

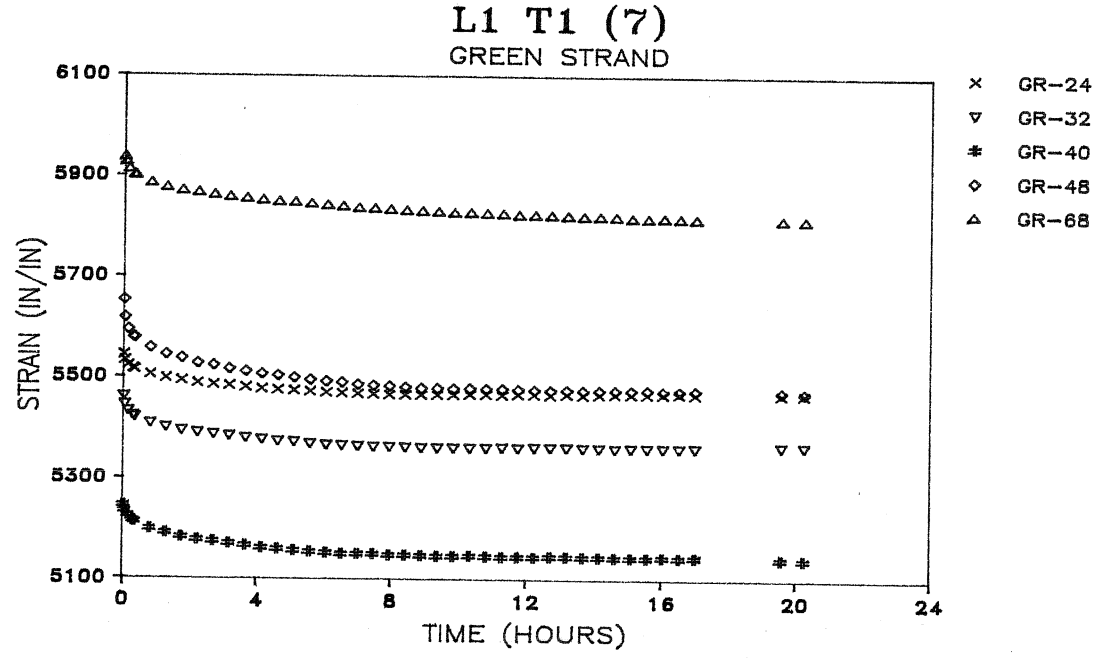

Fig. 4.1b L1 T1 (7): Strain redistribution with time after anchorage seating

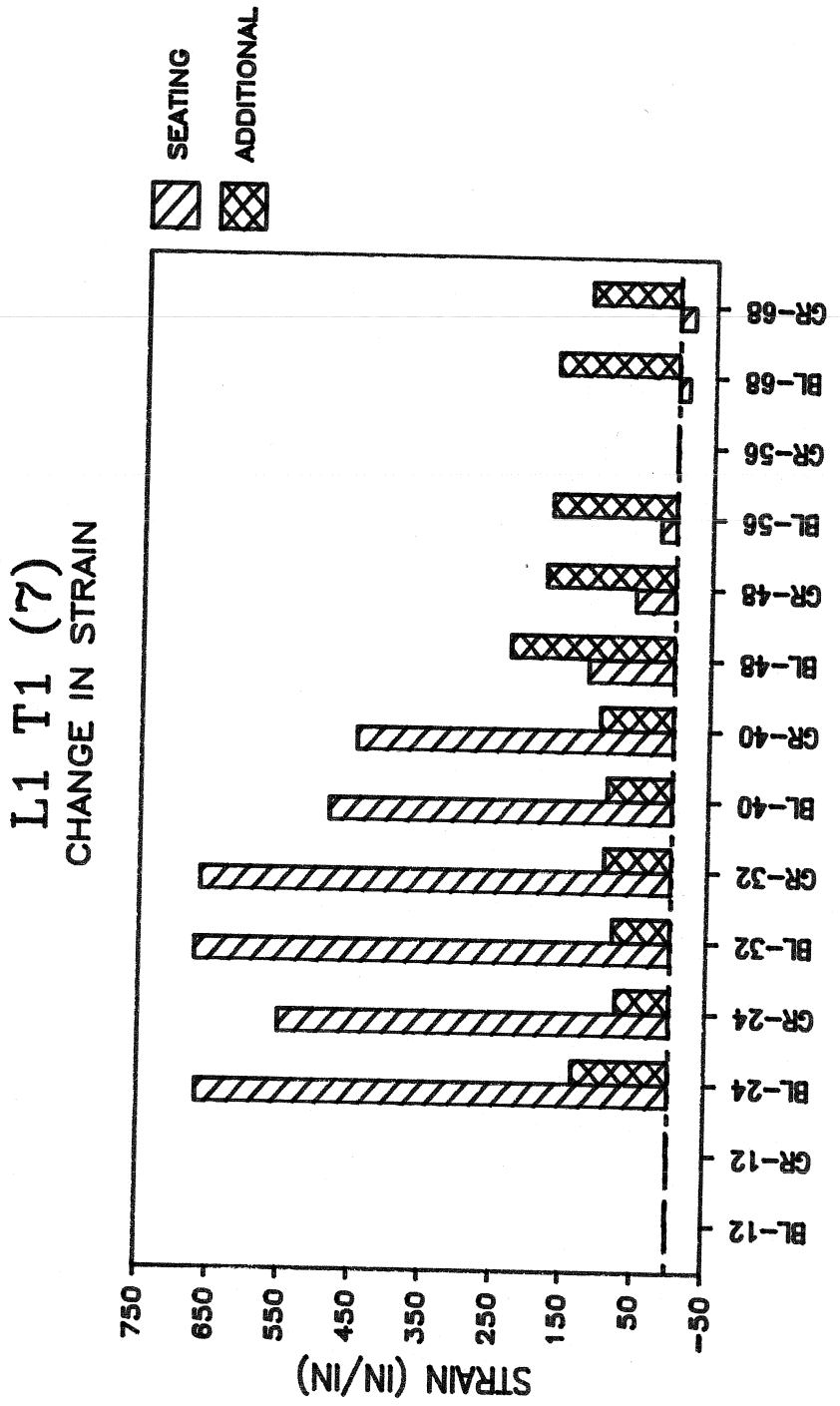

Fig. 4.1c L1 T1 (7): Seating and total-additional strain change

measured changes in strain at each blockout location. The measured strain change in tendons caused by seating is shown as a bar graph along with the additional change for the total monitored time period following seating at each blockout where data were available. A microstrain change of 100 is equivalent to a stress change of 3.05 ksi. Note that during stressing and seating of strands, some strain gages became ineffective thus rendering no useful data information.

Table 4.2 shows the average stress per tendon at the holding end for tests which incorporated a load cell. Excluding L1 T7 (7E), the change in stress following seating was very slight and might be considered negligible. The pattern of the holding end stress was to increase slightly with release of jacking force followed by a small decrease with time. The largest holding end stress decrease following seating was 2.7 ksi; a total reduction of 1.6 percent. This confirms that the rigid body specimen in general experienced little elastic shortening rebound, creep, or shrinkage in the observed time period.

4.3.2 Tendon Profile No.1. Tendon Profile No.1 was characterized by symmetry and a constant radius of curvature. In the first two tests, L1 T1 (7) and L1 T2 (7), tendon strains were monitored approximately every thirty minutes for twenty hours after seating (Figs. 4.1b and 4.2b). In the initial five hours following seating, strains decreased at varying rates between blockouts and accounted for approximately 95% of all additional dropoff. After five hours, strains leveled to a strain equilibrium plateau. Figure 4.1c shows that the largest additional strain losses occurred in the region closest to the holding end: BL-48, GR-48, BL-56, BL-68, and GR-68. Unique to L1 T1 (7), the two instrumented strands had uncommonly high strains following jacking near the holding end leading to the more substantial strain dropoff shown in Fig. 4.1c. More representative for this tendon profile is Fig. 4.2c which indicates additional strain loss was minimal near the ends with the interior region experiencing a larger decrease. Average additional stress loss along the specimen length was approximately 4 ksi and 3 ksi for L1 T1 (7) and L1 T2 (7), respectively.

In comparison with friction loss theory, measured strand stresses did not reproduce exactly the stresses predicted by *FLOSS* (Figs. 4.1a and 4.2a). Also, instrumented strand stresses varied somewhat sporadically from test to test due to frictional effects. In some instances the change in strand stresses measured at distances further from the jacking end were larger than those located at closer stations. For L1 T1 (7), friction caused the stress to decrease comparable to that predicted by theory to the layout between jacking end and midspan (BL-40/GR-40). Beyond that point, between midspan and the holding end, friction does not appear to continue to reduce the stress of the gaged strands. As noted previously, measured strand stresses at BL-68 and GR-68 were 10 ksi larger than at midspan. This apparent increase in stress more than likely can be explained by a faulty strain gage or initially incorrectly setting the gage reading to zero prior to stressing. A similar pattern was repeated for L1 T2 (7) except that stresses at BL-68 and

Test	Jacking Stress (ksi)	Seating Stress (ksi)	Final Stress (ksi)	Stress Change After Seating (ksi)
L1 T1 (7)	153.5	155.0	154.6	- 0.4
L1 T2 (7)	152.8	154.3	153.9	- 0.4
L1 T3 (7)	155.8	156.0	154.2	- 1.8
L1 T7 (7E)	140.1	139.5	125.1	-14.1
L2 T1 (7)	155.5	155.9	154.0	- 1.9
L2 T2 (7)	154.9	156.5	156.3	- 0.2
L2 T4 (7)	162.9	164.2	161.5	- 2.7
L2 T6 (2)	160.0	161.0	163.0	+ 2.0
L3 T1 (7)	118.7	118.9	118.7	- 0.2
L3 T2 (7)	110.8	113.0	113.7	+ 0.7
L3 T5 (2)	138.6	139.8	140.8	+ 1.0

Table 4.2 Load Cell Holding End Stress

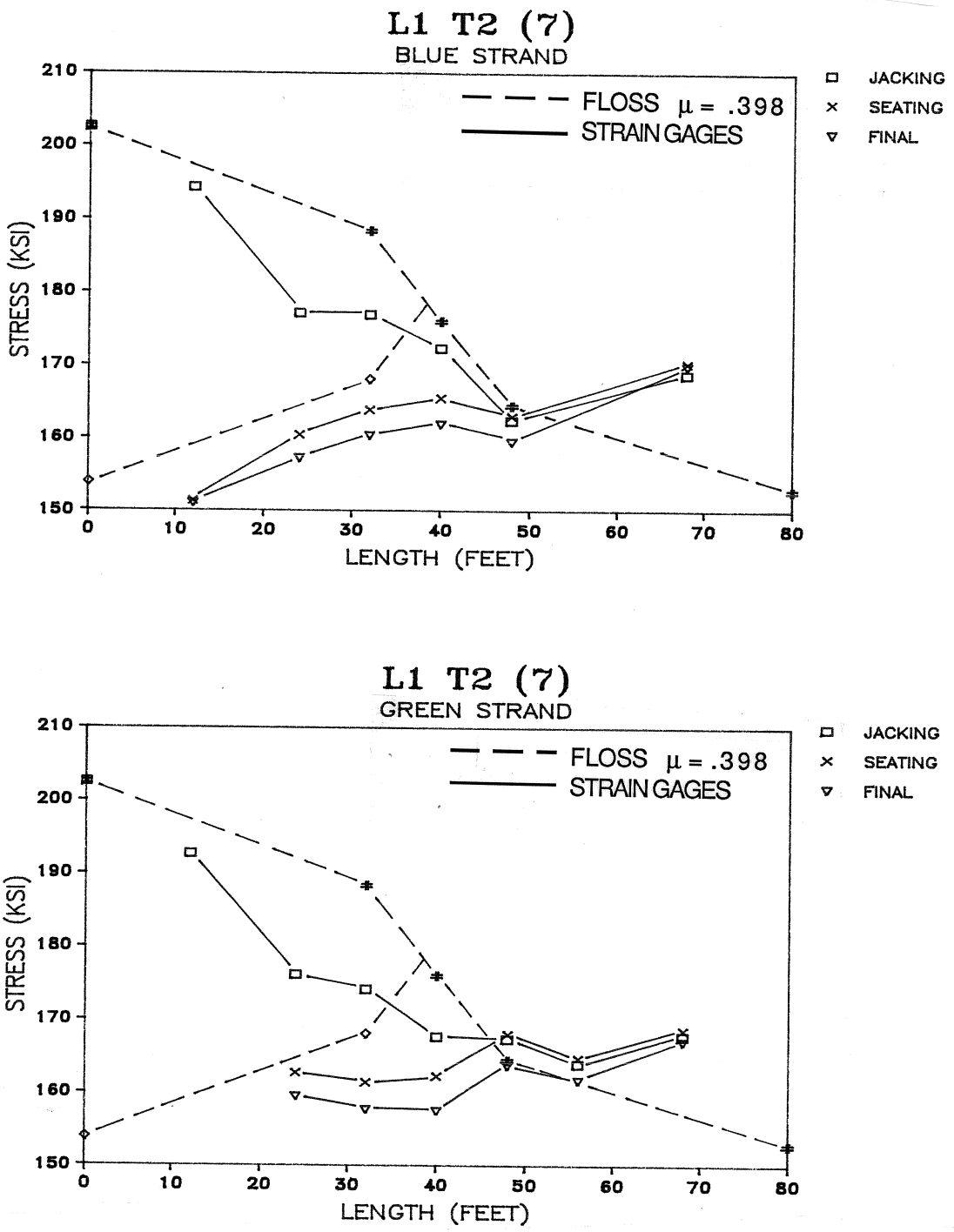

Fig. 4.2a L1 T2 (7): Jacking, seating, and final strand-stress variation

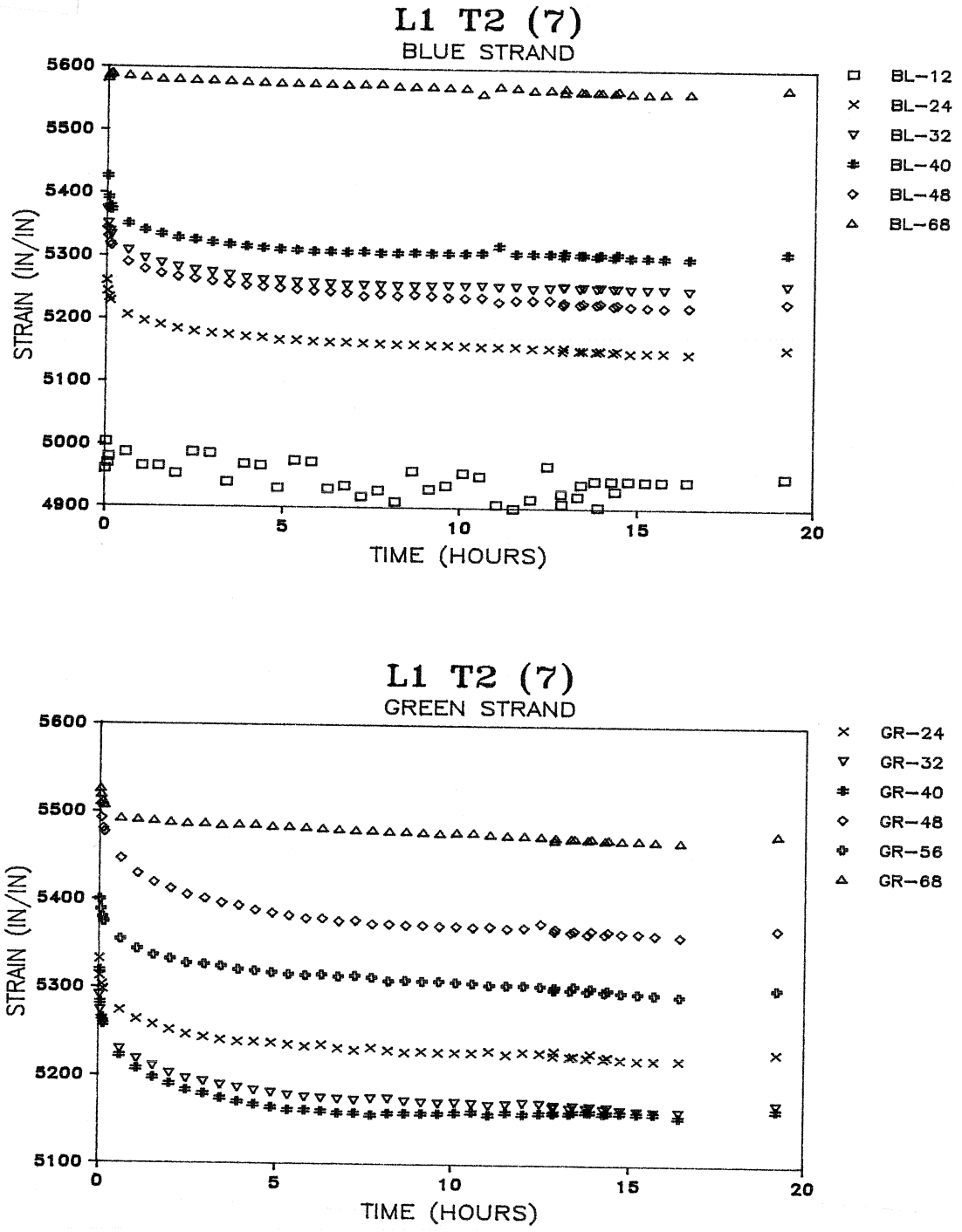

Fig. 4.2b L1 T2 (7): Strain redistribution with time after anchorage seating

GR-68 were approximately equal or slightly less than midspan. Thus, a uniform friction effect is not prevalent in the measured data between jacking and holding ends.

Upon anchorage seating, transfer decreased the strains 48 ft into the layout, 10 ft further than *FLOSS* predicted. Also, seating did not produce the theoretical sharp peak at midspan. Unlike jacking which is a gradual and consistently applied change in force, the transfer of force from pulling block to permanent anchor head is a sudden release of energy. For seven strands at $.75f_{pu}$, the released jacking force is equivalent to 217 kips. This force transfer induces and transmits a compressional wave force which propagates into the layout. The compressional wave is resisted by and consequently dampened by friction and strand stiffness as it propagates through the layout until completely damped. Also, as the layout path changes from a negative to positive slope or vice versa, the compressional wave is further damped as it is carried around the conduit curvature. This compressive wave increases strand slippage against the resistive friction force, leveling strand stresses up to the point where wave propagation ceased. If the jacking force were gradually released, then the anchor set curve of negative friction would correspond to the mirror image of the friction curve as is usually assumed. Instead, seating tended to equalize tendon stresses along layout length. Therefore, anchorage transformation losses as a result of sudden release appear to have a significant impact on the redistribution of tendon stresses initially varied by friction.

Again, tendon stresses decreased slightly in the monitored time period following seating but redistribution was minimal along profile length. The normal force and friction interaction between strands and conduit combined together to lock the strands in place. Further stress loss is a result primarily of strand relaxation plus minor creep and shrinkage effects.

L1 T3 (7) and L1 T4 (7) were monitored for longer periods of time following seating, 186 and 124 hours, respectively. Results were very similar to the previous two tests. Total additional stress loss averaged 5.3 and 3.8 ksi in the monitored time period with midspan stresses decreasing a slightly larger amount than the end stresses (Figs. 4.3c and 4.4c). As before, the majority of stress loss occurred in the initial five hours. Figures 4.3a and 4.4a show that the additional stress loss between seating and final stages can be approximated as uniform along the length with minimal redistribution. Also apparent is the absence of a predicted peak of high stress resulting from anchorage seating at midspan. Rather, transformation losses redistributed and equalized strand stresses to BL-48/GR-48 as observed earlier. Figures 4.3c and 4.4c show measured strand change caused by seating. The amount of change was dependent upon final jacking stress, relative position to the seating end, and the compressional wave leveling effect during transfer as discussed above.

Test results for L1 T5 (4) and L1 T6 (2), with reduced strand numbers, had a few

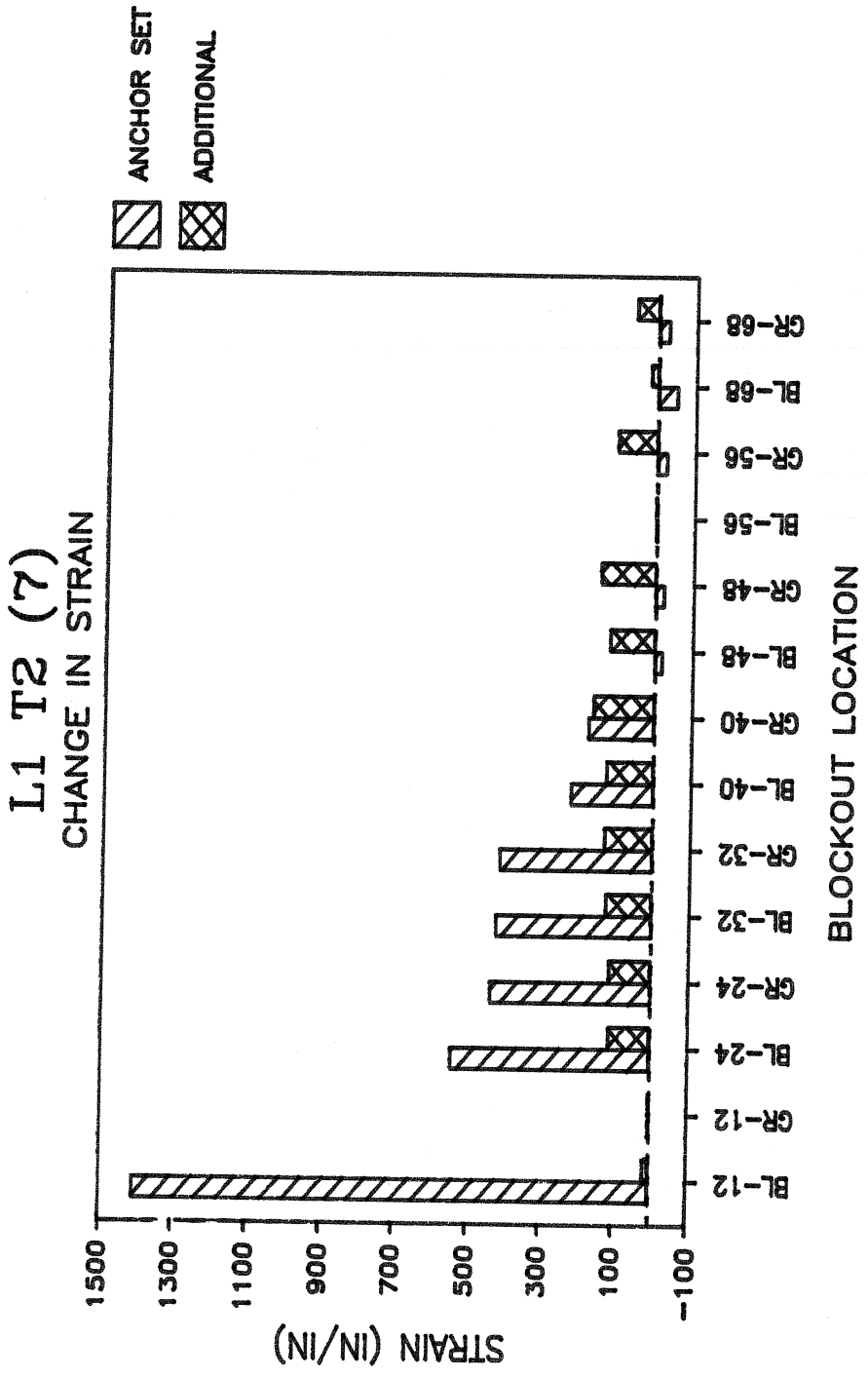

Fig. 4.2c L1 T2 (7): Seating and total- additional strain change

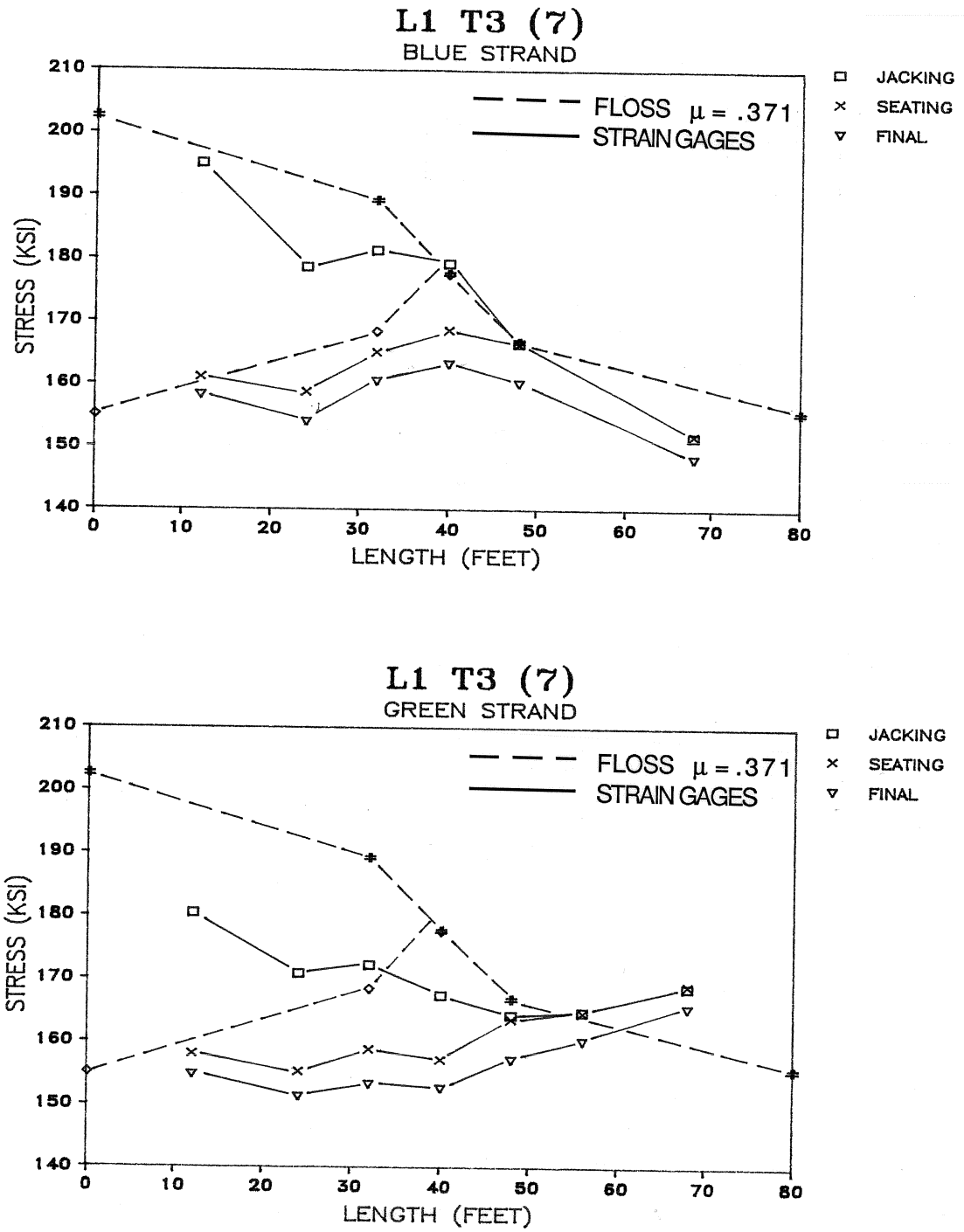

Fig. 4.3a L1 T3 (7): Jacking, seating, and final strand-stress variation

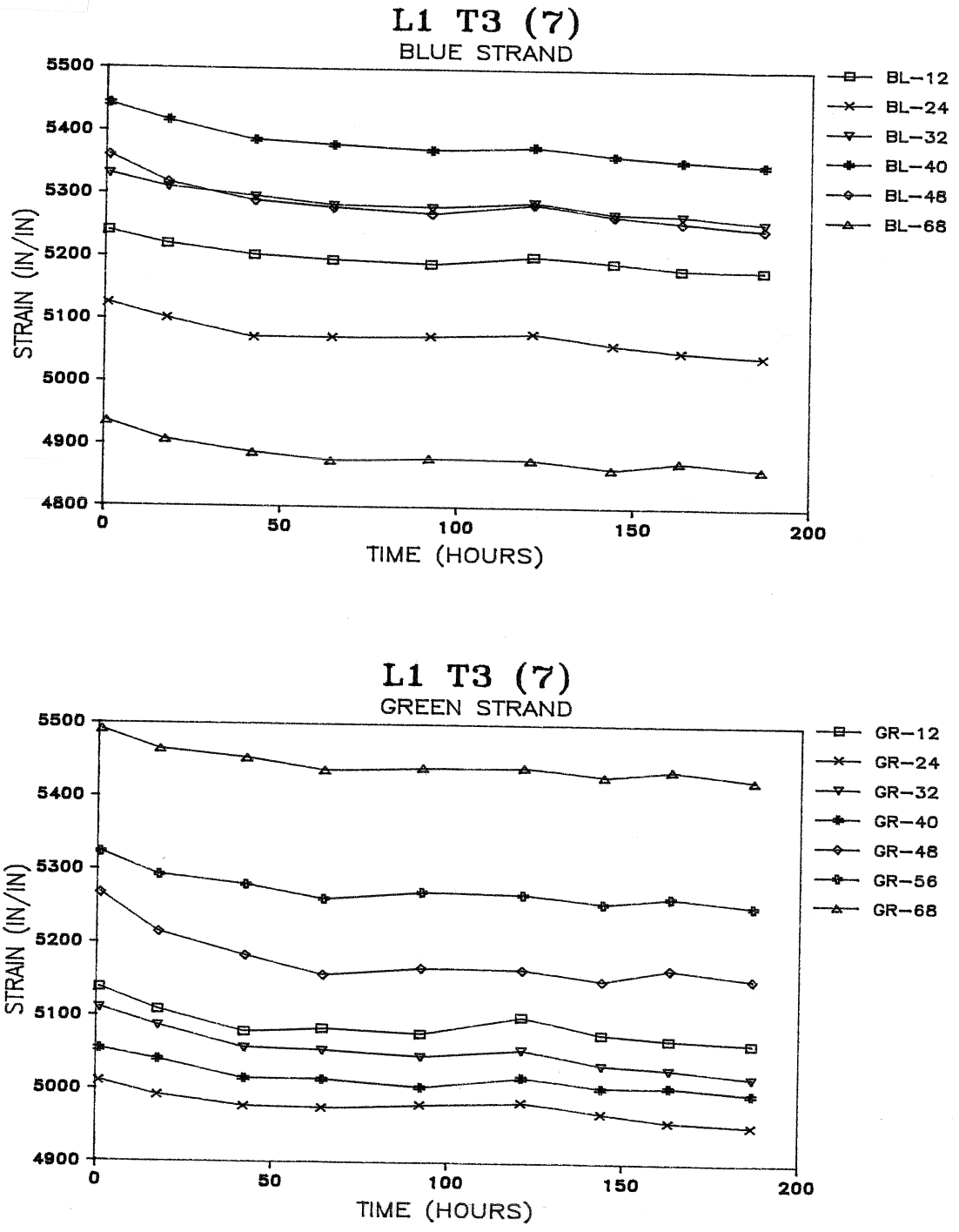

Fig. 4.3b L1 T3 (7): Strain redistribution with time after anchorage seating

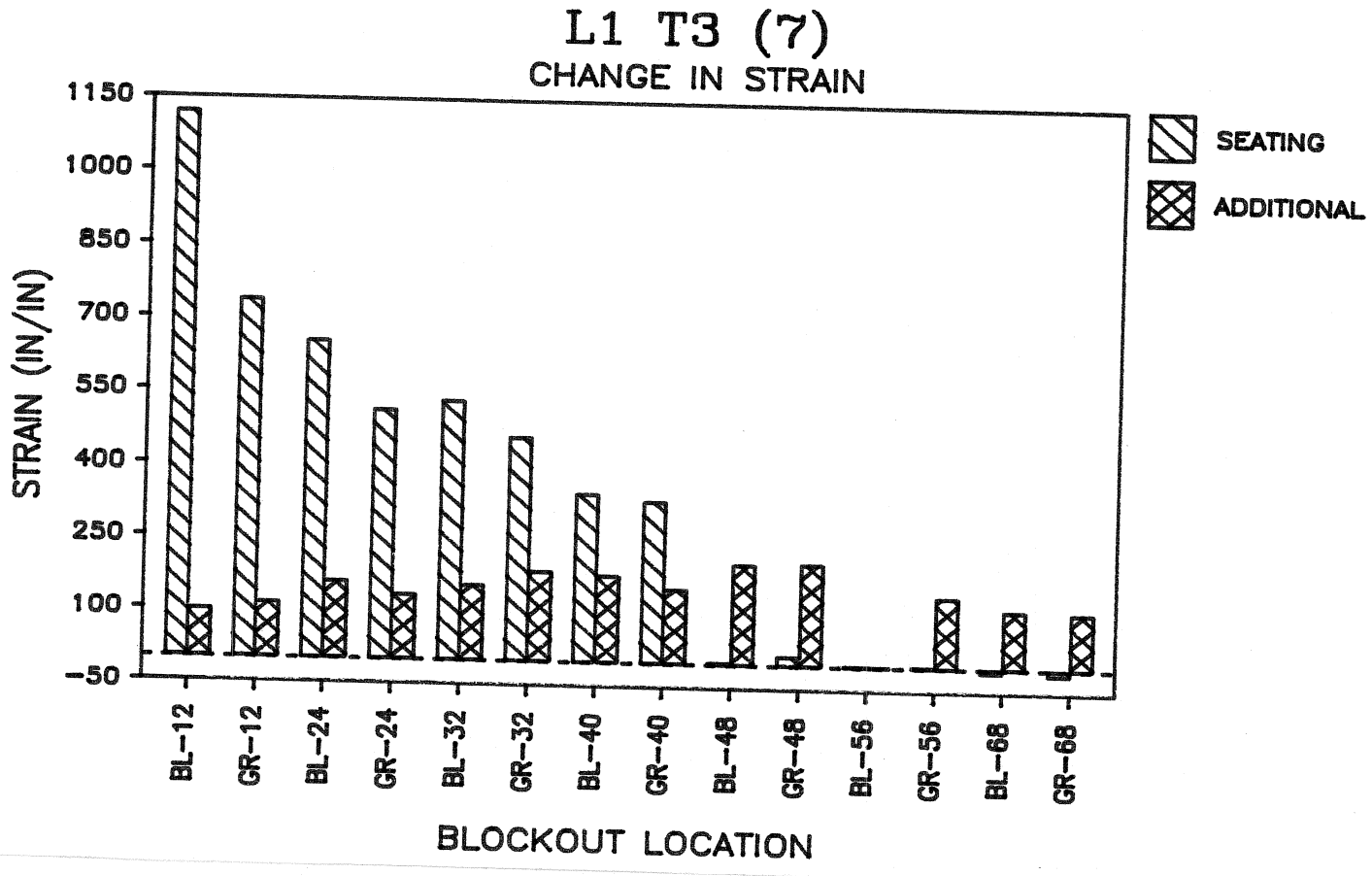

Fig. 4.3c L1 T3 (7): Seating and total additional strain change

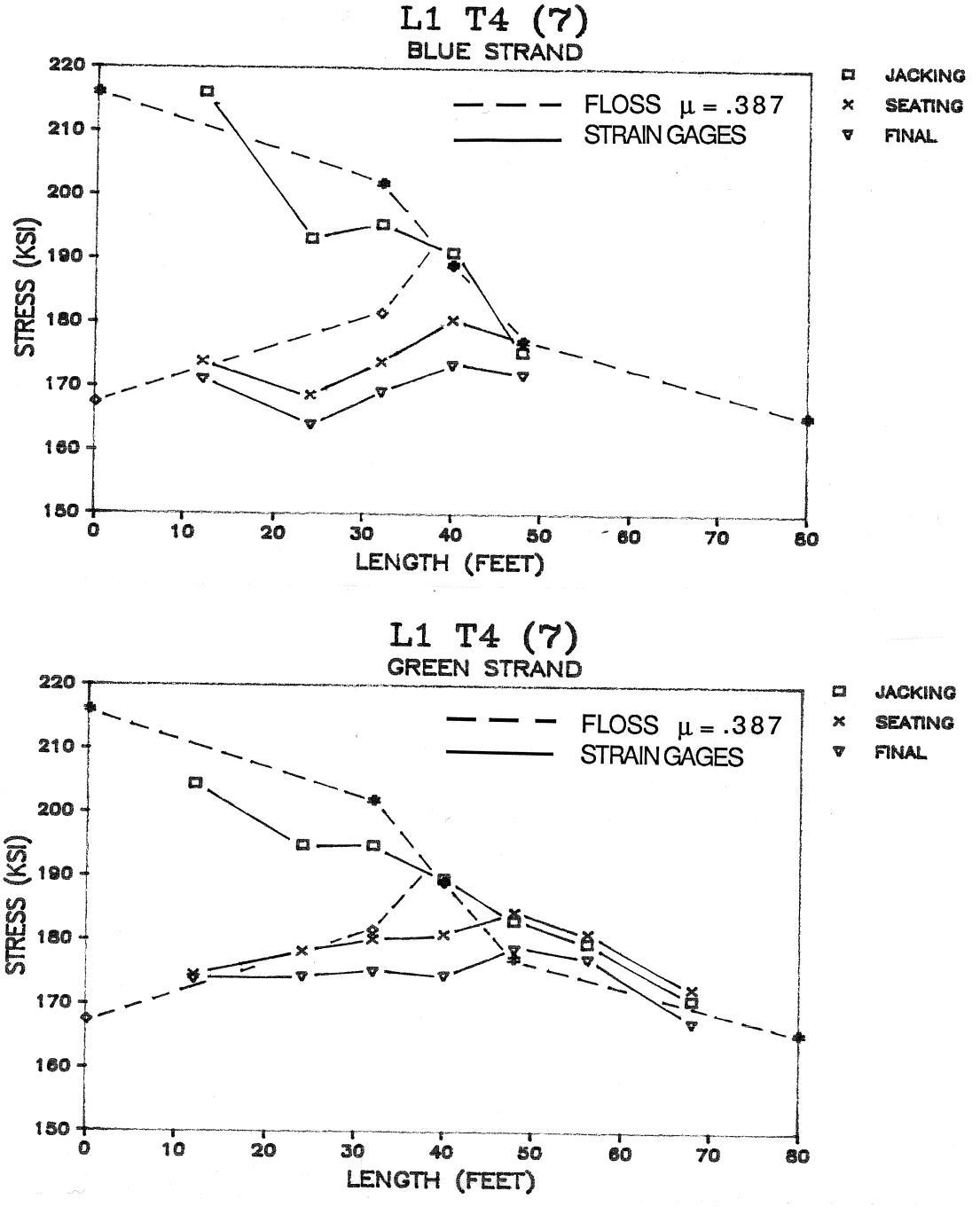

Fig. 4.4a L1 T4 (7): Jacking, seating, and final strand-stress variation

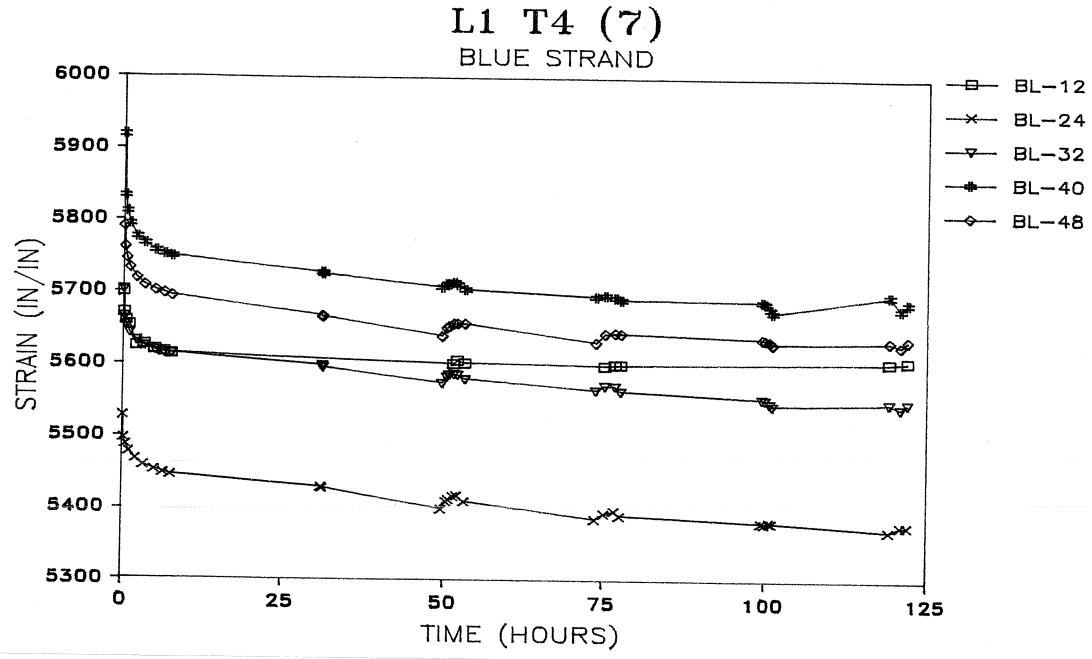

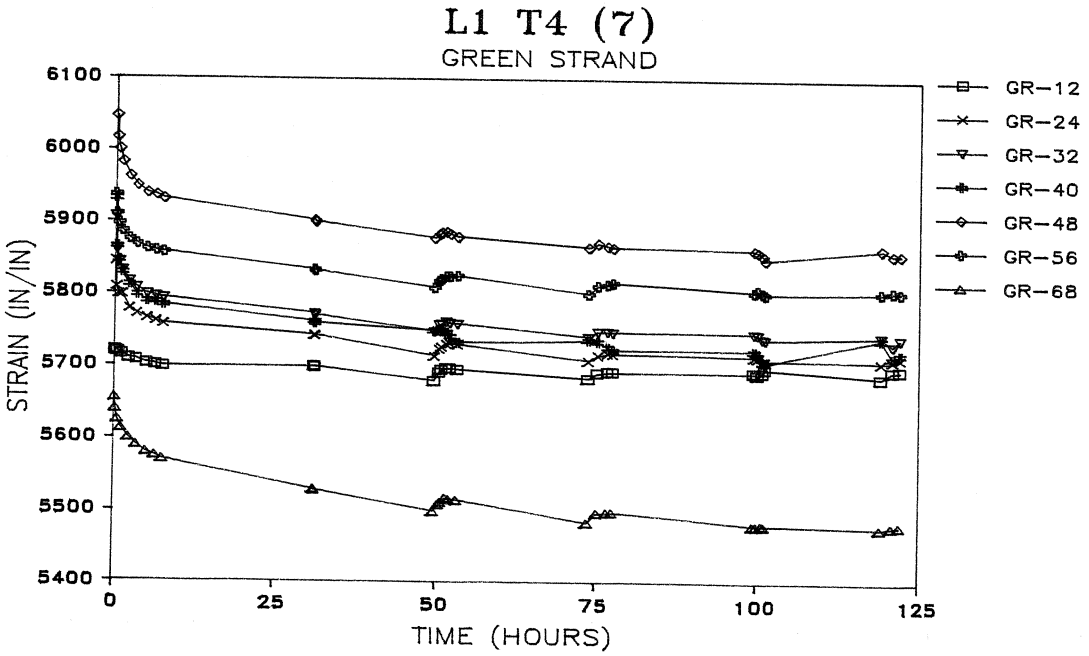

Fig. 4.4b L1 T4 (7): Strain redistribution with time after anchorage seating

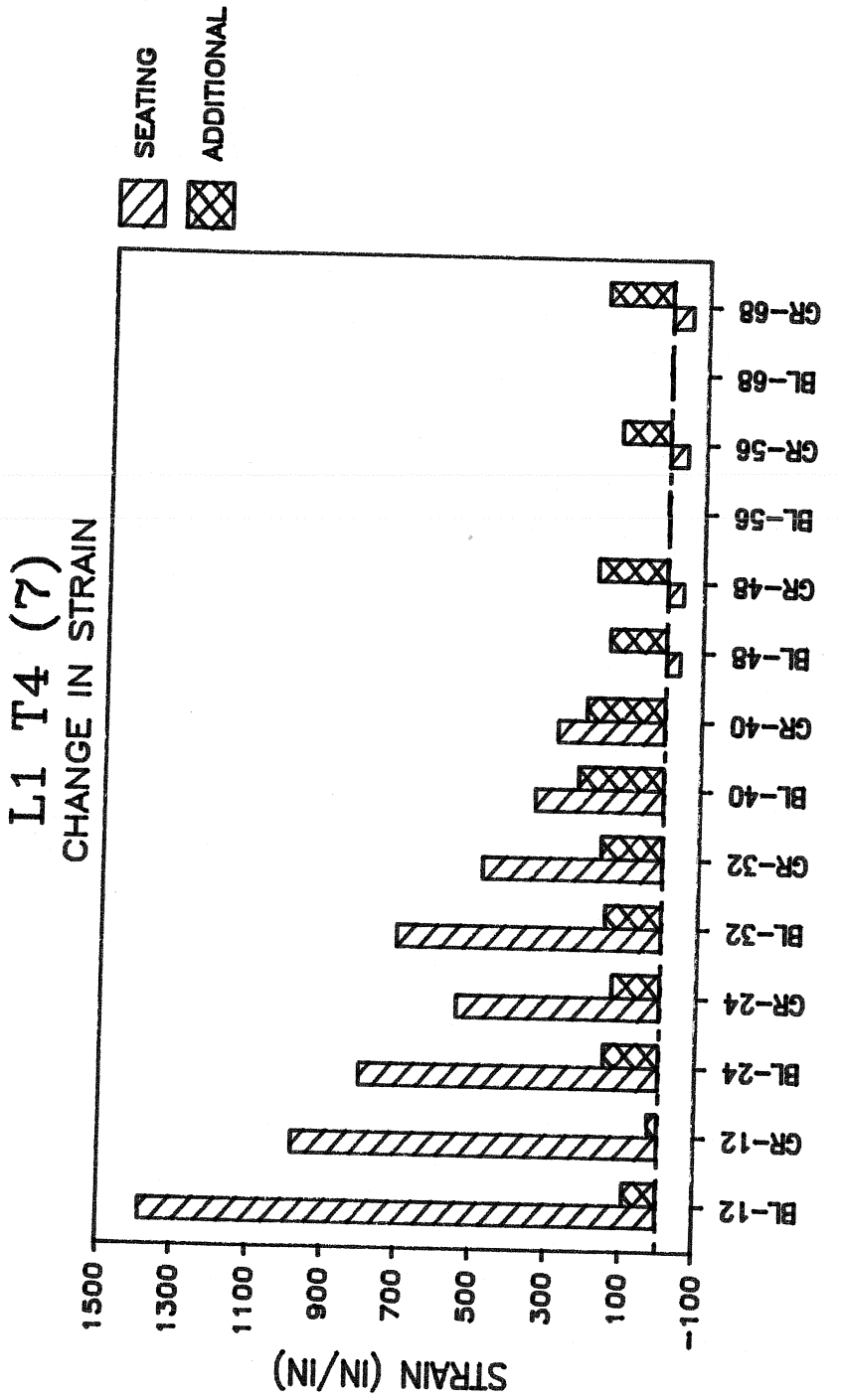

Fig. 4.4c L1 T4 (7): Seating and total additional strain change

notable differences from the 7 strand tests. Chiefly, tendon stresses were reduced along the entire layout by friction (Figs. 4.5a and 4.6a). Stresses measured at BL-68/GR-68 instead of being approximately equal to those at midspan (BL-40/GR-40) were more comparable to stresses predicted by *FLOSS*. This can be attributed to the fact that both instrumented strands were almost exclusively in contact with the conduit as opposed to contact with both surrounding strands and conduit with seven strands. For both tests, the seating loss curve intersected the friction loss curve at a distance 48 ft into the layout. Again for L1 T5 (4), anchorage seating leveled the tendon stresses to blockouts BL-48 and GR-48 although the 'green' strand displayed a sharp peak stress at GR-48 (Fig. 4.5a). But for L1 T6 (2), anchorage seating did not equalize to the magnitude of the 4 and 7 strand tests. In this case, friction resistance between strand and conduit reduced stress redistribution during seating. Also, the compressional wave force was not as significant because with fewer strands, the hydraulic ram was resisting a lower jacking pressure upon release. Hence, during transformation the internal ram resistance was more capable of gradually transferring the jacking force of two strands in comparison to seven strands.

Following seating, L1 T5 (6) and L1 T6 (2) were observed for 139 and 71 hours and experienced an additional stress loss of 4.5 and 4 ksi, respectively. These additional loss values were comparable to the 7 strand tests. Absence of a normal force from surrounding strands did not increase redistribution of strand stresses between blockouts. Following the pattern observed in previous tests, additional change in strain was largest in the midspan region with little observable change in the end regions (Figs. 4.5c and 4.6c).

To summarize test results for the symmetrical Tendon Profile No.1, the friction coefficient was consistently measured around .390. This value is 1.5 times the recommended value of 0.25. Although unusually large, no single reason reasonably explains the larger friction coefficient. Upon anchorage seating transfer, the seating loss curve intersected the friction loss curve at a distance 48 ft into the layout in every test. Furthermore, anchorage seating redistributed and leveled tendon stresses to the point of intersection. Additional average tendon strain losses ranged from 3 to 5 ksi with the majority of the additional losses occurring in the initial 5 hours following seating. In the time period following seating and prior to grouting, no further redistribution or equalization of strand stresses occurred. Based upon the results for Tendon Profile No.1, an average tendon stress would be a reasonable assumption for design along the 80-ft length.

4.3.3 Tendon Profile No.2. In contrast to the symmetrical layout in Tendon Profile No.1, Tendon Profile No.2 was characterized by a sharp increase in tendon curvature in the last 26 ft at the holding end. Again, during jacking, friction did not uniformly nor consistently reduce the measured tendon stresses over the entire length in accordance with friction loss theory. Two instrumented strands, even in the same test, displayed a different frictional stress loss reduction between blockouts. Overall frictional loss for all seven strands as a group closely approximated

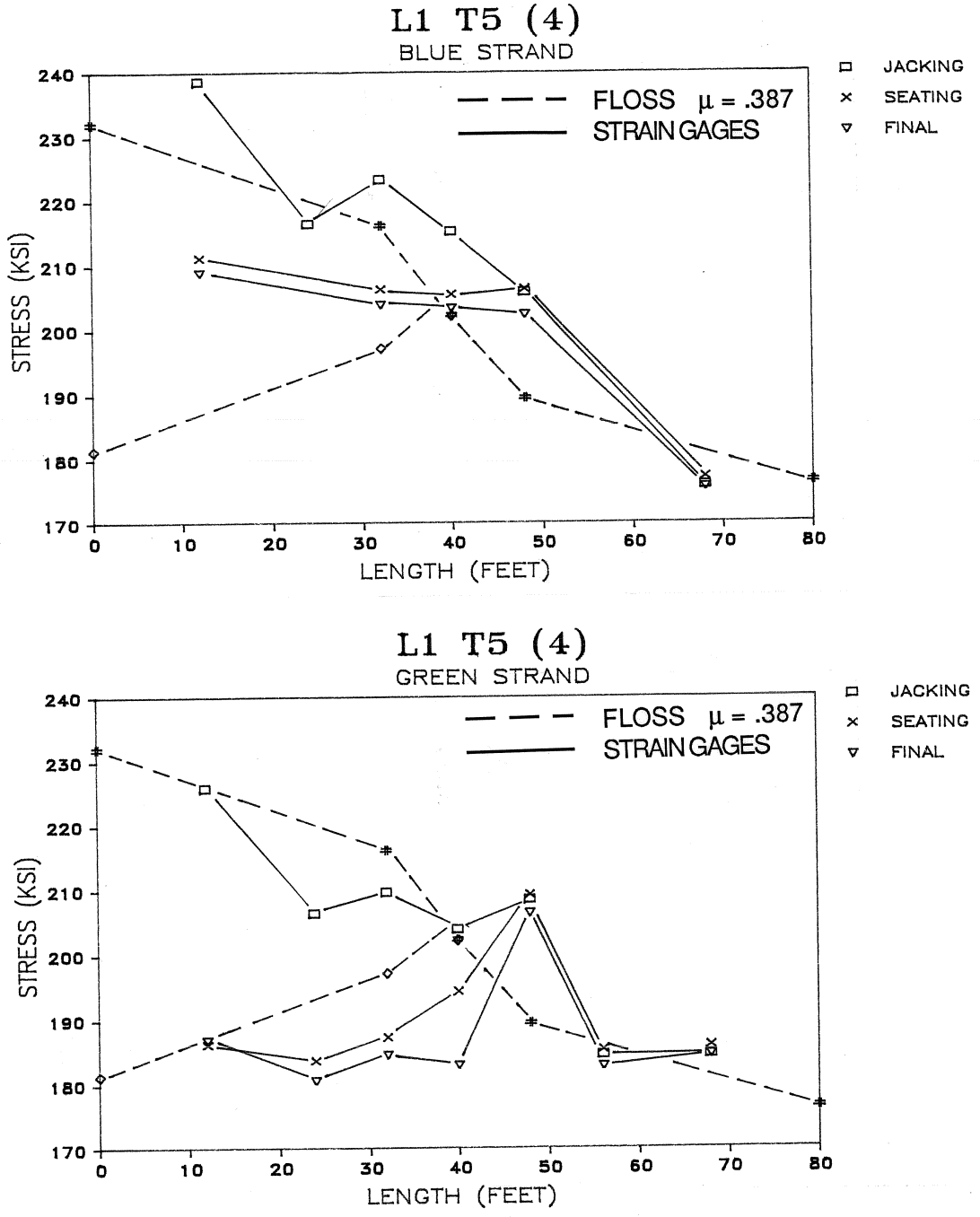

Fig. 4.5a L1 T5 (4): Jacking, seating, and final strand-stress variation

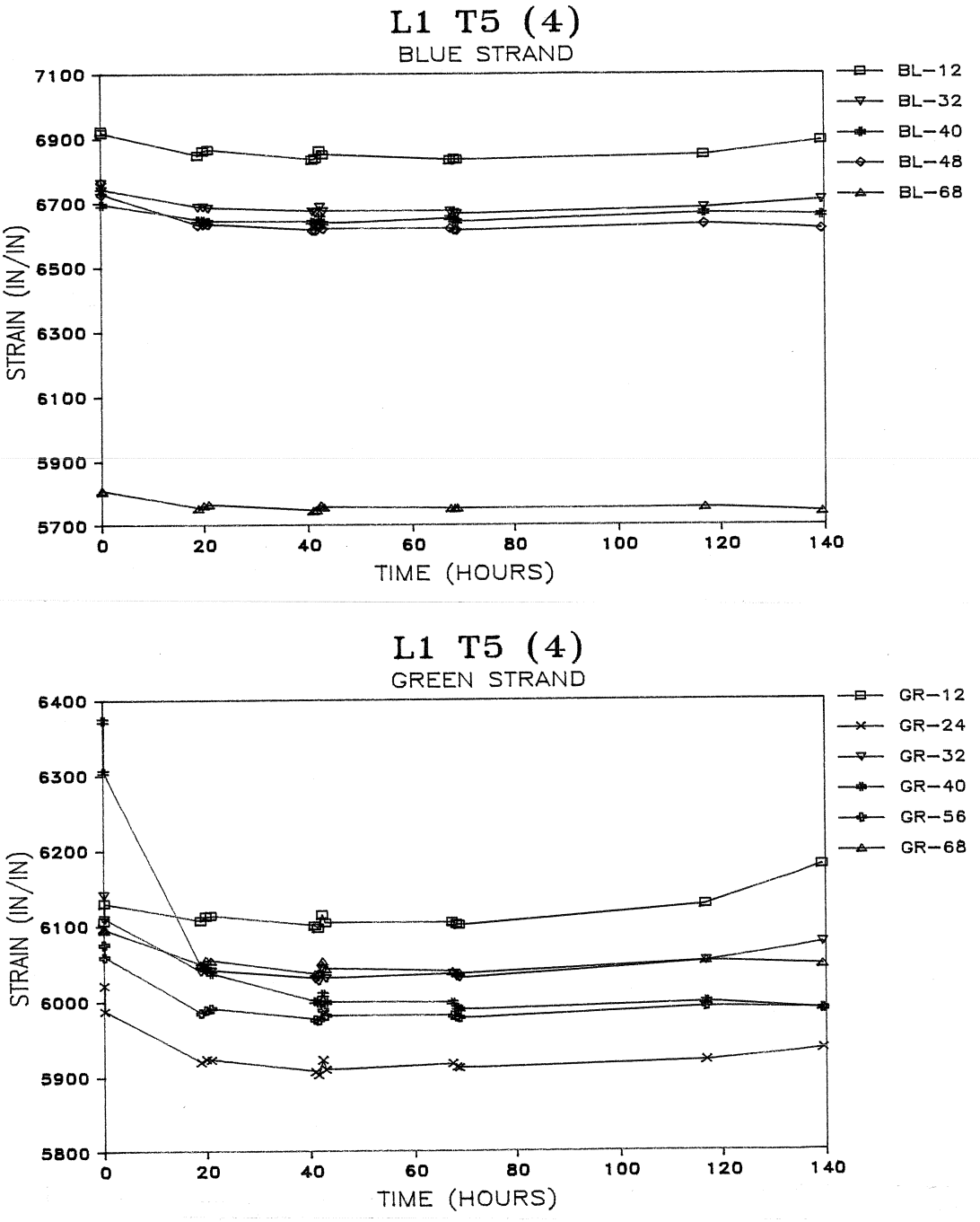

Fig. 4.5b L1 T5 (4): Strain redistribution with time after anchorage seating

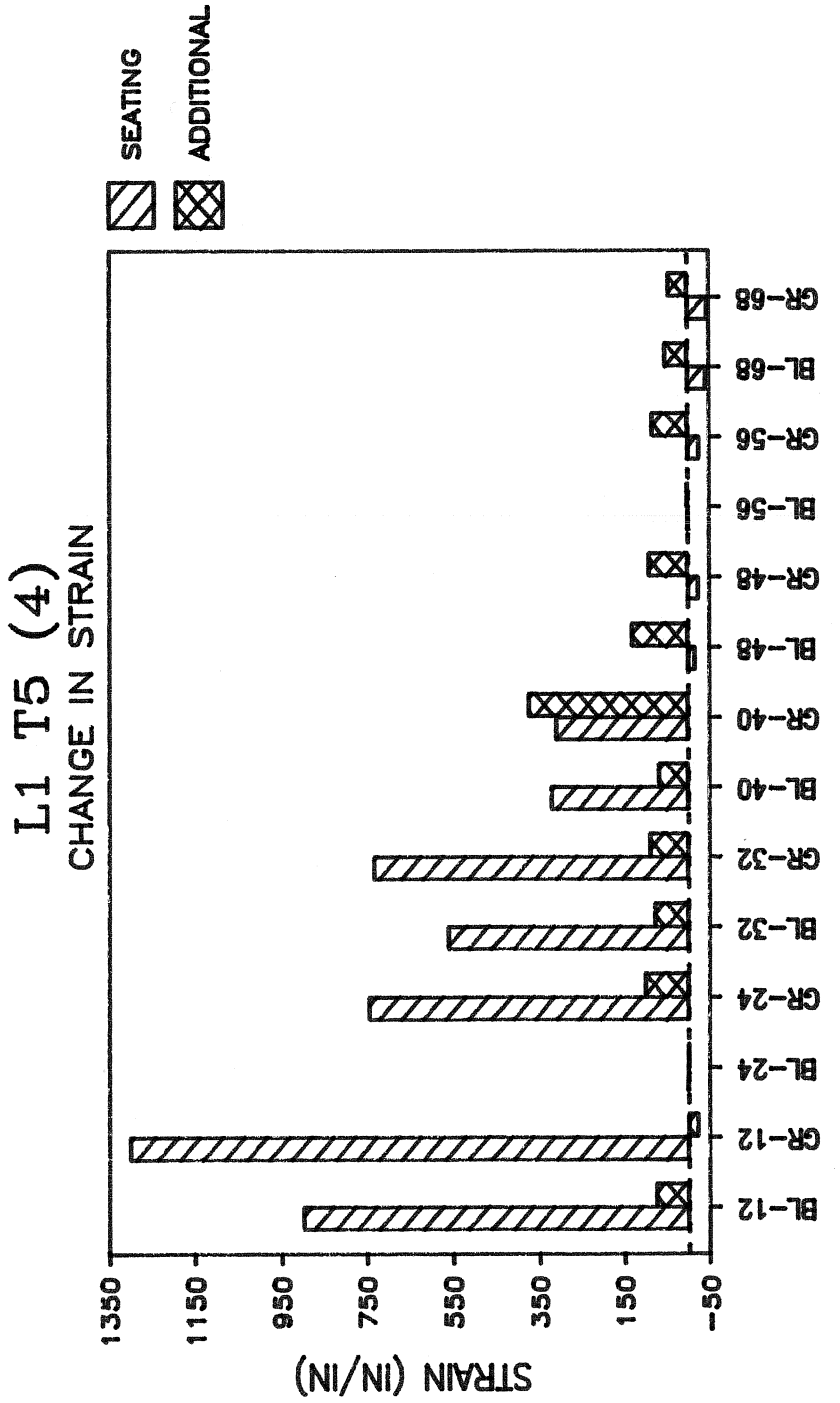

Fig. 4.5c L1 T5 (4): Seating and total additional strain change

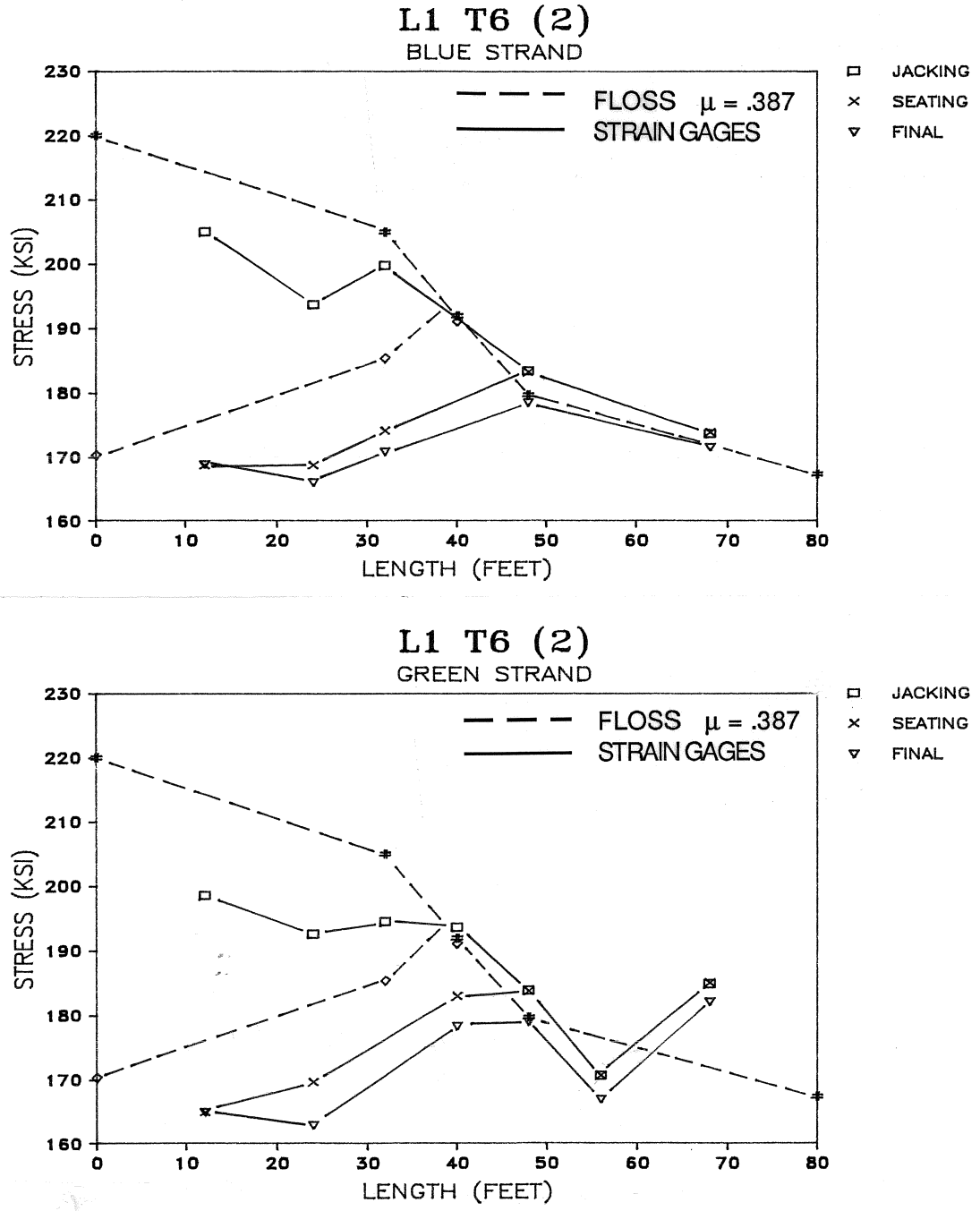

Fig. 4.6a L1 T6 (2): Jacking, seating, and final strand-stress variation

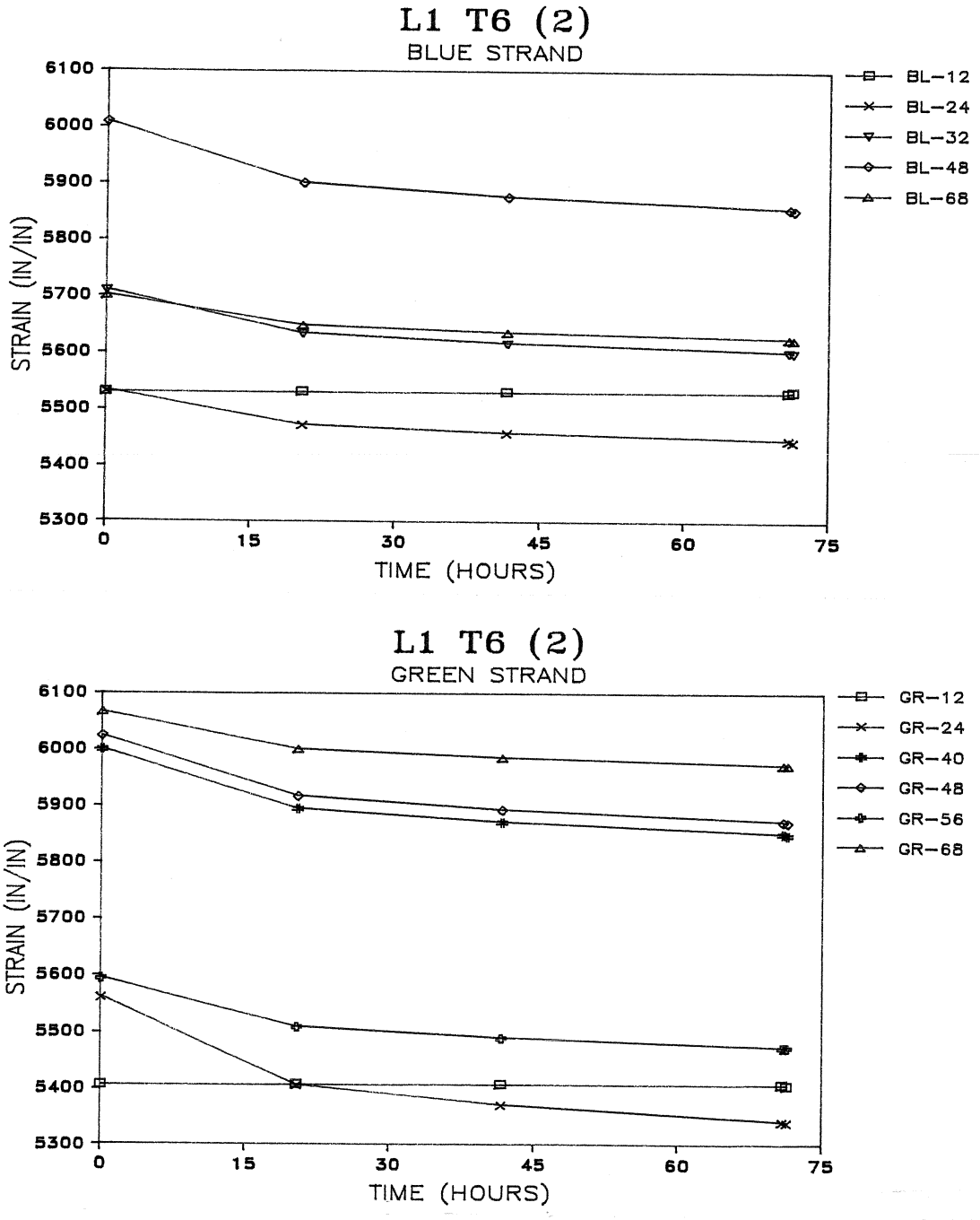

Fig. 4.6b L1 T6 (2): Strain redistribution with time after anchorage seating

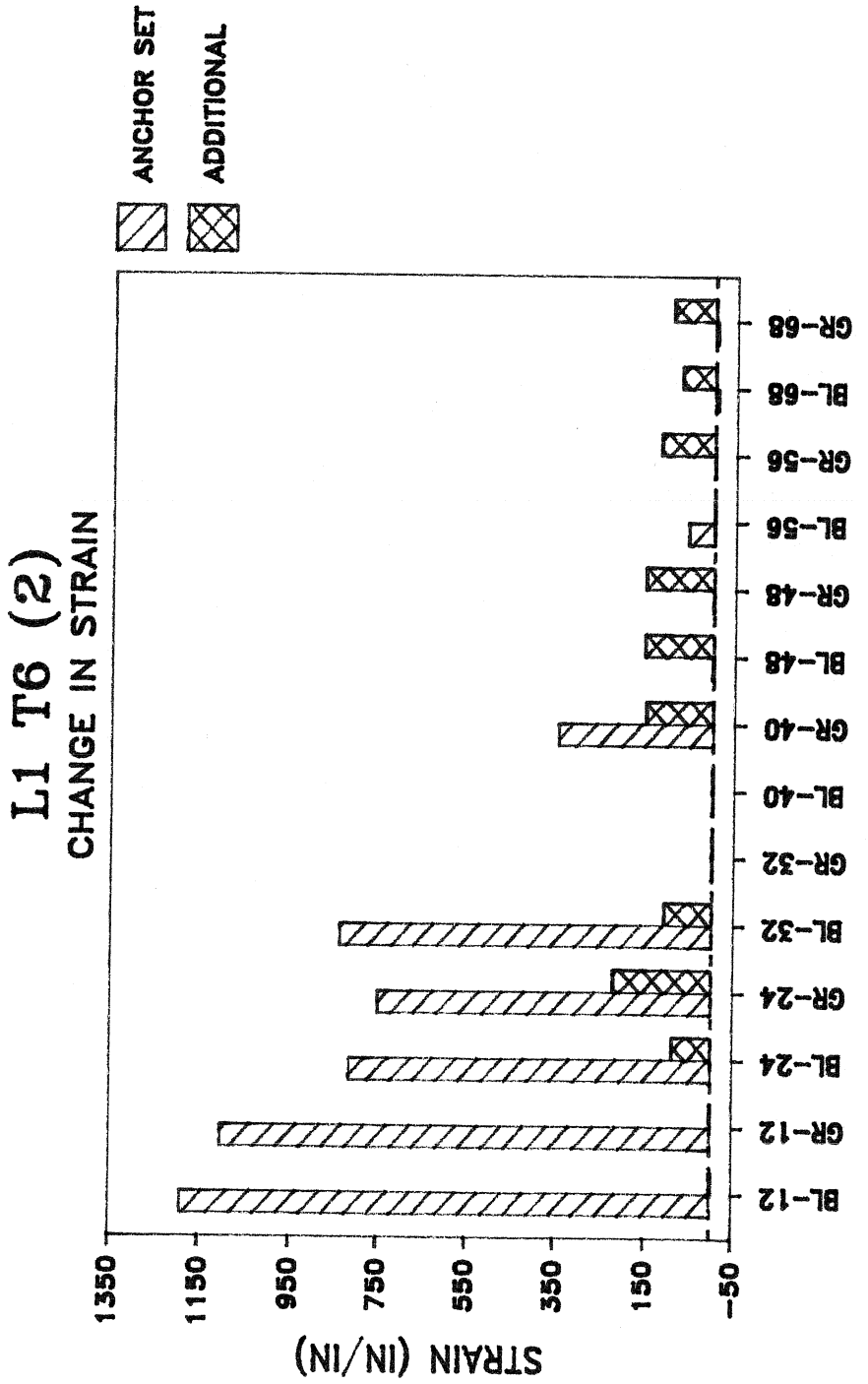

Fig. 4.6c L1 T6 (2): Seating and total additional strain change

those expected as the measured friction coefficient ranged from .25 to .29 for this layout. In comparison with *FLOSS* stresses, measured stresses generally were less than predicted especially in the 54 ft closest to the jacking end. But characteristic to all tests, the larger radius of curvature near the holding end (54 to 80 ft) significantly decreased strand stresses.

Figures 4.7a and 4.8a show the strand stresses for L2 T1 (7) and L2 T2 (7). In some regions, measured strand stress and/or slope of stress loss were almost identical to those predicted by *FLOSS*. But actual stresses varied widely; each strand proving to be unique. Based upon a 0.5-in. seating transformation, *FLOSS* predicts that the anchor set curve intercepts the friction curve 48 ft into the layout. An anchorage seating loss for L2 T1 (7) was observable to BL-54/GR-54 and effectively leveled strand stresses to that blockout. This equalization effect was not as apparent for L2 T2 (7). Here, anchorage seating loss was detected to BL-46/GR-46 yielding peaks and valleys of high and low stress regions. For these tests, the high stress region generally coincided between BL-46/GR-46 and BL-54/GR-54 for two reasons: 1.) the anchor set curve intercepts the friction curve in this region, and 2.) the radius of curvature became larger beginning at that point.

Following seating, the monitored time periods for L2 T1 (7) and L2 T2 (7) were quite short; 17.6 and 3 hours, respectively. Figures 4.7b and 4.8b show that again the majority of strand strain dropoff occurred within the initial five hours immediately following seating and following that time a strain equilibrium was achieved. For L2 T1 (7), average additional stress dropoff along the layout was 3.8 ksi and 2.4 ksi for L2 T2 (7). Measured strain change at each blockout (Figs. 4.7c and 4.8c) appeared more scattered but uniform. That is, no distinguishable pattern developed as for Tendon Profile No.1. The amount of additional strain change was independent of the relative blockout location yet no significant redistribution tendencies with time were observable.

Tests L2 T3 (7) and L2 T4 (7) were monitored for much longer time periods following seating, 572 and 124 hours, respectively. Test results were repetitive of the previously described tests except that the amount of additional strain loss increased slightly. Additional losses averaged 6.8 and 6.1 ksi which corresponded to a stress dropoff of 4.0%. Figure 4.9b shows that at approximately 180 hours for L2 T3 (7), strain equilibrium becomes altered but to a lesser magnitude and low stresses were redistributed and equalized. After jacking and seating (Figs. 4.9a and 4.10a), measured strand stresses generally fell below the predicted theoretical *FLOSS* stresses. Final strand stresses showed a high stress peak at BL-60, GR-60, BL-54, and GR-60. Anchorage losses appreciably leveled strand stresses to the intersection of the friction and anchor set curves. Anchorage seating loss progressed to BL- 54/GR-54 and BL-46/GR-46 for L2 T3 (7) and L2 T4 (7), respectively.

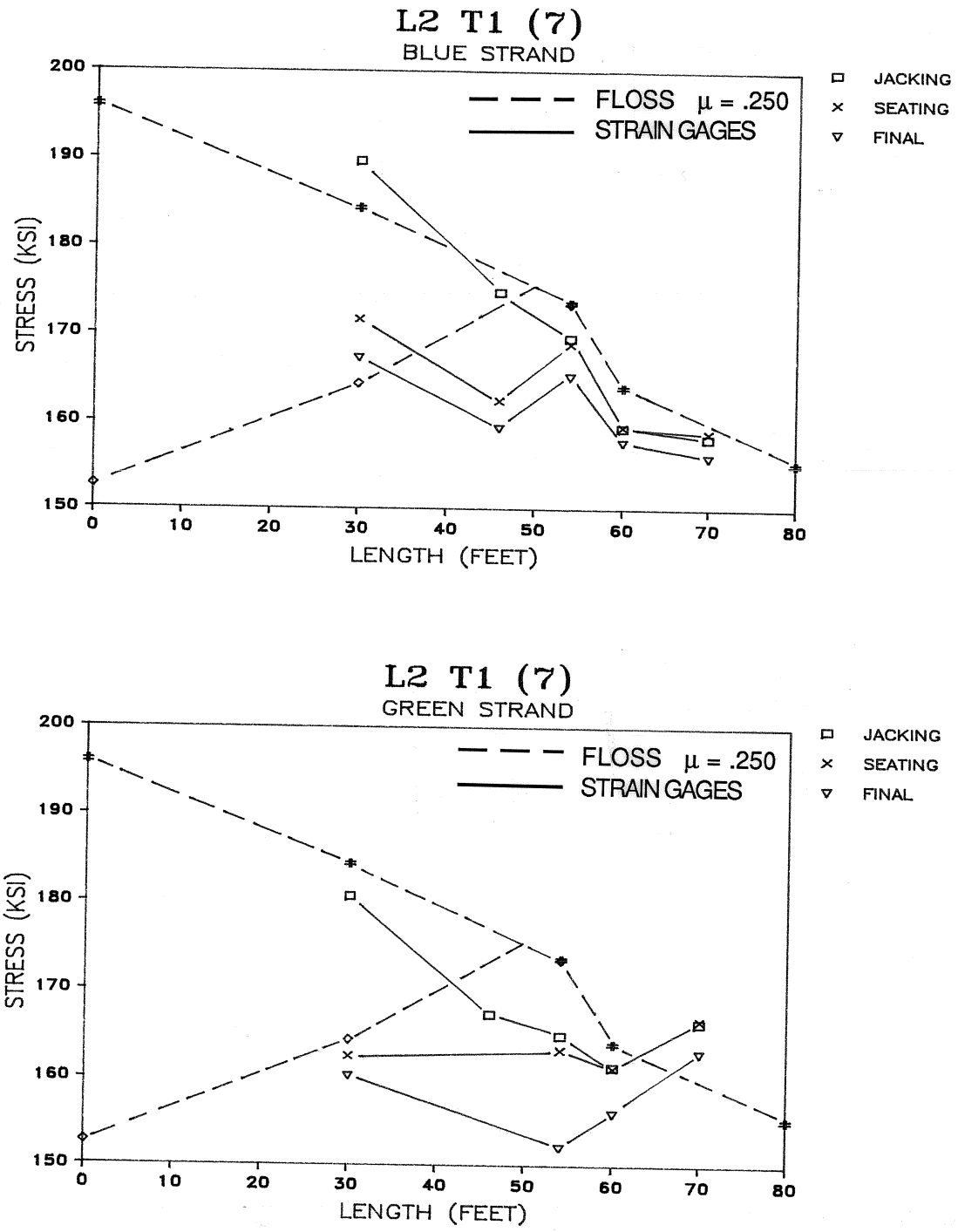

Fig. 4.7a L2 T1 (7): Jacking, seating, and final strand-stress variation

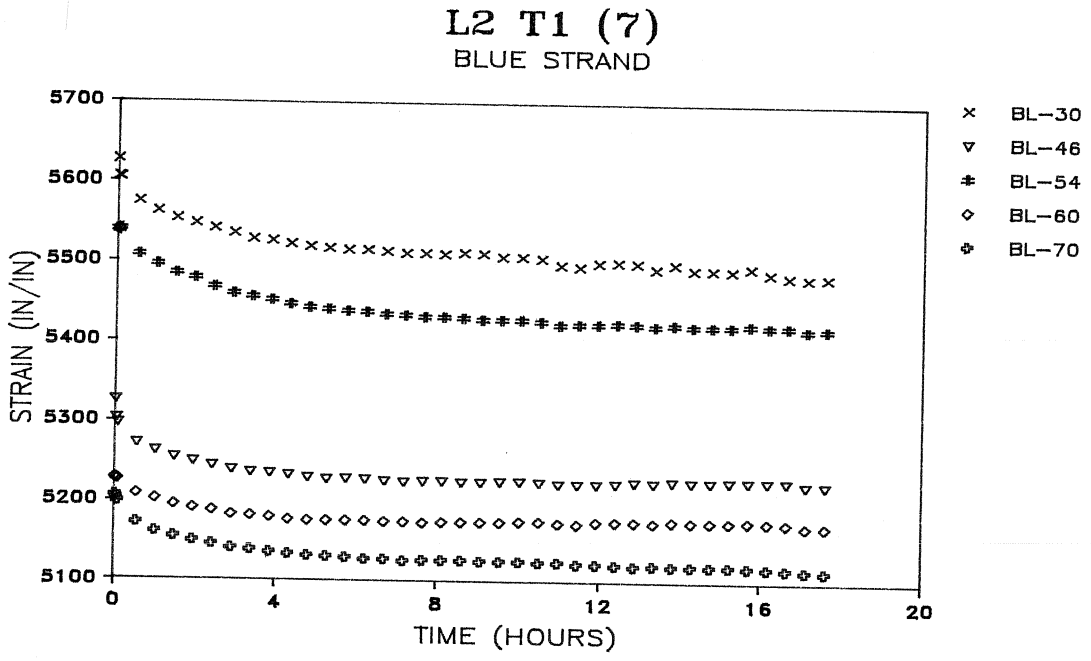

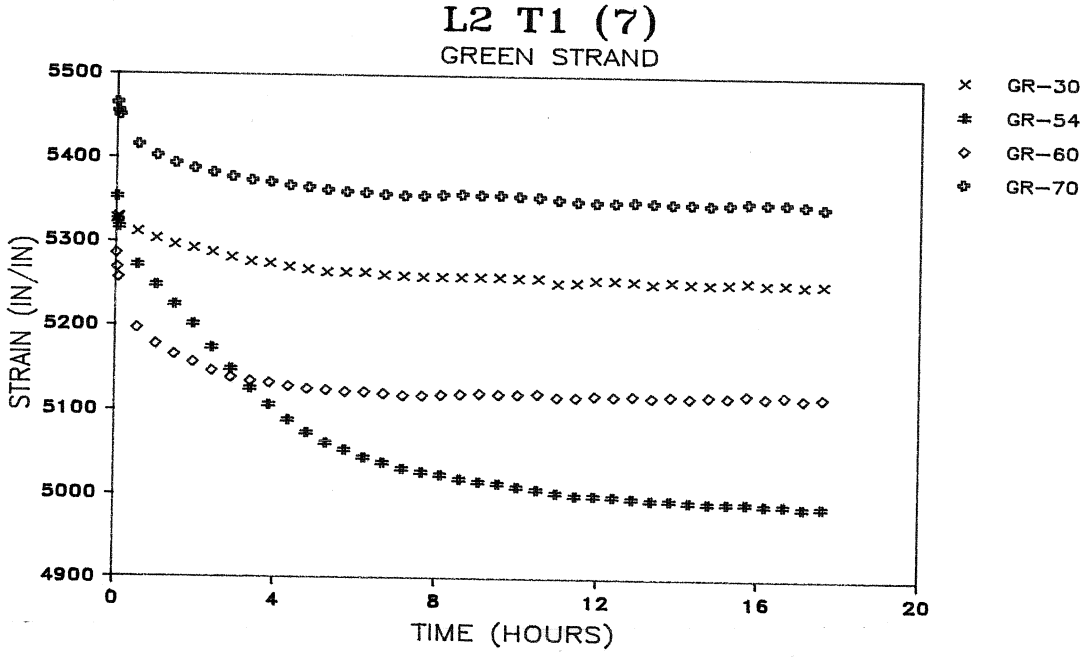

Fig. 4.7b L2 T1 (7): Strain redistribution with time after anchorage seating

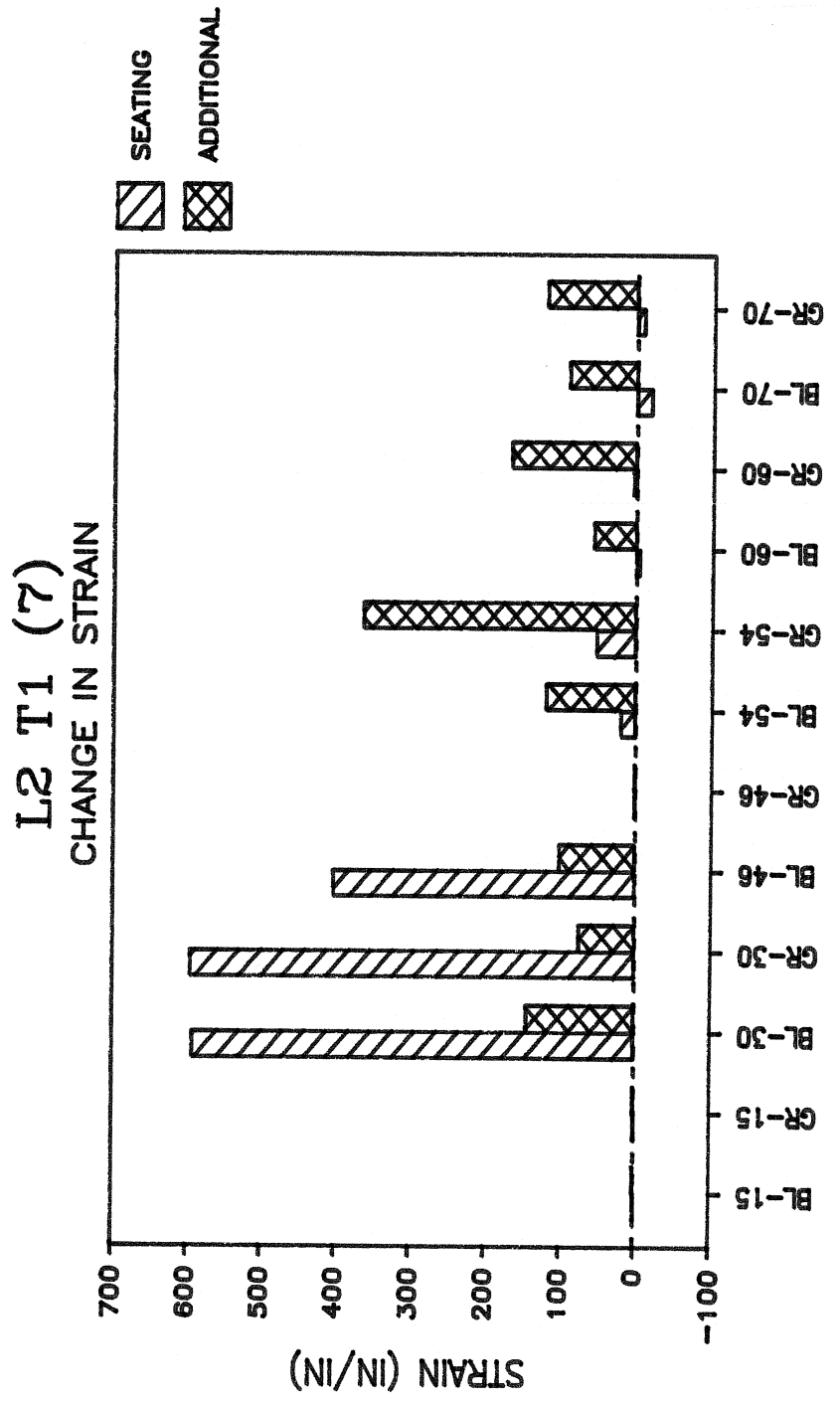

Fig. 4.7c L2 T1 (7): Seating and total additional strain change

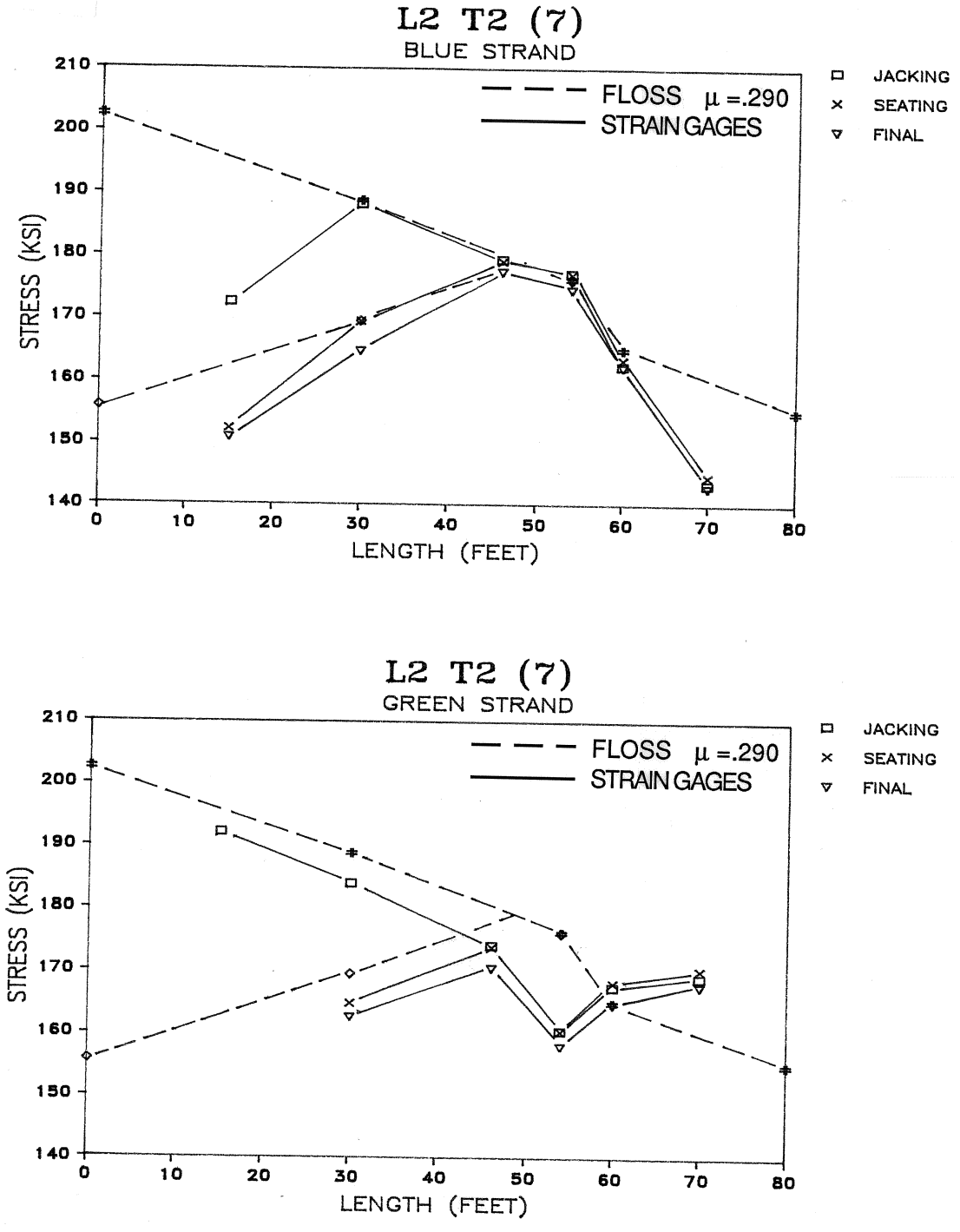

Fig. 4.8a L2 T2 (7): Jacking, seating, and final strand-stress variation

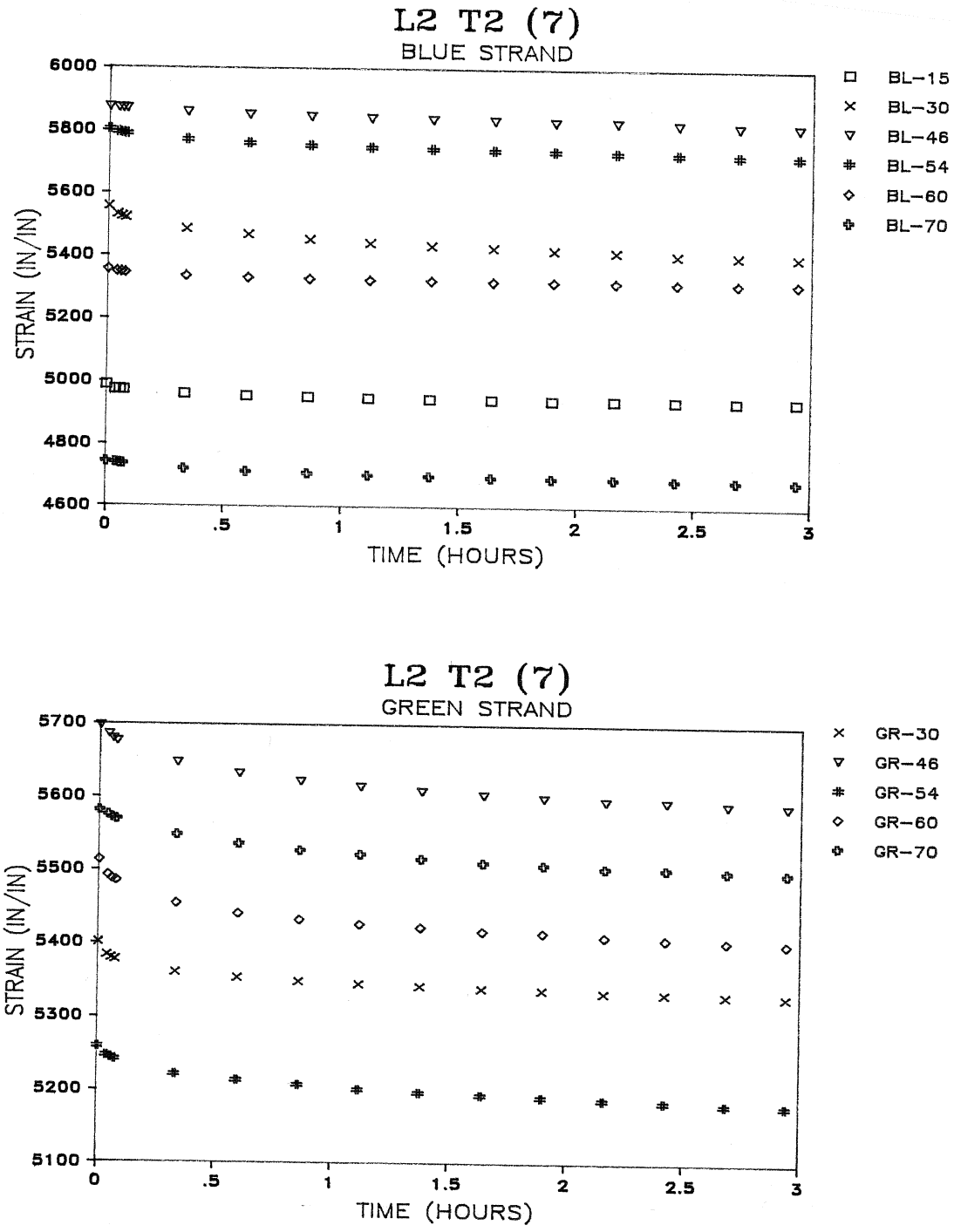

Fig. 4.8b L2 T2 (7): Strain redistribution with time after anchorage seating

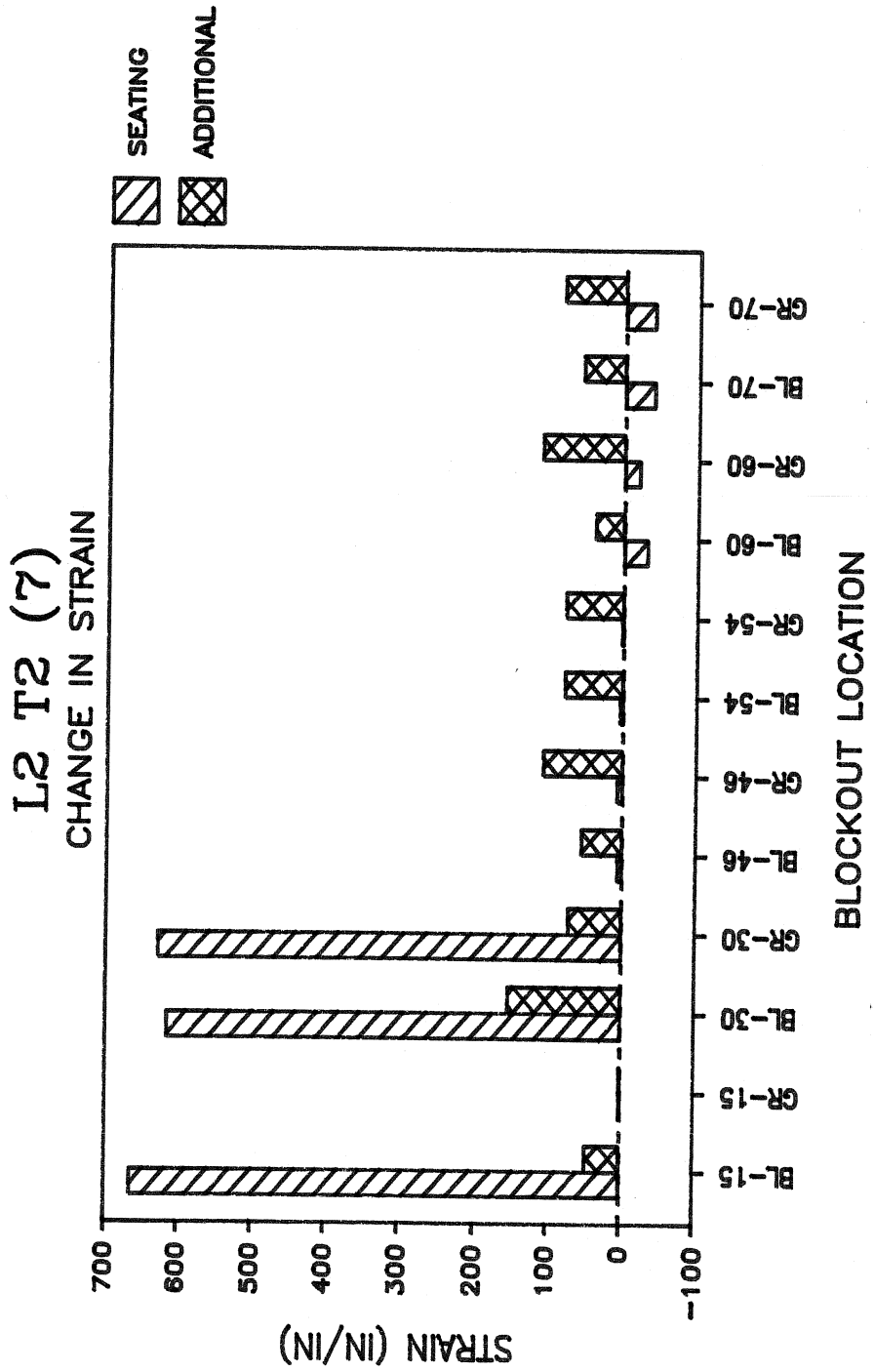

Fig. 4.8c L2 T2 (7): Seating and total additional strain change

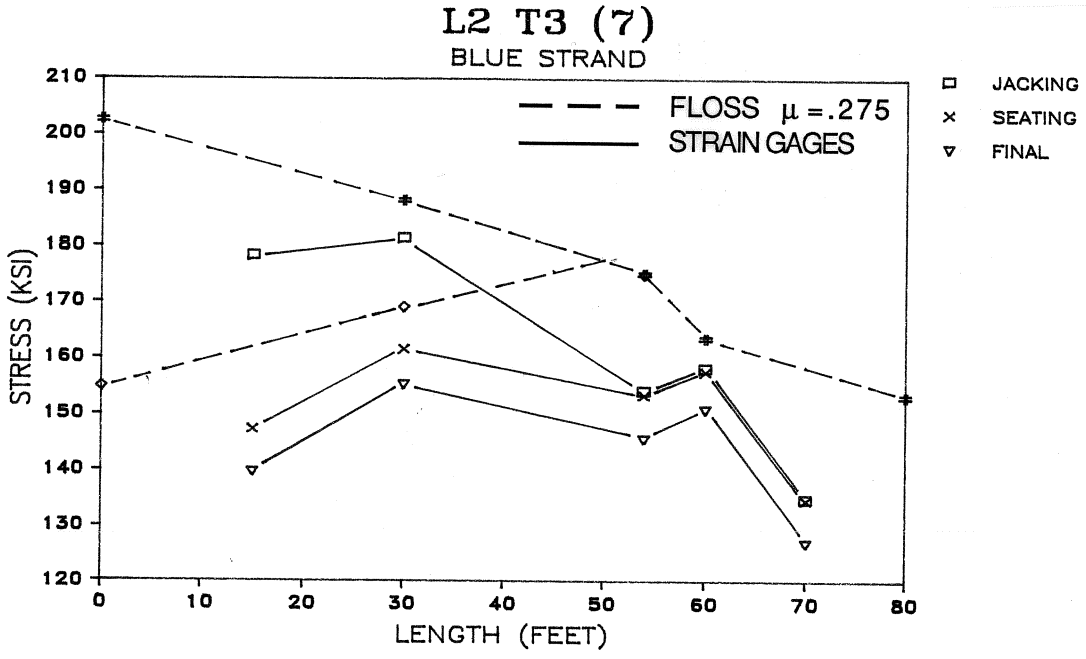

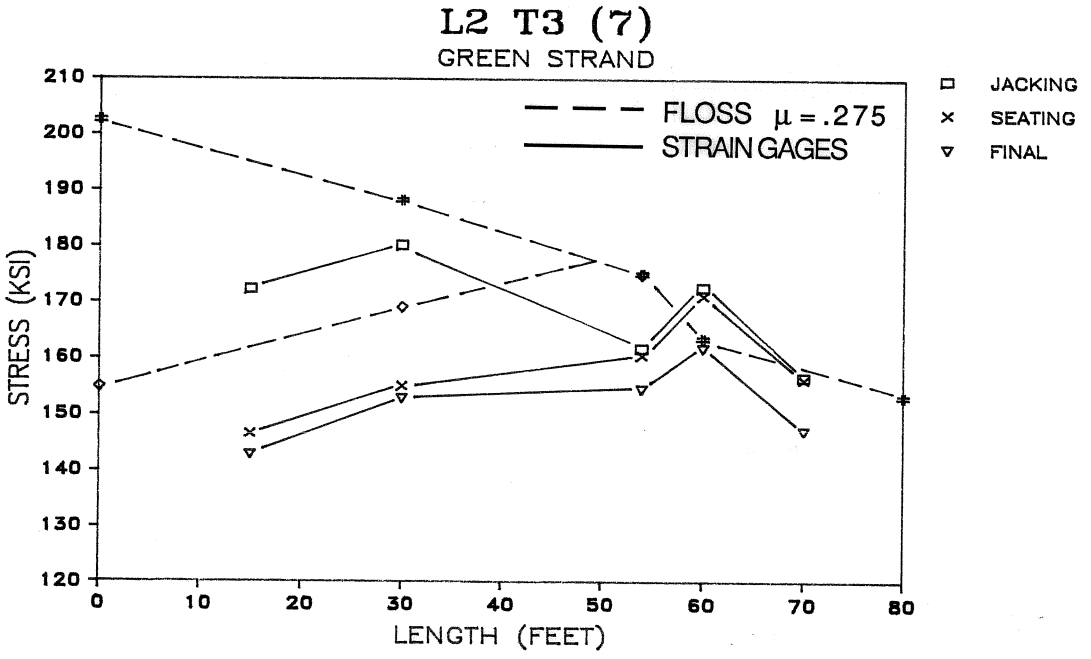

Fig. 4.9a L2 T3 (7): Jacking, seating, and final strand-stress variation

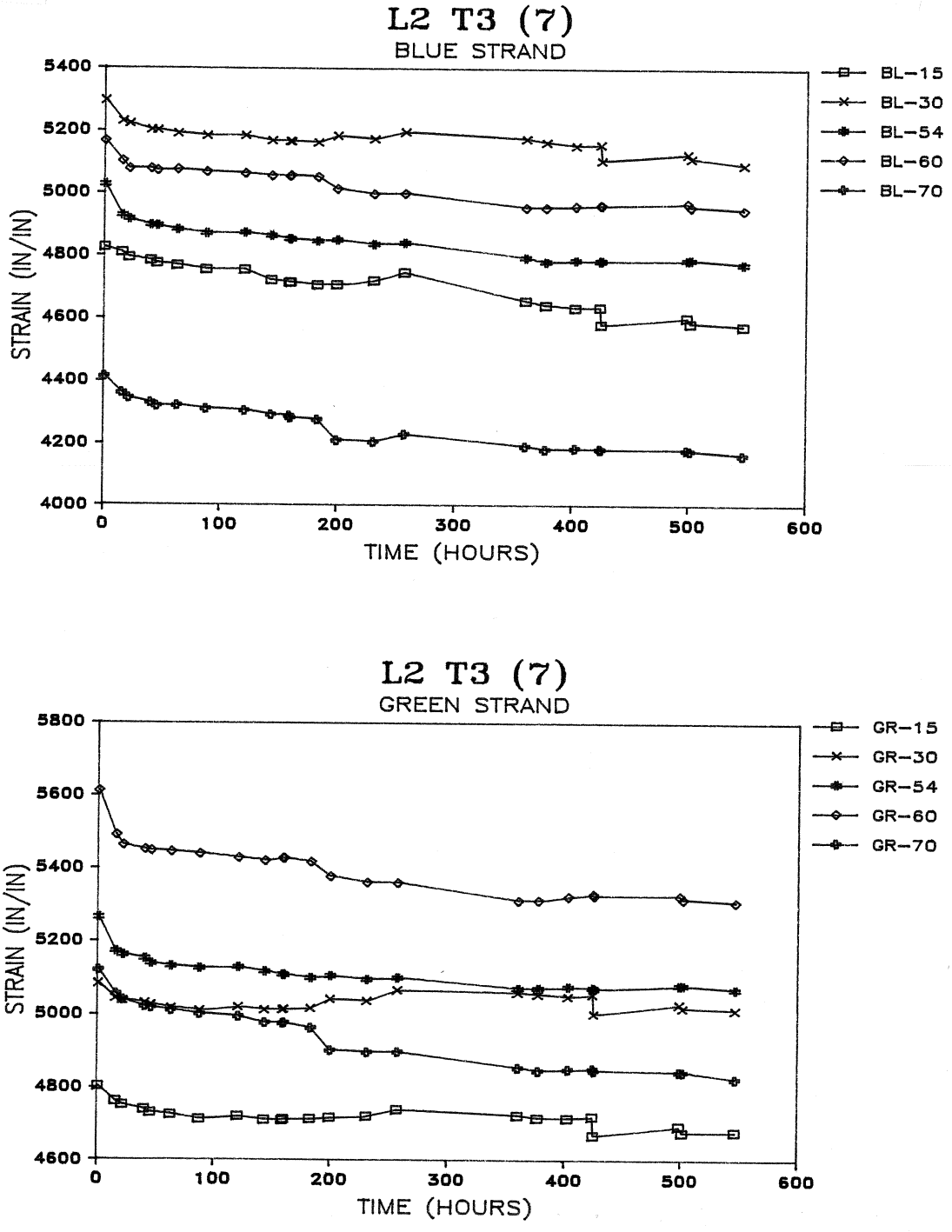

Fig. 4.9b L2 T3 (7): Strain redistribution with time after anchorage seating

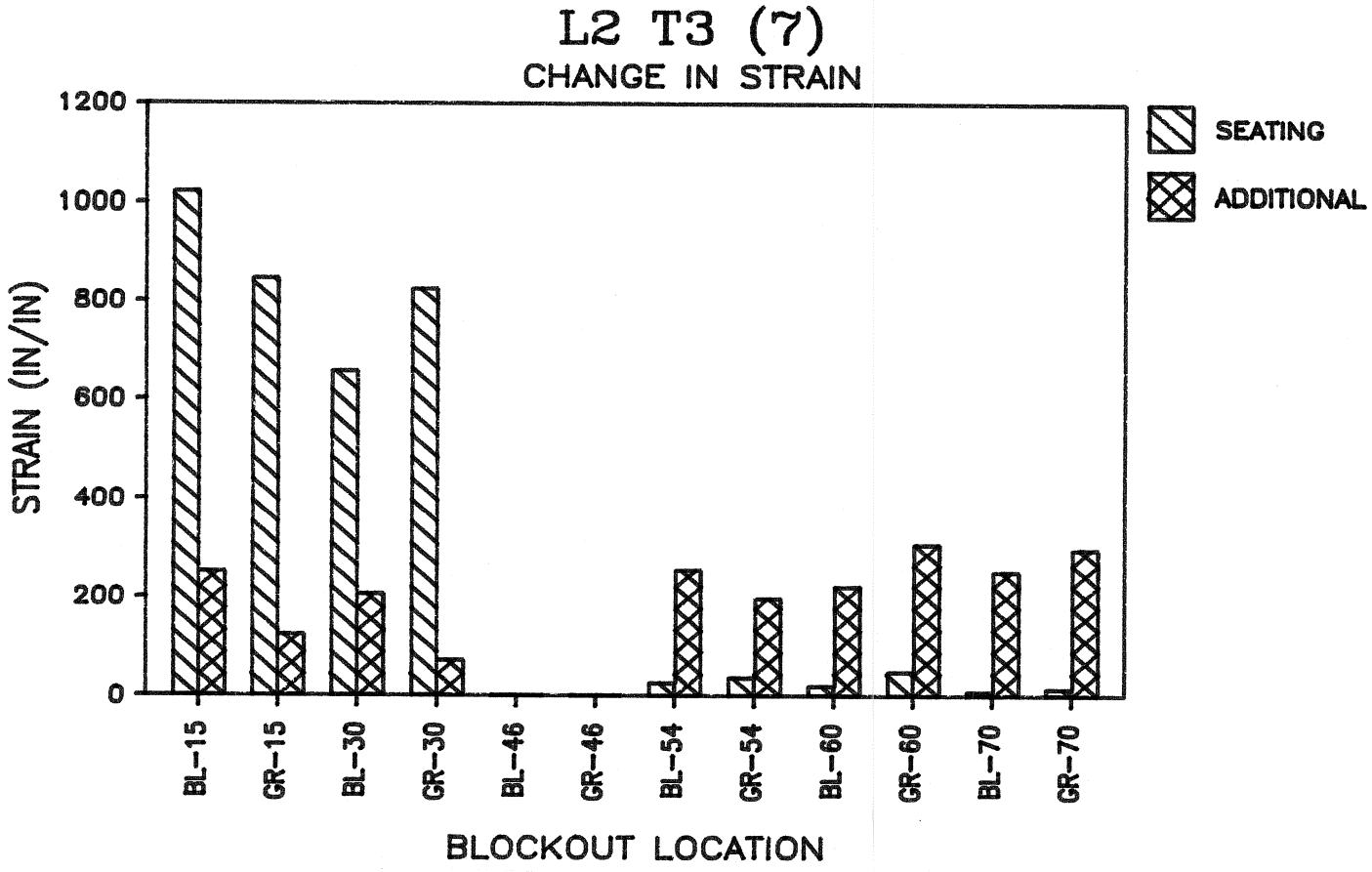

Fig. 4.9c L2 T3 (7): Seating and total additional strain change

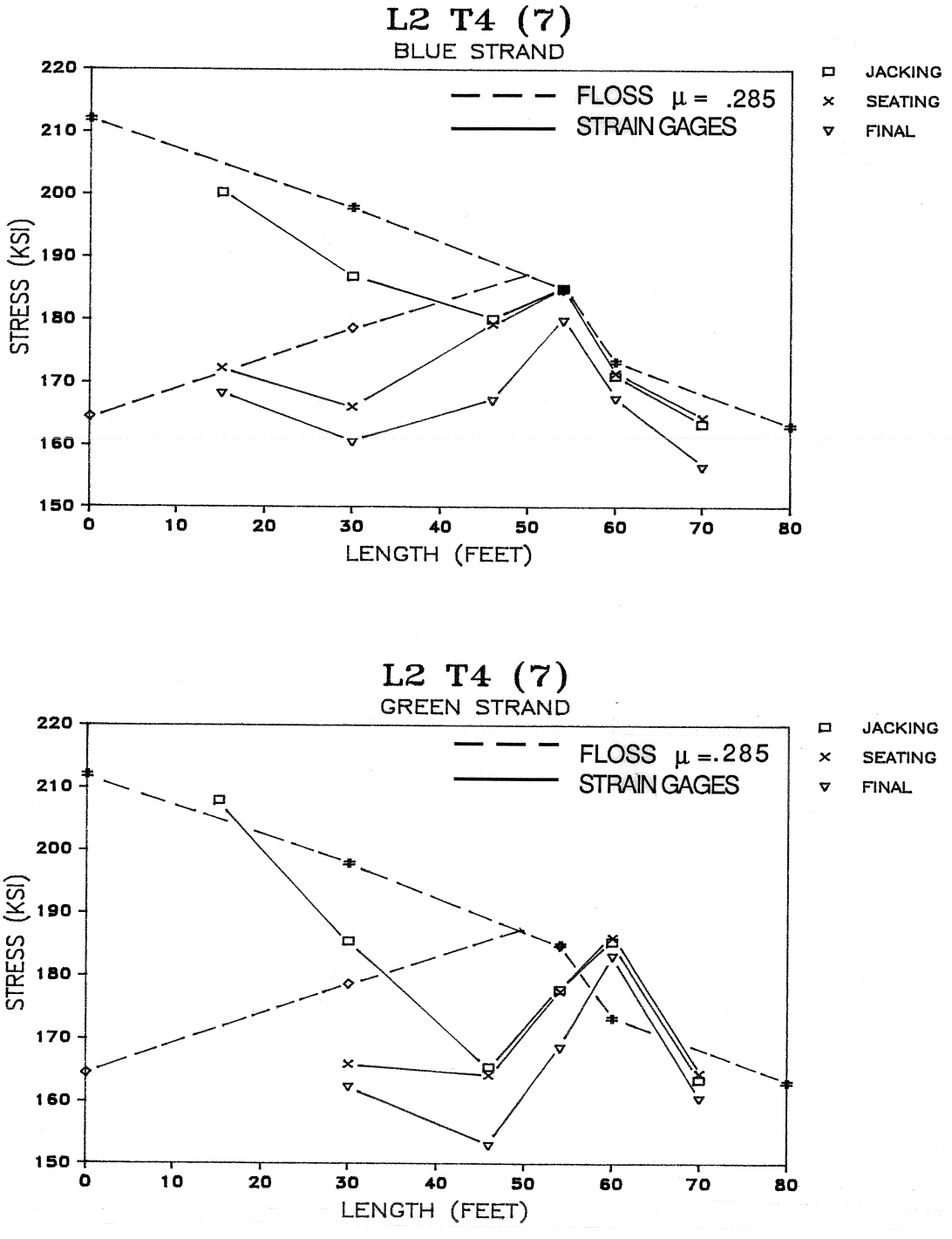

Fig. 4.10a L2 T4 (7): Jacking, seating, and final strand-stress variation

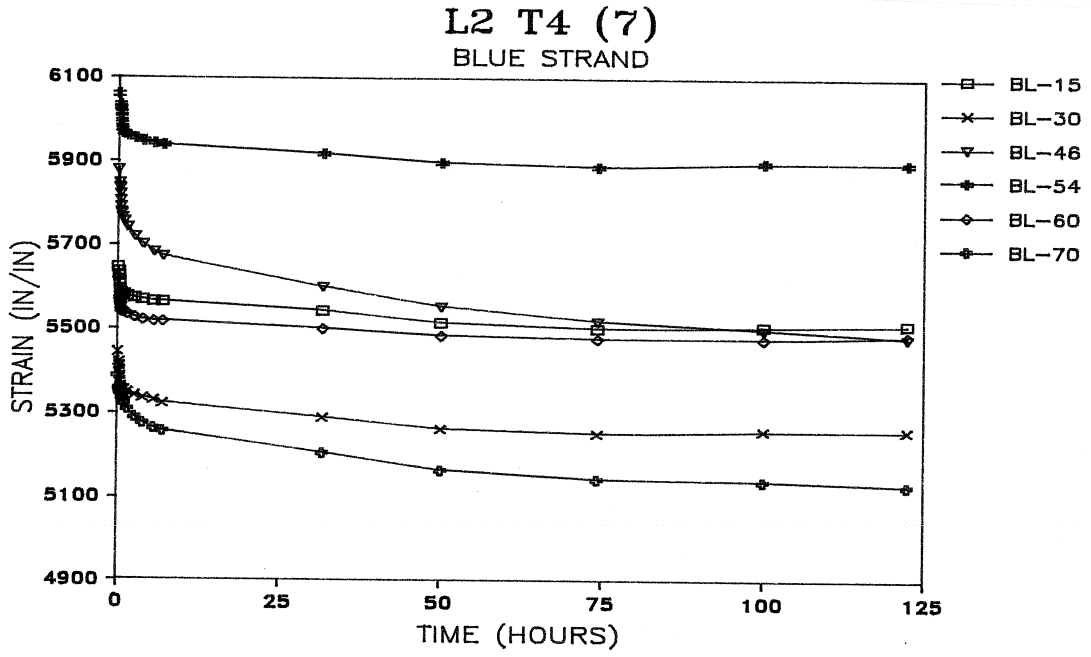

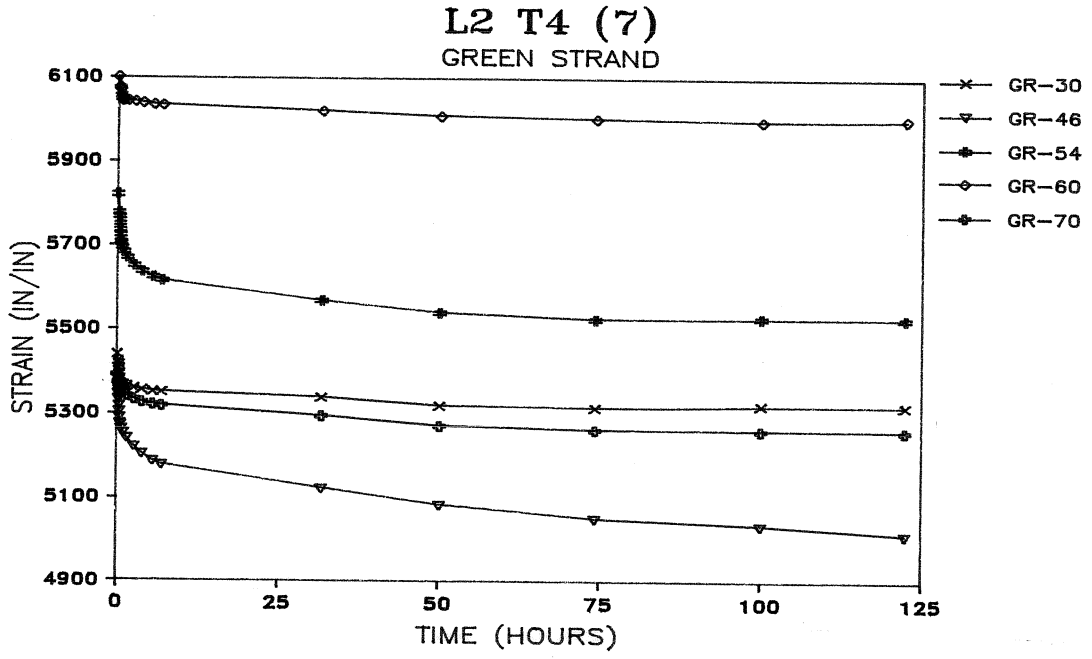

Fig. 4.10b L2 T4 (7): Strain redistribution with time after anchorage seating

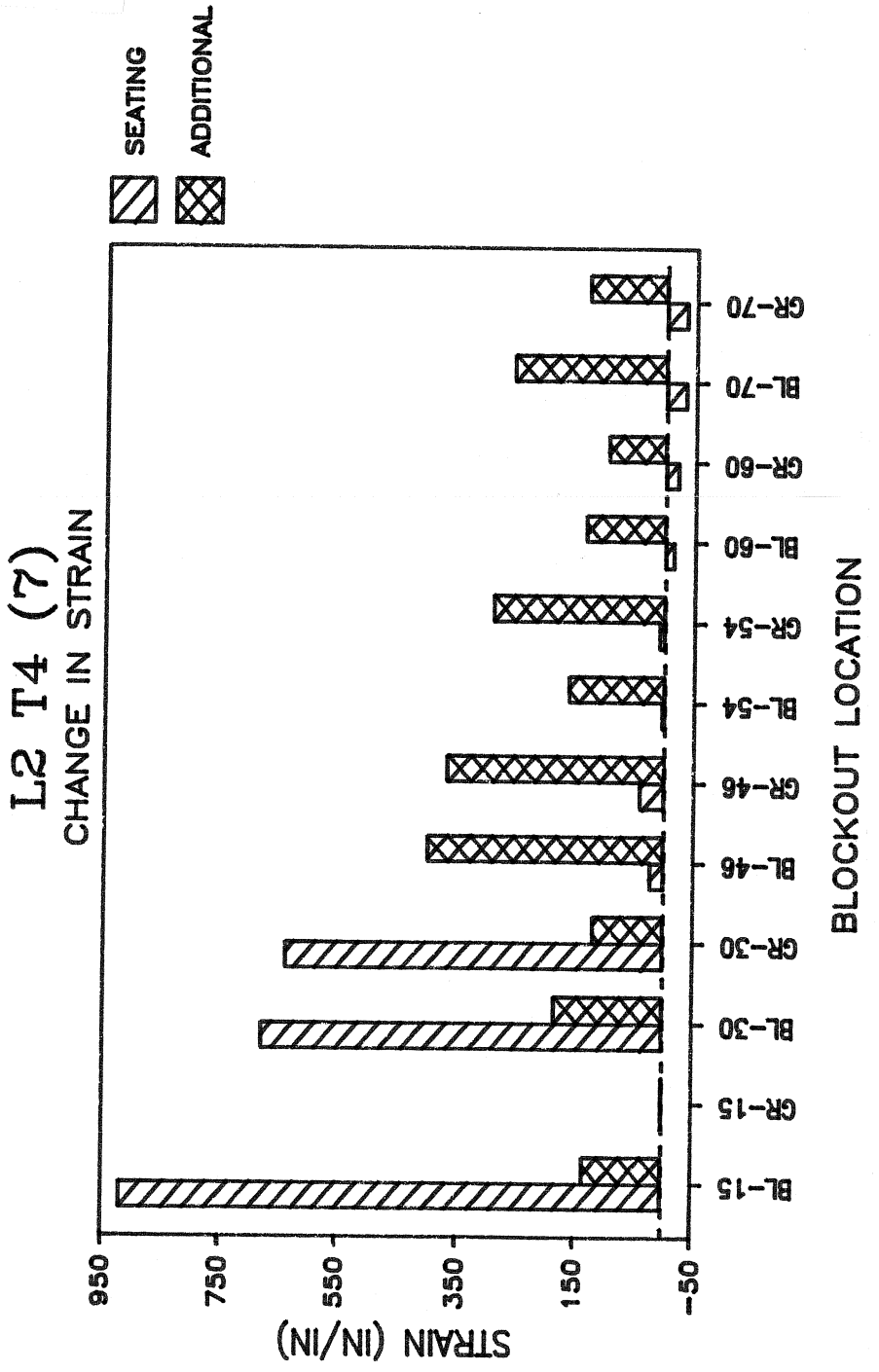

Fig. 4.10c L2 T4 (7): Seating and total additional strain change

L2 T5 (4) and L2 T6 (2) were stressed with fewer strands. For L2 T5 (4), the results (Figs. 4.11a, b, and c) followed the same pattern as that of the test with seven strands.

The average additional stress loss 215.5 hours after seating was 5.3 ksi. But L2 T6 (2) had different results. Measured stresses show a linear friction loss with each instrumented strand detecting virtually an identical stress at each blockout (Fig. 4.12a). The friction coefficient was unusually high in comparison to previous seven strand tests suggesting that an error occurred while monitoring the jacking stress. Strain gages at BL-15, GR-15, BL-30, GR-30, and GR-46 became ineffective upon releasing the jacking force so seating loss effects could not be observed. The average additional stress loss after 171 hours for the remaining strain gages was 3.5 ksi. Since additional stress loss for reduced strand tests are in the same range as seven- strand tests, one can conclude that additional losses are more relaxation related as opposed to creep and shrinkage. Even for extended time periods prior to grouting, additional stress loss is quite small ranging from 2 to 4 percent for time periods up to 24 days.

4.3.4 Tendon Profile No.3. Tendon Profile No.3 was characterized by large curvatures in the initial 34 ft inducing a rapid frictional tendon stress reduction followed by more shallow curvatures and less frictional loss. The calculated friction coefficient ranged from .244 to .289 closely approximating the recommended value. In the first test L3 T1 (7), Fig. 4.13a shows that the measured strand stresses compared favorably with theoretical values in the low stress region; BL-30/GR-30 to BL-74/GR-74. From blockouts BL-10/GR-10 to BL-30/GR-30, the slope of measured frictional loss is identical to *FLOSS* but at an offset of 15 ksi. This implies a very sharp frictional loss in the initial ten ft. Upon seating, the anchor set curve intercepted the friction curve at BL-30/GR-30 which is only three ft further than predicted by *FLOSS*. Redistribution and leveling of strand stresses was indeterminate for this test as strain gages were stripped off at BL-10, BL-26, and GR-30 during seating. From readings of gage GR-10, it appears that the stresses did equalize to the point of intersection. Figure 4.13c shows that the seating induced compressional wave propagated to the holding end and reflected back. The strand stresses at BL-50, GR-50, BL-74, GR-74; therefore experienced an increase in stress by approximately 3.0 ksi. This effect also occurred for L3 T3 (7) (Fig. 4.15c).

Following seating, additional strain behavior for L3 T1 (7) was monitored for 44.5 hours with readings at 30 minute intervals during the first 22.5 hours (Fig. 4.13b). As for the previous two layouts, the initial five hours accounted for approximately 95% of all additional losses and after that time a strain equilibrium was reached. After jacking and seating, a significant stress differential remained between jacking and holding ends because of extremely large frictional losses. The strand stress at GR-10 was measured as 168 ksi while only 125 ksi occurred at BL-74 and GR-74, a differential of 43 ksi. It should be noted that the average stress along the length was approximately 145 ksi, much lower than either Tendon Profile No.1 or No.2. Hence, the normal

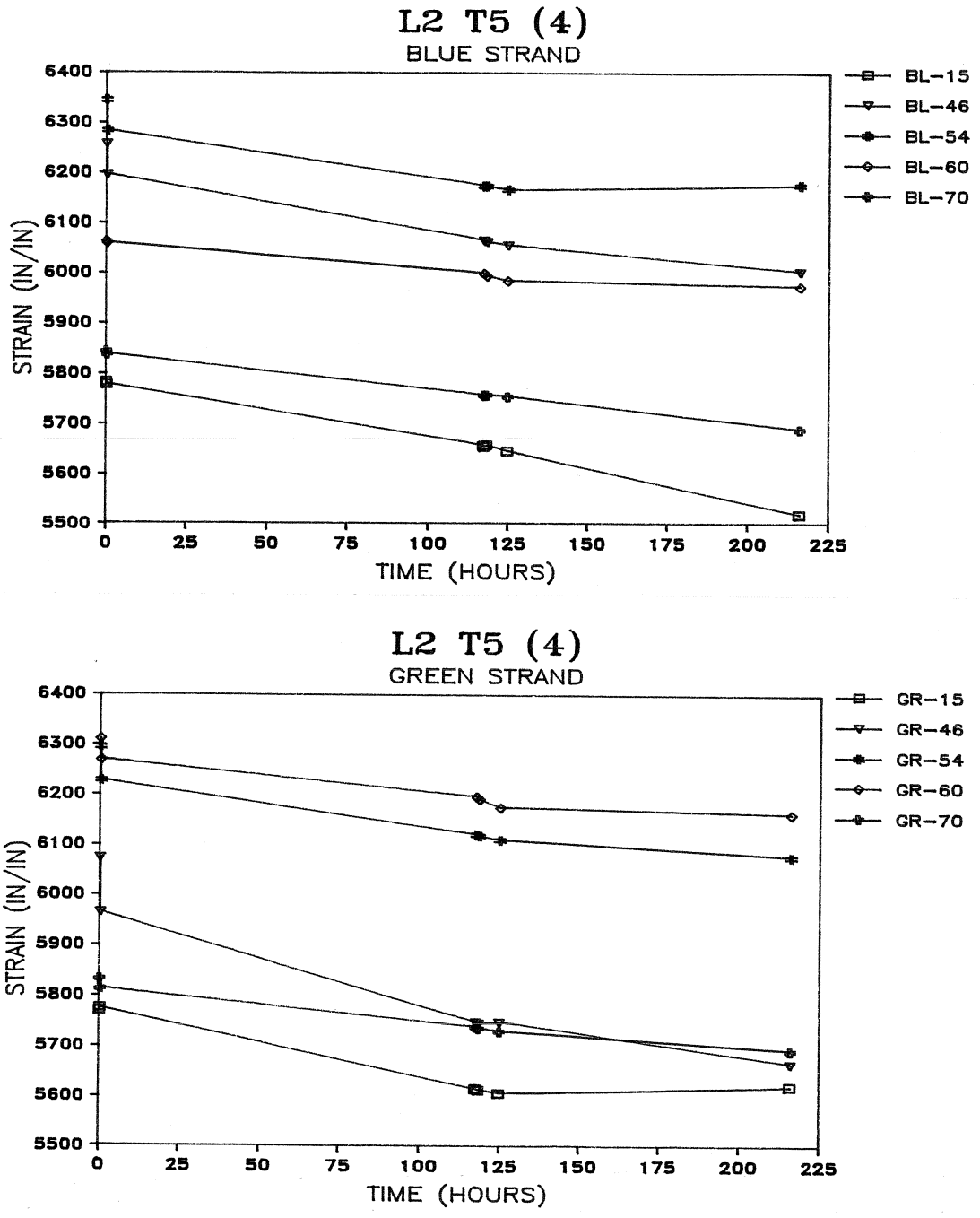

Fig. 4.11b L2 T5 (4): Strain redistribution with time after anchorage seating

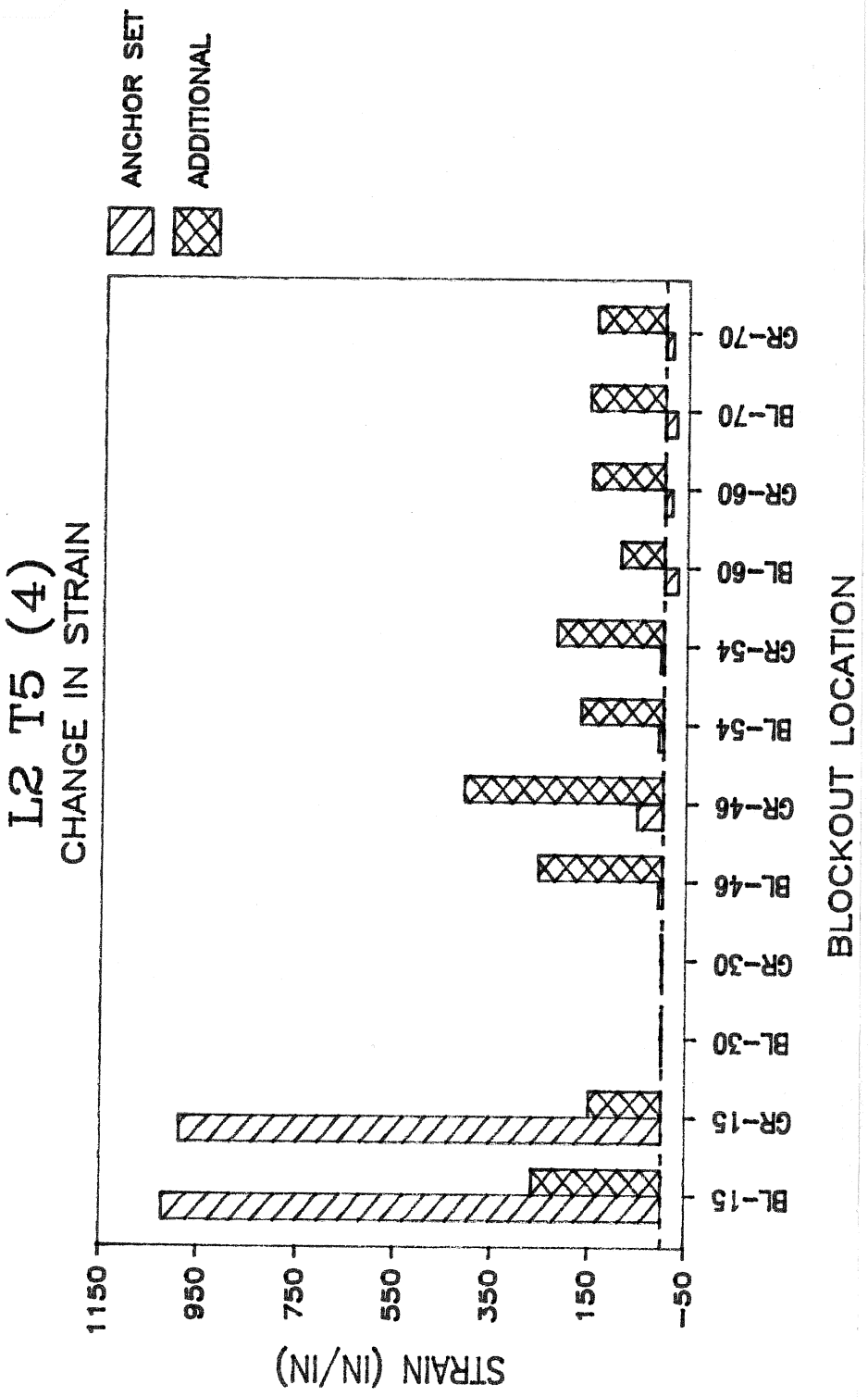

Fig. 4.11c L2 T5 (4): Seating and total additional strain change

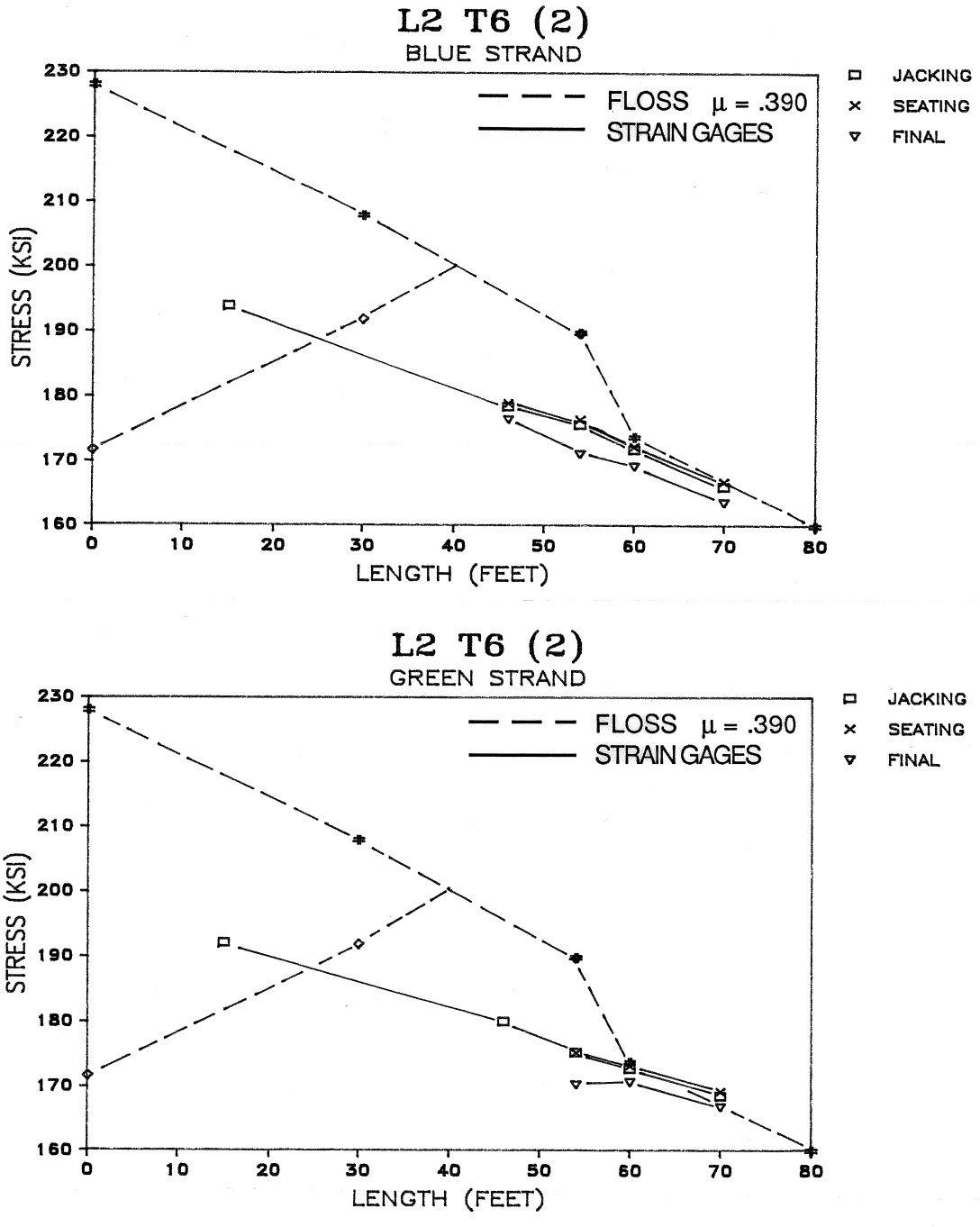

Fig. 4.12a L2 T6 (2): Jacking, seating, and final strand-stress variation

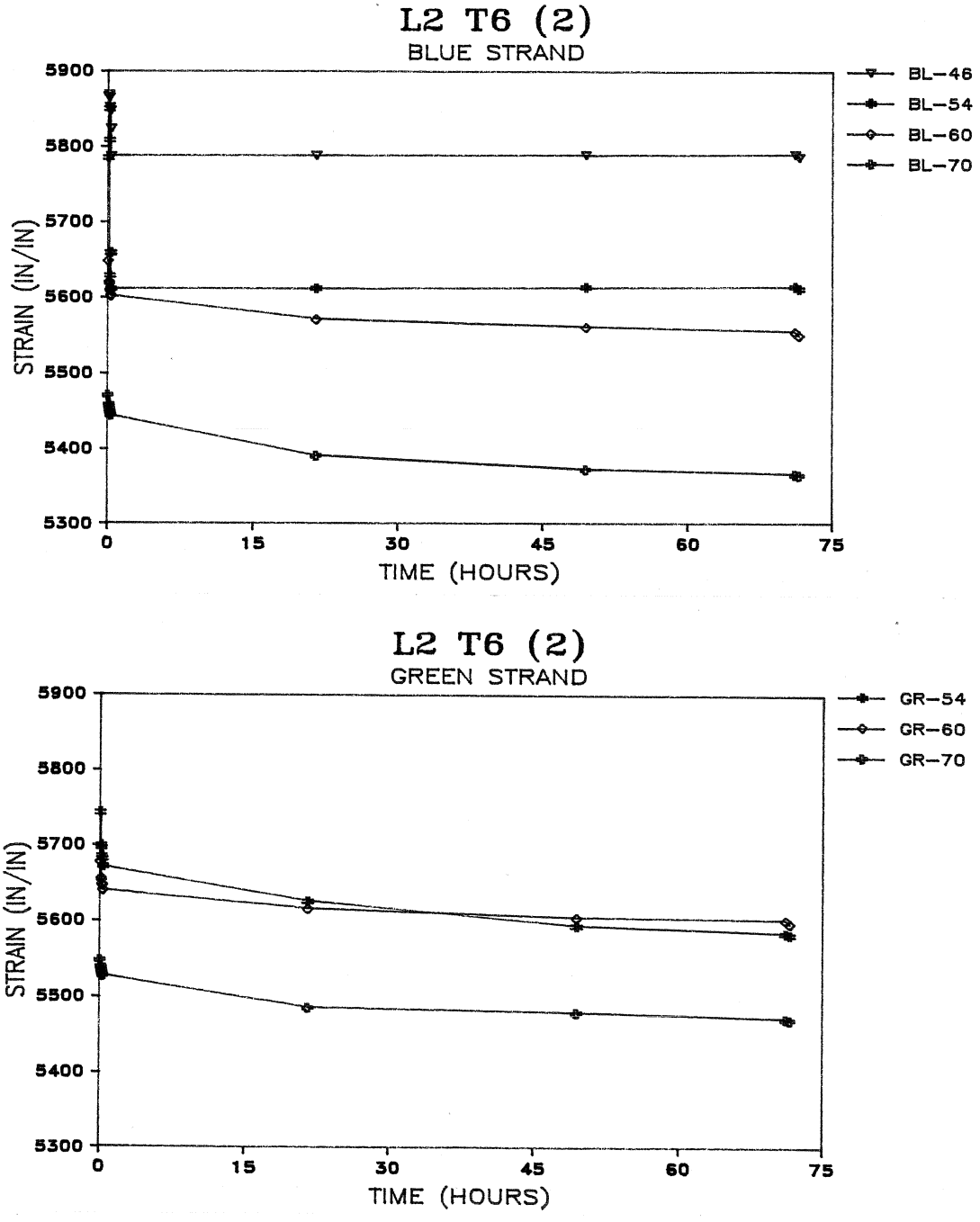

Fig. 4.12b L2 T6 (2): Strain redistribution with time after anchorage seating

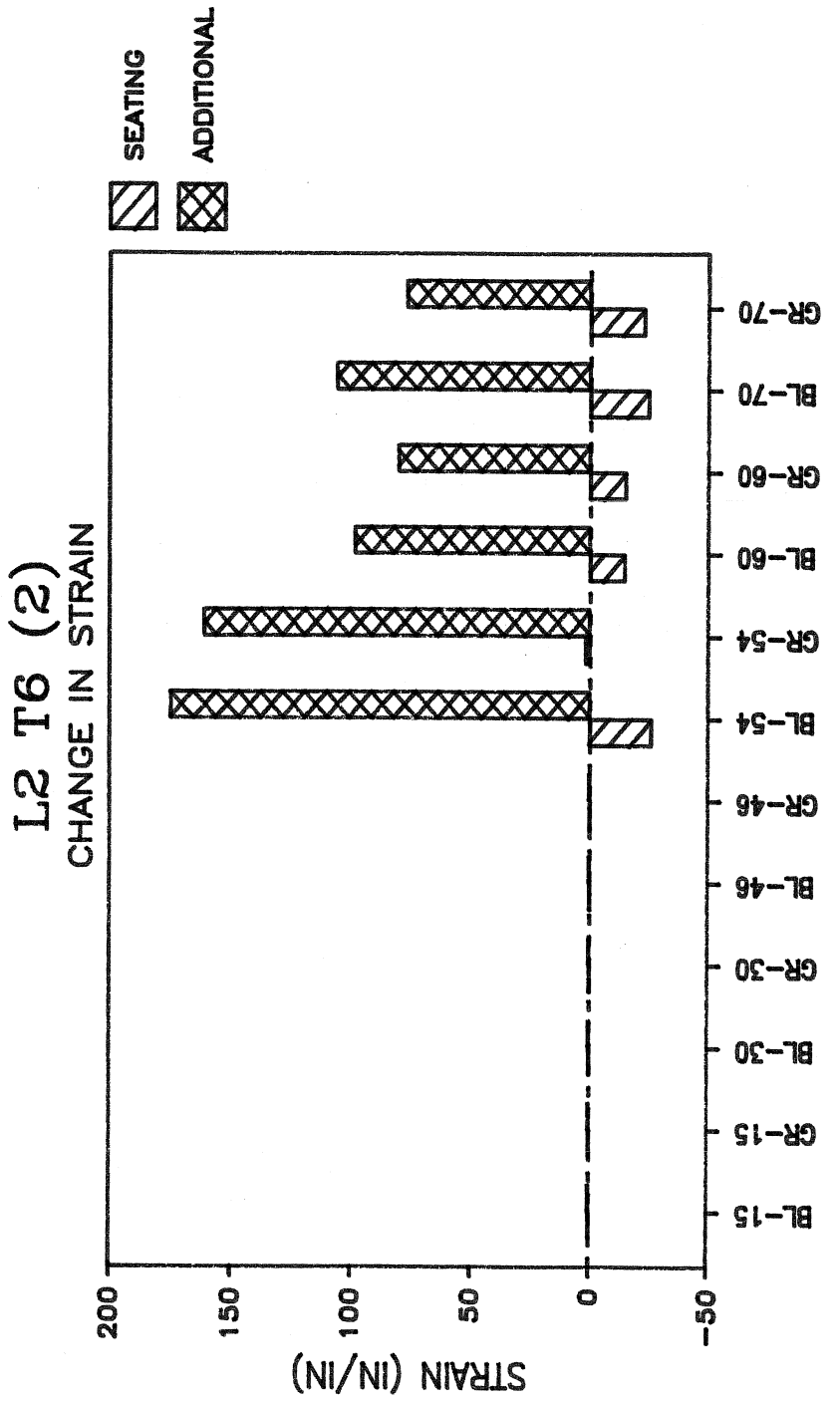

Fig. 4.12c L2 T6 (2): Seating and total additional strain change

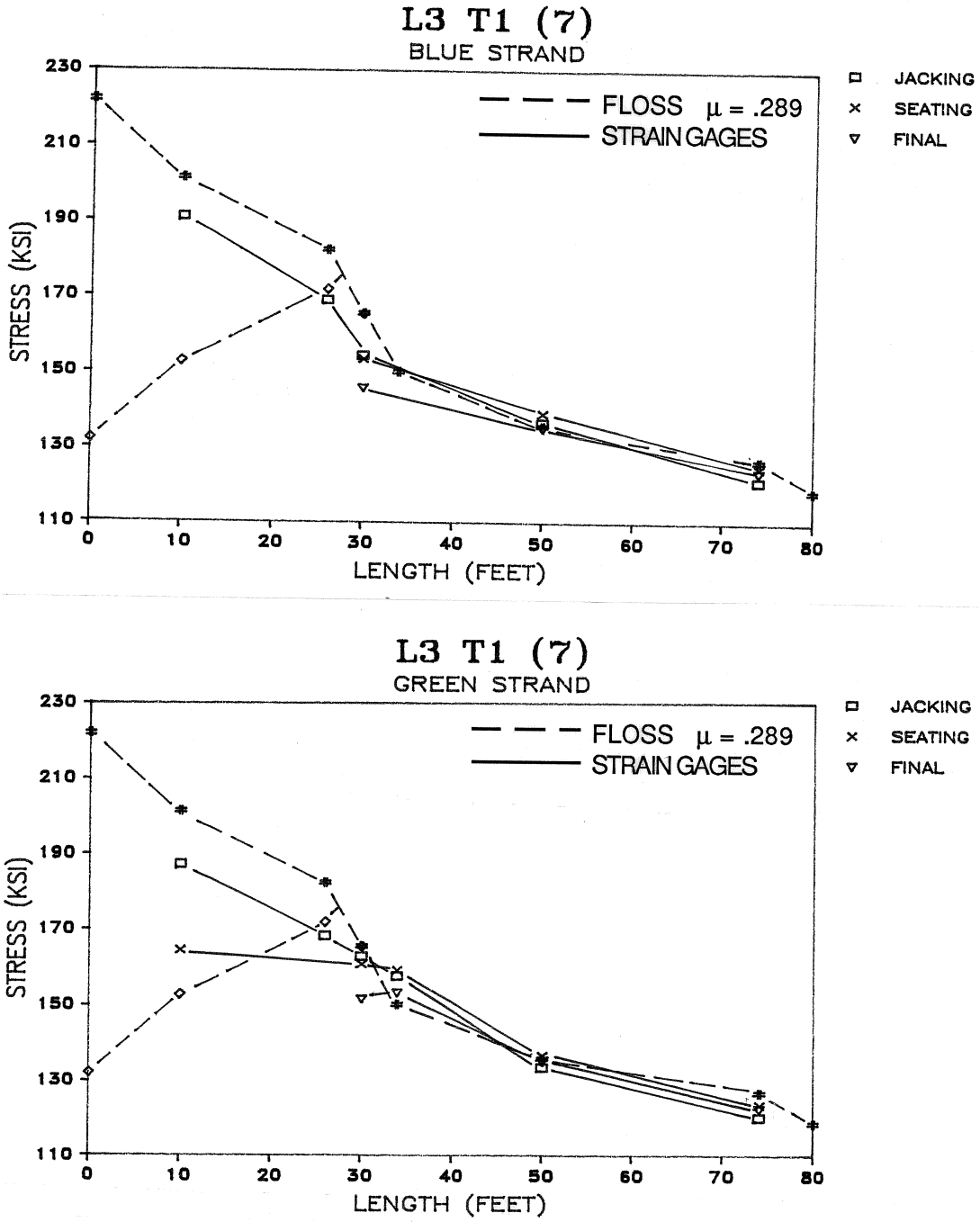

Fig. 4.13a L3 T1 (7): Jacking, seating, and final strand-stress variation

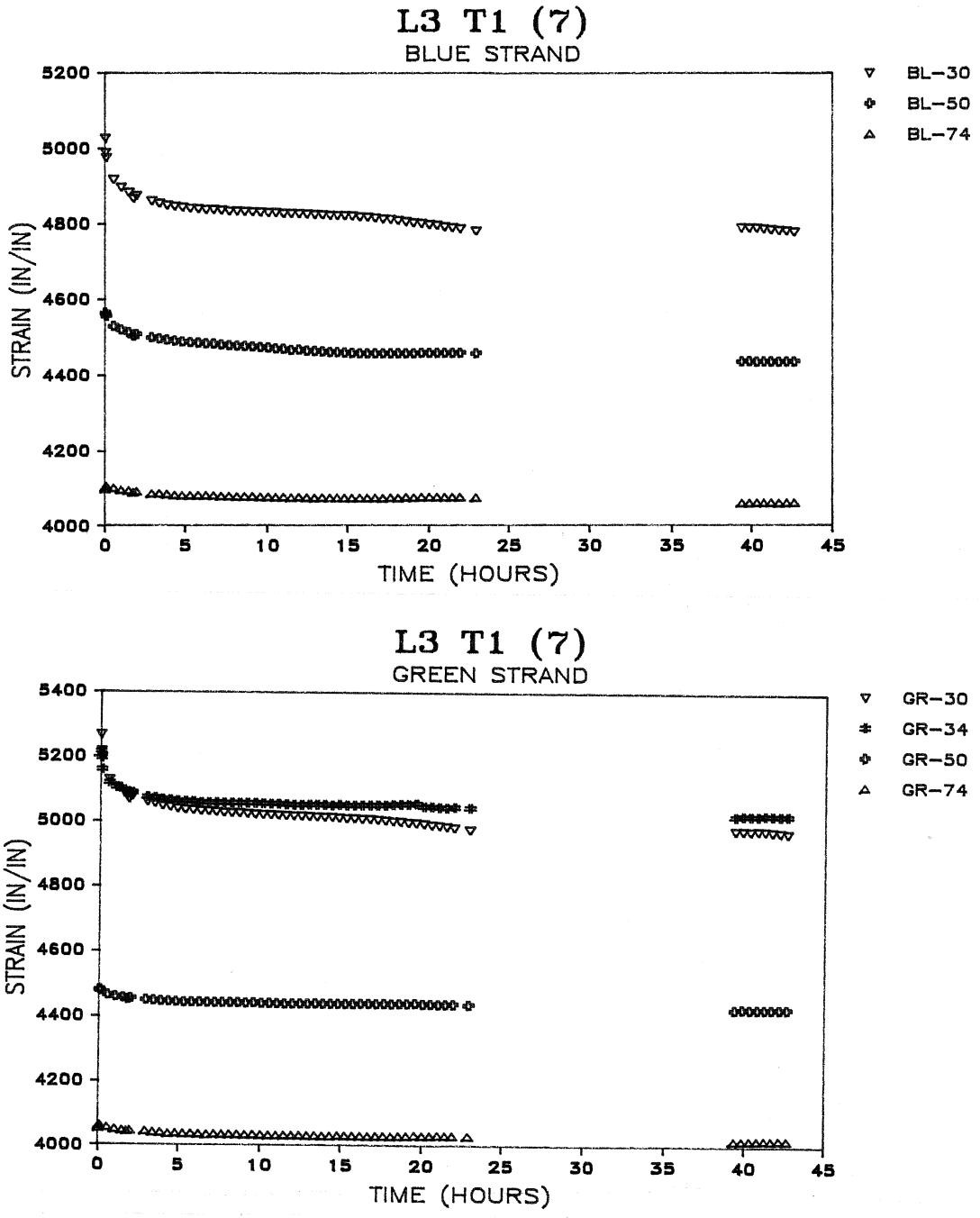

Fig. 4.13b L3 T1 (7): Strain redistribution with time after anchorage seating

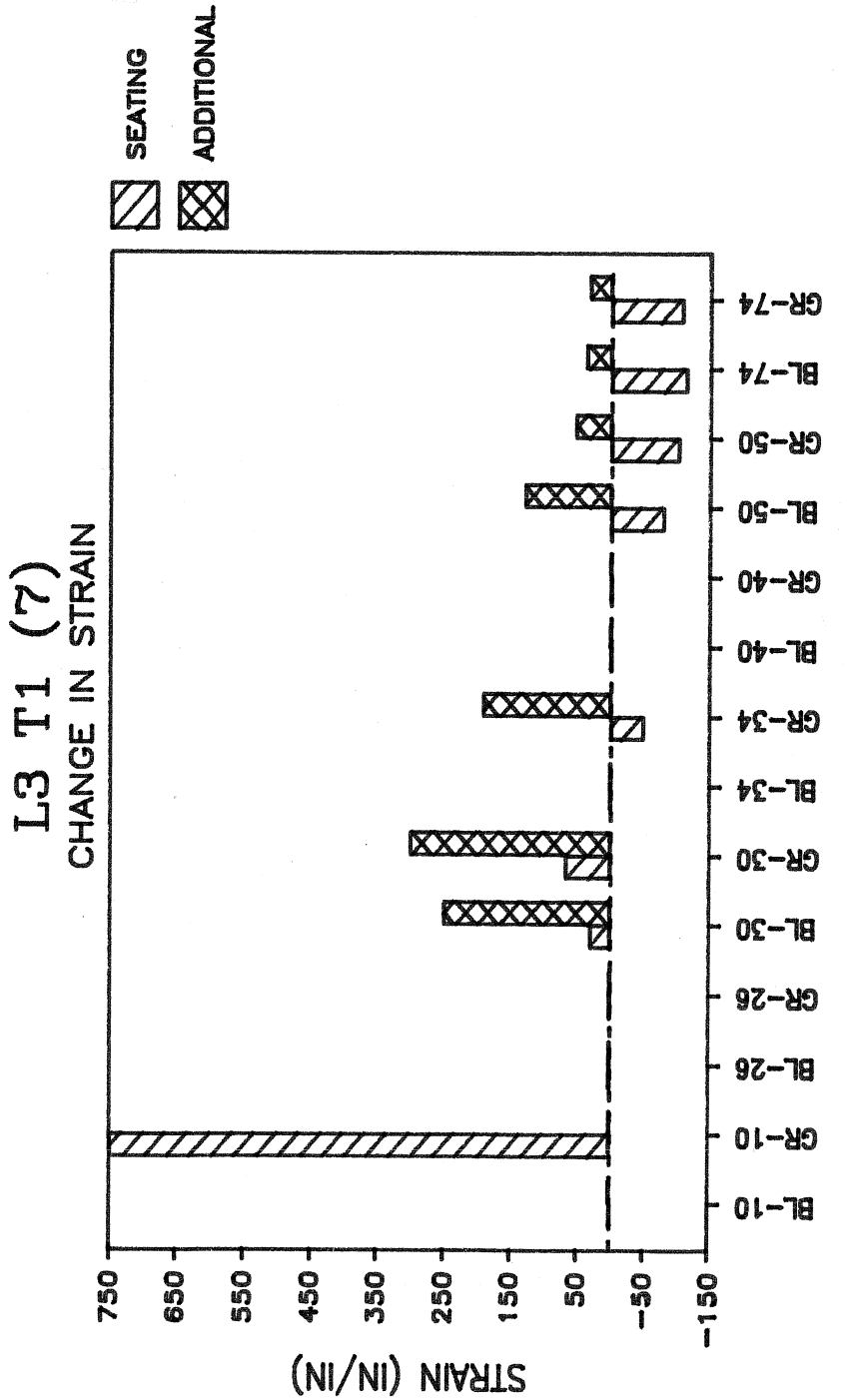

Fig. 4.13c L3 T1 (7): Seating and total additional strain change

force, i.e. friction, resisting tendon stress redistribution was also lower. These factors plus the tendon path of Layout #3 contributed to more substantial additional strain losses following seating. The pattern shown in Fig. 4.13c for L3 T1 (7) is a high strain dropoff at BL-30/GR-30 decreasing to a minimal dropoff at BL-74/GR-74. Final additional stress loss for these respective blockouts are 7.6 and 1.5 ksi, respectively.

Redistribution effects following seating are more pronounced for L3 T2 (7). In this test the strains were monitored for 337 hours (two weeks). Figures 4.14a and c show that BL-10/GR-10 experienced the largest additional strain loss with the change in strain diminishing to a minimal amount at BL-74/GR-74, corresponding to stress losses of 17.5 and 3.8 ksi, respectively. The average additional stress loss in this test was 10.5 ksi. Although more significant, redistribution following seating did not completely level the high and low stress regions caused by jacking and anchor set. In fact, additional losses are still approximately uniform along the layout. Note that redistribution effects occur when a high stress region decreases to a lower stress region. However, strand does not experience redistribution such that a low stress region increases its stress level.

Following the trend of previous tests, anchorage transformation with Layout #3 leveled the strand stresses until intercepting the friction loss curve at BL-34/GR-34 (Fig. 4.14a). Tests results for L3 T3 (7) (Figs. 4.15 a, b, and c) were comparable to both L3 T1 (7) and L3 T2 (7).

The final two tests, L3 T4 (4) and L3 T5 (2), with fewer strands closely approximated the predicted *FLOSS* friction loss curve but offset at a lower stress (Figs. 4.16a and 4.17a). Between blockouts, slope of the friction curve is offset by 20 ksi for L3 T4 (4) and 30 ksi for L3 T5 (2). Using the same hydraulic stressing ram to stress fewer strands as with seven strands, final pressure gage readings were located in the initial region of the calibration curve and accuracy of readings is more suspect. Also, eighty percent tendon elongations to check pressure gage readings depended upon an even lower pressure. Thus the measured maximum applied jacking stress appears to have been over estimated for the test with only two strands.

Measured strand stresses showed a consistent friction reduction compatible with friction theory in these tests where the instrumented strands exclusively contacted the conduit. With increasing strand numbers, an individual strand position changes along the layout as the curvature changes direction. There are three different strand locations: 1) in direct contact with conduit with normal forces from surrounding strands acting upon it, 2) interior of strand bundle away from conduit with fewer surrounding strands applying normal forces, and 3) exterior of bundle away from conduit and no normal force from surrounding strands. Therefore; an individual strand in multi-strand layouts (7 strands) will show a less consistent friction reduction during stressing in comparison to tests with fewer strands in the same size duct.

Also, the anchorage seating curve for tests with fewer strands more closely approximated

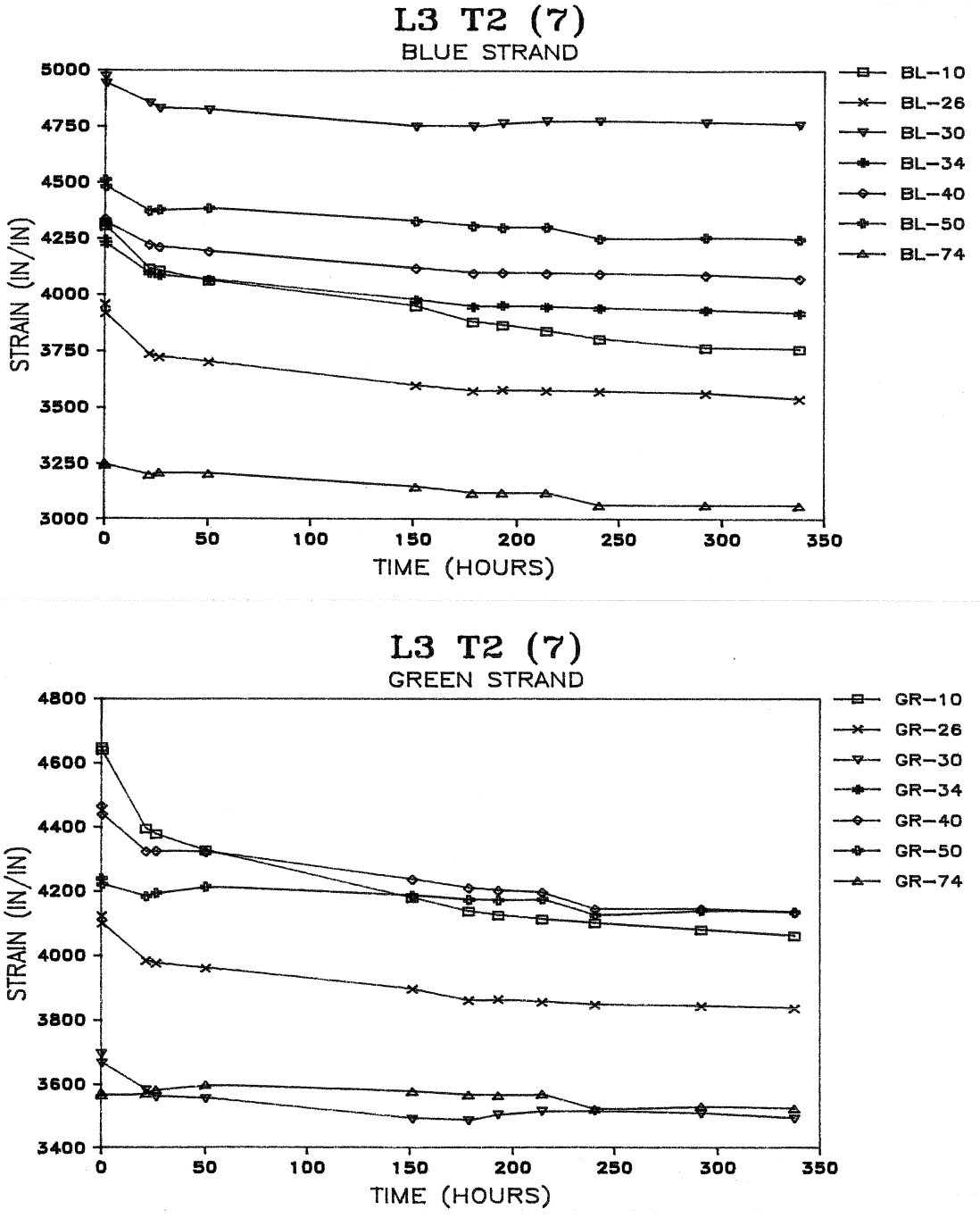

Fig. 4.14b L3 T2 (7): Strain redistribution with time after anchorage seating

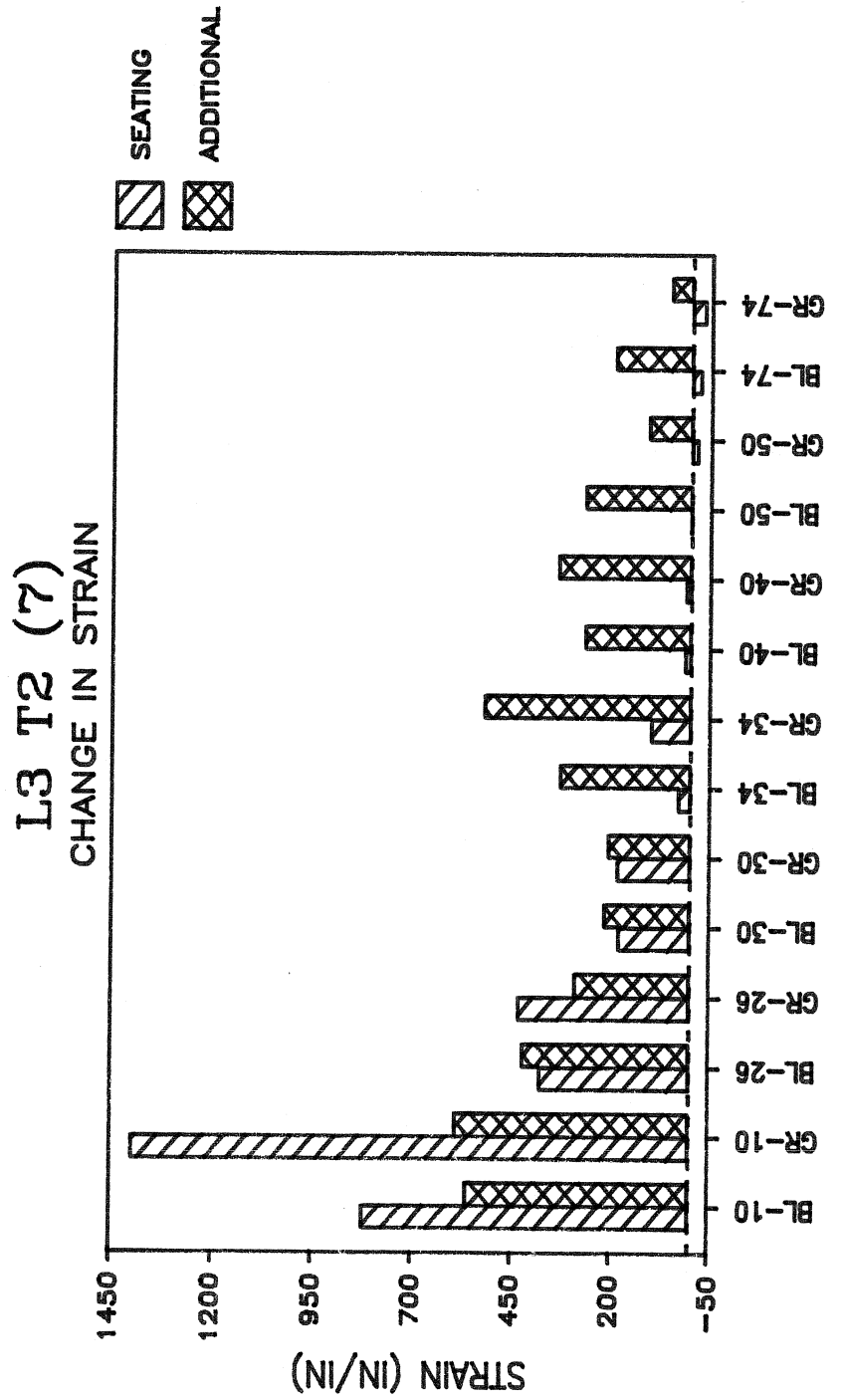

Fig. 4.14c L3 T2 (7): Seating and total additional strain change

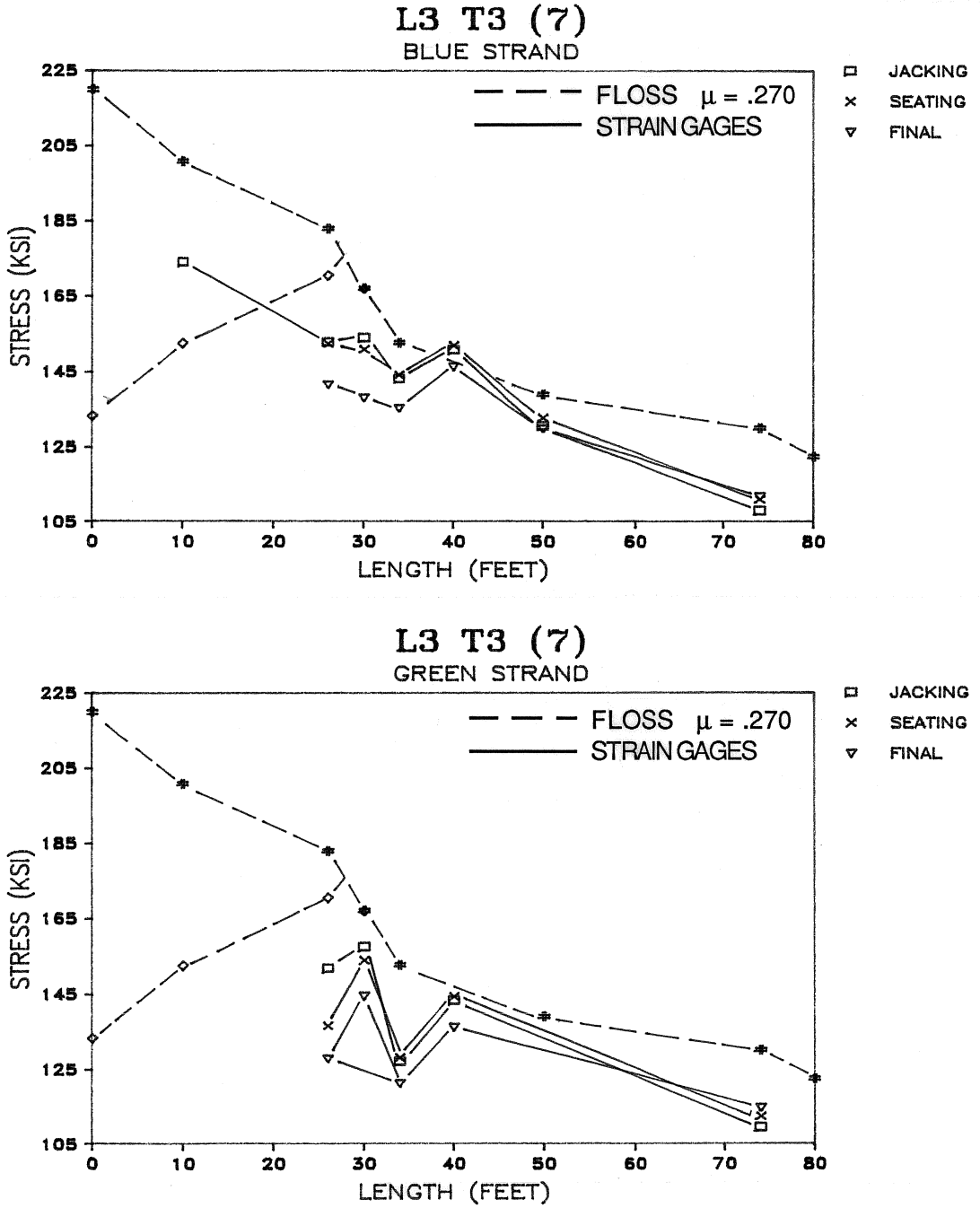

Fig. 4.15a L3 T3 (7): Jacking, seating, and final strand-stress variation

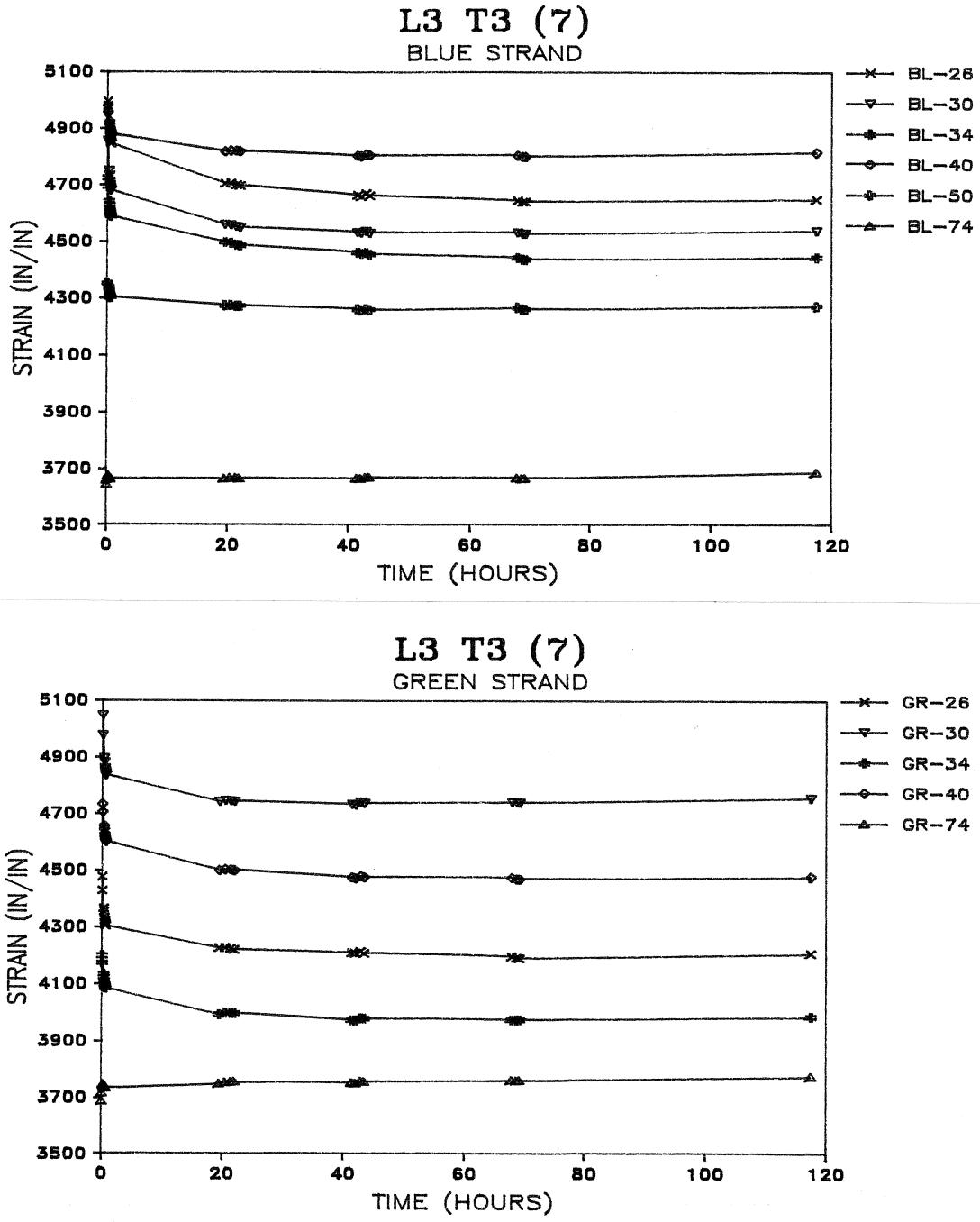

Fig. 4.15b L3 T3 (7): Strain redistribution with time after anchorage seating

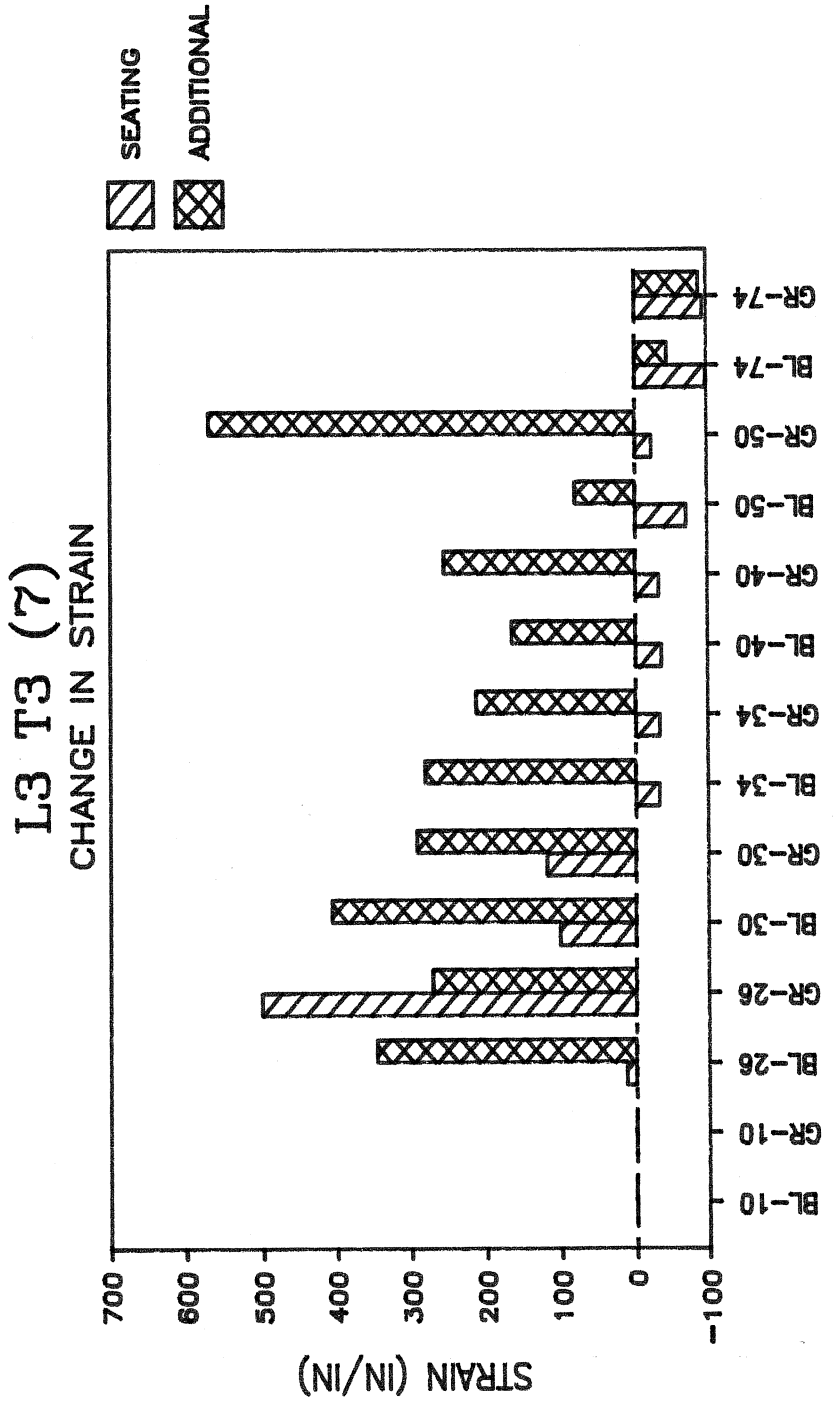

Fig. 4.15c L3 T3 (7): Seating and total additional strain change

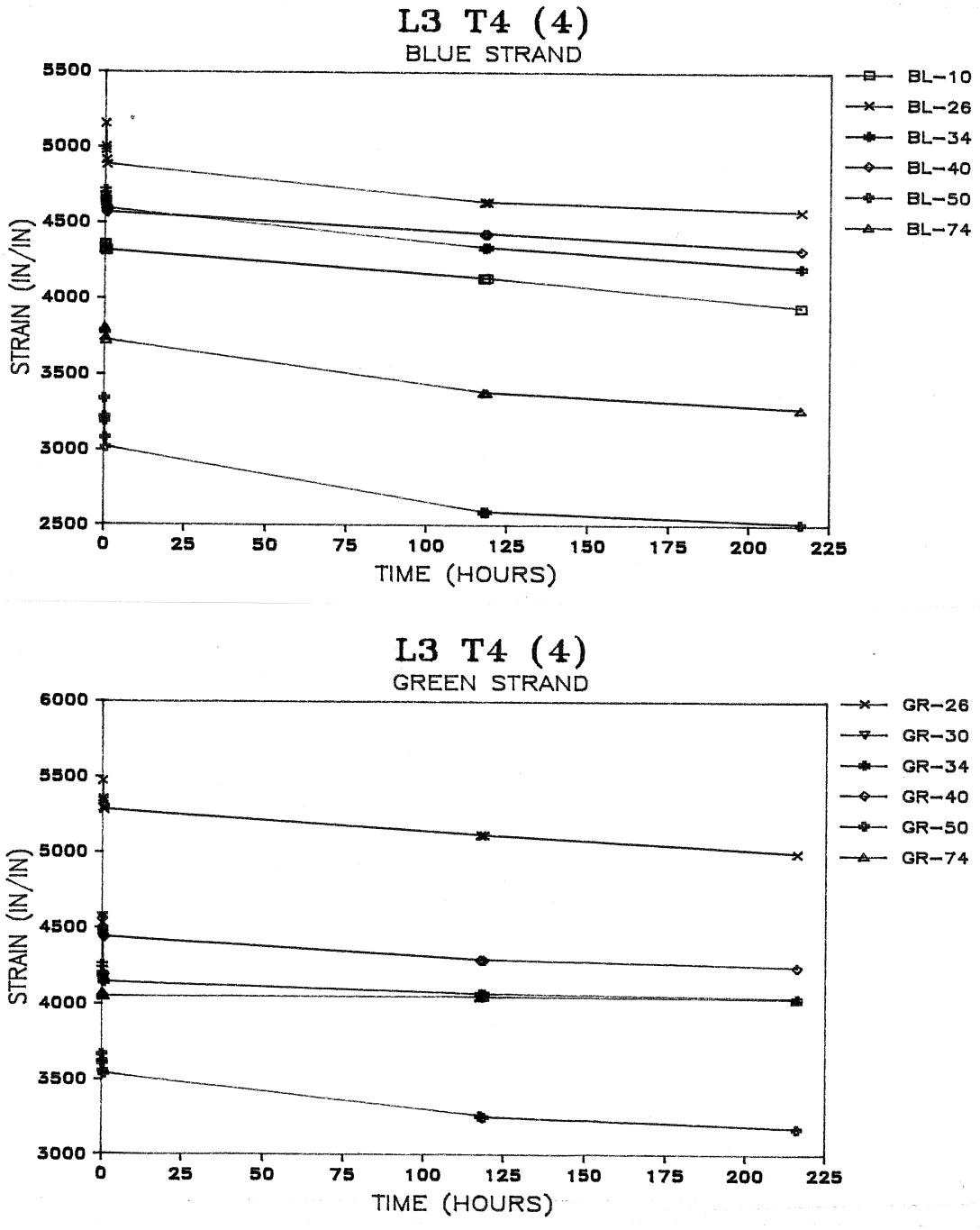

Fig. 4.16b L3 T4 (4): Strain redistribution with time after anchorage seating

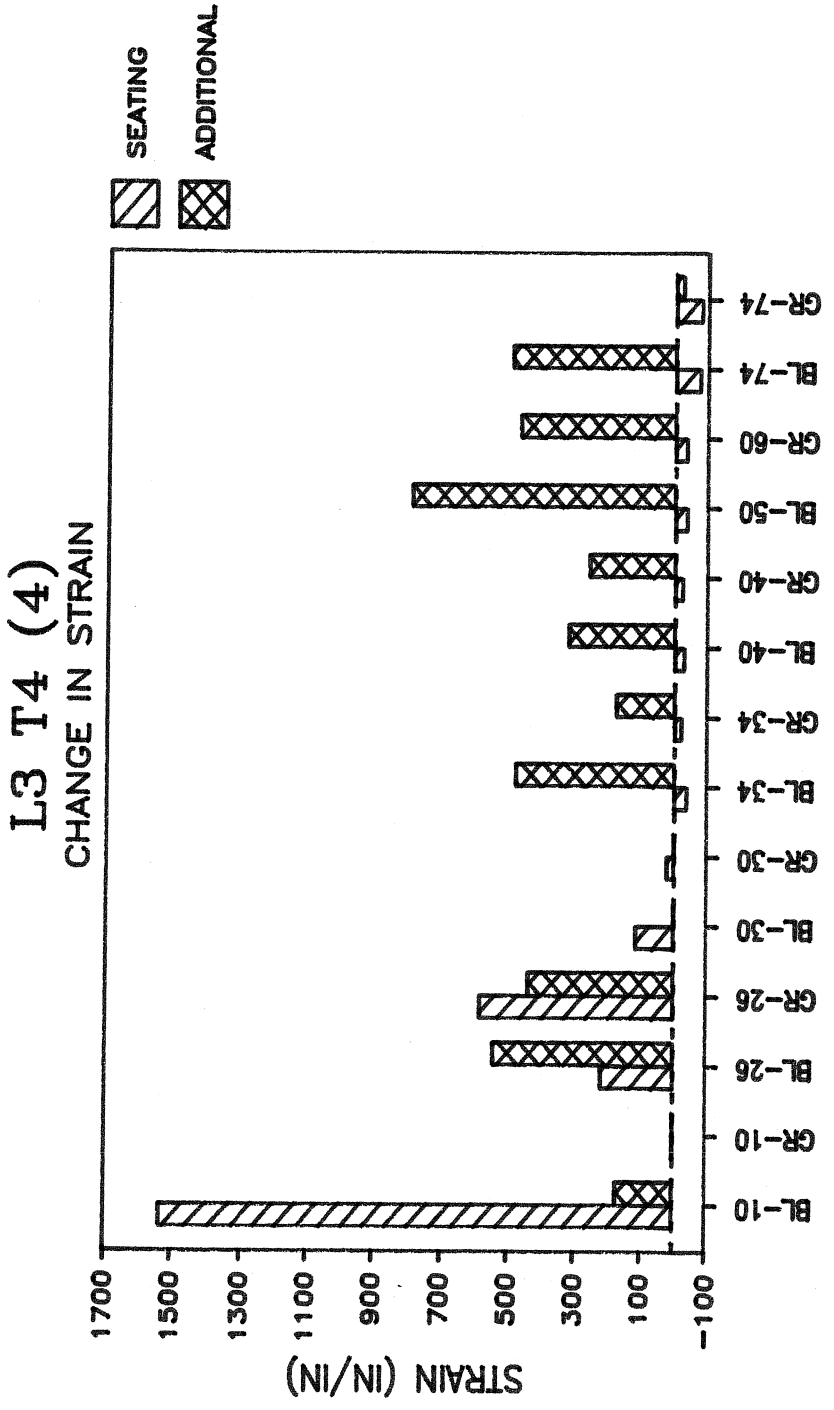

Fig. 4.16c L3 T4 (4): Seating and total additional strain change

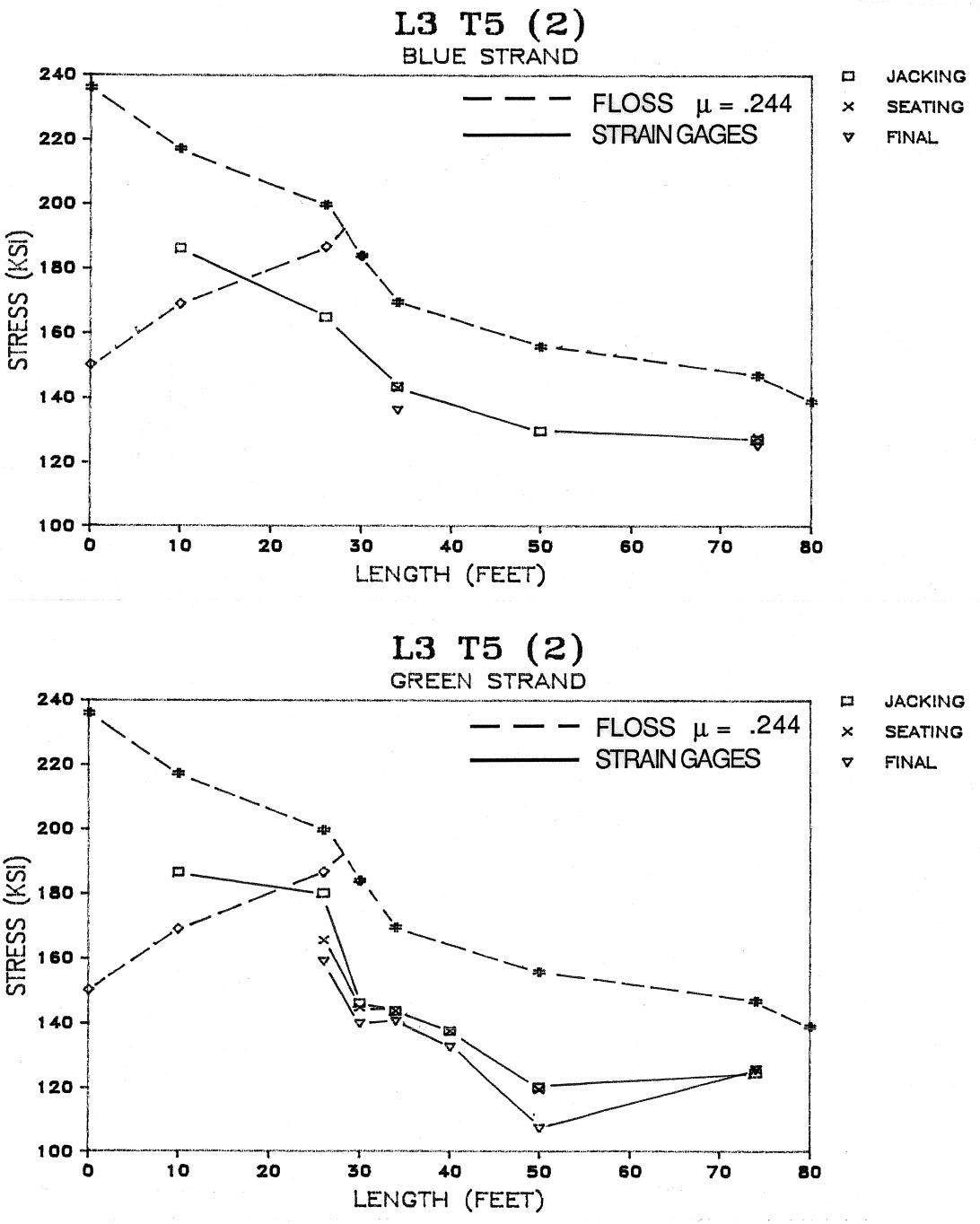

Fig. 4.17a L3 T5 (2): Jacking, seating, and final strand-stress variation

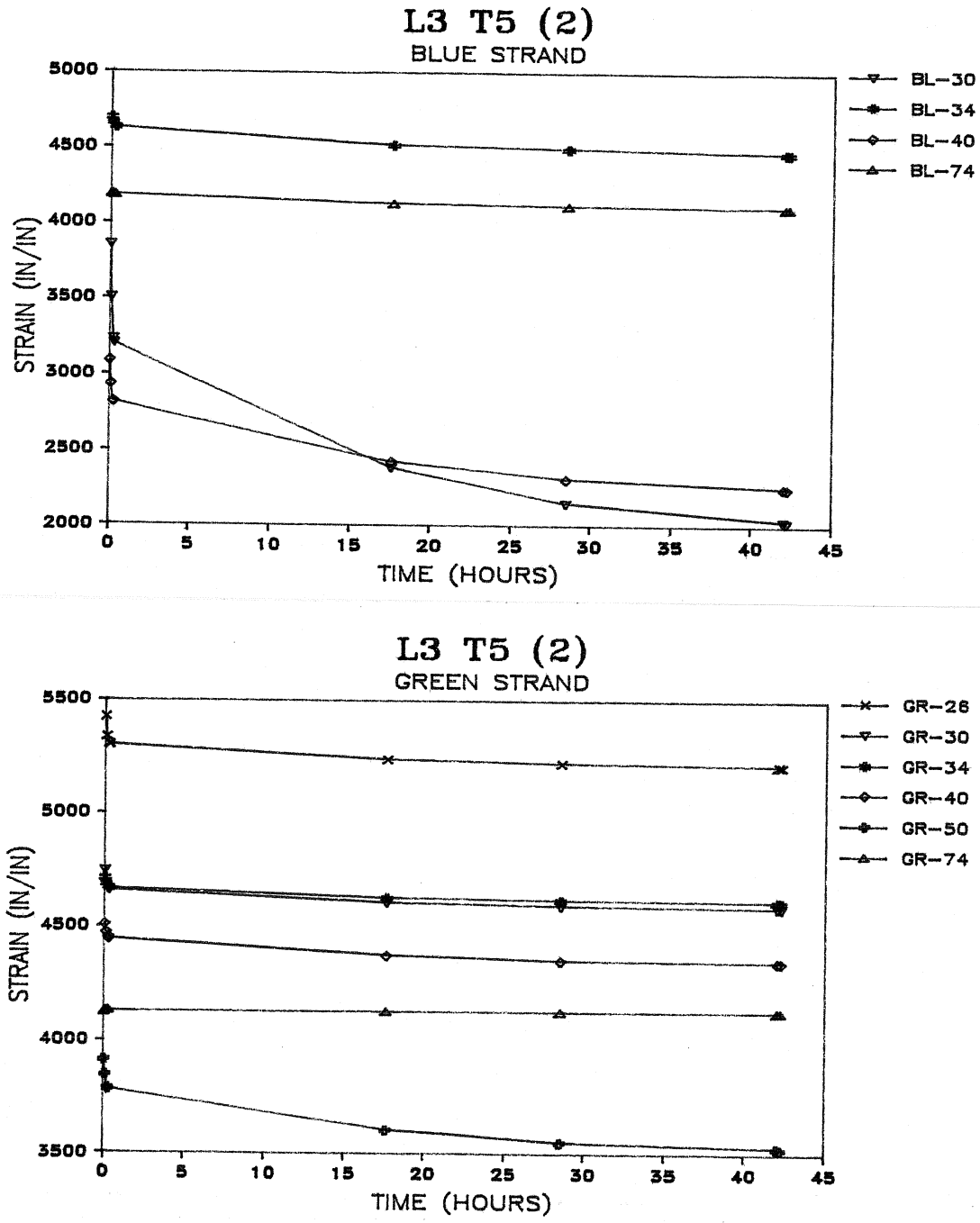

Fig. 4.17b L3 T5 (2): Strain redistribution with time after anchorage seating

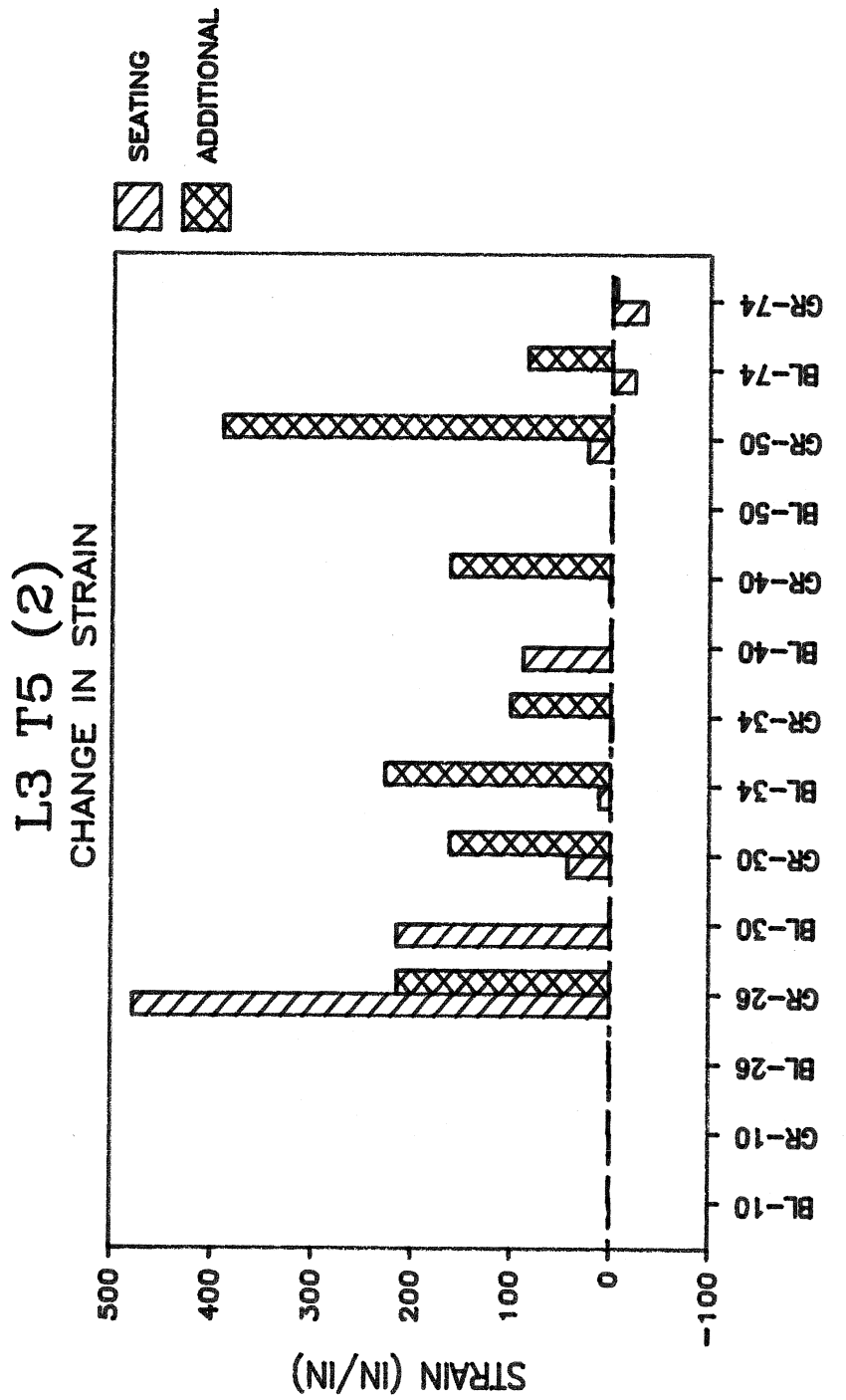

Fig. 4.17c L3 T5 (2): Seating and total additional strain change

the conventional practice of assuming a mirror image of the friction curve. The 'blue' strand for L3 T4 (4) (Fig. 4.16a) shows that the measured anchorage seating stress slope from BL-10 to BL-26 is reasonably identical to that of the predicted *FLOSS* slope. With fewer strands, anchorage seating does not redistribute or level strand stresses to the intersection of the two curves. Following seating, a large stress differential increased the additional losses between holding ends. After 216 hours, L3 T4 (4) had an average additional loss of 10 ksi. L3 T5 (2) decreased an average of 5.3 ksi after 43 hours. The additional strain generally decreased uniformly from end to end (Figs. 4.16c and 4.17c).

4.3.5 Epoxy Coated Strand. The grit embedded epoxy coated strand displayed extremely high frictional losses. Measured friction coefficients ranged from .530 to .610 for the rigid body layouts (Table 4.1). These values are approximately twice as large as the measured uncoated strand values and far exceeding the .318 value for galvanized metal conduit determined by the Florida Wire and Cable Report(6). Assuming a larger wobble coefficient, K, of .001/ft instead of .0002/ft, the friction coefficient ranges between 430 and 530. In this test, placement of seven epoxy coated strands in a conduit intended for seven uncoated strands accounted in part for more friction loss. The 30 mil epoxy coating increased the strand surface area in direct contact with conduit. However, the extremely coarse strand surface texture due to grit was the main cause of increased friction effects.

Figures 4.18a, 4.19, and 4.20 show the strand stress variation for tests L1 T7 (7E), L2 T7 (7E), and L3 T6 (7E), respectively. For L1 T7 (7E), the 'green' strand showed a consistent and substantial friction loss to GR-40 with no more reduction to GR-68. The 'blue' strand displayed a very inconsistent friction reduction along the length with a high stress at BL-68, 20 ksi greater than BL-56. The most probable explanation for large fluctuations such as these is a high localized strain for the particular gaged wire at BL-68. Overall, the measured strand stresses are within $\pm$10 ksi of *FLOSS* stresses with all measured strand stresses ranging between maximum jacking end stress and minimum holding end stress. But stress variation is highly variable in the interior region due to friction.

The coarse grit surface provided a friction interlock between the epoxy coated strands. Upon anchorage seating (Fig. 4.18c), a measurable strain loss was transmitted to BL-48/GR-48 and effectively ceased at that point, but a small strain loss was observable all the way to the holding end. The compressional anchorage seating wave in effect breaks the interlock in the lower stress region resulting in strand slippage throughout the specimen. Also, increased frictional losses resulted in a stress differential of 60 ksi from the jacking end to holding end. Thus, the normal force near the holding end provided less frictional resistance during seating. Strand stresses were redistributed and leveled for the 'green' strand to GR-40 but peaked to higher stresses at GR-48 (Fig. 4.19). Redistribution was not as significant for the 'blue' strand

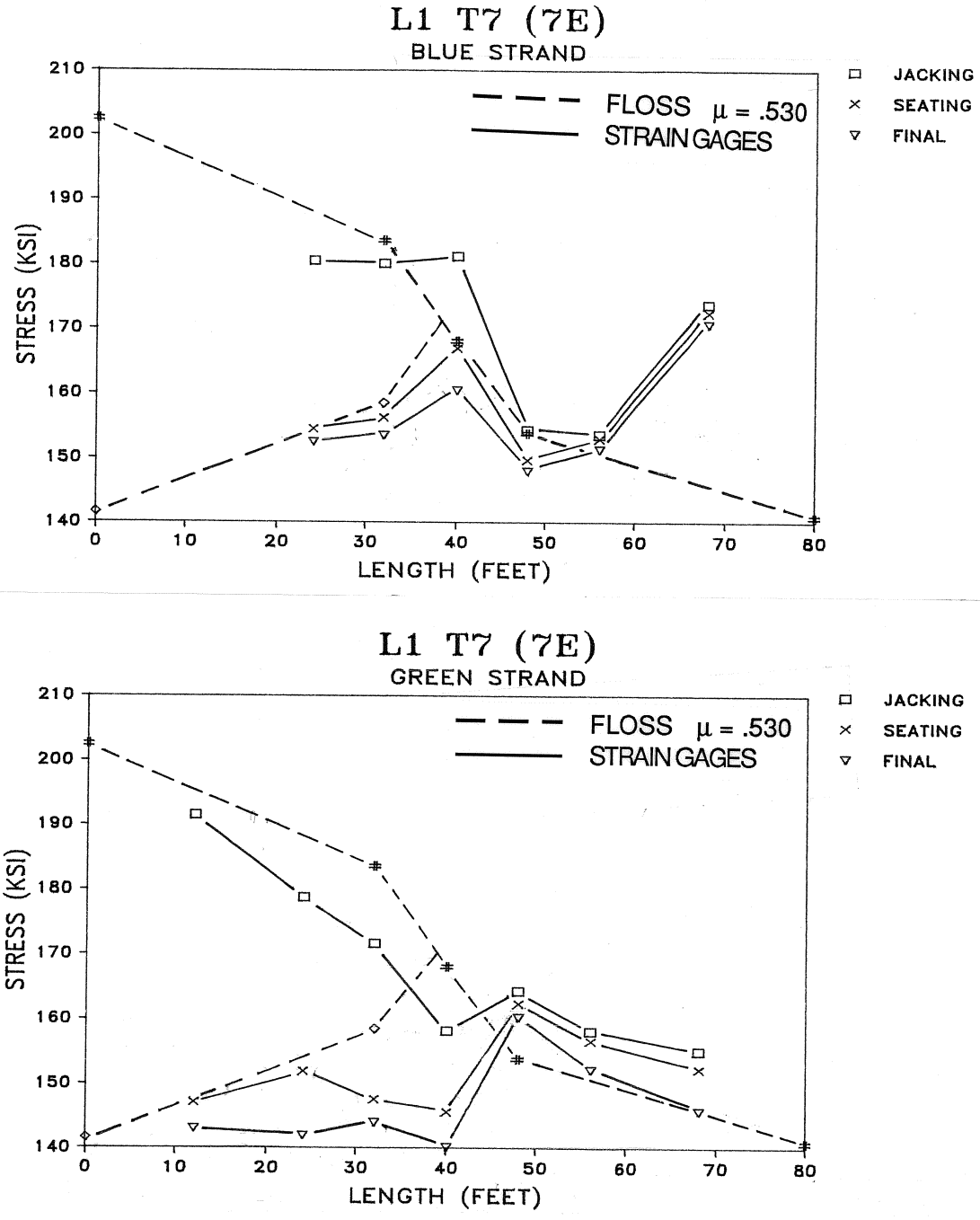

Fig. 4.18a L1 T7 (7E): Jacking, seating, and final strand-stress variation

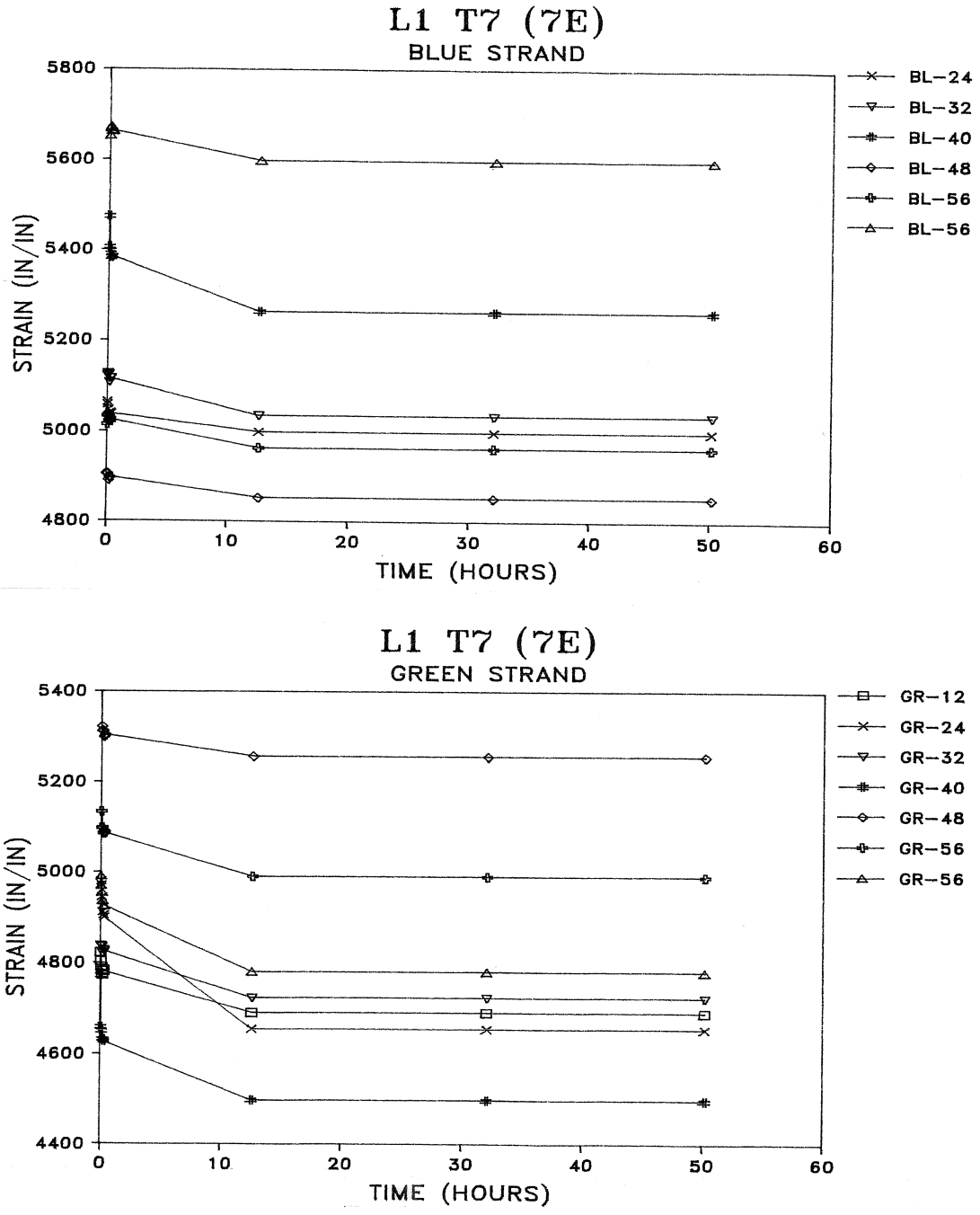

Fig. 4.18b L1 T7 (7E): Strain redistribution with time after anchorage seating

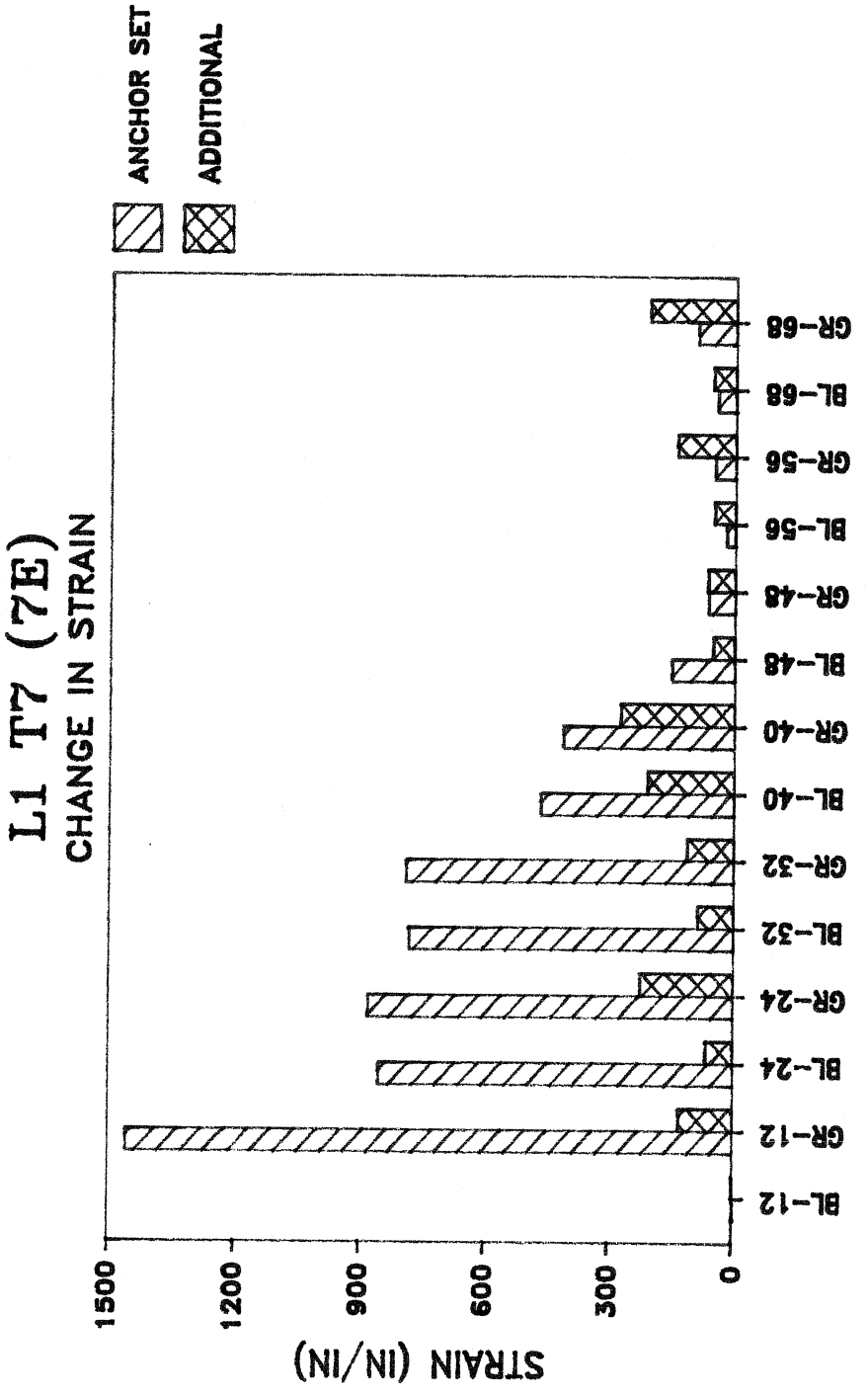

Fig. 4.18c L1 T7 (7E): Seating and total additional strain change

with a peak stress at BL-40. Yet Fig. 4.18c shows that the measured strain change for respective blockouts is almost identical. Therefore; upon seating, the larger normal force in the high stress region moved strands as a unit with leveling of strand stresses dependent on the initial friction stress variation for each strand. Additional redistribution was comparable to that of uncoated strands. Redistribution following seating was minimal in the monitored 52 hours with a total additional average stress loss of 4.5 ksi.

During stressing of L2 T7 (7E) and L3 T6 (7E), a wedge failure occurred at the holding end at jacking stresses of 157.5 and 135.0 ksi, respectively. In each case, only one of the seven strands failed. Failure was brittle and instantaneous as the wedge stripped the epoxy coating off strand a distance equal to post- tensioning elongation. These tests show that standard 3-piece wedges are not suitable for epoxy strands in post-tensioning systems. Measured strand stresses were extrapolated to a final jacking stress of 0.75f (202.5 ksi) from the jacking stress where failure occurred (Figs. 4.19 and 4.20). For these two tests, instrumented strand stresses favorably compared to the predicted *FLOSS* stresses. Note that the final stress differentials between jacking and holding ends were 82.5 and 142.5 ksi for L2 T7 (7E) and L3 T6(7E), respectively. Such high frictional losses would be considered impractical for design suggesting that an alternative to the epoxy coated with grit strand be used in post-tensioning.

4.4 Wichita Falls Bridge

4.4.1 Jacking Phase. In contrast to the three rigid body specimen layouts, a longer tendon profile length with shallow curvatures accounted for frictional losses in the Wichita Falls Taft Street Overpass Bridge (Figs. 3.2a and b). As both WF3 (19) and WF4 (19) exhibited similar results, only WF3 (19) will be discussed in detail. For initial first end jacking, an 18 percent tendon stress reduction due to friction was estimated. The measured friction coefficient for WF3 (19) was .309 corresponding to a twenty percent tendon stress reduction, slightly exceeding the assumed design values. For the four instrumented strands of WF3 (19), Figs. 4.21a and b show the measured strains at 1000 psi pressure gage increments for BO-89 and BO-183 (BO-X represents blockout distance from jacking end). Strain gage measurements displayed a linearly elastic behavior during stressing, but strains varied between strands. Strain variation in part occurred as the temporary wedges in the pulling block completely gripped the strands at slightly different intervals in the initial extension of the stressing ram piston. Note that a slight strain differential was measured between two strain gages spaced six in. apart on the same strand. At maximum jacking pressure, the corresponding maximum/minimum measured stresses were 183.9/165.6 ksi and 168.4/155.7 ksi with averages of 174.3 and 161.4 ksi at BO-89 and BO-183, respectively.

Figure 4.22 shows the measured strand stresses in comparison to the theoretical *FLOSS*

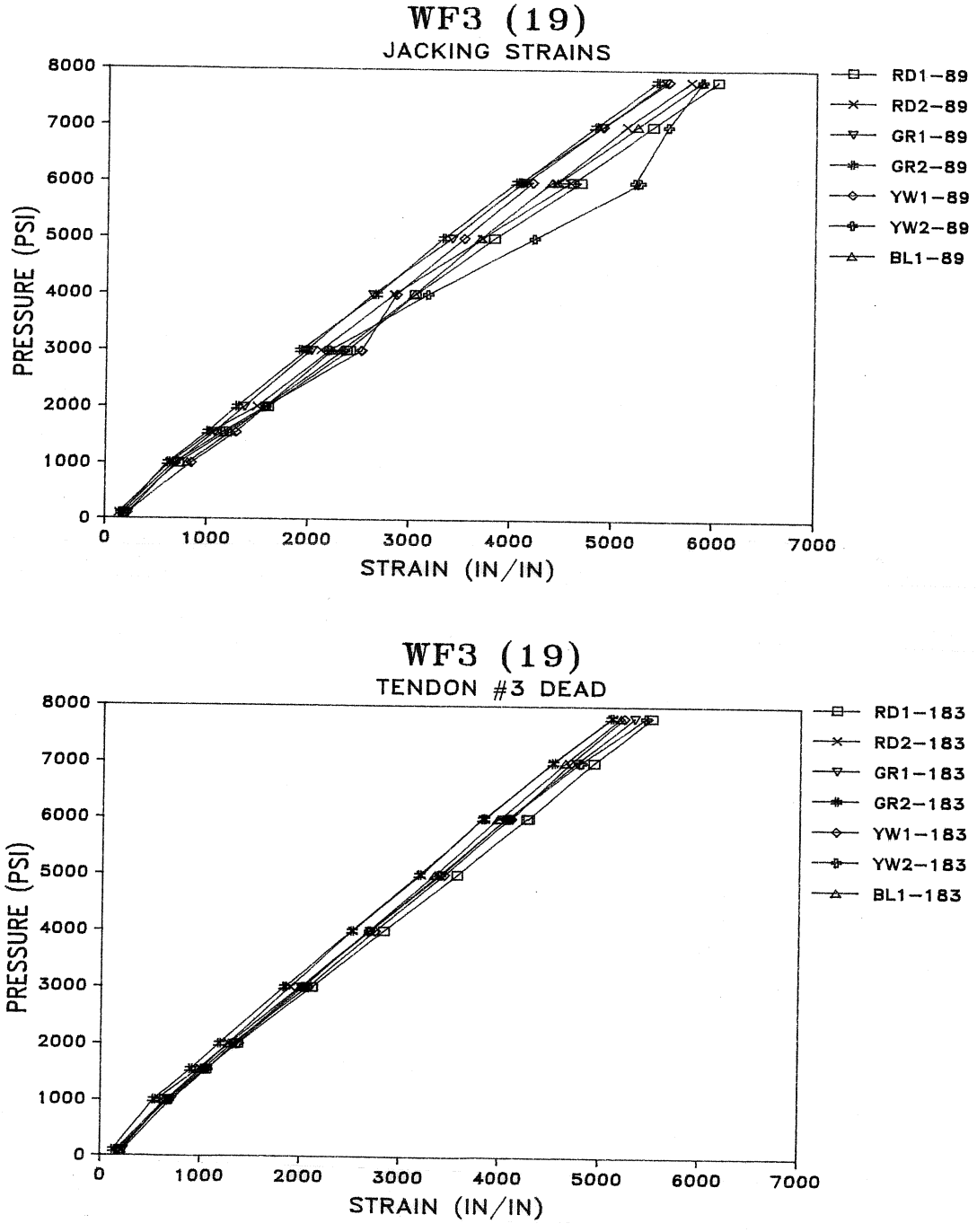

Fig. 4.21 WF3 (19): Strains at a distance from jacking end of (a) 89 ft and (b) 183 ft

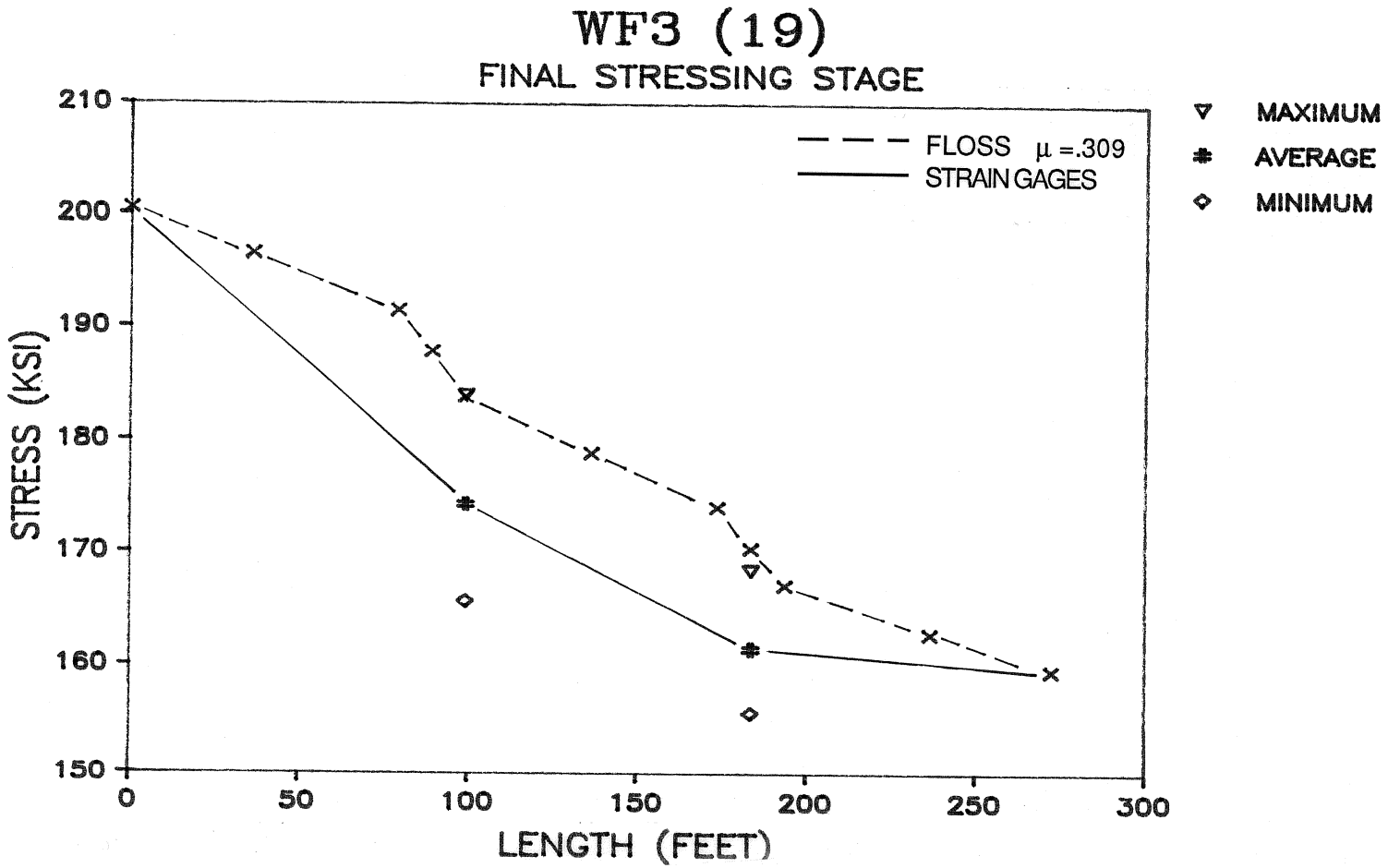

Fig. 4.22 WF3 (19): Strand stresses during jacking

stresses. Based on strain gage measurements, frictional losses greatly reduced tendon stress in the first 90 ft by 26.2 ksi. From 90 to 180 ft, a further reduction of 12.9 ksi occurred with an assumed final reduction of 1.9 ksi in the final 90 ft. Although derivation of theoretical friction formulas accounted for decrease in tendon tension and normal force, test results show that the high normal force close to the jacking end decreases tendon stress much faster than the natural logarithmic exponential predicts. Instrumented strands were located on the exterior of the strand bundle away from the conduit at the blockouts. Between blockouts, instrumented strands were in direct contact with conduit with the normal force of the remaining 15 strands increasing the instrumented strand pressure against the conduit. Also, instrumented strands were positioned against the conduit surface along the majority of profile length due to the low curvatures of this layout. Hence, a significantly greater frictional loss resulted for the monitored strands in comparison to the theoretical average friction loss for all strands as a unit as shown in Fig. 4.22. Measured stressing strand data for WF4 (19) were very similar to WF3 (19).

4.4.2 Anchorage Seating. Unlike the hydraulic stressing ram used in laboratory testing, the hydraulic field stressing ram used a pressure control value in the electric pump to regulated the maximum pressure release. Thus, an induced compressional wave during force transfer was not a contributing factor for strand stress redistribution. The average anchorage transformation loss was consistently measured at 9/16 of an in. Figure 4.23 shows that *FLOSS* estimates the anchor set curve to intercept the friction loss curve at BO-89. Detected seating induced strain change for the instrumented strands is shown in Fig. 4.25a and b. At BO-89, the strains correspond to stress losses which ranged from 2.7 to 5.5 ksi with an average of 4.5 ksi. Note that observed strain changes for two strain gages on an individual color coded strand were nearly identical. No change was detected at BO-183.

Gradual release of jacking pressure did not produce the theoretical peak stress at BO-89 (Fig. 4.23). Instead, the anchorage transformation loss simply allowed the strands to slip back to a lower stress level. After seating, final jacking end stress was 178.3 ksi decreasing to 159.5 ksi at the holding end. Hence, for the shallow curvature profile, anchorage seating significantly redistributed and leveled strand stresses.

4.4.3 Time Period Prior to Grouting.

4.4.3.1 Additional Losses. Figures 4.24a and b show strand strain redistribution pattern with time following seating for each blockout. Elastic shortening in the subsequent stressing of the remaining 32 tendons accounted for the majority of additional strain decrease. As would be expected, elastic shortening for WF3 (19) was largest while stressing the interior tendons with the furthest exterior strands having a negligible effect. Each strain gage detected an almost identical reduction at each respective blockout suggesting that in a given cross sec-

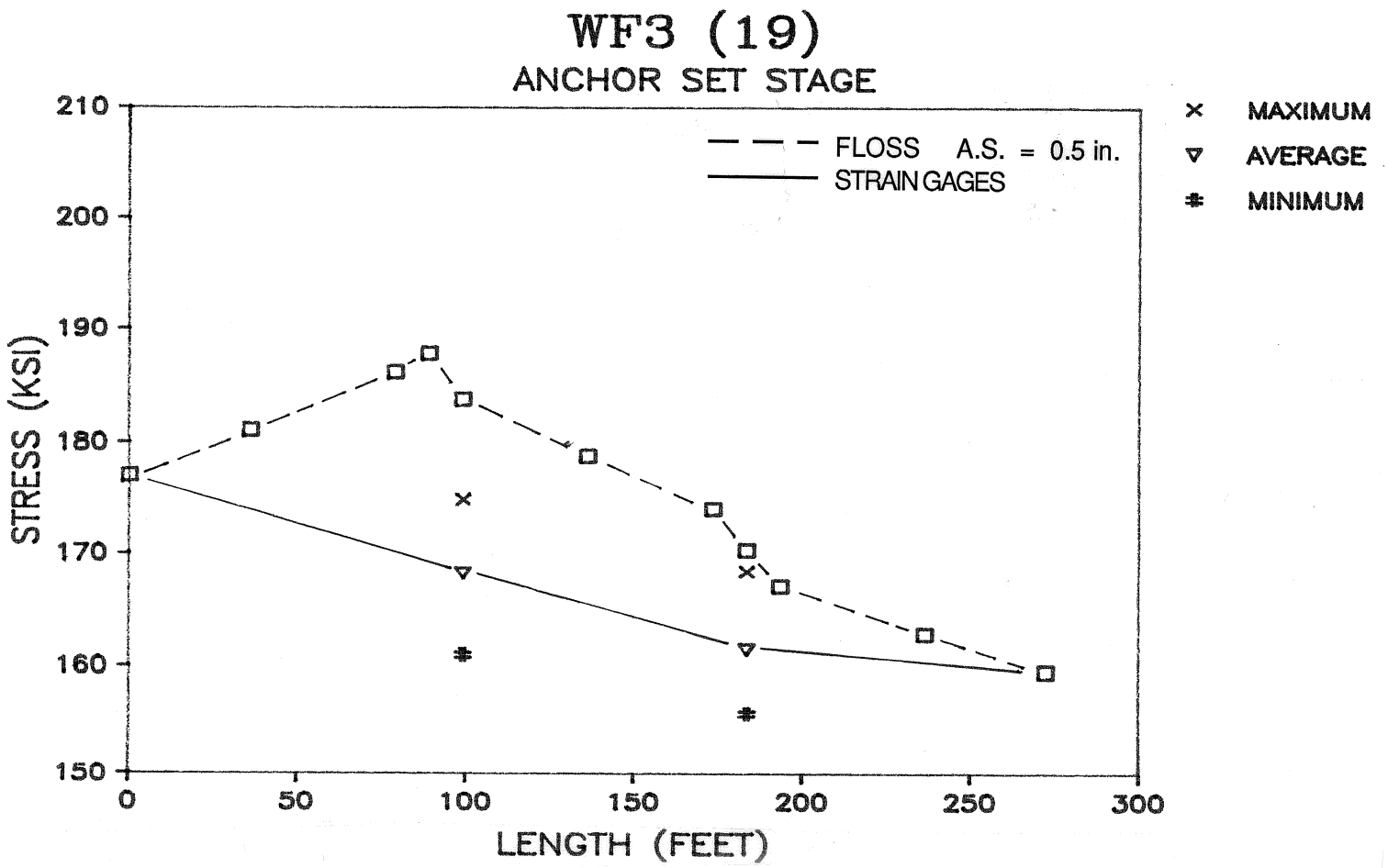

Fig. 4.23 WF3 (19): Strand stresses following seating

tional plane, the strands can be treated as a unit. At 64 hours following seating, total observed additional strain change is show in Figs. 4.25a and b. Corresponding total measured stress losses were 10.0 and 8.7 ksi for BO-89 and BO-183, respectively. Excluding the elastic shortening losses; creep, shrinkage, and relaxation losses accounted for 2.3 and 1.0 ksi at BO-89 and BO-183. Therefore, elastic shortening accounted for approximately 7.3 and 7.7 ksi of the additional stress loss. In design, elastic shortening was estimated with the following equation:

$$ES = (E_s/E_c)\, f_{cir} \tag{4.1}$$

where

E_s = modulus of elasticity of prestressing strand

E_c = initial modulus of elasticity of concrete

f_{cir} = stress in the concrete at c.g.s. due to prestress force

The above equation yields a stress loss of 8.4 ksi. Second end stressing should slightly increase the elastic shortening loss for WF3 (19) surpassing the estimated value. But WF3 (19) experienced more elastic shortening than exterior tendons so the estimated value is a reasonably close approximation. The holding end stress for all 19 strands as monitored with the load cell decreased a total of 8.4 ksi. Note that a slight redistribution of instrumented strand stresses occurred due to a combination of elastic shortening, creep, and shrinkage of the bridge slab.

4.4.3.2 Second End Stressing. Since WF3 (19) had a load cell at the holding end, second end stressing effects will be described for WF4 (19). Table 4.3 shows WF4 (19) average measured instrumented strand stresses for BO-89 and BO-183 at different phases of stressing. Note that just prior to second end stressing (after time dependent losses), tendon stresses at BO-89 were just 6.7 ksi larger than BO-183. Hence the stress level is approximately equal along the tendon profile. Referring to Figs. 3.2a and b, measured strand stresses at this stage are 32.0 and 24.5 ksi below the estimated friction loss design curve for BO-89 and BO-183, respectively. Also, second end stressing was calculated to produce an increased stress level of 15.0 ksi at BO-183 as shown in Fig. 3.2b.

The maximum second end jacking stress (Table 4.3) at BO-183 showed a stress increase of 15.9 ksi, closely approximating the theoretical estimate. But the stress level remained 22.8 ksi below the design curve. In addition, the BO- 183 stress was slightly less than the maximum initial jacking stress experienced at BO-89. Thus, the friction effect again decreased the instrumented strand stresses in the 90 ft between jacking end and blockout location. Note that at BO-89, the stress level increased slightly by 1.3 ksi.

	Average Stresses of Instrumented Strands	
	Blockout 89 (ksi)	Blockout 183 (ksi)
Initial Jacking	171.4	157.3
Seating	167.4	157.3
Time Dependent Effects	157.5	150.8
2nd End Jacking	158.8	166.7
Seating	158.8	166.5
Final	159.0	165.3

Table 4.3 WF4 (19) Second End Stressing

To achieve the maximum second end force, the required tendon elongation was 1.125 in. Upon anchorage seating, the transformation loss was not detected at BO-183. After seating, the stress level at BO-183 was 7.7 ksi larger than at BO-89. Hence, after second end stressing and seating, the stress level remained approximately uniform along the tendon profile. Figures 4.26a and b show the measured instrumented strand's strain change redistribution with time for WF4 (19).

4.5 T-Section Beam

4.5.1 Jacking Phase. For the 30-ft simply supported, T-Section beam (L4 TB (7)), four of the seven strands were instrumented with strain gages with a load cell at the holding end. Instrumented strands were in direct contact with galvanized metal conduit. Normal forces from the non- instrumented strands acted through the instrumented strands. Figures 4.28a and b show the measured strand strains at BO-9.5 and BO-20.5, respectively, at 500 psi pressure gage increments during jacking . Each strand displayed a linear elastic behavior with approximately the same slope. Slope variation between individual strands was a result of the temporary pulling block wedges gripping an individual stand at different intervals in the initial extension of hydraulic ram.

The measured friction coefficient for L4 TB (7) was 0.305. Figure 4.29a shows that the average of measured strand stresses at the maximum jacking force closely approximated the predicted *FLOSS* stresses. Individual strand stresses ranged from 174.1 to 213.2 ksi at BO-9.5 and 175.2 to 195.1 ksi at BO-20.5. The sharpest friction stress reduction occurred between the two blockouts. In this region, tendon curvature changed from a negative to positive slope. Note that the 'green' strand had the highest stress at BO-9.5 and the lowest at BO-20.5. The 'green' strand location was such that normal force components from surrounding strands acted through it. This indicates that an individual strand stress is dependent on the normal force interaction between strands and relative location in the strand bundle.

4.5.2 Anchor Set Phase. The hydraulic stressing ram used in the laboratory released jacking pressure instantaneously. For this test, anchorage transformation loss was 0.5 in. Figure 4.31 shows that the detected seating loss was nearly uniform throughout the layout. Averaged measured strand stress loss was 36.2 ksi. Assumed stress loss at the jacking end was 56.5 ksi with a measured stress loss of 32 ksi at the holding end. The seating induced compressional wave effectively redistributed and leveled strand stresses for L4 TB (7) (Fig. 4.29b). Hence, final tendon stress level could be reasonably approximated as uniform and equal throughout this short (30 ft) beam with low tendon curvature.

4.5.3 Redistribution Following Seating. THe tendon stresses following jacking and seating are approximately constant along the length, thus redistribution effects in the monitored time

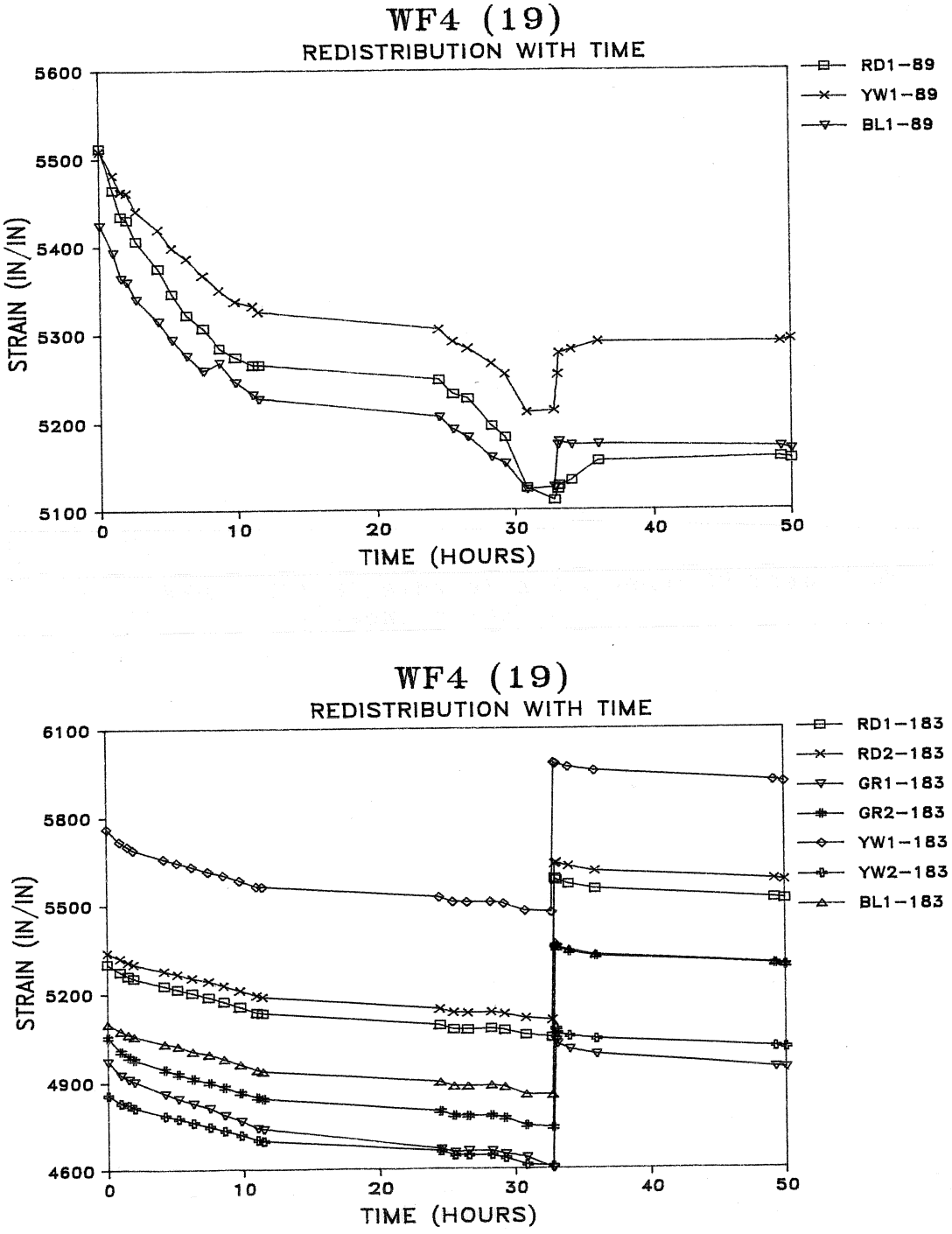

Fig. 4.26 WF4 (19): Strains at a distance from jacking end of (a) 89 ft and (b) 183 ft

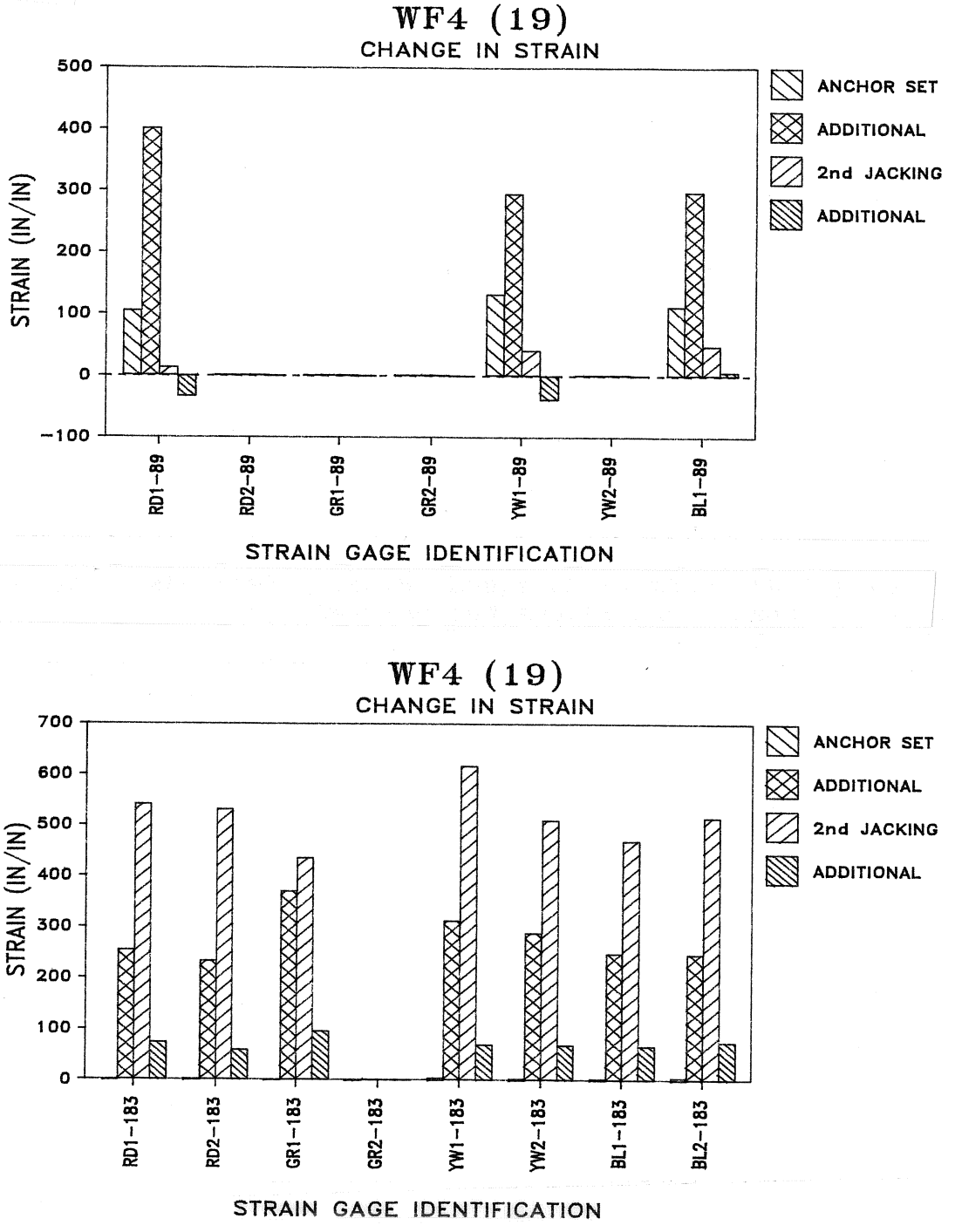

Fig. 4.27 WF4 (19): Strain change due to seating and additional losses (a) at blockout 89 and (b) at blockout 183

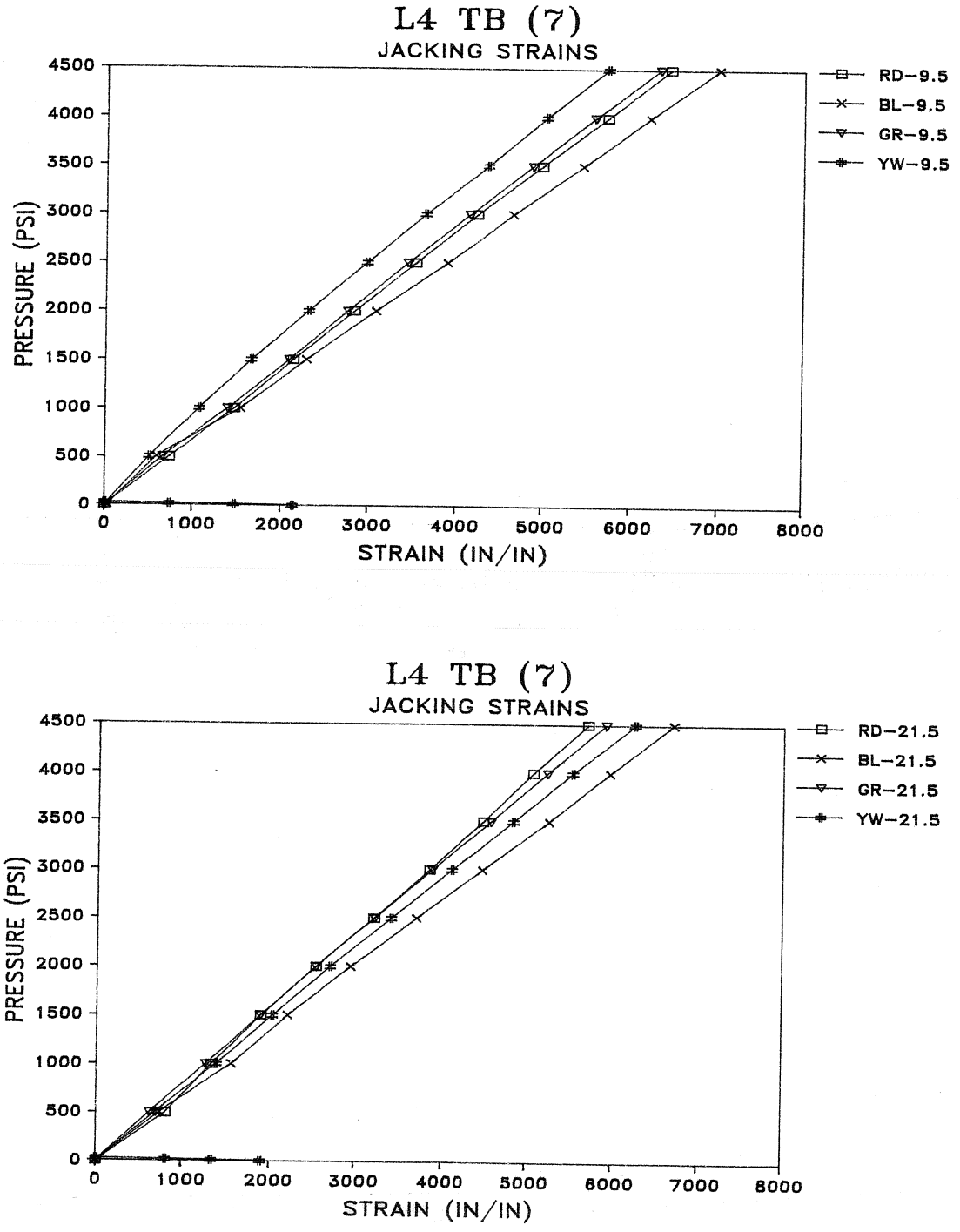

Fig. 4.28 L4 TB (7): Strand strains during jacking at blockout (a) 9.5 ft and (b) 20.5 ft

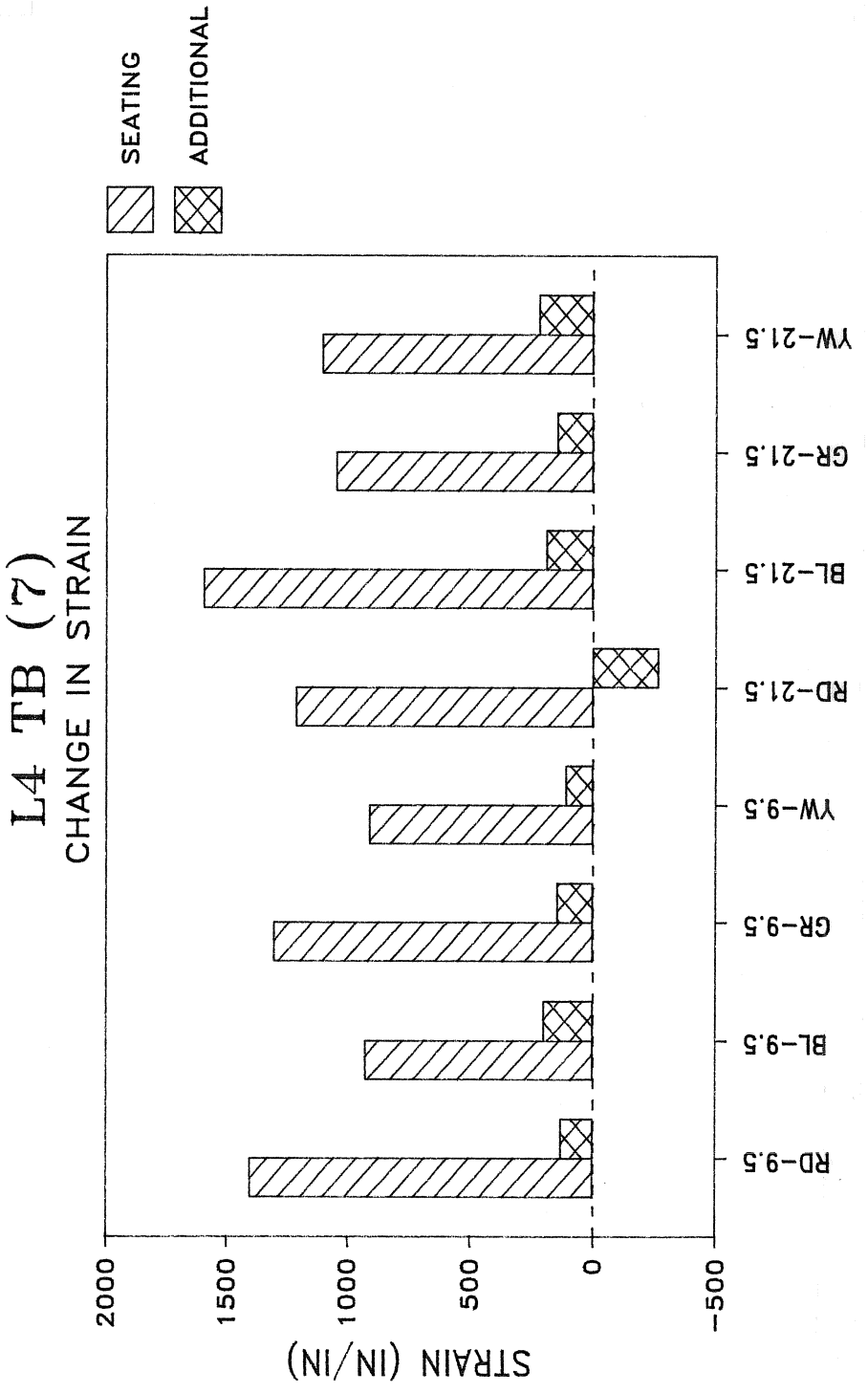

Fig. 4.31 L4 TB (7): Seating and total additional strain change

period for leveling peak and valley stresses was insignificant. Figures 4.30a and b show the strand strain change due to the combined time dependent effects of creep, shrinkage, and relaxation. Slight upward camber developed from creep which made a very small contribution to strand stress losses. After 167 hours, the total average stress loss was 4.7 ksi corresponding to a 3.0 percent reduction. This additional loss falls in the same range as those observed for the rigid body layouts.

CHAPTER FIVE CONCLUSIONS

Based on the test results of the three tendon profiles in the rigid body specimen, the 30-ft simply supported T–Beam, and the tendon profile in the 275-ft three span Wichita Falls bridge evaluated in this research study, the following conclusions can be made for the three different phases prior to grouting.

5.1 Jacking Phase

1. The coefficient of friction, μ, is highly variable for similar materials and stressing systems. But for galvanized rigid metal conduit and uncoated seven-wire strand, a value of $\mu = .30$ is a reasonable approximation for design based on these test results. This value is larger than the current recommended value. The number of strands per tendon did not significantly influence the coefficient of friction value.

2. Using the conventional friction loss formula with recommended wobble coefficient and friction coefficient values yields a reasonable estimation of the tendon stress along the tendon profile and the holding end force. No change in the current design procedure is necessary.

3. Individual strand stresses between the jacking end and holding end are influenced by their relative position in the strand bundle as strands change positions along the tendon profile length. Interaction between strand and conduit, strand and strand, and the normal force of surrounding strands leads to a highly variable strand stress variation along the layout length which is not uniformly influenced by the coefficient of friction.

4. The individual stress variation at design control points between the jacking and holding ends did not consistently achieve the stress level predicted with the conventional friction loss formula. In the regions closest to the jacking end, individual strand stresses were overestimated. As the distance from the jacking end increased, individual strand more closely approximated the predicted stresses from the friction loss formula. This reinforced the current practice of using the critical tendon stress region for design rather than an average tendon stress along several spans in a multi-span structure.

5. As the number of strands per tendon increased, the increased normal force from surrounding strands lead to larger stress reduction along the layout between the jacking and holding ends.

5.2 Anchorage Seating Phase

1. The change in the stress at the jacking end and the length influenced by the seating transformation loss are reasonably estimated by the procedure outlined in the Post-Tensioning Manual.

2. Anchorage seating tended to redistribute and equalize individual strand stresses along the length influenced by seating. This is a change in the current design procedure which assumed a mirror image seating loss curve to the friction loss curve.

3. The anchorage seating curve can be reasonably approximated as a linear transformation between the resulting jacking end stress and friction loss stress at the distance influenced by seating. This linear transformation is a straight line between these two points, not the linear transformation mirror image of the friction loss curve.

4. For design, the Post-Tensioning Manual procedure for determining the change in stress and the influenced length are recommended based upon a mirror image seating curve. Then based upon these values, a straight line drawn between the resulting jacking end stress and the intersection of the friction loss curve stress should replace the mirror image curve.

5.3 Following Seating and Prior to Grouting Phase

1. Within five hours of seating, individual strand stresses had essentially achieved an equilibrium stress level.

2. Following seating, redistribution of individual strand stresses was minimal. There was no significant equalization of strand stresses to level the friction and seating induced stress variation along the tendon path. Based on these results, designers cannot assume that an average tendon stress for design represents the actual tendon stress. However, the calculated force along the path of the tendon, after seating, gives a very good estimate of the general profile of the tendon force along the length of the beam following transfer. With time, losses will occur which reduce prestress to the final effective prestress force values along the member. This same general profile, considering further losses along the path in addition to friction loss, should be the basis for design of prestressed concrete structures.

3. Individual strand stresses experienced a stress loss which ranged between 2.0 ksi and 6.0 ksi for monitored time periods of up to two weeks. Ninety-five percent of the stress loss occurred within five hours and the change in stress was approximately uniform along the tendon profile length.

REFERENCES

1. American Concrete Institute, *Building Code Requirements for Reinforced Concrete and Commentary (ACI 318-83)*, Detroit, Michigan, 1983.

2. Post-Tensioning Institute, *Post-Tensioning Manual*, 4th Edition, Phoenix, Arizona, 1985.

3. *American Association of State Highways and Transportation Officials, Standard Specification for Highway Bridges*, 13th Edition, 1983.

4. Lin, T.Y., and Burns, Ned H., *Design of Prestressed Concrete Structures*, 3rd Edition, John Wiley & Sons, New York, 1981.

5. Lin, T.Y., "Cable Friction in Posttensioning," *Journal of the Structural Division*, American Society of Civil Engineers, November, 1956.

6. Presswalla, Hoshi, "Friction and Related Properties of Tendons for Harlem River Bridge: Test Report," Florida Wire and Cable Company, Jacksonville, Florida, 1982.

7. Stone, W.C., and Breen, J.E., "Design of Post- Tensioned Girder Anchorage Zones," *Research Report 208-3F*, Center for Transportation Research, The University of Texas at Austin, June 1981.

8. Dorsten, Victor, Hunt, Frederick F., and Preston, H. Kent, "Epoxy Coated Seven-Wire Strand for Prestressed Concrete," *Prestressed Concrete Institute Journal*, Vol. 29, No.4, July-August 1984.

9. "Tentative Recommendations for Prestressed Concrete," Report by ACI-ASCE Committee 423, *Journal of the American Concrete Institute*, Vol. 54, No. 7, January 1958.

APPENDIX A

COMPUTER PROGRAM FLOSS

```
      PROGRAM FLOSS(INPUT,OUTPUT,TAPE5=INPUT,TAPE6=OUTPUT)
      DIMENSION CGS(100), SL(100), TAC(100), STRA(100)
      DIMENSION STR(100), TP(100), SLT(100), DIFF(100)
C
C     DESCPRITION OF ENTRY PARAMETERS
C
C         WOBLE              WOBBLE COEFFICIENT
C
C         AMU                FRICTION COEFFICIENT
C
C         PJACK              JACKING STRESS (KSI)
C
C         PER                PERCENTAGE FOR SLACK FORCE (%)
C
C         E                  ELASTICITY OF STEEL TENDON (KSI)
C
C         ANSET              ANCHOR SET (INCHES)
C
C         N                  COUNTER VALUE (NUMBER OF SEGMENTS)
C
C         SL(I)              SEGMENT LENGTH OF ELEMENT I (FEET)
C
C         CGS(I)             ELEVATION DIFFERENCE BETWEEN ENDS
C                            OF SEGMENT (INCHES)
C
C         TP(I)              SHAPE OF SEGMENT
C
C
C     ENTER THE ABOVE REQUIRED INPUT DATA FOR
C     THE CHOSEN TENDON LAYOUT PROFILE
C
C     ENTER VALUES OF WOBLE, AMU, PJACK, PER, E, AND ANSET
C
      READ(5,*) WOBLE, AMU, PJACK, PER, E, ANSET
C
      WRITE(6,10) WOBLE, AMU, PJACK, PER, E, ANSET
   10 FORMAT(///,20X,'WOBBLE COEFFICIENT',11X,'=',F10.4,
     1          /,20X,'FRICTION COEFFICIENT',9X,'=',F10.3,
     1          /,20X,'JACKING STRESS',15X,'=',F10.2,1X,'KSI',
     1          /,20X,'SLACK PERCENTAGE',13X,'=',F10.1,1X,'PERCENT',
     1          /,20X,'STEEL MODULUS OF ELASTICITY',2X,'=',F10.1,1X,'KSI',
     1          /,20X,'ANCHOR SET',19X,'=',F10.3,1X,'INCHES')
C
C
C     ENTER COUNTER VALUE  N  FOR THE NUMBER
C     OF DIFFERENT SEGMENTS
C
      READ(5,*) N
C
C     ENTER THE SEGMENT LENGTH, ELEVATION DIFFERENCE OF ENDS,
C     WHETHER THE SEGMENT IS TANGENT OR PARABOLIC IN SHAPE
C
C           NOTE: ENTER  0  FOR TANGENT SEGMENT
C                 ENTER  1  FOR PARABOLIC SEGMENT
C
      DO 20 I=1,N
C
            READ(5,*) SL(I), CGS(I), TP(I)
C
   20 CONTINUE
C
C
C
C     CALCULATE INCREMENTAL ANGLE CHANGES
C
      DO 30 I=1,N
C
            IF(TP(I) .EQ. 0) THEN
            TAC(I) = 0.0
            ELSE
            TAC(I) = CGS(I)/SL(I)/6.0
            ENDIF
C
   30 CONTINUE
```

```
C
      SLT(1) = SL(1)
C
      DO 40 I=2,N
C
            SLT(I) = SLT(I-1)+SL(I)
C
   40 CONTINUE
C
      SUM = 0.0
C
      DO 50 I=1,N
C
            SUM = SUM-(SL(I)*WOBLE+AMU*TAC(I))
            STR(I) = PJACK*EXP(SUM)
C
   50 CONTINUE
C
C     WEIGHTED STRESSES FOR AVERAGING
C
      TOTAL = 0.0
      PRE = PJACK
C
      DO 60 I=1,N
C
            TOTAL = TOTAL+(STR(I)+PRE)/2.0*SL(I)
            PRE = STR(I)
C
   60 CONTINUE
C
C     AVERAGE THE STRESSES
C
      AVG = TOTAL/SLT(N)
C
C     CALCULATE TENDON ELONGATION
C
      ELONG = AVG*SLT(N)/E*12.0
      PX = 1.0-(PER/100.0)
      PE = PX*ELONG
C
C     RENUMBER THE CONSTANTS
C
      DO 70 I=1,N
C
            STR(N+2-I) = STR(N+1-I)
            SLT(N+2-I) = SLT(N+1-I)
            TAC(N+2-I) = TAC(N+1-I)
            CGS(N+2-I) = CGS(N+1-I)
            SL(N+2-I) = SL(N+1-I)




            TP(N+2-I) = TP(N+1-I)
C
   70 CONTINUE
C
      STR(1) = PJACK
      SLT(1) = 0.0
      TAC(1) = 0.0
      CGS(1) = 0.0
      SL(1) = 0.0
      TP(1) = 1.0
C
C     CALCULATE THE LOSSES DUE TO ANCHOR SET
C
      DO 80 I=1,N
C
            DIFF(I) = 2.0*(STR(I)-STR(I+1))
C
   80 CONTINUE
C
      DIFF(N+1) = 0.0
      DELTL = 0.0
C
      DO 100 I=1,N
C
            M = I
            DELTL = DELTL+DIFF(I)*SL(I+1)*6.0/E
            IF(DELTL .GE. ANSET) GOTO 110
            IF(I .EQ. 1) GOTO 100
C
```

```
C
                    DELTL = DELTL+DIFF(I)*12.0/E*SL(J+1)
                    IF(DELTL .GE. ANSET) GOTO 110
C
   90         CONTINUE
C
  100 CONTINUE
C
  110 SLOPE = DIFF(M)/2.0/SL(M+1)
      DELTL1 = ANSET
      IF(M .EQ. 1) GOTO 150
C
      DO 130 I=1,M-1
C
             DELTL1 = DELTL1-DIFF(I)*SL(I+1)*6.0/E
C
             IF((M-2) .LT. I) GOTO 130
             DO 120 J=I,M-2
C
                    DELTL1 = DELTL1-DIFF(J+1)*12.0/E*SL(I+1)
C
  120        CONTINUE
C
  130 CONTINUE
C
      B = 0.0
C
      DO 140 I=1,M-1
C
             B = B+SL(I+1)*12.0/E
C
  140 CONTINUE



C
      A = 3.0/SLOPE/E
      DELTF = (0.0 - B+SQRT(B**2+4*A*DELTL1))/2.0/A
      GOTO 160
  150 DELTF = SQRT(E*DELTL1*SLOPE/3.0)
  160 H = DELTF/2.0/SLOPE
      IF(M .EQ. N) GOTO 170
      GOTO 220
  170 IF(H .LT. SL(M+1)) GOTO 220
      DELTL1 = ANSET
C
      DO 190 I=1,M
C
             DELTL1 = DELTL1-DIFF(I)*SL(I+1)*6.0/E
             IF(M .EQ. I) GOTO 190
C
             DO 180 J=I,M-1
C
                    DELTL1 = DELTL1-DIFF(J+1)*12.0/E*SL(I+1)
C
  180        CONTINUE
C
  190 CONTINUE
C
      DELTF = DELTL1*E/12.0/SLT(N+1)
C
      DO 210 I=1,M+1
C
             STRA(I) = STR(I)-DELTF
C
             DO 200 J=I,M
C
                    STRA(I) = STRA(I)-DIFF(J)
C
  200        CONTINUE
C
  210 CONTINUE
C
      GOTO 260
C
  220 DO 240 I=1,M
C
             STRA(I) = STR(I)-DELTF
             IF(M .EQ. I) GOTO 240
C
             DO 230 J=I,M-1
C
                    STRA(I) = STRA(I)-DIFF(J)
```

```
C
  240 CONTINUE
C
      STINT = STR(M)-DELTF/2.0
C
      DO 250 I=M+1,N+1
C
            STRA(I) = STR(I)
C
  250 CONTINUE
C
  260 TOT = 0.0




C
      DO 270 I=1,N
C
            TOT = TOT+(STRA(I+1)+STRA(I))/2.0*SL(I+1)
C
  270 CONTINUE
C
      AVG1 = TOT/SLT(N+1)
C
      WRITE(6,280)
  280 FORMAT(///,1X,'INCREMENT',3X,'SEGMENT',3X,'ELEVATION',3X,
     1       'INCREMENTAL',2X,'CUMULATIVE',2X,'STRESSES',3X,'STRESSES',
     1       /,2X,'NUMBER',6X,'LENGTH',3X,'DIFFERENCE',4X,
     1       'ANGULAR',6X,'TENDON',5X,'AFTER',6X,'AFTER',
     1       /,23X,'OF ENDS OF',4X,'CHANGE',7X,'LENGTH',
     1       4X,'FRICTION',4X,'ANCHOR',
     1       /,24X,'SEGMENT',30X,'LOSSES',6X,'SET',
     1       /,15X,'(FT)',5X,'(INCHES)',4X,'(RADIANS)',
     1       6X,'(FT)',7X,'(KSI)',5X,'(KSI)',//)
C
      DO 320 I=1,N+1
C
            K = I-1
            IF(TP(I) .EQ. 0) GOTO 300
C
            WRITE(6,290) K, SL(I), CGS(I), TAC(I),
     1                   SLT(I), STR(I), STRA(I)
  290       FORMAT(3X,I3,5X,F7.2,'P',5X,F7.3,5X,F8.4,
     1             4X,F8.2,4X,F7.2,4X,F7.2)
C
            GOTO 320
C
  300       WRITE(6,310) K, SL(I), CGS(I), TAC(I),
     1                   SLT(I), STR(I), STRA(I)
  310       FORMAT(3X,I3,5X,F7.2,'T',5X,F7.4,5X,F8.4,
     1             4X,F8.2,4X,F7.2,4X,F7.2)
C
  320 CONTINUE
C
      WRITE(6,330)
  330 FORMAT(/,17X,'P = PARABOLIC SEGMENT, T = TANGENT SEGMENT')
C
      J = PX+100
      IF(M .EQ. N) GOTO 340
      GOTO 350
  340 IF(H .GT. SL(N+1)) GOTO 370
C
  350 WRITE(6,360) ELONG, J, PE, AVG, H, M, STINT, AVG1
  360 FORMAT(///,7X,'TENDON ELONGATION',12X,'=',F10.3,1X,'INCHES',
     1       /,7X,I2,' PERCENT TENDON ELONGATION =',F10.3,1X,'INCHES',
     1       //,7X,'THE AVERAGE TENDON STRESS AFTER FRICTION ',
     1       'LOSSES IS',F7.2,1X,'KSI',
     1       //,7X,'THE ANCHOR SET LOSS CURVE INTERSECTS THE ',
     1       'FRICTION CURVE',F7.2,' FEET INTO',/,7X,'SEGMENT ',
     1       I3,' AT A STRESS OF',F7.2,' KSI',
     1       //,7X,'THE AVERAGE TENDON STRESS AFTER FRICTION ',
     1       'AND ANCHOR SET LOSSES IS',F7.2,1X,'KSI')
C
      GOTO 390
C
  370 WRITE(6,380) ELONG, J, PE, AVG, AVG1
  380 FORMAT(///,7X,'TENDON ELONGATION',12X,'=',F10.3,1X,'INCHES',
```

```
     1        /,7X,I2,' PERCENT TENDON ELONGATION =',F10.3,1X,'INCHES',
     1        //,7X,'THE AVERAGE TENDON STRESS AFTER FRICTION ',
     1        'LOSSES IS',F7.2,1X,'KSI',
     1        //,7X,'ANCHOR SET LOSS GOES TO DEAD END ANCHOR',
     1        //,7X,'THE AVERAGE TENDON STRESS AFTER FRICTION ',
     1        'AND ANCHOR SET LOSSES IS',F7.2,1X,'KSI')
C
C
  390 STOP
      END
```